CONCEPTUAL DESIGN OF A GLYCEROL BIOREFINERY

by

BAHIZIRE MARTIN MUKERU

submitted in accordance with the requirements for

the degree of

MAGISTER TECHNOLOGIAE

in the subject

CHEMICAL ENGINEERING

at the

UNIVERSITY OF SOUTH AFRICA

SUPERVISOR: PROFESSOR BILAL PATEL

December 2021

DECLARATION

Name: BM MUKERU

Student number: 53389913

Degree: MAGISTER TECHNOLOGIAE

CONCEPTUAL DESIGN OF A GLYCEROL BIOREFINERY

I declare that the above dissertation is my own work and that all the sources that I have used or quoted have been indicated and acknowledged by means of complete references.

I further declare that I submitted the dissertation to originality checking software and that it falls within the accepted requirements for originality.

I further declare that I have not previously submitted this work, or part of it, for examination at Unisa for another qualification or at any other higher education institution.

_____ _____

SIGNATURE DATE

ACKNOWLEDGEMENTS

I kindly express my heartfelt gratitude to God for his abundant love and grace. Without him I could not be able to finish this work. All glory and honour to Him.

I'm forever grateful to my supervisor Professor Bilal Patel for his daily guidance on how to plan, design, implement and present a research project. He has always been there for me whenever I need help. It is such a privilege to have him as a supervisor. His quick feedback and insights played a significant role in completing this study.

I would like to take this opportunity to thank my brothers Safari Mukeru and Bahati Mukeru as well as their respective wives Furaha Namulambi and Genevieve Mugangu for their sacrifice during my academic adventure. Without their financial and moral support, I would not finish this work.

I owe special gratitude to the University of South Africa (UNISA) for funding. This financial support helped me keep moving during hard times.

My gratitude to Mr Josaphat Fahari Chokoro for the love he has been showing me during my tough times.

I am grateful to my friend Ndishimana Thierry for showing me how to use the Aspen Plus simulation software. Without him I would not be able to complete this study.

I am grateful to my colleague Mrs Lucy Khumalo for her encouragement during tough times.

I am also grateful to Dr Sigwadi Rudzani for checking upon me during my studies.

ABSTRACT

Glycerol is considered as the major waste from biodiesel production since every 1L of biodiesel produced is accompanied by 0.1 L of glycerol by-product. Utilizing this waste as a biorefinery feedstock will not only promote biodiesel production but also reduce challenges related to waste disposal. There are various ways through which glycerol can be transformed into valuable products. This study used an insight-based approach (CHO ternary diagrams) to determine the performance of glycerol-biorefinery via reforming pathway prior to a detailed design. It was shown that to produce syngas that fulfils the requirement for methanol synthesis$\left(\frac{H_2}{CO} \sim 2\right)$, glycerol should be mixed with methane in a ratio of 1/2 (in terms of molar ratio) using steam as a reforming agent. A high-level economic as well as environmental analysis in terms of economic potential, carbon efficiency, atom economy, and E-factor was assessed. It was found that the price of raw glycerol has a significant impact on the economic potential during the synthesis of methanol. The raw glycerol price range that generated a positive economic potential was found to be \$0.025/kg - \$ 0.90/kg. At this raw glycerol price range, the approximate economic potential of the entire process was found to be \$ 7169.12 - 239.12 \$ million per year. The carbon efficiency, atom economy, and E-factor were also calculated and found to be 100%, 100 %, and 0 respectively.

Based on these CHO ternary diagram targets an entire flowsheet for methanol synthesis was developed using Aspen Plus. It was determined that Aspen Plus could not exceed targets set by CHO ternary diagrams in terms of methanol flow rate, carbon efficiency as well as atom economy. CHO ternary diagrams further revealed that it is possible to synthesize DME from a mixture of glycerol and linear low-density polyethylene (LLDPE) (25% glycerol-75% LLDPE). It can be inferred from various analysis conducted that the production of methanol from glycerol obtained from biodiesel is economical.

Key Terms: Glycerol, CHO ternary diagrams, Syngas, LLDPE, reforming, Carbon deposition boundary, Aspen Plus.

Table of Contents

List of Figures

List of Tables

CHAPTER ONE

1.0 INTRODUCTION

1.1 Background to the study

Energy is considered as the most important driving force of any economic activity (Matsumoto *et al*., 2018)**.** It plays a significant role in the economic development of a nation (Babajide, 2013). Most of this energy is generated from fossil fuels, which are regarded as non-renewable resources (these include coal, natural gas, and petroleum) (Hook and Tang, 2013).

Once these non-renewable resources undergo combustion processes, greenhouse gases such as carbon dioxide as well as various particulate matter are released which results in environmental issues such as global warming, air, and water pollution. Global warming can be regarded as the most significant environmental threat in recent years and it has negative impacts on humans as well as animals (Menezes *et al*., 2018),(Sharma *et al*., 2008). Therefore, due to the above-mentioned issues related to conventional fuels, the development of a more sustainable economy, based on alternative renewable sources of energy, has become of significant importance.

Currently, South Africa being a developing country, is considered the biggest energy consumer in Africa (Akinbami *et al.,* 2021). It is the 12th highest emitter of greenhouse gases worldwide (Statista, 2021). Most of its energy is generated from non-renewable sources with 83% generated from coal, which makes the country coal- dependent for the foreseeable future (DoE, 2018)**.** In this regard, South Africa has signed an agreement in Paris on global warming in order to lower the annual quantity of CO_2 that is emitted into the atmosphere to 4.5 % by 2030 (Pachón *et al*., 2018). To achieve this goal, the use of sustainable renewable energy is becoming the main priority of the country. This will help South Africa move from fossil fuels economy into a greener or sustainable circular (bio) economy.

Various renewable energy sources that can generate energy with high economic value are available worldwide. These natural resources include biomass (wood, algae, and crops), wind, solar, hydropower, and geothermal (REN21, 2021). Among all these different types of renewable resources, biomass is the only resource that contains renewable carbon. This characteristic makes biomass a unique alternative source of energy. Some other benefits of using biomass as an alternative renewable source of energy include its availability as well as low emissions of harmful

substances in the atmosphere (Tey *et al.*, 2021), (Junginger *et al.*, 2006). Due to these unique benefits of biomass, it is important to sustainably process it into value-added products.

A biorefinery is defined as the processing of raw materials (biomass) into chemicals and fuels with high economic value (IEA, 2012b). There are numerous types of biomass that are available for a biorefinery. Some of these types include energy and food crops, algae, industrial, forestry, and agricultural residues, municipal solid waste (Tursi, 2019). The effective utilization of biomass as a biorefinery feedstock for the generation of transportation biofuels (such as biodiesel, methanol, and ethanol) and other related biofuels (such as hydrogen and dimethyl ether) as well as high-value chemicals has gained interest in recent years. Producing these biofuels and other commodities from biomass not only assists in combating climate change and reducing the global reliance on petroleum but could also play a significant role in developing rural areas, creating job opportunities and investment in these areas (Pradhan and Mbohwa, 2014).

Biofuel (bioethanol and biodiesel) production has significantly increased worldwide in recent years, from 128 (73.3 % bioethanol and 26.7 % biodiesel) to 140.2(66.9% bioethanol and 33.1% biodiesel) billion liters in 2016 and 2018 respectively (WBA, 2020). While in 2019, the production of biofuel worldwide reached approximately 161 billion liters (71.4 % bioethanol and 28.6 % biodiesel). This increase was curtailed in 2020 due to the Covid-19 pandemic. This pandemic caused global biofuel production to decrease to 152 billion liters in 2020 (69.1 % bioethanol and 30.9 % biodiesel). The United States and Brazil were the leading biofuel producers in 2020 with 36 and 26% respectively(REN21, 2021). The global production of biofuel is forecasted to increase and reach approximately 182 billion liters (72.5 % bioethanol and 27.5 % biodiesel) in 2030 (OEDC/FAO, 2021). This continued growth of biofuel production is due to the fact that various countries have adopted biofuel policies and targets (Pradhan and Mbohwa, 2014). For example, the European Union Directive (2009/28/EC) and 2018/2001 stipulated that all country members were required to use 10 % and 14 % of biofuel in the transportation sector at the end of 2020 and 2030 respectively (EU, 2009), (EU, 2018).

South Africa has also adopted a strategy to increase the production of biofuels. The main objective of this strategy was to introduce 2% of biofuel in the transportation sector by 2013. This 2% was equivalent to approximately 0.4 billion liters. Achieving this target, approximately 2500 jobs could

have been created (DoME, 2007). Unfortunately, this strategy has been delayed due to multiple reasons such as issues related to food security. This delay has caused the country's biofuel production to stay stagnant and contribute almost nothing to global biofuel production (less than 0.01%) (Pradhan and Mbohwa, 2014). Zimbabwe has also launched a biofuel program whereby at the end of 2030, 22% (20% ethanol and 2% biodiesel) of biofuel should be mixed with diesel (REN21, 2021). This increase in biofuel production has reduced the global unemployment rate in recent years. Records reveal that biofuel production approximately created 3.58 million jobs in 2019 (WBA, 2020).

Although these biofuels are characterized as a reliable, renewable, and sustainable alternative to petroleum, their economic feasibility is still a major concern (Fan *et al*., 2010). Unfortunately, there is an inevitable generation of a significant amount of waste (by-products) during the production of these biofuels, which negatively affect their market as well as the environment.

Many researchers have considered biodiesel as one of the most promising biofuels. Biodiesel generation is seen as a promising alternative to produce clean, biodegradable, non-toxic and renewable fuels (Harabi *et al.*, 2019). This biofuel can also serve as an additive for conventional diesel (Asri, 2018). It can be utilized alone without mixing it with any other fuel (Murillo *et al*., 2007), or as a mixture with diesel, for example, B5 (where 5% of biodiesel is mixed with 95% diesel) (Kousoulidou *et al.*, 2010). Animal tallow, vegetable or waste cooking oils serve as feedstock to produce biodiesel via a process called transesterification. A homogeneous or heterogeneous catalyst is typically required. However, various wastes are generated such as glycerol, unconverted methanol/ethanol, biodiesel washing wastewaters, and solid residues (Plácido and Capareda, 2016). During the production of biodiesel, 10 to 20% by volume of glycerol is generated, and therefore it is considered as the main by-product of biodiesel. In other words, if 100 L of biodiesel are to be produced, at least 10 L of crude glycerol is obtained. This means that high production of biodiesel will always lead to considerable quantities of glycerol (D'Avino *et al.*, 2015). For example, biodiesel industries approximately generated 3.42 billion liters of crude glycerol in 2016 and this production increased to 3.6 billion liters in 2018. It is estimated that this trend will keep on increasing and reach approximately 5 billion liters in 2030 (WBA, 2020).

An increase in biodiesel global production has not only caused a dramatic reduction in crude glycerol pricing in recent years, but also has raised environmental concerns due to the way glycerol

is disposed because crude glycerol is a contaminated by-products (Seadira *et al.*, 2018)**.** The price of crude glycerol has dropped significantly in recent years from $3200/ton to $500/ton in European Union and from $2000/ton to $600/ton in the USA due to a fast growth of biodiesel production (Bagnato *et al.*, 2017)**.** Despite these low prices of crude glycerol, the cost involved in its purification is exceedingly high and therefore this limits its applications as a purified product (Harabi *et al.*, 2019)**.**

Presently, some industries are utilizing glycerol as an additive to produce various products. Soap and cosmetics industries consume 28% of glycerol whereas other industries like polyglycerol, food, and beverage consume more than 47% of glycerol. However, these applications will not accommodate an oversupply of crude glycerol. This means that global biodiesel producers will encounter severe problems because the demand of crude glycerol will always be less than its supply (Seadira *et al.*, 2018)**.**

It is crucial to look for alternative industrial uses of crude glycerol to improve and promote the biodiesel industry's economic viability. The economy of biodiesel depends on the way crude glycerol is utilized by various industries (Fan *et al*., 2010). The sustainable utilization of crude glycerol as a biorefinery feedstock to produce various products with high economic value will not only promote biodiesel production but also contribute to its economy and ease pressure on waste management. Glycerol-based biorefineries are able to produce more than two thousand products via different industrial processes (Rodrigues *et al*., 2017). These processes include biochemical, chemical as well as thermochemical processes. Since glycerol-based biorefineries are dependent on biodiesel production, these biorefineries can be regarded as promotors of a circular (bio) economy (Lari *et al*., 2018). For example, glycerol-based biorefinery can produce methanol through a thermochemical process such as reforming. Biodiesel industries can in turn use this methanol to generate biodiesel and crude glycerol.

1.2 Purpose of study

Like other biorefineries, a glycerol-based biorefinery is faced with certain challenges with regard to sustainability. This challenge can be addressed by means of effective process design at the early stage. Thus, the main purpose of this study is to apply two process design techniques (targeting

and conceptual design) to effectively convert glycerol into valuable products. Targeting plays an important role in biorefinery design as it allows the designer to evaluate the quality and benchmark of the process prior to a detailed design (El-Halwagi, 2012). The most common types of process targets are mass, energy, and entropy balance. One can use the mass balance for example, to determine the amount of products as well as the amount of waste from a given feedstock (Patel, 2007). This study uses carbon-hydrogen-oxygen (CHO) ternary diagram as an insight-based approach to set the target for glycerol-based biorefinery. Once the outputs are known, Aspen Plus simulation can be used to develop a flowsheet for the entire process.

1.3 Aim and Objectives

The aim of the current study is to utilize raw glycerol in an efficient way to promote a circular bioeconomy. This aim is expected to be achieved through the following objectives:

1. Identify the different chemical reactions through which glycerol can be transformed into high-value chemicals and fuels
2. Determine the thermodynamic equilibrium of glycerol conversion by using CHO ternary diagrams (systems).
3. Utilize the CHO diagram (equilateral triangle) to identify the most suitable products that can be generated from glycerol via a thermochemical pathway
4. Use an Aspen Plus simulation to show the technical feasibility of the glycerol biorefinery based on CHO ternary diagram targets
5. Compare CHO ternary diagram results with results generated from Aspen Plus.

1.4 Dissertation structure

A brief outline of the dissertation and the remaining chapters are provided below:

Chapter Two: Literature review

The main objective of this chapter is to address the necessity of utilizing alternative sources of energy. It begins with a discussion of the different environmental issues caused by non-renewable resources and the need for alternative energy sources such as biomass. It also discusses the similarities and differences between a biorefinery and petrochemical refinery. The co-production

of biodiesel and crude glycerol is also discussed in this chapter. The necessity of promoting glycerol as a circular bio-economy feedstock is addressed as well. The chapter further discusses previous work on glycerol biorefineries. Lastly, the chapter discusses the process synthesis and design of a biorefinery.

Chapter Three: Methodology

This chapter provides the methodology used in the synthesis of a glycerol biorefinery. It starts by discussing the significance of CHO ternary diagrams as a glycerol biorefinery synthesis tool. It further describes the simulation of a glycerol biorefinery in Aspen Plus.

Chapter Four: Results and discussions

This chapter is split into two sections. The first section is based on CHO ternary diagrams. In this section, the model used in chapter 3 is validated by comparing it with published data. After the validation of the model, two processes (pyrolysis and reforming) are used to convert glycerol into value-added products. The second section is based on the Aspen Plus simulation. The model used in this section is also validated using published data. Finally, the results generated by both CHO ternary diagrams and Aspen Plus are compared.

Chapter Five: Conclusion and recommendations

This chapter gives a few concluding remarks on converting glycerol into value-added products. Because the conversion of glycerol into value-added products is a relatively recent area of research, the chapter also gives some recommendations for future studies.

1.5 References

Akinbami, O. M., Oke, S. R. and Bodunrin, M. O. (2021) 'The state of renewable energy development in South Africa: An overview', *Alexandria Engineering Journal*, 60(6), pp. 5077–5093.

Asri, N. P. (2018) 'Alumina supported zinc oxide catalyst for production of biodiesel from kesambi oil and optimization to achieve highest yields of biodiesel', *Euro-Mediterranean Journal for Environmental Integration*, 3(1), pp. 1–7.

Babajide, O. (2013) 'Sustaining Biodiesel Production via Value-Added Applications of Glycerol', *Journal of Energy*, 2013, pp. 1–7.

Bagnato, G., Iulianelli, A., Sanna, A. & Basile, A. (2017) 'Glycerol production and transformation: A critical review with particular emphasis on glycerol reforming reaction for producing hydrogen in conventional and membrane reactors', *Membranes*, 7(2), pp. 1–31.

D'Avino, L., Rizzuto, G., Guerrini, S., Sciaccaluga, M., Pagnotta, E. & Lazzeri, L. (2015) 'Environmental implications of crude glycerin used in special products for the metalworking industry and in biodegradable mulching films', *Industrial Crops and Products*, 75, pp. 29–35.

DoE (2018) *South African Energy Sector Report. Department of Energy, Republic of South Africa*. [Accessd on 11th August 2021]

DoME (2007) *Biofuels industrial strategy of the Republic of South Africa. Department of Minerals and Energy. South Africa.[Accessed on 7th August 2021]*

El-Halwagi, M. M. (2012) *Sustainable Design Through Process Integration:Fundamentals and Applications to Industrial Pollution Prevention, Resource Conservation, and Profitability Enhancement*. Second ed. Boston, MA: Butterworth-Heinemann.

EU, 2009, Directive 2009/28/EC of the European Parliament and of the Council of 23 April 2009 on the promotion of the use of energy from renewable sources and amending and subsequently repealing Directives 2001/77/EC and 2003/30/EC. [Accessed on 8 August 2021]

EU, 2018, Directive (EU) 2018/2001 of the European Parliament and of the Council of 11 December 2018 on the promotion of the use of energy from renewable sources. [Accessed on 8 August 2021]

Fan, X., Burton, R. and Zhou, Y. (2010) 'Glycerol (byproduct of biodiesel production) as a source for fuels and chemicals - Mini review', *Open Fuels and Energy Science Journal*, 3, pp. 17–22.

Harabi, M., Bouguerra, S. N., Marrakchi, F. & Chrysikou, L. P. (2019) 'Biodiesel and Crude Glycerol from Waste Frying Oil: Production, Characterization and Evaluation of Biodiesel Oxidative Stability with Diesel Blends', *Sustainability*, 11, pp. 1–15.

Hook, M. and Tang, X. (2013) 'Depletion of fossil fuels and anthropogenic climate change — A review', *Energy Policy*, 52, pp. 797–809.

IEA, 2012b. Bio-based Chemicals: Value Added Products from Biorefineries. Report for IEA.Biorefinery- Task 42. International Energy Agency (IEA), Paris,France [Accessed on 8 August 2021].

Junginger, M., Junginger, M., de Visser, E., Hjort-Gregersen, K., Koornneef, J., Raven, R., Faaij, A. & Turkenburg, W. (2006) 'Technological learning in bioenergy systems', *Energy Policy*, 34(18), pp. 4024–4041.

Kousoulidou, M., Fontaras, G., Ntziachristos, L. & Samaras, Z. (2010) 'Biodiesel Blend effects on a common-rail diesel combustion and emmissions', *Fuel*, 89, pp. 3442–3449.

Lari, G., Pastore, G., Haus, M., Ding, Y., Papadokonstantakis ,S., Mondelli, C. & Pérez-Ramírez, J.(2018) 'Environmental and economical perspectives of glycerol biorefinery', *Energy Environ. Sci.*, 11(5), pp. 1012–1029.

Matsumoto, K., Doumpos, M. and Andriosopoulos, K. D. (2018) 'Historical energy security analysis of EU countries', *Renewable and Sustainable Energy Reviews,* 82, pp.1737-1748.

McEwan, C. (2017) 'Spatial processes and politics of renewable energy transition: Land, zones

and frictions in South Africa', *Political Geography*, 56, pp. 1–12.

Menezes, J. P. da S. Q., Manfro, R. L. and Souza, M. M. V. M. (2018) 'Hydrogen production from glycerol steam reforming over nickel catalysts supported on alumina and niobia: Deactivation process, effect of reaction conditions and kinetic modeling', *International Journal of Hydrogen Energy*, 43(32), pp. 15064–15082.

Murillo, S., Miguez, J.L, Porteiro, J., Granada, E. & Moran, J.C. (2007) 'Performance and exhaust emmissions in the use of biodiesel in outboard diesel engines', *Fuel*, 86(12–13), pp. 1765–1771.

OEDC/FAO (2021) *OECD-FAO Agricultural Outlook 2021-2030*. OECD Publishing, Paris.

Pachón, E. R., Vaskan P., Raman, J.K. and Gnansounou, E. (2018) 'Transition of a South African sugar mill towards a biorefinery. A feasibility assessment', *Applied Energy* 229: 1–17

Patel, B. (2007) '*Fundamental Targets for the Synthesis and Evaluation of Chemical Processes*', PhD thesis, University of Witwatersrand, Johannesburg.

Plácido, J. and Capareda, S. (2016) 'Conversion of residues and by-products from the biodiesel industry into value-added products', *Bioresources and Bioprocessing*, 3(1), pp. 1–12.

Pradhan, A. and Mbohwa, C. (2014) 'Development of biofuels in South Africa: Challenges and opportunities', *Renewable and Sustainable Energy Reviews*, 39, pp. 1089–1100.

REN21 (2021) *Renewables 2021: Global Status Report*.[Accessed on 8th August 2021]

Rodrigues, A., Bordado, J. . and does Santos, R. G. (2017) 'Upgrading the Glycerol from Biodiesel Production as a Source of Energy Carriers and Chemicals — A Technological Review for Three Chemical Pathways', *Energies*, 10(11), p. 1817.

Seadira, T., Sadanandam, G., Ntho, T. A., Lu, X., Masuku, C. M. & Scurrell, M. (2018) 'Hydrogen

production from glycerol reforming: conventional and green production', *Rev Chem Eng*, 34(5), pp. 695–726.

Sharma, Y. C., Singh, B. and Upadhyay, S. N. (2008) 'Advancements in development and characterization of biodiesel: A review', *Fuel*, 87(12), pp. 2355–2373.

Statista (2021) *Carbon dioxide emissions in 2009 and 2019, by select country*.[Accessed on 6th August 2021]

Tursi, A. (2019) 'A review on biomass : importance , chemistry , classification , and conversion', *Biofeuel Reserch Journal*, 22, pp. 962–979.

Tey, T. O., Chen, S., Cheong, Z.X., Chaong, A. S.X, Ng, L.Y. & Chemmangattuvalappil, N.G (2021) 'Synthesis of a sustainable integrated biorefinery to produce value-added chemicals from palm-based biomass via mathematical optimization', *Sustainable Production and Consumption*, 26, pp. 288–315.

WBA (2020) *Global Bionergy Statistics 2020*.[Accessed on 8th August 2021]

CHAPTER TWO

2.0 LITERATURE REVIEW

2.1 Background

The consumption and demand of energy worldwide have dramatically escalated in the past two-centuries. The main driving forces of this increase are factors such as population growth, economic activities in developed and developing nations, and technological advancements (Earis, 2007). Records reveal that the total energy consumption in 2016 was roughly 102.70 billion GJ whereas it increased to 105.82 billion in 2019 (IEA, 2020). 2020 was characterized by uncertainties due to the Covid-19 pandemic which caused the energy demand to decrease by 4%. This decline is considered as the largest since World War II (IEA, 2021)**.** Due to vaccine rollouts against the pandemic, it is approximated that energy demand is going to increase by 4.6% at the end of 2021 exceeding pre-Covid-19 levels (ibid). Nearly 80% of global energy is obtained from non-conventional resources commonly known as fossil fuel resources such as natural gas, crude oil, and coal (Hook and Tang, 2013). This implies that the world will still rely on these non-renewable resources.

Oil reserves on planet earth have been estimated to be 1734 billion barrels at the end of 2019, meaning these reserves can be globally exploited for 50 years without any shortage at a rate of 95 192 thousand barrels per day. The natural gas reserves are 198.8 trillion cubic meters at end of the same year which is enough to meet 49.8 years of worldwide exploitation. The global coal reserves were estimated at 1070 billion tons at the end of 2019 which can be exploited for the next 132 years (BP, 2020). This shows that fossil reserves will deplete in the near future, resulting in an energy crisis across the world if no action is taken.

However, the prolonged reliance on fossil fuel resources has placed more pressure on the global environment, resulting in air pollution, global warming, and climate change. Fossil fuels undergo different chemical reactions such as combustion and subsequently release greenhouse gases (like CO_2, NO_x) and other pollutants in the environment (Gutiérrez *et al*., 2017). These greenhouse gases cause health-related problems such as cardio-pulmonary, neurological, cancer, respiratory,

and other chronic diseases (Lelieveld *et al.*, 2019), (Kotcher *et al*., 2019). Perera (2018) points out that children are the most vulnerable to these health-related issues.

Martins *et al*. (2019) point out that, besides environmental and health consequences of non-renewable resources, their uneven distribution around the world increases concerns regarding energy security. This uneven distribution is because the formation of these fossil resources depends on the type of climate, types of organisms that have lived in a specific region for thousands of years, and depends on the geological processes that have taken place. All countries that form part of OPEC (Organization of the Petroleum Exporting Countries) have high reserves of these resources. Records reveal that these countries have around 71% of global petroleum reserves (BP, 2020).

It can be further noted that major oil consumers do not produce sufficient quantities to sustain their internal consumption and this leads them to import 35% from members of OPEC. As it was seen earlier, there is a high demand of fossil fuel resources (oil, natural gas, and coal) which puts more pressure on their prices. Oil supply and demand are also considered as fundamental market factors and hence influence the global prices of oil. Socio-political disruptions between both consumers and suppliers also play a significant role in oil prices (Madathil and Velmurugan, 2019). The balance between oil supply-demand can be disrupted by natural causes and this results in high/low oil prices. This is the case of Covid-19. Asare *et al*. (2020) explain how Covid-19 has affected the demand-supply of fossil fuel resources which resulted in decreased prices in 2020. For example, in South Africa, the petrol (gasoline) price decreased from 1.14 USD in January 2020 to 0.87 USD in May 2020, whereas in the USA, crude oil price fell almost to zero USD as there was high supply with low demand due to lockdowns (Nkosi *et al.*, 2021).

Taking into consideration what has been mentioned in the above paragraphs, it is necessary to take action so that the dependency on non-renewable resources can be minimized. One of the most sustainable measures is the deployment of renewable energy (Hamelinck *et al*., 2005). There are various types of renewable energy and the most common are solar, wind, biomass, and geothermal energy (Gundekari *et al*., 2020). Among different renewable sources of energy, biomass is viewed as the most promising candidate to substitute fossil resources (Tey *et al.*, 2020), (Junginger *et al.*, 2006). Hamelinck *et al*. (2005) point out that, global biomass availability is the main reason for it

to be a promising alternative source of energy. During the utilization or transformation of biomass into biofuels, carbon dioxide is quickly transferred into the environment and this same carbon dioxide is used again by plants for the production of biomass as depicted in figure 2.1 (Tursi, 2019). Litheko (2017) also explains that biochemical, transportation fuels, and other biomaterials are obtained directly only from biomass.

The biomass global reserves are estimated to be around 1804 trillion kg (1800 trillion kg of land and 4 trillion of aquatic biomass) (Tursi, 2019). This total reserve can produce 33.000 exajoules which corresponds to more than 80 times the global energy consumption across the world on an annual basis (WBA, 2018).

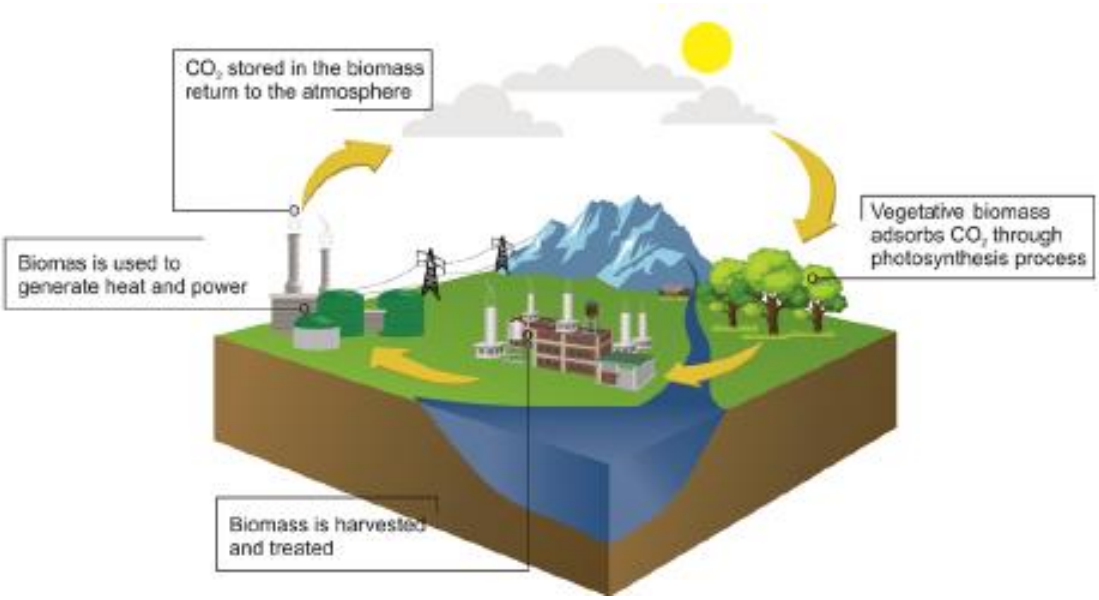

Figure 2. 1: Carbon cycle during the production and utilization of biomass (Tursi, 2019)

2.2 Biomass production and its classification

Biomass can be defined as any organic matter that can be generated from living or recently living organisms (Khan *et al.*, 2009). Biomass is naturally produced by plants from water and carbon dioxide in the presence of sunlight and this overall process is commonly known as photosynthesis (Ptasinski, 2015). During this process, carbohydrates are formed which are considered as the building blocks of biomass (McKendry, 2002).

Figure 2.2 illustrates the different natural factors involved in biomass production as well as the different agricultural production stages. The principal stages during the production of biomass are cultivation, harvesting, and logistics. Several factors (either climatic or environmental) affect the cultivation of biomass. These factors include insolation, precipitation, temperature, humidity, and soil quality.

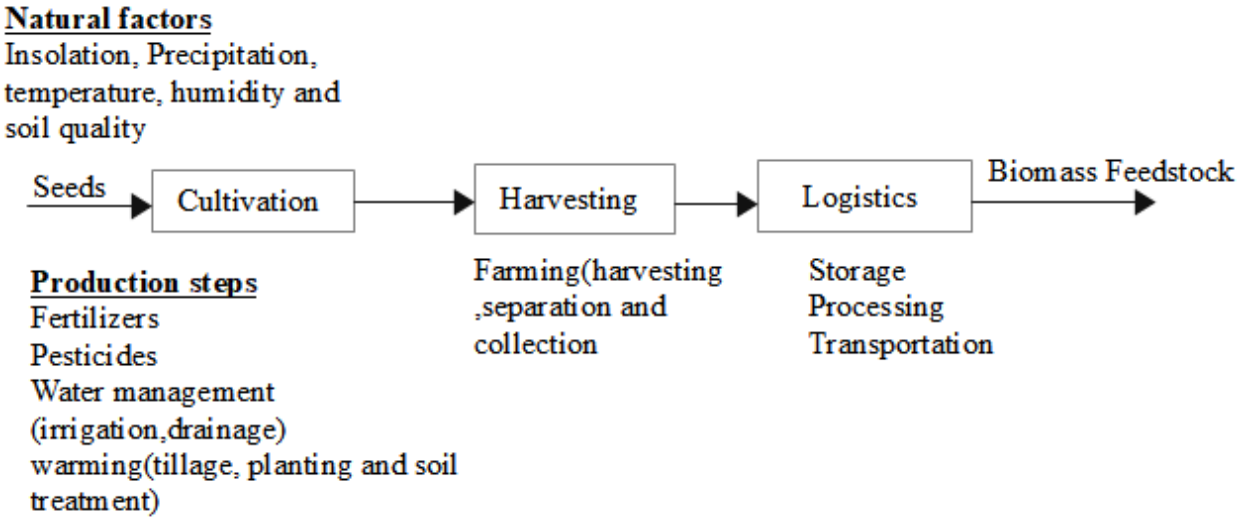

Figure 2. 2: Natural factors and production stages of Biomass

There is no unique way used to classify biomass due to their different varieties. Therefore, biomass can be classified in various ways depending on the scope of the study. In this study, the classification of biomass is based on three approaches which are chemical composition, sources as well as origin. Based on their sources, biomass can be classified into six major groups namely animal, industrial, agricultural, and forestry residues, municipal solid waste (MSW) as well as sewage (Tursi, 2019). Taking their chemical composition into consideration, biomass can be classified as carbohydrates (cellulose, starch, and hemicellulose), lignin, essential oils, vegetable oils (e.g. sunflower, soybean, and rapeseed oil) , animal fats, and natural resins (Gundekari *et al*., 2020). Based on their origin, biomass can be classified as first (animal fats, energy crop, food crops), second (lignocellulose, hemicellulose), and third generation (e.g. algae).

2.3 Concept of a biorefinery

2.3.1 Definition of a biorefinery

Biorefinery has been defined in many ways, but all these definitions essentially have a similar meaning. The IEA (International Energy Agency) provides the most comprehensive definition of a biorefinery: The word biorefinery is explained as the "sustainable processing of biomass into a spectrum of products which are marketable. These products include feed, materials, chemicals, food, fuels, power, and heat'' (IEA, 2012b). Another essential definition of a biorefinery is given as follows: "A biorefinery is any facility that aims to integrate different processes to convert biomass into fuels, power and biochemical *"*(Moncada *et al*., 2016). Figure 2.3 illustrates the biorefinery system concept.

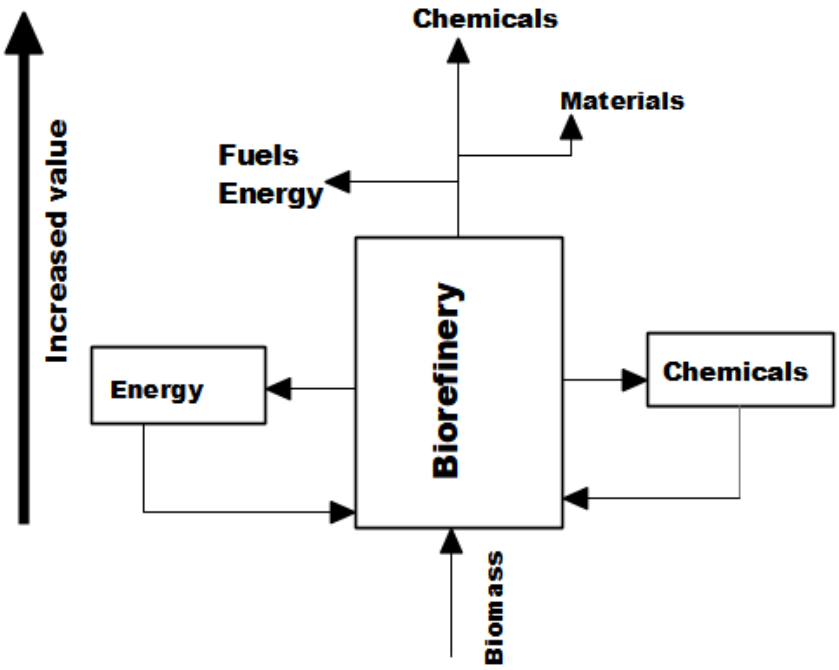

Figure 2. 3: Concept of a biorefinery (Carvalheiro, Duarte and Girio, 2008)

2.3.2 Similarities and differences between a biorefinery and a petrochemical refinery

An analogy exists between a biorefinery and an oil refinery (petrochemical refinery) (Kokossis and Yang, 2010). The main analogy is that both biorefineries and refineries aim to produce high-

value products and fuels from their feedstocks. There are also some differences between a biorefinery and a petrochemical refinery (Ghatak, 2011). The nature of raw materials, transformation method, product spectrum, economic aspects, and the impact on the environment are the main elements differentiating a biorefinery from a refinery. The feedstock used in the oil refineries is very expensive but the cost to process this feedstock is quite low, whereas for the biorefineries, the feedstock costs are lower, but the processing costs are high. The main raw materials used in the petrochemical refinery are crude oil and natural gas whereas biorefineries use biomass as their feedstock (Prasetyo *et al.*, 2020). A refinery uses exclusively chemical processes whereas a biorefinery uses a combination of both chemical and biotechnological processes (Cherubini and Ulgiati, 2010).

A condensed comparison between a biorefinery and a petrochemical refinery is summarized in table 2.1.

Table 2. 1: Similarities and differences between refineries and biorefineries, extracted from (de Jong and Jungmeier, 2015)

	Petrochemical refinery	Biorefinery
Raw material	Homogenous raw material Low O_2 content The product weight (mole/mole) increases with processing Sometimes high sulfur content	Heterogeneous raw material such as e.g. carbohydrates and oils Most of the raw materials are present in a polymeric form High O_2 content The product weight (mole/mole) decreases with processing The sulfur content is low
Main building block	Toluene, propylene, ethylene, benzene, methane, xylene isomers are the main building blocks	Xylose, fatty acids, and glucose
(Bio)chemical processes	Mostly chemical Atoms such as S, O, and N are introduced	Chemical and biotechnological processes may be used Removal of O_2
Chemical intermediates produced at commercial scale	Various intermediate products	Few intermediate products

2.3.3 Feedstock and Classification of a Biorefinery

A biorefinery system requires raw materials that are sustainable and renewable for the production of fuels and biochemicals (Prasetyo *et al.*, 2020). Taking into consideration the definition of biomass given in section 2.2, it is clear that biomass is the main biorefinery feedstock (Mahlia *et al.*, 2020). This biomass originates from various resources with high availability as stated in section 2.2.

Given that, there are various types of biomass, many technological transformations are required to convert the physical and chemical properties of a broad range of raw materials (Espinoza Pérez *et al.*, 2017). Biorefinery classification can be in terms of different aspects such as type of raw materials, type of intermediate products (syngas and or sugar), conversion processes (such as thermochemical and biochemical processes), and also the technological status (such as conventional and advanced) (Takkellapati *et al.*, 2018).

A biorefinery can be categorized as first, second, third or fourth generation according to the nature of raw materials that are used as feedstock to obtain chemicals with high economic value as well as biofuels. Biorefineries that use food crop resources like vegetable oil, corn, sugarcane, wheat as their feedstock are referred to as 1st generation (1G). If the raw materials to be used in a biorefinery are for example, wood, agricultural, and animal debris and energy crops high in lignocellulose, the biorefineries that process these types of materials into chemicals and fuels are referred to as second-generation (2G) (Palmeros *et al.*, 2017). There are other biorefineries that do not use food crops (e.g. soybean oil) as feedstock but they use instead algae biomass as their feedstock, such biorefineries are regarded as third-generation (3G) (Parajuli *et al.*, 2015**).** The fourth generation biorefineries use products obtained via industrial processes as their feedstock. These products are considered as pollutants and they include carbon dioxide (Mata *et al.*, 2010).

Second and third generation biorefineries are not yet implemented at an industrial scale due to their economic and or technical challenges but 1st generation biorefineries have been implemented and established. First-generation feedstock biorefinery which uses edible vegetable oil (sunflower, soya bean, and canola oils), cane, rice or wheat faces various challenges such as social, political, environmental, and even economic challenges since they are obtained from food crops. Using these food crops, can negatively impact food prices or result in pressure on land usage (Moncada *et al.*, 2016).

Biorefineries can also be classified by using four different features, which are platforms, products, feedstocks, and processes. A biorefinery system from raw materials to final products can be defined once all the four features are combined. Platforms are intermediates that connect the raw materials (feedstock) used in the biorefineries with the final products. Platforms are considered as the most important feature one can use when the specification of a biorefinery type is required (Cherubini *et al*., 2009).

There are various types of platforms such as biogas (which is a combination of CH_4 and CO_2), obtained from anaerobic digestion, syngas (CO, H_2) is produced by gasification or reforming. Hydrogen (H_2) is obtained through different processes such as steam reforming and fermentation. Sugars that contain six atoms of carbon (such as glucose, fructose and galactose are obtained from a hydrolysis process of hemicellulose, cellulose, starch, and sucrose. Whereas sugars with five carbon atoms (such as xylose and arabinose) are produced from the hydrolysis of hemicellulose and food streams. Triglycerides are also considered as a type of a platform that are obtained from algae, oil-based residues as well as oilseed crops (ibid).

Energetic and non-energetic products are the two main products that are generated when raw materials are processed inside a biorefinery. An example of an energetic product is bioethanol and glycerol can be considered as a non-energetic product. The third feature is the feedstock: to get product from a biorefinery, there is a need of raw materials, which are always renewable, and these renewable materials are called feedstocks (biomass). Every biorefinery uses one of the following feedstock: agriculture (food crops), forestry (wood), industrial wastes, organic residues and, algae (Cherubini, 2010). The fourth feature is the processes: biorefineries use different processes to convert their feedstock into products such as mechanical, biochemical, chemical, and thermochemical processes (Cherubini *et al*., 2009).

A biorefinery can also be classified as phase I, II, and phase III biorefinery (Clark and Deswarte, 2008), (Takkellapati *et al*., 2018). Figure 2.4 gives a concise definition of these types of biorefineries.

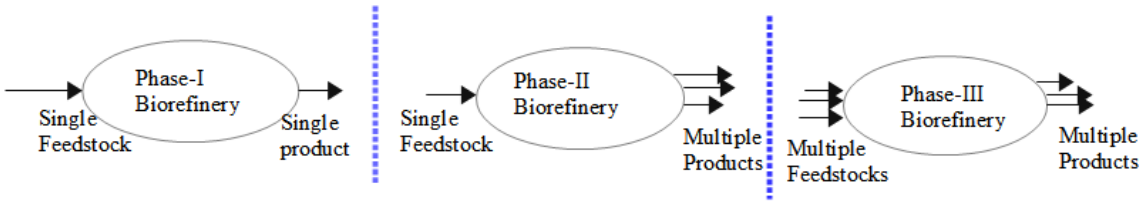

Figure 2. 4: Three types of biorefinery systems (Ptasinski, 2015)

A phase-I biorefinery is a type of biorefinery whereby a single primary product is produced from one feedstock. Biodiesel production from vegetable oils is considered as a phase-I biorefinery (Naik *et al.*, 2010). Figure 2.5 shows how biodiesel is generated from vegetable oil via transesterification process. A phase-II biorefinery is like a phase-I biorefinery but it is able to generate different products from one raw material. Using starch as a raw material for the production of various chemicals falls under a phase-II biorefinery (Takkellapati *et al.*, 2018). Phase-III biorefinery is a type of biorefinery that utilizes different feedstocks to generate various products by using different technologies (Takkellapati *et al.*, 2018).

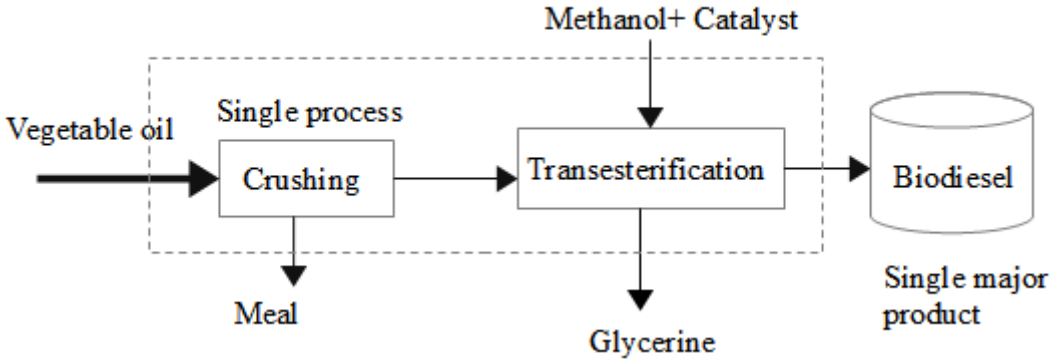

Figure 2. 5:Illustration of Phase-I Biorefinery using biodiesel production (Clark and Deswarte, 2008)

Because Phase-III biorefinery uses various feedstock to generate multiple products, this biorefinery can be grouped into four different classes (ibid). These four classes are whole-crop biorefinery, lignocellulosic biorefinery, green biorefinery, and two-platform concept biorefinery. These biorefinery types are not explained in detail here, but their explanations can be found in (Clark and Deswarte, 2008),(Takkellapati *et al.*, 2018), (Ptasinski, 2015), (Naik *et al.*, 2010) and (Xuan *et al.*, 2012).

2.4 Glycerol biorefinery

2.4.1 Promoting a sustainable circular (bio) economy through glycerol

As shown earlier, the world has been relying on non-renewables for the production of transportation fuels, biomaterials, and other different products. But the exploitation of these sources has resulted in negative environmental consequences such as greenhouse gas (GHG) emissions and air pollution. Various solutions to these environmental issues have been proposed, but the most sustainable, effective, and efficient is to change the production system from a linear economy (LE) into a circular economy (CE) as well as circular bioeconomy (CBE) (Gatto and Re, 2021). Leong *et al.* (2021) define CBE as the sustainable use of

renewable resources (biomass) including wastes to produce different products such as bioenergy, biomaterials, and food. CBE presents various advantages such as reducing the dependence on fossil fuels and valorizing waste products from different industries like biodiesel and bioethanol.

In section 2.3.3, different types of biorefineries were explained. It was shown that a phase-I biorefinery uses a single feedstock for the synthesis of a single major product. The production of biodiesel is an example of this type of biorefinery as biodiesel is the main product from the transesterification process with glycerol as the main by-product. Biodiesel is viewed as an alternative source of energy. This is due to its properties such as non-toxicity, biodegradability and, eco-friendliness (Habibullah *et al*., 2015). Another property that makes biodiesel an important fuel is that engines can use it alone or mix it with different proportions of diesel (Singh *et al*., 2020). It has been shown that for every $1m^3$ of biodiesel there is 0.1 m^3 of glycerol produced as waste (Vivek *et al.*, 2017), (Kaur *et al.* 2020). The production of biodiesel is estimated to reach approximately 40 billion liters in 2027, this means that 4 billion liters of glycerol will be generated as waste (D'Angelo *et al.*, 2018). The disposal of glycerol has become an environmental threat and this could affect the biodiesel industry (Costa-Gutierrez *et al.*, 2021). An efficient, effective, and sustainable transformation of glycerol into products with high economic value will not only promote the production of biodiesel but also contribute to its economy as well to reduce its environmental impacts. The main objective of a glycerol biorefinery is to optimize the utilization of raw materials (glycerol), minimize the production of waste, maximize profitability, and to minimize the environmental effects. Because the production of glycerol is dependent on other production industries (biodiesel) it is viewed as a promotor of CE/CBE (Lari *et al.*, 2018). In other words, glycerol-based biorefinery can generate products that can be used again by biodiesel production processes such as energy generation and methanol production via biochemical and thermochemical processes respectively (Mahabir *et al.*, 2021). Figure 2.6 shows how methanol is produced from glycerol via steam reforming and this same methanol is used again to produce biodiesel.

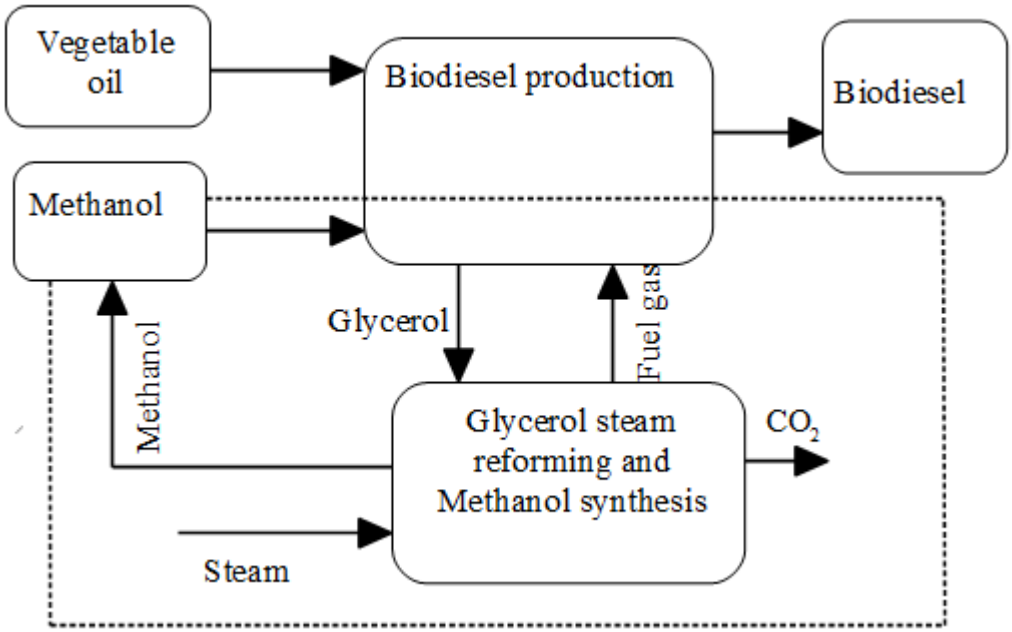

Figure 2. 6: Promoting CE through glycerol, extracted from (van Bennekom et al., 2009)

Several studies have been done on the valorization of glycerol as a biorefinery feedstock. D'Angelo *et al.* (2018) analyzed an economic performance glycerol-based biorefinery by selecting products, namely glycerol carbonate, allyl alcohol, 1, 2-propanediol, acrylic acid, lactic acid as well as 1, 3-propanediol. It was found that, among these products, glycerol carbonate gave the highest profit for the amount of glycerol used. Kaur *et al.* (2020) showed that glycerol can serve as a raw material to synthesize chemicals such as butanol, glyceric acid, tartronic acid, acrolein, syngas, polyglycerols, 1-3 propanediol, and glyceric acid via different conversion processes. Costa-Gutierrez *et al.* (2021) point out that, microbiological industries synthesize different bioproducts such as biogas, pigments, and biosurfactants from glycerol. Glycerol is valorized as a feedstock for the synthesis of fuel additives (Smirnov *et al*., 2018). Table 2.2 gives a summary of some of the pertinent literature on the valorization of glycerol-based biorefinery. The next section focuses on different routes through which glycerol can be converted into value-added products.

Table 2. 2: Glycerol an important promotor of a circular (bio) economy

Reference		Summary
1	(Mahabir *et al.*, 2021)	Discuss two transformation pathways which valorize glycerol as a promotor of circular economy. These two pathways are anaerobic digestion as well as reforming.
2	(Kaur *et al.*, 2020)	Different transformation pathways used in the synthesis of value-added chemicals and fuels from glycerol. Environmental and economic analysis of these different transformation routes are considered.
3	(Lari *et al.*, 2018)	Synthesis of different chemicals such as lactic acid, glycerol bicarbonate, propanediols as well as acrylic acid. The analysis for the synthesis of these products based on environmental and economical approach is also carried out.
4	(D'Angelo *et al.*, 2018)	Used various capital estimation methods as well as Aspen Plus to evaluate the investment costs during the manufacture of different products from glycerol.
5	(Martın, 2018)	Give a review of different pathways through which glycerol can be transformed into syngas, glycerol ethers and epichlorohydrin.
6	(Trifoi *et al.*, 2016)	Different techniques and approaches for the synthesis of fuel additives (ketals and acetals) from glycerol
7	(Chen and Liu, 2016)	Discusses some metabolic engineering aspects and different challenges during the synthesis of various products from glycerol such as diols, biofuels as well as organic acids.
8	(Gargalo *et al.*, 2016)	Assess some economical risks related to glycerol biorefinery at the early stage
9	(Schultz *et al.*, 2014)	Discuss different challenges and opportunities related to glycerol biorefinery as well as various transformation pathways.
10	(Zhou *et al.*, 2013)	Give a detailed review on different catalytic transformations of glycerol into value-added products

11	(Almeida *et al*., 2012)	Give a summary of different products from glycerol via microbial fermentation
12	(Posada *et al*., 2012)	Design and analyze a glycerol biorefinery for the synthesis of different products via chemical and biochemical pathways.

2.4.2 Transformation pathways used in a glycerol biorefinery

Different methods can be used for the synthesis of various chemicals from glycerol. Figure 2. 7 gives a summary of the major conversion processes used in glycerol biorefinery.

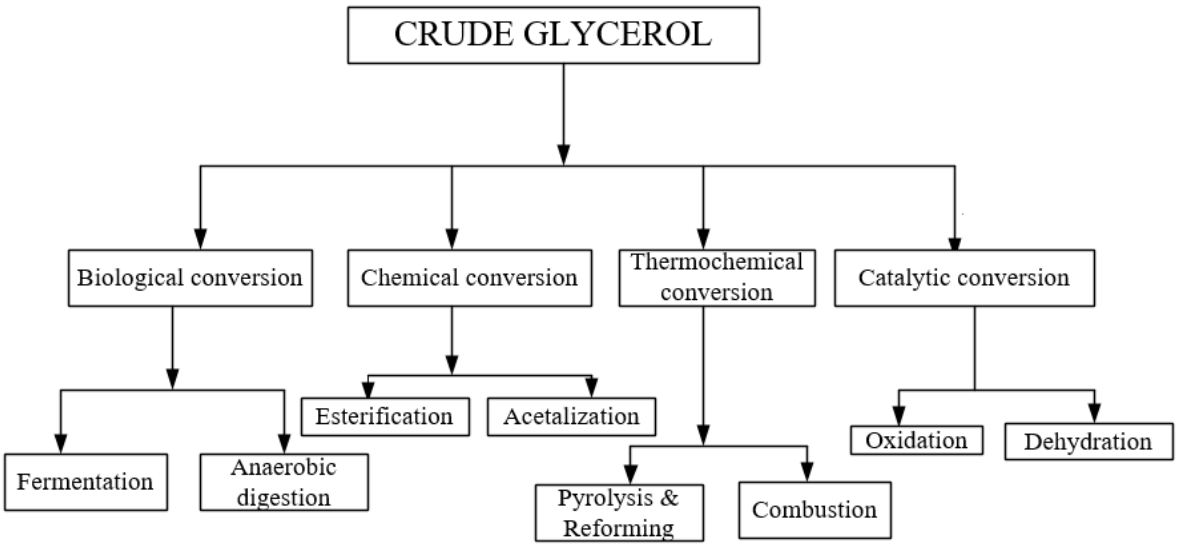

Figure 2. 7: Conversion processes used in glycerol biorefinery, extracted from (Kaur et al., 2020)

2.4.2.1 Chemical and catalytic transformation of glycerol

Chemical conversion is viewed as the main process used to transform glycerol into valuable products (Kaur *et al.*, 2020). Some selected products that can be synthesized from glycerol via chemical processes with their industrial applications are explained below.

- Solketal is an important chemical produced from glycerol via an acetalization process (Nda-umar *et al.*, 2018). This chemical can be used as a fuel additive (Smirnov *et al*., 2018).
- Using an esterification process, glycerol serves as a feedstock to produce different esters such as polyglycerol esters, acylated esters, and glyceryl diacetate. These esters are also used as fuel additives (Kaur *et al.*, 2020).

Catalytic transformation of glycerol into various chemicals includes processes such as oxidation, reduction, and dehydration. Different catalysts are used in this process, but the most preferred catalysts are heterogeneous catalysts which give high conversion and selectivity *(ibid).* Glycerol can be oxidized by using various metal catalysts such as palladium, platinum, and gold to produce chemicals like glyceric, hydroxypyruvic, tartaric, oxalic, and mesoxalic acids as well as dihydroxyacetone.

Glycerol can also undergo a catalytic reduction to obtain various types of chemicals like propylene glycol, ethylene glycol, and lactic acid. Cu, Zn, Ni, and Co are the main catalysts used in the reduction processes of glycerol. High pressures and temperatures are required so that this process can be effective (Posada *et al*., 2012). Zhang *et al.*(2015) point out that, dehydration is considered as the most important catalytic process of glycerol. Glycerol is dehydrated to produce acrolein which serves as a raw material to manufacture acrylic acid and acrylic acid esters (Tan *et al*., 2013). Rosas *et al*. (2017) studied the catalytic dehydration of glycerol using Pd/LaY Zeolite catalysts for the production of acrolein. In the study, three main dehydration reactions of glycerol occurred. Acrolein and acetol were considered the main products whereas methanal and ethanal were taken as minor products.

2.4.2.2 Glycerol conversion via biochemical processes

Fermentation and anaerobic digestion are the two main biochemical routes (Kaur *et al.*, 2020). Through fermentation processes, different chemicals can be generated from glycerol at low temperatures and rates (Cherubini, 2010). The most common chemicals are, 1, 3-propanediol, D-lactic, succinic, and propionic acid, ethanol and poly-3-hydroxybutyrate. 1,3- propanediol can be obtained via a biological process in the presence of bacterial strains such as Klebsiella-pneumoniae (Posada *et al*., 2012). It is also possible to synthesize 2-3 butanediol from glycerol through a fermentative pathway. This product serves as a raw material for the production of bioplastics as well solutions (Almeida *et al*., 2012).

Anaerobic digestion is another type of biochemical conversion of glycerol that is used to transform glycerol into biogas (Romano and Zhang, 2008). It uses bacteria at low temperatures between 303 and 338K in the absence of oxygen (Cherubini, 2010).

2.4.2.3 Thermochemical conversion of glycerol

Like coal and biomass, glycerol can also undergo thermochemical conversion processes for the synthesis of fuels and chemicals. Direct combustion, partial oxidation, pyrolysis and reforming are the main thermochemical conversion routes of glycerol (Earis, 2007). Combustion is a process whereby glycerol undergoes complete oxidation to produce heat as a final product. The conversion of glycerol via a complete combustion route is not feasible as it emits CO_2 into the atmosphere causing global warming (Kaur *et al.*, 2020). Pyrolysis is a process whereby glycerol is transformed into products like gas and liquids without using oxygen. Whereas reforming uses a reforming agent such as H_2O, O_2, and CO_2 to transform

glycerol into syngas. Both gasification and reforming processes work on the same principles and therefore lead to the same products. The only difference is that gasification refers to the conversion of solid feedstock such as wood, whereas reforming refers to the transformation of liquid and gaseous feedstock such as methane and glycerol into syngas.

2.4.2.3.1 Reforming processes

Reforming is a chemical process where glycerol is subjected to high temperatures (823K-1623K) to generate synthesis gas (H_2, CO, H_2O, CO_2, CH_4) (Kelloway and Daoutidis, 2014). This process is divided into two parts namely catalytic and non-catalytic reforming. Temperatures around 1573 K are required for non-catalytic reforming whereas catalytic reforming requires temperatures below less than 1573 K (Naik *et al.*, 2010).

Certain reforming pathways (e.g. partial oxidation, dry reforming, and steam reforming) consist of four stages which are drying, pyrolysis, oxidation, and reduction. During the drying stage, the moisture present in glycerol is transformed into steam at a temperature range of 373-473K (Ferreira *et al.*, 2019). At this stage, glycerol is not yet decomposed because no chemical reaction has taken place already. During the stage of pyrolysis, the dry glycerol is now devolatilized at a temperature range of 423-973 K (complete absence of O_2). During this stage, volatile components are released as well as ash and char. During the oxidation stage, hydrogen and carbon are oxidized to form H_2O and CO_2. During the reduction stage, various reactions (endothermic) take place at high temperatures roughly 1073-1273 K generating H_2, CO, and CH_4 from H_2O, CO_2 and char respectively (Puig-Arnavat *et al.*, 2010). Some of the chemical reactions that occur during reforming processes are summarized in Equations 2.i-2.v, but other reactions can be found in (Ptasinski, 2015*)*.

Incomplete combustion: $C + 0.5O_2 \leftrightarrow CO$ 2.i

Water gas reaction: $C + CO_2 \leftrightarrow CO + H_2$ 2.ii

Boudouard reaction: $C + CO_2 \leftrightarrow 2CO$ 2.iii

Water-gas-shift: $CO + H_2O \leftrightarrow CO_2 + H_2$ 2.iv

Steam reforming: $CH_4 + H_2O \leftrightarrow CO + 3H_2$ 2.v

Partial combustion, Boudouard, and water-gas-shift reactions are considered as the most important reactions and lead to a high quantity of CO and H_2 (main syngas constituent) (*ibid)*. Parameters like reforming agents, pressure, and temperature affect the quality of syngas

produced from glycerol reforming process (Ferreira *et al.*, 2019). Different glycerol reforming processes are explained below.

Reforming of glycerol using H_2O

Steam (H_2O) can be used to transform glycerol into syngas and the process is known as glycerol steam reforming (GSR) (Charisiou *et al.*, 2020), (Adhikari *et al.*, 2007). There are two main reactions that take place during GSR, namely glycerol decomposition (2.2i), as well as water-gas shift reaction (2.2ii), and 2.2iii represents the overall GSR (Roslan *et al.*, 2020).

$$C_3H_8O_3 \leftrightarrow 3CO + 4H_2 \quad \text{2.2i}$$

$$CO + H_2O \leftrightarrow CO_2 + H_2 \quad \text{2.2ii}$$

$$C_3H_8O_3 + 3\,H_2O \leftrightarrow 3\,CO_2 + 7H_2 \quad \text{2.2iii}$$

GSR requires high temperatures for the production of syngas as at low temperatures significant amount of H_2O, CH_4, and CO_2 can be generated. GSR is an endothermic process that requires energy (Schwengber *et al.*, 2016). Besides reactions 2.2i-2.2iii, there are other side reactions that take place during GSR such as methanation and Boudouard reactions (Roslan *et al.*, 2020). Various conditions such as temperature, pressure, and steam to glycerol ratios (SGRs) affect this process and can lead to the deposition of carbon. Adhikari *et al*. (2007) applied the minimization of Gibbs energy to model the transformation of glycerol into H_2 and CO by using H_2O as a reforming agent. It was revealed that increasing the temperature and SGR produced a high yield of H_2 while the production of CO is minimized. For example, at a temperature, pressure, and SGR of 1000 K, 1 atm, and 9:1 respectively, roughly 6 moles of H_2 were produced. While at the same condition, roughly 1 mole of CO was generated. Freitas and Guirardello (2014) also performed a thermodynamic analysis of glycerol (using the minimization of Gibbs energy approach). Results revealed that a temperature of 1073.15K, and an SGR of 3:1 glycerol produced a syngas ratio (H_2:CO) of 2.34 (61.9% H_2 and 26.5% CO).

Silva *et al*. (2015) point out that, carbon deposition deactivates the catalyst used in GSR and thus lowers syngas yield and suggest that high steam to glycerol ratios (SGRs) must be used to prevent it. Various heterogeneous catalysts can be used in GSR such as nickel, platinum, and cobalt-based catalysts (Silva *et al*., 2015). A thermodynamic analysis using the minimization Gibbs free energy approach of GSR was performed for hydrogen production (Ismaila *et al.*, 2021). It was revealed that, a temperature range of 900K-1050K and an SGR of 10:1 were

optimal for the GSR process where an insignificant amount of coke was formed at a pressure of 1 atm.

Glycerol can also undergo a catalytic aqueous-phase reforming (APR) so that it can be transformed into synthetic gas. During this reaction, water is heated by increasing the operating conditions such as pressure (around 3000 kPa) and temperature (270 °C). During the aqueous-phase reforming process, hydrocarbons that have been oxygenated are now converted into hydrogen (H_2), carbon dioxide, water, and alkene (C_nH_{2n}). Equation 2.2iv depicts the entire reaction of an APR process of glycerol for the generation of hydrogen (Seadira *et al*., 2018).

$$C_3H_8O_3 + xH_2O \rightarrow (2x + 1)H_2 + xCO_2 \qquad 2.2\ iv$$

When water is heated up to its critical temperature (374 °C) and then compressed at a pressure of 22100 kPa so that glycerol can be converted into H_2, this process is known as supercritical water reforming (Fan *et al*., 2010).

Reforming of glycerol using O_2/air

Glycerol can also produce syngas by using O_2/air and this process is commonly known as glycerol partial oxidation (GPO). During this process, a sub-stoichiometric number of oxygen is required to avoid the complete combustion of glycerol (Polychronopoulou *et al.*, 2018). This process is exothermic and thus does not require energy and thus no extra heat needed to drive the process once it has started (Roslan *et al.*, 2020). The GPO overall reaction is summarized by equation 2.3

$$C_3H_8O_3 + 1.5O_2 \rightarrow 4H_2 + 3CO_2 \qquad 2.3$$

Various studies have been carried on GPO. Wang (2010) used the minimization of Gibbs energy to study the thermodynamic analysis of GPO for the synthesis of hydrogen. The optimal conditions for hydrogen synthesis such as reaction temperatures (727-827 °C) and oxygen to glycerol ratios (OGRs) (0.4-0.6) were identified. At these conditions, glycerol was completely converted while the yield H_2 was 78.93% at an OGR of 0.4 and 87.31% at a ratio of 0.6

Reforming of glycerol using CO_2

Glycerol can also react with carbon dioxide to produce syngas and this process is known as glycerol dry reforming (GDR) (Roslan *et al.*, 2020). This process is summarized by equation 2.4

$$C_3H_8O_3 + CO_2 \rightarrow 4H_2 + 3CO_2 + H_2O \qquad 2.4$$

Using CO_2 to convert glycerol into syngas can be advantageous since CO_2 is a greenhouse gas (Garcia *et al.*, 2001). Catalysts such as Ni, Rh, Re, and Pt which are supported on different oxides like CeO_2, Al_2O_3, CaO, and SiO_2 can be used in GDR (Siew *et al.*, 2014), (Arif *et al.*, 2019). Several thermodynamic studies have been carried out to study GDR. Wang *et al*. (2009) revealed that the optimal conditions to produce H_2 and CO from GDR are: $CO_2/C_3H_8O_3$ (CGR) ratio must be in a range of 0-1 and temperature higher than 975K. At these conditions, the H_2/CO was found to be 1. Freitas and Guirardello (2014) studied the GDR process using the minimization of Gibbs Energy at different temperatures, constant $CO_2/C_3H_8O_3$ ratio (3:1) and at a pressure of 1 bar. It was revealed that higher composition of CO than H_2 was generated at temperatures above 973 K and the syngas ratio was close to 1. For example, a temperature of 800K produced a syngas ratio of 1.17 (29% H_2 and 24.7% CO). While at 973K, 43.7% and 32.1 % of CO and H_2 was generated respectively.

Reforming of glycerol using a combination of reforming agents

Instead of using H_2O, O_2, and CO_2 as glycerol reforming agents, one can also use a combination of H_2O with O_2, H_2O with CO_2 as well as O_2 with CO_2 to transform $C_3H_8O_3$ into syngas. A process whereby a mixture of H_2O and O_2 is used as a reforming agent to convert glycerol into syngas is commonly known as auto-thermal reforming (GAUR) (Liu *et al*., 2013). This process offers several advantages such as no additional heat needed to drive the reaction because it supplies itself the heat (Schwengber *et al.*, 2016). In other words, GSR consumes all the heat released by GPO (Liu and Lawal, 2015). The overall process of GAUR is summarized by equation 2.5 (Liu *et al*., 2013).

$$C_3H_8O_3 + H_2O + O_2 \rightarrow H_2 + CO + 2CO_2 \qquad 2.6$$

Even though GAUR presents several advantages, it generates a syngas ratio less than GSR. Freitas and Guirardello (2014), performed a thermodynamic analysis of glycerol. Results showed that at a temperature of 1073.15K, GSR and GAUR generated a syngas ratio of 2.34 and 1.84 respectively.

A mixture of O_2 and CO_2 can also be used to convert glycerol into syngas. This process is known as glycerol dry auto-thermal reforming (GPO + GDR)(Kale and Kulkarni, 2010). Wang *et al.* (2017) studied the dry autothermal reforming of glycerol using different conditions such as $CO_2/C_3H_8O_3$ and $O_2/C_3H_8O_3$ and temperature range of 850K-900K based on minimization of Gibbs energy. It was revealed that thermoneutral conditions were reached at an $O_2/C_3H_8O_3$ ratio of 0.15. Kale and Kulkarni (2010) conducted a thermodynamic analysis of $C_3H_8O_3$ via dry auto-thermal reforming at a temperature range of 600K-1000K, O_2/C ratio from 0.1 to 0.5 and CO_2/C ratio from 1 to 5 at a pressure of 1 bar. The results revealed that high O_2/C and CO_2/C ratios generated a syngas ratio of 1 with an insignificant amount of solid carbon and CH_4. It was further revealed that carbon formation was higher in GDR than GPO.

Lastly, glycerol can be converted into syngas by combining H_2O with CO_2 (GSR+GDR). There is no paper found in the literature evaluating either the thermodynamic behaviour or experimental approach of glycerol using a combination of H_2O and CO_2. However, Jabbour (2020) performed a thermodynamic study (using minimization of Gibbs energy) at different conditions such as temperature (473-1273), pressure (1-20 bar), and feed ratio to convert CH_4 into syngas using a combination of CO_2 and H_2O. It was found that running this process at a temperature higher than 1073K with $\frac{CO_2+H_2O}{CH_4}$ ratio of around 1 and a pressure of 1 bar were feasible and minimized the formation of coke. Bio-oil reforming using a combination of CO_2 and H_2O for H_2 and CO production was evaluated by (Xie *et al.*, 2020). It was found that, during this process, increasing the amount of H_2O increased the total amount of H_2 as well as CO as well as the temperature, whereas increasing the amount of CO_2 decreased the temperature as well as the amount of H_2 and CO.

Co-reforming of glycerol with linear low-density polyethylene (LLDPE) plastic wastes

Even though glycerol reforming using different reforming agents has gained academic interest in recent years, there are no published works on the co-reforming of glycerol with LLDPE. Plastic waste has become another environmental threat in recent years due to its non-biodegradable nature. It is also important to target syngas composition using a mixture of glycerol and LLDPE via different reforming routes as indicated in previous sections. Instead of co-reforming glycerol with LLDPE, it is also possible to co-reform with CH_4. Based on its stoichiometry, it was shown that glycerol reforming processes generate a significant amount of CO_2. For example, 1 kmol of glycerol produces 3 kmol of CO_2 via GSR process. Co-reforming glycerol with CH_4 can be an advantage as this later will continuously react with the generated

CO_2 (Huang et al. (2018). Equation 2.7 shows the overall process of co-feeding glycerol with methane in the presence of H_2O as a reforming agent.

$$C_3H_8O_3 + 3CH_4 + 3H_2O \rightarrow 13H_2 + 6CO \qquad 2.7$$

It can be seen that 1 kmol of glycerol can be co-fed with 3 kmol of methane to produce 13 kmol of H_2 and 6 kmol of CO using 3 kmol of steam. This shows that introducing CH_4 in GSR can increase the syngas ratio (H_2: CO) up to 2.17.

2.4.2.3.2 Pyrolysis of glycerol

Pyrolysis is a process where any temperature ranging from 300℃ to 600℃ is employed to transform glycerol/biomass into syngas and liquids products such as bio-oil without using any reforming agent. The main objective of pyrolysis is to recover biofuels with a medium-low calorific value (Naik *et al.*, 2010). However, gasification is preferred over pyrolysis because downstream processing of bio-oil generated from biomass via pyrolysis is not an easy task (Puig-Arnavat *et al*., 2010). Valliyappan *et al*. (2008) studied glycerol pyrolysis for syngas production using a temperature range of 923 -1073 K and 1 atm. Results showed that the composition of H_2 increases with an increase in temperature and decrease in CO composition. For example, at 923K, this process produced 17% H_2 and 54% CO. While at 1073K, 48.6% H_2 and 44.9% CO were generated.

2.4.3 Applications of glycerol-derived syngas in downstream processes

It was shown that syngas (H_2 and CO) can be generated from glycerol via different reforming routes as well as pyrolysis. The ratio of these two compounds is very critical during the synthesis of various products like FT, DME, and methanol. Other parameters such as temperature, pressure, and catalysts are also important during the transformation of CO and H_2 into these different products (Spath and Dayton, 2003). Figure 2.8 gives a summary of the different uses of syngas.

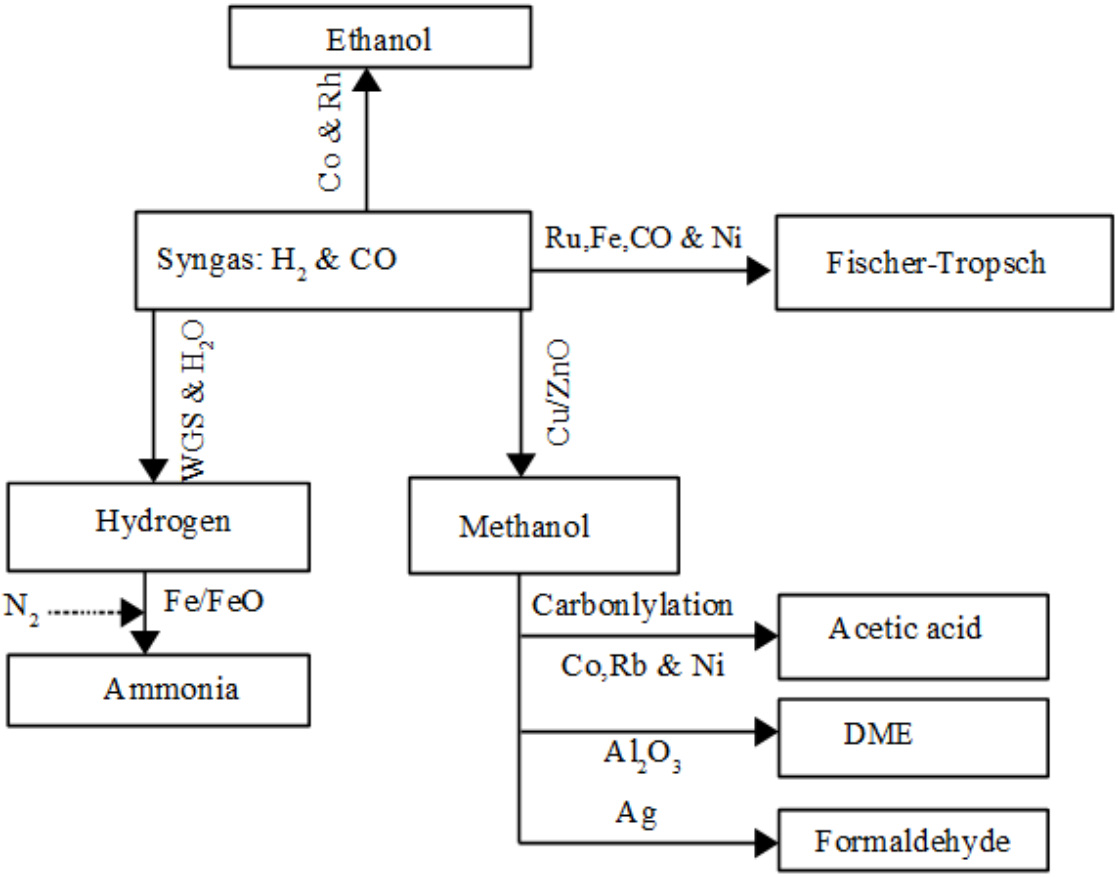

Figure 2. 8: Different uses of syngas, extracted from (dos Santos and Alencar, 2020)

- *Synthesis of methanol from syngas*

Methanol can be synthesized by reacting carbon monoxide with hydrogen and steam using different catalysts such as Cu-Zn oxides with a small amount of carbon dioxide (Ciferno and Marano, 2002). A temperature and pressure of 260°C and 70 bars respectively are required during this synthesis (Paisley and Anson, 1997). Two reactions occur during the synthesis of methanol, viz. WGS and hydrogenation of carbon dioxide reactions (Equation 2.8 and 2.9).

$$CO + H_2O \rightarrow H_2 + CO_2 \qquad \Delta H_r = -49.67 \frac{kJ}{mol} \qquad 2.8$$

$$CO_2 + H_2 \rightarrow CH_3OH + H_2O \qquad \Delta Hr = 41.47\ kJ/mol \qquad 2.9$$

Equation 2.8 and 2.9 can be combined to generate equation 2.10

$$CO + 2H_2 \rightarrow CH_3OH \qquad \Delta Hr = -90.64\ kJ/mol \qquad 2.10$$

During the production of methanol from syngas, the ratio of H_2 and CO must not be lower than 2. In order to synthesize methanol, carbon dioxide and carbon monoxide ratio should be around

0.6 to keep the catalyst activated (Ciferno and Marano, 2002). Tsubaki *et al*. (2001) point out that, the maximum conversion of CO during the synthesis of methanol from syngas is 50%.

- *Synthetic FT fuels from syngas*

The syngas gas produced during reforming process can be used to produce synthetic FT fuels such as paraffins and olefins. Equation 2.10 shows the production of paraffins whereas equation 2.11 shows the production of olefins (Kelloway and Daoutidis, 2014).

$$CO + (2n + 1)H_2 \rightarrow C_nH_{2n+2} + H_2O \qquad 2.10$$

$$CO + 2nH_2 \rightarrow C_nH_{2n} + nH_2O \qquad 2.11$$

The hydrogenation of CO during the synthesis of Fischer-Tropsch (FT) fuels synthesis is a catalytic process. Metals such as Ru, Fe, Co are used in FT fuels synthesis as catalysts for commercial applications (dos Santos and Alencar, 2020). The synthesis of FT requires a low temperature range (473-513K) or a high temperature range (573-623K) depending on the types of products needed. Low temperature favours the production of waxes with high molecular weight whereas high temperature range is recommended for the synthesis of gasoline as well as olefins with low molecular weight. Co (used for low temperature range) and Fe (high temperature range) are the two main catalysts used during the synthesis of FT (Spath and Dayton, 2003). A water gas shift reaction (WGS) occurs when Fe is used as the catalyst. The synthesis of FT requires a syngas ratio of 2.15 when Co catalysts is used but this ratio is decreased down to 1.7 when Fe is used as a catalyst due to WGS. A pressure range of 1000-40000 kPa is needed during the synthesis of FT from H_2 and CO (ibid). CH_4 is not a desired product during the synthesis of FT, hence it should be minimized. When Co catalysts are used, the selectivity of CH_4 decreases with an increase in CO conversion (Yang *et al*., 2014). For example, the CO conversion of 0.91 decreases the CH_4 selectivity from 0.118 to 0.091 by using Co catalysts (Ma *et al*., 2020).

- *Mixed alcohols from syngas*

It is also possible to use H_2 and CO as feedstocks for the synthesis of mixed alcohols (Forzatti *et al*., 1991). The overall process is summarized by equation 2.12

$$nCO + 2nH_2 \rightarrow C_nH_{2n+1} + (n-1)H_2O \qquad 2.12$$

where n = $\{1,2,3,4,5,6,7,8\}$

The catalysts used for the synthesis of mixed alcohols are grouped in 4 classes namely modified high pressure methanol synthesis catalysts: alkali-doped ZnO/Cr_2O_3 (temperature range: 573-698 K, pressure range: $12.5\times10^3 - 30\times10^3$ kPa and CO conversion range: 5-20%), modified low pressure methanol synthesis catalysts: Cu/ZnO and $Cu/ZnO/Al_2O_3$ (temperature range: 548-583K and pressure range of 5000-10000 kPa),modified Fischer-Tropsch catalysts: alkali-doped $CuO/CoO/Al_2O_3$ (temperature range: 533-613K, pressure range:6×10^3- 20×10^3 kPa, CO conversion range 5-30%) as well as alkali-doped catalysts such as MoS_2.

- *DME from syngas*

It is also possible to produce DME (dimethyl-ether) from syngas. The synthesis of DME can be done via two pathways commonly known as direct and indirect pathway. Equations 2.12 and 2.13 give a summary of indirect and direct pathways respectively.

$$4H_2 + 2CO \rightarrow C_2H_6O + H_2O \qquad 2.12$$

$$3H_2 + 3CO \rightarrow C_2H_6O + CO_2 \qquad 2.13$$

The indirect pathway is a two-step process whereby methanol is produced first from syngas and then undergoes a dehydration process to generate DME while in the direct pathway DME is directly generated from syngas. This makes the direct pathway to be more favourable over the indirect method from a thermodynamic and economical point of view (Dadgar *et al.*, 2016). The pressure and temperature range for the synthesis of DME $1\times10^3 - 20\times10^3$ kPa and 523-573K in the presence of γ- Al_2O_3, zeolites and silica-modified alumina as catalysts (Peinado *et al.*, 2020). Syngas ratio is another crucial parameter during the synthesis of DME. Equation 2.12 shows that a minimum syngas ratio of 1 is required in the synthesis of DME via indirect pathway while a ratio of 2 is needed via the direct pathway.

Table 2.3 gives a summary of syngas properties for the synthesis of various chemicals as well as fuels.

Table 2. 3: Properties of syngas for the synthesis of various products, extracted from, (Ciferno and Marano, 2002)

Products	Synthetic fuels	Methanol	H_2	Fuel gas	
	FT gasoline & Diesel			Boiler	Turbine
H_2:CO	0.6 [a]	~2.0	High	Unimportant	Not necessary
CO_2	Low	Low [c]	Not important [b]	Not critical	Not important
Hydrocarbons	Low[d]	Low [d]	Low [d]	High	High
Nitrogen	Low	Low	Low	Note e	Note [g]
H_2O	Low	Low	High [f]	Low	Note [g]
Contaminants	<1 ppm sulfur, Low particulates	<1 ppm sulfur, Low particulates	<1 ppm sulfur, low particulates	Note [k]	Low particulates and metals
Heating value	Unimportant [h]	Unimportant [h]	Not important [h]	High [i]	High [i]
Pressure, bar	~20-30	~50 (liquid phase) ~140 (vapor phase)	~28	Low	~400
Temperature, ℃	200-300 [j] 300-400	100-200	100-200	250	500-600

[a] it depends on a type of the catalyst, 0.6 is satisfactory when Fe catalyst is used but when Co is used as a catalyst a ratio of around 2.0 should be used

[b] a WGS reaction is necessary for the conversion of CO to H_2. The CO_2 present in the syngas is removed simultaneously with the CO_2 formed during the water gas shift reaction

[c] traces of CO_2 are tolerated when the ratio of H_2 and CO is greater than 2.0 and CO_2 can be converted into methanol provided there is enough H_2

[d] heavier hydrocarbons as well as methane should be recycled and converted into syngas

[e] nitrogen reduces the HV. Its level is not necessary if the syngas can be burnt with a stable flame

[f] during WGSR, water is needed

[g] water high levels can be tolerated if steam is added to adjust the combustion temperature

[h] if the ratio of H_2 and CO is achieved as well as impurities levels, the heating value is not an issue

[i] there is an improvement in efficiency as HV increases

[j] catalyst dependent. Fe catalyst operates at elevated temperatures than Co catalyst.

[k] insignificant quantities of impurities can be tolerated

2.4.4 Design of a glycerol - integrated biorefinery

Before explaining how a design and synthesis of a biorefinery may be performed, it is imperative to discuss what is meant by an integrated biorefinery. An integrated biorefinery is a type of biorefinery whereby various transformation pathways are integrated (e.g. feedstock handling, pre-treatment, gasification, pyrolysis, combustion, fermentation, and anaerobic digestion) to produce multiple products (Goh and Ng, 2015).

Biorefineries are always designed to meet some crucial objectives such as ensuring energy security in industrialized countries where biomass is being produced on a large scale (Martinez-Hernandez *et al*., 2013). The next objective is to minimize or reduce some environmental impacts, which could be associated with the generation of biomass-based chemicals. This emphasizes that there should be less waste produced and less greenhouse gases emitted into the environment**.** The other objective is to develop rural areas and also to increase the life quality of societies that are involved in the supply chain of biomass-derived products (Cherubini and Ulgiati, 2010)**.**

Ng *et al*. (2009) point out that, the design and synthesis of integrated-biorefineries is a challenging and complex task than petrochemical refineries. This is due to the fact that different properties such as thermodynamic properties (such as Gibbs energy, enthalpy as well as entropy) of biorefinery feedstock are not established. But also, biorefinery feedstock presents different structures as well as compositions (Ng, 2010). Therefore, various methods that are used to design petrochemical refineries are not directly applied in biorefineries (Ibid). Siirola (1996) divides different methods used in chemical design into four main phases which are targeting, conceptual, refined, and final phase. Taking into consideration the scope of this study, only the two first phases are discussed.

2.4.4.1 Targeting Phase

Fundamentally, targets of a chemical process describe its theoretical limits of performance. Targeting plays a crucial role in designing a given chemical process as it allows the designer to evaluate the quality and performance (benchmark) of the process before carrying out a detailed design (El-Halwagi, 2012). Patel (2007) discusses three important targets used in the design of a chemical process. These three targets are mass balance, energy balance, and entropy. Using a mass balance as a target, one can determine the exact minimum amount of

input required to produce a specific product and the amount of waste that can be generated from the process. One can also perform an overall energy balance across the entire process in order to determine the energy flows in and out of the process. Patel *et al.* (2007) point out that, one does not need to know the structure or a process flowsheet in order to set these targets. This makes a target an important tool in process design.

2.4.4.2 Conceptual design phase

A conceptual design of a particular biorefinery is a phase whereby the assumption of new challenges have been made such as the wide range of raw materials and the development of local or even regional areas (Aristizábal-Marulanda and Cardona Alzate, 2019).

The conceptual design phase consists of four phases which are problem formulation, synthesis, analysis, and evaluation (Siirola, 1996). During the problem formulation phase, a process designer defines the characteristics of the problem such as objective function, feedstocks that have to be transformed as well as products (Bertran *et al.*, 2016).

Once the problem has been identified and defined, the next stage is the synthesis of a process. Process synthesis (generation of multiple alternatives) is a stage whereby the flowsheet structure of a chemical process is developed and this should satisfy various objectives of the process (Patel, 2007). At this point, only process input (raw materials) and outputs (products) are known, the flowsheet structure is not yet known. A process synthesis is summarized in figure 2.9

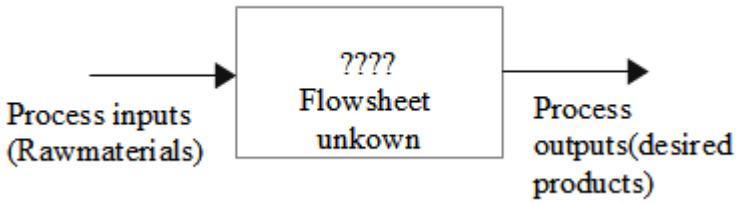

Figure 2. 9: Representation of a process synthesis (El-Halwagi, 2012)

The stage whereby each generated alternative from the synthesis phase is analyzed is known as the process analysis (Carno-Ruiz and McRae, 1998). During this stage, various streams (e.g. flow rates, composition, temperature, and pressure) that characterize the process are estimated using several analysis techniques (El-Halwagi, 2012). These analysis techniques include mathematical programming, empirical correlations, and computer-aided simulations such as Aspen Plus (Patel, 2007). At this stage, one seeks to know the outputs since the inputs and flowsheet are known as indicated in figure 4.10

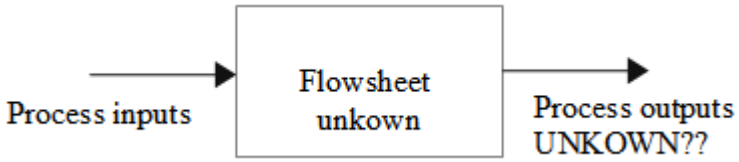

Figure 2. 10: Representation of a process analysis

Lastly, once all alternatives have been analyzed it is now imperative to evaluate one by one depending on the objective of the identified and formulated problem. At this stage, if the solution is satisfactory, then the conceptual design is complete. In the case where the solution is not satisfactory, the process designer will have to generate a new alternative, analyze and evaluate it. This makes the entire conceptual design phase an iterative task (Carno-Ruiz and McRae, 1998).

It must be noted that the process synthesis is the cornerstone of a biorefinery conceptual design (Goh and Ng, 2015). This is due to the fact that it provides all the information required to identify the different types of main equipment (such as reactors, separators, heat exchangers), design operating conditions, flow rates, and also it shows how different unit operations are interconnected in order to come up with a comprehensive flowsheet (Yuan *et al*., 2013).

The classic biorefinery synthesis problem is based on the following statement: given a set of biomass resources and a set of multiple products, a systematic approach is needed in order to select products that have a high yield and also to select the most sustainable processing method with high energy efficiency (Ibid).

Given that, various conversion technologies take place in an integrated biorefinery to convert glycerol into products, it is imperative to use some systematic approaches to screen and design this type of biorefinery. Process systems engineering (PSE) is considered as the most important tool that can be used to screen and design a particular integrated biorefinery. This is due to the fact that using a PSE, all these alternative conversion routes and technologies that take place in an integrated biorefinery are compared and evaluated at the same time. For example, gasification, pyrolysis, fermentation, and anaerobic digestion can be compared and evaluated simultaneously during the production of various products from glycerol which makes the whole glycerol integrated biorefinery a complex task.

Tay *et al*. (2011) point out that, process systems engineering (PSE) play a crucial role during the synthesis and design of an integrated biorefinery as these tools aid in minimizing the consumption of feedstock as well as the consumption of energy. Kokossis and Yang (2010)

and Dimian (2007) also show the main advantages of incorporating these PSE tools in the design and synthesis of an integrated biorefinery. Stephanopoulos and Reklaitis (2011) point out that, these process systems engineering approaches deploy systematic computer-aided tools to design, control and optimize various processes.

Process design and synthesis approaches are subdivided into three categories. These categories are heuristics-based approach (hierarchical decomposition approach), insights-based approach, and superstructure-based optimization approach or mathematical programming approach (Li *et al*., 2020). An explanation of these different synthesis approaches is given in the following sections.

2.4.4.2.1 Hierarchical approach in synthesis design

Hierarchical decomposition approach consists of decomposing a large and complex design problem into small multiple problems which can be easily tackled (ibid). The synthesis flowsheet problem of a chemical process can be decomposed into six hierarchical levels (Douglas, 1985). These levels have been adapted and modified by Goh and Ng (2015) to accommodate integrated biorefineries. These adapted and modified hierarchical levels are explained below.

Level-1: the operation mode is selected as either continuous, batch, or semi-batch process but also all information regarding the input is listed such as desired product as well as reaction data. Level-2, at this level, the raw material/biomass is characterized and standardized. Level-3: the input-output structure of the entire flowsheet is considered. The type of raw materials that is fed into the process should be known as well as the type of main products but also the type of any by-products. Level 4, the recycle structure of the flowsheet is considered, at this level it is imperative to know if there will be any recycle stream or not. Level 5, at this level the separation system is synthesized so that vapour and liquid can be recovered. Level 6 deals with mass and energy integration.

To apply hierarchical approaches in the synthesis of a chemical process, the designer should have some experience in order to come up with a good design. It implies that these approaches may not be applied when considering new chemical processes. Due to the sequential nature of these approaches, sometimes an optimal solution is achieved (Ng *et al*., 2017).

2.4.4.2.2 Mathematical programming and optimization

The second approach is mathematical programming and optimization. El-Halwagi (2012) defines optimization as a process that seeks to identify the best solution among various solutions. An optimization problem deals with the minimization or maximization of an objective function. An objective function during the optimization of an integrated biorefinery is to maximize the economic potential and minimize the emission of dangerous GHGs into the atmosphere or the use of raw material resources. An optimization problem with one objective function is called a single-optimization problem while a multi-optimization problem considers various objectives (Sadhukhan *et al*., 2014). Any optimization problem where the objective function and constraints are linear is commonly known as a linear program (LP) and if neither the objective function nor the constraints are linear it is called non-linear programming (NLP). If all the variables in the model are integers the optimization is called integer programming (IP). Mixed-integer programming (MIP) is a type of optimization that contains real variables (e.g., flow rates, temperature, and pressure) and also integer variables. If the objective function and the constraints are linear the MIP becomes MILP and it is called MINLP (constraints and objective function are non-linear) (El-Halwagi, 2012). Tey et al. (2021) point out that, when optimizing an integrated biorefinery, three parameters should be kept in mind, viz. economic, environmental, and social. Mathematical programming is a useful approach as it helps the designer to consider all alternatives simultaneously. Even though this approach is useful, it presents some limitations such as (Patel, 2007):

- Sometimes the process designer can end up formulating a complex and non-linear mathematical problem. Therefore, the optimum solution to this problem is not guaranteed.
- The input of the process designer is not taken into consideration when using this approach.

Mathematical programming approaches have been widely used to design and synthesize integrated biorefineries. Kong and Shah (2016) used a MILP model for the synthesis of biorefinery to produce chemicals from D-limonene, and itanic acid. This optimization model was based on the economic potential as the objective function. Martin and Grossmann (2014) developed an MINLP optimization model for simultaneous production of hydrogen and liquid fuel using glycerol as a raw material. The objective function was to maximize the production of liquid fuel production and H_2 by minimizing the energy input.

A superstructure network seeks to find feasible alternative pathways during the synthesis of a chemical process (Li *et al.*, 2020). A simple superstructure network is shown in figure 2.11. This figure can be explained as follows: Feedstock F undergoes 3 processing stages before product P can be generated. These processing stages include different unit operations such as mixers, reactors, separators, and distillation columns. For example, feedstock F-1 can either be processed alone or can be mixed with feedstock-F2 to generate product P-1. Product P-2 is generated by either processing feedstock F-2 alone or mixing it with feedstock F-1. Arrows indicate different streams.

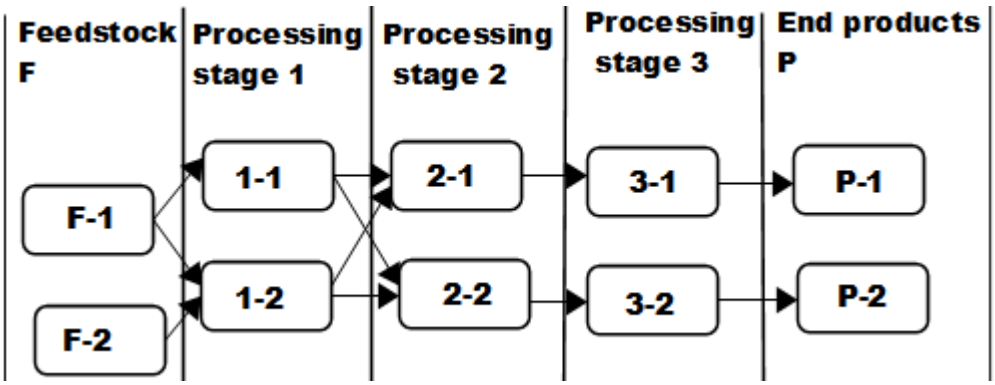

Figure 2. 11: Representation of a simple superstructure *network, extracted from (ibid)*

Loureiro da Costa Lira Gargalo *et al*. (2017) developed a superstructure network to generate 7 products (polyhydroxybutyrate, lactic, and succinic acid, 1, 3 and 1, 2-propane diol, acrolein, and epichlohydrin) from glycerol. The developed network consisted of 5 stages viz. taking glycerol from biodiesel production plants to the glycerol processing site, removing different impurities from glycerol, transforming glycerol into products, separating, and purifying these products from impurities and finally supplying the end products to different markets. The objective of this network was the maximization of the net present value (NPV). Zondervan *et al*. (2011) also developed a superstructure network model which consisted of 7 processing stages to optimize an integrated biorefinery for the production of various chemicals such as ethanol, succinic acid, and butanol from two types of feedstocks (biomass and crude-oil). This superstructure model resulted in a MINLP problem. The objective function was to maximize the profit, minimizing the generation of waste, and minimize fixed costs.

2.4.4.2.3 Approaches based on insights

The third approach is the insights-based approach: Some of the insights-based approaches are the automated targeting approach, the P-graph approach, and the carbon-hydrogen-oxygen ternary diagram approach (Tey *et al.*, 2020). These insights-based approaches are very useful as they reveal important information such as the performance of the entire process ahead of a detailed design by means of a graphical representation. Inaccuracy is seen as one of the main disadvantages of these approaches.

Yi *et al*. (2020) describe a P-graph as a type of a bipartite graph consisting of two main vertices which are material vertex (such as material balance, intermediate product) which is represented by a dot, and an operating unit vertex which is represented by a rectangular bar. Atkins *et al*. (2016) applied a P-graph approach to study the economic feasibility of five wood processing residues viz. pulp logs, wood chips, sawdust, landing, and cutover residues. Different products were taken into consideration based on gasification, pyrolysis, and fermentation as processing routes. Among these products, only six were found to be economically viable and profitable.

2.4.5 Significance of CHO ternary systems in the synthesis of a glycerol-based biorefinery

Carbon-hydrogen-oxygen or simply CHO ternary systems play a significant role in various fields such as combustion, gasification, reforming, and torrefaction processes as well as fuel cells (Cairns and Tevebaugh, 1964). A triangle is used to plot these ternary diagrams whereby each vertex represents pure carbon, hydrogen, and oxygen (100 percent concentration). The points inside the triangle represent the ternary mixtures of the three elements (Basu, 2013). Any chemical substance that consists of CHO can be plotted on these ternary diagrams.

Cairns and Tevebaugh (1964) calculated the gas phase compositions of different species present in equilibrium with carbon at a temperature range of 25- 1227°C and a fixed pressure of 1atm and a H/O ratio from 0.026 to 4.5. These authors found that the only chemical species present at equilibrium are H_2, CO, CH_4, CO_2, H_2O and C(s). The compositions of these different species were converted into C:H:O ratios and plotted on the CHO ternary diagrams in order to determine the carbon deposition boundaries at different temperatures. The carbon deposition boundary was decreasing with an increase in temperature. For example, at 298K, the carbon deposition was a curve but at a temperature of 1050K, it became a straight line. At high temperatures, the most stable species are carbon monoxide and hydrogen whereas at low

temperatures methane, water, and carbon dioxide are the most stable species (Tevebaugh and Cairns, 1965).

Muramoto *et al*. (2017) investigated the compositions of fuel gas used in the solid oxide fuel cells (SOFCs) through thermochemical equilibrium calculations at pressures up to 30 bars and temperatures up to 1000°C. Because most conventional fuel gas that contains hydrogen consists of carbon, hydrogen, and oxygen, CHO ternary diagrams were used to study the carbon deposition regions within the diagrams at different pressures and temperatures. The results revealed that the carbon deposition region shrinks in the area rich in hydrogen and it enlarges in the area rich in oxygen with an increase in total pressure. The minimum amount of different oxidising agents (steam, oxygen, and carbon dioxide) required to prevent the deposition of carbon was calculated at the highest pressure (30 bars).

Prins *et al.* (2006) applied these CHO ternary diagrams so that the efficiency of wood gasification and torrefaction can be analyzed whereas Ptasinski *et al*. (2007) used these diagrams in order to compare the gasification process of various biofuels and coal.
Tay *et al*. (2011) used these CHO ternary diagrams to produce methanol from biomass. During this synthesis, it was revealed that 1 ton of biomass can be co-gasified with methane in presence of H_2O to generate a syngas that meets methanol synthesis requirement (H_2:CO). Litheko (2017) used also these ternary diagrams in conjunction with the atomic balance to synthesize DME from 1 ton of biomass. Results revealed that, in order to produce DME (H_2: CO =1) via a direct pathway from biomass, a combination of H_2O/CO_2 or H_2O/O_2 should be used as a gasifying agent. The author used the lever-rule to determine the minimum amount of these gasifying agents needed to convert 1 ton of biomass to generate a syngas from which DME is produced.

2.4.6 Modelling of a glycerol reforming process

Reforming models are required to determine not only the composition of syngas but also other different species present at equilibrium as well. Puig-Arnavat *et al*. (2010) point out that reforming models can be grouped into four types namely kinetic, thermodynamic equilibrium, Aspen Plus as well as neural network models. Only the thermodynamic equilibrium model is discussed here, but the explanations of other models can be found in (Puig-Arnavat *et al*., 2010),(Puig-Arnavat *et al.*, 2013), (Nikoo and Mahinpey, 2008), (Baruah *et al*,. 2014).

The thermodynamic equilibrium model is divided into two methods which are stoichiometric and non-stoichiometric (Ptasinski, 2015). In a stoichiometric model (based on the equilibrium constants of the main reforming reactions), the reforming chemical reactions, as well as chemical species present at equilibrium are required (Tay *et al.*, 2011).

The non-stoichiometric approach is based on the minimization of Gibbs energy and no chemical reactions are required, only the chemical species present at equilibrium are required (Ferreira *et al.*, 2019). At a temperature range of 327-1227°C, the main chemical species present at equilibrium with a concentration higher than 0.0001% are H_2, CO, H_2O, CO_2, CH_4, C(graphite), and N_2 (Desrosiers, 1979).

Equation 2. 14 shows the general reforming process of glycerol process using oxygen as a gasifying agent.

$$C_3H_8O_3 + iH_2O + mO_2(g) \rightarrow n_1H_2(g) + n_2CO(g) + n_3H_2O(g) + n_4CO_2(g) + n_5CH_4(g) + n_6C(s) \quad 2.14$$

where; n_1-n_6 are the molar quantities of H_2, CO, H_2O, CO_2, CH_4 and C respectively, i the glycerol moisture content and m the amount of oxygen needed for the reforming of 1 kmol of glycerol.

When combining all the three reforming agents, the global reforming of glycerol process can be given by equation 2.15.

$$C_3H_8O_3 + eCO_2 + iH_2O\,(l) + mO_2 + H_2O \rightarrow n_1H_2 + n_2CO + n_3H_2O + n_4CO_2 + n_5CH_4 + n_6C(s) \quad 2.15$$

To use the non-stoichiometric model of glycerol reforming to determine the syngas composition at different temperatures, the first step is to obtain the atomic balances. Since glycerol is composed of three atoms (C, H, and O), three equations can be obtained from the atomic balances from equations 2.14 and 2.15. Considering 1 kmol of glycerol, the following atomic balance equations can be generated from equation 2.15 (using pure oxygen):

Carbon balance: $3 + e = n_2 + n_4 + n_5 + n_6$ 2.16

Hydrogen balance: $8 + 2w + 2i = 2n_1 + 2n_3 + 4n_5$ 2.17

Oxygen balance: $3 + w + 2m + 2e + i = n_2 + n_3 + 2n_4$ 2.18

Extensive studies have been carried out to study the thermodynamic analysis of glycerol reforming using either non-stoichiometric or stoichiometric methods. In section 2.4.2.3 it was shown that glycerol can be transformed into syngas by using a non-stoichiometric approach (based on the minimization of Gibbs energy). Dieuzeide and Amadeo (2010) used a stoichiometric method to convert glycerol into syngas using H_2O as a reforming agent. Results revealed that high temperatures and SGRs increased the amount of H_2 but decreased the formation of coke as well as CH_4. Three operating conditions viz. temperature (600-1200K), SGRs (0.1-10), and pressure (1-9 atm) were used in this process. The effect of pressure was also studied, and it was revealed that increasing the pressure tended to favour the formation of coke at temperatures higher than 900K.

Carbon deposition is considered as major issue in all glycerol reforming processes and it leads to catalyst deactivation. During the modelling of glycerol reforming process, it is crucial to determine at which conditions carbon deposition is favoured or disfavoured. Various tools have been developed to address these challenges that occur during reforming processes. Taking the scope of this study into consideration, CHO ternary diagrams are used to address these challenges. CHO ternary diagram can be used to determine the operating conditions of glycerol reforming processes.

2.5 Conclusion

The main objective of this chapter was to discuss different concepts related to glycerol biorefinery. It started by discussing the sustainability challenges caused by the usage of non-renewable resources as well as the deployment of sustainable and renewable resources such as biomass. It further gave brief similarities and differences between a biorefinery and a petrochemical refinery. Finally, the chapter discussed the need of glycerol as a promotor of a circular (bio) economy (CE/CBE) through different transformation pathways. It also discussed different tools used in the design and synthesis of a glycerol biorefinery in order to establish it as a promotor of CE (CBE).

It was shown that glycerol can be transformed into value-added products via different pathways such as chemical, biochemical and thermochemical. Different studies have been carried out to study the thermodynamic analysis of glycerol reforming via different processes. It has been shown that the main issue during these processes is the deposition of carbon or coke. These studies have been considering operating conditions such as temperature and reforming agent

to glycerol ratio. There is no published article that has assessed the thermodynamic analysis of glycerol reforming using CHO ternary diagrams. The following four questions arise:

1. At which conditions should glycerol reforming processes be performed in order to avoid the deposition of carbon?
2. What can be the optimum amount of reforming agent required to convert 1 kmol of glycerol into syngas without carbon deposition?
3. What is the suitable reforming agent for the conversion of 1 kmol of glycerol into syngas?
4. Is it possible to mix glycerol with linear low- density polyethylene plastics to produce syngas?

These four questions will be answered in chapter 4 by means of CHO ternary diagram.

2.6 References

Adhikari, S., Fernandoa, S., Gwaltney, S.R., To, S.D.F., Brick, R.M., Steele, P.H. & Haryanto, A. (2007) 'A thermodynamic analysis of hydrogen production by steam reforming of glycerol', *International Journal of Hydrogen Energy*, 32, pp. 2875–2880.

Adhikari, S., Fernando, S. and Haryanto, A. (2007) 'A comparative thermodynamic and experimental analysis on hydrogen production by steam reforming of glycerin', *Energy & Fuels*, 21, pp. 2306–2310.

Almeida, J.R ., Fávaro, L. C. & Quirino, B. F.(2012) 'Biodiesel biorefinery: opportunities and challenges for microbial production of fuels and chemicals from glycerol waste', *Biotechnology for Biofuels*, 5(48) pp.1-16.

Arif, N. N., Abidin, S.Z., Osazuwa, O.U., Vo, D.V.N., Azizan, M.T. & Taufiq-Yap, Y.H. (2019) 'Hydrogen production via CO_2 dry reforming of glycerol over Re-Ni/CaO catalysts', *International Journal of Hydrogen Energy*, 44(37), pp. 20857–20871.

Aristizábal-Marulanda, V. & Cardona Alzate, C. A. (2019) 'Methods for designing and assessing biorefineries: Review', *Biofuels, Bioproducts and Biorefining*, 13(3), pp. 789–808.

Asare, J., Reguant, M. & Sacchetto, C. (2020) *Low oil prices during COVID-19 and the case for removing fuel subsidies, International Growth Centre*.

Atkins, M. J., Walmsley, T.G., Ong, B.H.Y., Walmsley, M. R. W. & Neale, J. R .(2016) 'Application of P-graph Techniques for Efficient use of Wood Processing Residues in Biorefineries', *Chemical Engineering Transactions*, 52, pp. 499–504.

Baruah, D. & Baruah, D. C. (2014) 'Modeling of biomass gasification: A review', *Renewable and Sustainable Energy Reviews*, 39, pp. 806–815.

Basu, P. (2013) *Biomass Gasification, Pyrolysis and Torrefaction: Practical Design and Theory*. Second Ed. Burlington, MA: Academic Press.

van Bennekom, J.G., Vos, J., Venderbosch, R.H., Paris Torres, M.A., Kirilov, V.A., Heeres,

H.J., Knez, Z., Bork, M. & Penninger, J.M.L.(2009) 'Supermethanol: reforming of crude glycerine in supercritical water to produce methanol for re-use in biodiesel plants', in *17th*

European Biomass Conference and Exhibition,. Hamburg, pp. 899–902.

Bertran, M.O., Frauzem, R., Zhang, L. & Gani, R. (2016) 'A generic Methodology of Superstruture Optimization of Different Processing Networks', *Computer Aided Chemical Engineering*, 38, pp. 685–690.

BP. 2020 'BP Statistical Review of World Energy June 2020. https://www.bp.com/Statistical review [Accessed 25 May 2021].

Cairns, E. J. & Tevebaugh, A. D. (1964) 'CHO Gas Phase Compositions in Equilibrium with Carbon, and Carbon Deposition Boundaries at One Atmosphere', *Journal of Chemical and Engineering Data*, 9(3), pp. 453–462.

Carno-Ruiz, J. & McRae, G. (1998) 'Environmentally Conscious Chemical Process Design', *Ann. Rev. Energy Environ*, 23(1), pp. 499–536.

Carvalheiro, F., Duarte, L. C. & Girio, F. M. (2008) 'Hemicellulose biorefineries: a review on biomass pretreatments', *Journal of Scientific & Industrial research*, 667, pp. 849–864.

de Jong, E. & Jungmeier, G.(2015) 'Chapter-1: Biorefinery Concepts in Comparison to Petrochemical Refineries', in *Industrial Biorefineries & White Biotechnology*, pp. 3–33.

Charisiou, N. D., Italiano, C., Pino, L., Sebastian, V., Vita, A. & Goula, M.A. (2020) 'Hydrogen production via steam reforming of glycerol over Rh/γ-Al_2O_3 catalysts modified with CeO_2, MgO or La_2O_3', *Renewable Energy*, 162(2020), pp.908–925.

Chen, Z. & Liu, D. (2016) 'Toward glycerol biorefinery: metabolic engineering for the production of biofuels and chemicals from glycerol', *Biotechnology for Biofuels*, 9(205).pp. 1-15

Cherubini, F. (2010) 'The biorefinery concept: Using biomass instead of oil for producing energy and chemicals', *Energy Conversion and Management*, 51(7), pp. 1412–1421.

Cherubini, F. & Ulgiati, S. (2010) 'Crop residues as raw materials for biorefinery systems - A LCA case study', *Applied Energy*, 87(1), pp. 47–57.

Cherubini, F., Wellisch, M. & Willke, T. (2009) 'Toward a common classification approach for biorefinery systems', *Biofuels, Bioproducts and Biorefining*, 3(1), pp. 534–546.

Ciferno, J. P. & Marano, J. J. (2002) *Benchmarking Biomass Gasification Technologies for Fuels, Chemicals and Hydrogen Production*. Pittsburgh, PA, USA.

Clark, J. H. & Deswarte, F. E. I. (2008) 'The biorefinery concept-An Integrated Approach. Introduction to chemicals from biomass', *Wiley, Chichester*, pp. 1–20.

Costa-gutierrez, S. B.,Saez, J.M, Aparicio, J.D, Raimondo, E.E., Benimeli, C.S. &Polti, M.A.(2021) 'Glycerol as a substrate for actinobacteria of biotechnological interest : Advantages and perspectives in circular economy systems', *Chemosphere*, 279, p. 130505.

D'Angelo, S. C., Dall'Ara, A., Mondelli, C., Pérez-Ramírez**,** J. & Papadokonstantakis, S. (2018) 'Techno-Economic Analysis of a Glycerol Biorefinery', *ACS Sustainable Chemistry and Engineering*, 6(12), pp. 16563–16572.

Dadgar, F., Myrstad, R., Pfeifer, P., Holmen, A. & Venvik, H.J. (2016) 'Direct dimethyl ether synthesis from synthesis gas: The influence of methanol dehydration on methanol synthesis reaction', *Catalysis Today*, 270, pp. 76–84.

Desrosiers, R. (1979) 'Thermodynamics of gas-char reactions.In: Reed TB,edition. A survey of biomass gasiciation. Colorado: Solar Energy Research Institute'

Dieuzeide, M.L & Amadeo, N. (2010) ' Thermodynamic Analysis of Glycerol Steam reforming ', *Chemical Engineering & Technology*, 33(1), pp.89-96.

Dimian, A.(2007) 'Renewable raw materials: chance and challenge for computer-aided process engineering', *Computer Aided Chemical Engineering*, 24(1), pp. 309–318.

Douglas, J. M.(1985) 'A hierarchical decision procedure for process synthesis', *AIChE Journal*, 31, pp. 353–362.

Earis, P. (2007) *Handbook of Alternative fuel technologies*. Second edi. Edited by S. Lee, J. Speight, and S. Loyalka. London: CRC Press: Taylor & Francis Group.

El-Halwagi, M. M. (2012) *Sustainable Design Through Process Integration:Fundamentals and Applications to Industrial Pollution Prevention, Resource Conservation, and Profitability Enhancement*. Second ed. Boston, MA: Butterworth-Heinemann.

Espinoza Pérez, A. T., Camargo, M., Rincón, P.C.N. & Marchant, M.A. (2017) 'Key

challenges and requirements for sustainable and industrialized biorefinery supply chain design and management: A bibliographic analysis', *Renewable and Sustainable Energy Reviews*, 69(October 2016), pp. 350–359.

Fan, X., Burton, R. and Zhou, Y. (2010) 'Glycerol (byproduct of biodiesel production) as a source for fuels and chemicals - Mini review', *Open Fuels and Energy Science Journal*, 3, pp. 17–22.

Ferreira, S., Monteiro, E., Brito, P. & Vilarinho, C. (2019) 'A Holistic Review on Biomass Gasification Modified Equilibrium Models', *Energies*, 12(160), pp. 1–31.

Forzatti, P., Tronconi, E. & Pasquon, I. (1991) 'Higher Alcohol Synthesis', *Catalysis Reviews*, 33(1&2), pp. 109–168.

Freitas, A. C. & Guirardello, R. (2014) 'Comparison of several glycerol reforming methods for hydrogen and syngas production using Gibbs energy minimization', *International Journal of Hydrogen Energy*, 39, pp. 17969–17984.

Garcia, L., Salvador, M.L., Arauzo, J. & Bilbao, R. (2001) 'CO_2 as a gasifying agent for gas production from pine sawdust at low temperatures using a Ni/Al coprecipitated catalyst', *Fuel Processing Technology*, 69, pp. 157–174.

Gargalo, C. L., Cheali, P., Posada, J.A., Gernaey, K.V. & Sin, G.(2016) 'Economic Risk Assessment of Early Stage Designs for Glycerol Valorization in Biorefinery Concepts', *Ind. Eng. Chem. Res.*, 55(24), pp. 6801–6814.

Gatto, F. & Re, I. (2021) 'Circular bioeconomy business models to overcome the valley of death. A systematic statistical analysis of studies and projects in emerging bio-based technologies and trends linked to the sme instrument support', *Sustainability (Switzerland)*, 13(4), pp. 1–37.

Ghatak, H.R.(2011) 'Biorefineries from the perspective of sustainability: Feedstocks, products, and processes', *Renewable and Sustainable Energy Reviews*, 15(8), pp. 4042–4052.

Goh, W. S. & Ng, D. K. S. (2015) 'Hierarchical decomposition approach for process synthesis of integrated biorefinery', *Chemical Engineering Transactions*, 45, pp. 1693–1698.

Gundekari, S., Mitra, J. & Varkolu, M. (2020) *Classification, characterization, and properties*

of edible and non-edible biomass feedstocks, Advanced Functional Solid Catalysts for Biomass Valorization.

Gutiérrez, C. D. B., Serna, D. L. R. & Alzate, C. A. C. (2017) 'A comprehensive review on the implementation of the biorefinery concept in biodiesel production plants', *Biofuel Research Journal*, 4(3), pp. 691–703.

Habibullah, M., Masjuki, H.H., Kalam, M.A., Ashrafur Rahmand, S.M., Mofijur, M., Mobarak, H.M. & Ashraful, A.M. (2015) 'Potential of biodiesel as a renewable energy source', *Renewable and Sustainable Energy Reviews*, 50, pp. 819–834.

Hamelinck, C. N., Suurs, R. A. A. & Faaij, A. P. C. (2005) 'International bioenergy transport costs and energy balance', *Biomass and Bioenergy*, 29(2), pp. 114–134.

Hook, M. and Tang, X. (2013) 'Depletion of fossil fuels and anthropogenic climate change-A review', *Energy Policy*, 52(2013), pp. 797–809.

Huang, C., Xu, C., Wang, B., Hu, X., Li, J., Liu, J.& Li, C. (2018) 'High production of syngas from catalytic steam reforming of biomass glycerol in the presence of methane', *Biomass and Bioenergy*, 119, pp. 173–178.

IEA, 2012b. Bio-based Chemicals: Value Added Products from Biorefineries. Report for IEA.Biorefinery- Task 42. International Energy Agency (IEA), Paris,France [Accessed on 8 August 2021].

International Energy Agency (IEA). 2020. World Energy Outlook 2020. http://www.iea.World Energy Outlook 2013, [Accessed on 25 May 2021]

International Energy Agency (IEA).2021. Monthly Energy Review. http://www.iea.World Energy Outlook 2021, [Accessed on 25 May 2021]

Ismaila, A., Chen, X., Gao, X. & Fan, X.(2021) 'Thermodynamic analysis of steam reforming of glycerol for hydrogen production at atmospheric pressure', *Chem. Sci. Eng.*, 15(1), pp. 60–71.

Jabbour, K. (2020) 'Tuning combined steam and dry reforming of methane for "metgas" production: A thermodynamic approach ad state-of the art catalysts', *Journal of Energy Chemistry*, 48, pp. 54–91.

Junginger, M., de Visser, E., Hjort-Gregersen, K., Koornneef, R.R., Faaij, A. & Turkenburg, W. (2006) 'Technological learning in bioenergy systems', *Energy Policy*, 34(18), pp. 4024–4041.

Kale, G. & Kulkarni, B. (2010) 'Thermodynamic analysis of dry autothermal reforming of glycerol', *Fuel Processing Technology*, 91, pp. 520–530.

Kaur, J., Sarma, A.K., Jha, M.K. & Gera, P (2020) 'Valorisation of crude glycerol to value-added products : Perspectives of process technology , economics and environmental issues', *Biotechnology Reports*, 27, pp. 1–23.

Kelloway, A. & Daoutidis, P. (2014) 'Process synthesis of biorefineries: Optimization of biomass conversion to fuels and chemicals', *Industrial and Engineering Chemistry Research*, 53(13), pp. 5261–5273.

Khan, A. A., de Jong, W., Jansens, P.J. & Spliethoff, H. (2009) 'Biomass combustion in fluidized bed boilers: Potential problems and remedies', *Fuel Processing Technology*, 90(1), pp. 21–50.

Kokossis, A. C. &Yang, A. (2010) 'On the use of systems technologies and a systematic approach for the synthesis and the design of future biorefineries', *Computers and Chemical Engineering*, 34(9), pp. 1397–1405.

Kong, Q. & Shah, N. (2016) 'An optimisation-based framework for the conceptual design of reaction-separation processes', *Chem.Eng.Res.Des.*, 113, pp. 206–222.

Kotcher, J., Maibach, E. & Choi, W.T. (2019) 'Fossil fuels are harming our brains: Identifying key messages about the health effects of air pollution from fossil fuels', *BMC Public Health*, 19(1), pp. 1–12.

Lari, G., Pastore, G., Haus, M., Ding, Y., Papadokonstantakis ,S., Mondelli, C. & Pérez-Ramírez, J.(2018) 'Environmental and economical perspectives of glycerol biorefinery', *Energy Environ. Sci.*, 11(5), pp. 1012–1029.

Lelieveld, J., Klingmüller, K., Pozzer, A., Burnett, R.T., Haines,A. &Ramanathan, V.(2019) 'Effects of fossil fuel and total anthropogenic emission removal on public health and climate', *Proceedings of the National Academy of Sciences of the United States of America*, 116(15), pp. 7192–7197.

Leong, H. Y.,Chang, C.K., Khoo, K.S., Chew, K.W., Chia, S.R., Lim, J.W., Chang, J.S. & Show, P.L. (2021) 'Waste biorefinery towards a sustainable circular bioeconomy: a solution to

global issues', *Biotechnology for Biofuels*, 14(1), pp. 1–15.

Li, Y., Zhang, L., Yuan, Z. & Gani, R.(2020) 'Synthesis and design of sustainable integrated process , water treatment , and power generation networks', *Computers and Chemical Engineering*, 141, p. 107041..

Litheko, L. A. (2017) Conceptual design of gsification-based biorefineries using the C-H-O ternary diagrams, University of South Africa, Pretoria,

Liu, Y., Farrauto, R. & Lawal, A. (2013) 'Autothermal reforming of glycerol in a dual layer monolith catalyst', *Chemical Engineering Science*, 89, pp. 31–39.

Liu, Y. & Lawal, A. (2015) 'Catalyst, Kinetic study of autothermal reforming of glycerol in a dual layer monolith', *Chemical Engineering and Processing: Process Intensification*, 95, pp. 276–283.

Loureiro da Costa Lira Gargalo, C., Carvalho, A., Gernaey, K.V. & Sin, G. (2017) 'Optimal design and planning of glycerol-based biorefinery supply chains under uncertainty', *Ind. Eng. Chem. Res.*, 56(41), pp. 11870–11893.

Madathil, J.&Velmurugan, P.(2019) 'Impact of crude oil price on the socio-political environment of global countries', *Restaurant Business*, 118(3),pp.110–123.

Mahabir,J., Koylass, N., Samaroo, N., Narine, K. & Ward, K. (2021) 'Towards resource circular biodiesel production through glycerol upcycling', *Energy Conversion and Management*, 233(December 2020), p. 113930.

Mahlia, T. M. I., Syazmi, Z.A.H.S., Mofijur, M., Abas, A.E.P., Bilad M.R., Ong, H.C. & Silitonga, A.S. (2020) 'Patent landscape review on biodiesel production: Technology updates', *Renewable and Sustainable Energy Reviews*, 118(October 2019), pp. 1–9.

Ma, W., Jacobs, G., Sparks, D.E., Todic, B., Bukur, D.B. & Davis, B.H. (2020) ' Quantitative comparison of iron and cobalt based catalysts for the Fischer-Tropsch synthesis under clean and poisoning conditions', *Catalysis Today*, 343(1),pp.125-136.

Martin, M. & Grossmann, I. E. (2014) 'Optimal Simultaneous Production of Hydrogen and Liquid fuels from Glycerol: Integrating the use of biodiesel byproducts', *Industrial and Engineering Chemistry Research*, 53(18), pp. 7730–7745.

Martinez-Hernandez, E., Sadhukhan, J. and Campbell, G. M. (2013) 'Integration of bioethanol as an in-process material in biorefineries using mass pinch analysis', *Applied Energy*, 104, pp.

517–526.

Martins, F., Felgueiras, C., Smitkova, M. & Caetano, N. (2019) ‘Analysis of Fossil Fuel Energy Consumption and Environmental Impacts in European Countries’, *Energies*, 153(12), pp. 1–11.

Martín, M., Díez, M., Alemena, A. & Bueno, L. (2018) ‘Integrated biodiesel facilities : review of glycerol-based production of fuels and chemicals’*Clean Technologies and Environmental Policy*, pp. 1639–1661.

Mata, T. M., Martins, A. A. and Caetano, N. S. (2010) ‘Microalgae for biodiesel production and other applications: A review’, *Renewable and Sustainable Energy Reviews*, 14(1), pp. 217–232.

McKendry, P. (2002) ‘Energy production from biomass (part 1): Overview of biomass’, *Bioresource Technology*, 83(1), pp. 37–46.

Moncada B, J., Aristizábal M, V. & Cardona A, C. A. (2016) ‘Design strategies for sustainable biorefineries’, *Biochemical Engineering Journal*, 116, pp. 122–134.

Muramoto, A., Kikuchi, Y., Tachikawa, Y., Lyth, S.M., Shiratori, Y., Taniguchi, S. & Sasaki, K.(2017) ‘High-pressure C-H-O diagrams: Fuel composition, carbon deposition, and open circuit voltage of pressurized SOFCs’, *International Journal of Hydrogen Energy*, 42(52), pp. 30769–30786.

Naik, S.N., Goud, V.V., Rout, P.K. & Dalai, A.K. (2010) ‘Production of first and second generation biofuels: A comprehensive review’, *Renewable and Sustainable Energy Reviews*, 14(2), pp. 578–597.

Nda-umar, U. I., Ramli, I., Taufiq-Yap, Y. & Muhamad, E.V. (2018) ‘An Overview of Recent Research in the Conversion of Glycerol into Biofuels , Fuel Additives and other’, *Catalysts*, 9(15), pp. 1–47.

Ng, D. K. S.,Pham, V., El-Halwagi, M.M., Jiminez-Gutierrez, A. & Spriggs, H.D.(2009) ‘Hierarchical approach to the synthesis and analysis of of integrated biorefineries’, in *Proceeding of Seventh International Conference n Foundations of Computer-Aided Process Design*, pp. 425–432.

Ng, D.K.S., Ng, K.S. & Ng, R.T.L ‘Integrated Biorefineries ’. Encyclopedia of Sustainable Technologies, edited by Abraham, M.A., Elsevier, 2017, pp.299-314.

Ng, D. K. (2010) 'Automated targeting for the synthesis of an integrated biorefinery', *Chemical Engineering Journal*, 162(1), pp. 67–74.

Nikoo, M. B. & Mahinpey, N. (2008) 'Simulation of Biomass gasification in fluidized bed reactor using Aspen Plus', *Biomass and Bioenergy*, 32, pp. 1245–1254.

Nkosi, N., Muzenda, E., Gorimbo, J. & Belaid, M.(2021) 'Developments in waste tyre thermochemical conversion processes: gasification, pyrolysis and liquefaction', *RSC Advances*, 11(20), pp. 11844–11871.

Paisley, M. A. & Anson, D. B. (1997) 'Biomass Gasification for Gas Turbine Based Power Generation', *Presented at the International Gas Turbine & Aeroengine Congress & Exhibition, 1997.*, pp. 1–6.

Palmeros Parada, M., Osseweijer, P. & Posada Duque, J. A. (2017) 'Sustainable biorefineries, an analysis of practices for incorporating sustainability in biorefinery design', *Industrial Crops and Products*, 106, pp. 105–123.

Parajuli, R., Dalgaard, T., Jørgensen, U., Adamsen, A. S., Knudsen, M. T., Birkved, M., Gylling, M. & Schjørring, J. K. (2015) 'Biorefining in the prevailing energy and materials crisis: A review of sustainable pathways for biorefinery value chains and sustainability assessment methodologies', *Renewable and Sustainable Energy Reviews*, 43, pp. 244–263.

Patel, B. (2007) '*Fundamental Targets for the Synthesis and Evaluation of Chemical Processes*', PhD thesis, University of Witwatersrand, Johannesburg.

Patel, B., Hildebrandt, D., Glasser, D. & Hausberger, B. (2007) 'Synthesis and Integration of Chemical Processes from a Mass , Energy, and Entropy Perspective', *Industrial and Engineering Chemistry Research*, 46, pp. 8756–8766.

Peinado, C., Liuzzi, D., Ladera-Gallardo, M., Retuerto, M., Ojeda, M, Pena, M.A.&Rojas, S. (2020) ' Effects of support and reaction pressure for the synthesis of dimethyl ether over heteropolyacid catalysts', *Sci Rep*, 10,pp.8551.

Perera, F. (2018) 'Pollution from fossil-fuel combustion is the leading environmental threat to global pediatric health and equity: Solutions exist', *International Journal of Environmental Research and Public Health*, 15(1). pp.1-27.

Polychronopoulou, K., Charisiou, N., Papageridis, K., Sebastian, V., Hinder, S., Dabbawala, A., Alkhoori, A., Baker, M., Goula, M. (2018) 'The effect of Ni addition onto a Cu-based ternary support on the H_2 production over glycerol steam reforming reaction', *Nanomaterials*,

8(11), p. 931.

Posada, J. A., Rincón, L. E. and Cardona, C. A. (2012) 'Design and analysis of biorefineries based on raw glycerol: Addressing the glycerol problem', *Bioresource Technology*, 111, pp. 282–293.

Prasetyo, W. D., Putra, Z.A., Bilad, M. R., Mahlia, T. M. I., Wibisono, Y., Nordin, N. A. H.& Wirzal, M. D. H. (2020) 'Insight into the sustainable integration of bio- and petroleum refineries for the production of fuels and chemicals', *Polymers*, 12(5), pp. 1–24.

Prins, M. J., Ptasinski, K. J. and Jansens, F. J. (2006) 'More efficient biomass gasification via torrefaction', *Energy*, 31(1), pp. 3458–34570.

Ptasinski, K. J. (2015) *Efficiency of Biomass Energy: An Exergy Approach to Biofuels, power, and Biorefineries*. Haboken, New Jersey: John Wiley & Sons.

Ptasinski, K. J., Prins, M. J. and Pierik, A. (2007) 'Exergetic evaluation of biomass gasification', *Energy*, 32(1), pp. 568–574.

Puig-Arnavat, M., Hernandez, J. A., Bruno, J. C. & Coronas, A. (2013) 'Artificial neural network models for biomass gasification in fluidized bed gasifiers', *Biomass and Bioenergy*, 49, pp. 279–289.

Puig-Arnavat, M., Bruno, J. C. & Coronas, A. (2010) 'Review and analysis of biomass gasification models', *Renewable and Sustainable Energy Reviews*, 14(9), pp. 2841–2851.

Romano, R. T. & Zhang, R. (2008) 'Co-digestion of onion juice and wastewater sludge using an anaerobic mixed biofilm reactor', *Bioresource Technology*, 99(3), pp. 631–637.

Rosas, I. P., Contreras, L., Salmones, J., Tapia, C., Zeifert, B., Navarrete, J., Tamara, V. & Carolina, D. (2017) 'Catalytic Dehydration of Glycerol to Acrolein over a Catalyst of Pd / LaY Zeolite and Comparison with the Chemical Equilibrium', *Catalysts*, 7(73), pp. 1–29.

Roslan, N. A., Abidin, S. Z., Ideris, A. & Vo, D.N. (2020) 'A review on glycerol reforming processes over Ni-based catalyst for hydrogen and syngas productions', *International Journal of Hydrogen Energy*, 45(36), pp. 18466–18489.

Sadhukhan, J., Ng, K. S. & Martinez-Hernandez, E. (2014) *Biorefineries and Chemical processes: Design, Integration and Sustainability Analysis*. First Edit. West Sussex, UK: Wiley.

dos Santos, R. & Alencar, A. c. (2020) 'Biomass-derived syngas production via gasification

process and its catalytic conversion into fuels by Fischer Tropsch synthesis: A review', *Internation Journal of Hydrogen Energy*, 45, pp. 18114–18132.

Schultz, E. L., de Souza, D. T. and Damaso, M. C. T. (2014) 'The glyerol biorefinery: a purpose fro Brazilian biodiesel prouction', *The glycerol biorefinery: a purpose for Brazilian biodiesel production*, 1(7), pp. 1–9.

Schwengber, C. A.; Alves, H.J.; Schaffner, R.A.; da Silva, F.A.; Sequinel, R.; Bach, V.R. & Ferracin, R.J. (2016) 'Overview of glycerol reforming for hydrogen production', *Renewable and Sustainable Energy Reviews*, 58(July 2014), pp. 259–266.

Seadira, T., Sadanandam, G., Ntho, T. A., Lu, X., Masuku, C. M. & Scurrell, M. (2018) 'Hydrogen production from glycerol reforming: conventional and green production', *Rev Chem Eng*, 34(5), pp. 695–726.

Siew, K. W.; Lee, H.C.; Gimbun, J. & Cheng, C.K. (2014) 'Production of CO-rich hydrogen gas from glycerol dry reforming over La-promoted Ni/Al_2O_3 catalyst', *International Journal of Hydrogen Energy*, 39(13), pp. 6927–6936.

Siirola, J. (1996) 'Industrial Applications of Chemical Process Synthesis', *Advances in Chemical Engineering*, 23, pp. 1–62.

Silva, J.; Soria, M. & Madeira, L.(2015) 'Challenges and strategies for optimization of glycerol reforming process', *Rebewable and Sustainable Energy Reviews*, 42, pp. 1187–1213.

Singh, D., Sharma, D., Soni, S.L., Sharma, S., Sharma, P.K., Jhalani, A. (2020) 'A review on feedstocks, production processes, and yield for different generations of biodiesel', *Fuel*, 262(116553).

Smirnov, A. A.; Selishcheva, S. A. &Yakovlev, V.A.(2018) 'Acetalization Catalysts for Synthesis of Valuable Oxygenated Fuel Additives from Glycerol', *Catalysts*, 8(595), pp. 1–25.

Spath, P.L.&Dayton, D. C. (2003) *Preliminary screening – technical and economic assessment of synthesis gas to fuels and chemicals with emphasis on the potential for biomass-derived syngas*. National Renewable Energy Laboratory, pp.1-160. [Accessed on 25 June 2021]

Stephanopoulos, G. and Reklaitis, G. V (2011) 'Process systems engineering : From Solvay to modern bio- and nanotechnology . A history of development , successes and prospects for the

future', *Chemical Engineering Science*, 66(19), pp. 4272–4306.

Takkellapati, S., Li, T. and Gonzalez, M. A. (2018) 'An overview of biorefinery - derived platform chemicals from a cellulose and hemicellulose biorefinery', *Clean Technologies and Environmental Policy*, 20(7), pp. 1615–1630.

Tan, H. W., Abdul Aziz, A. R. and Aroua, M. K. (2013) 'Glycerol production and its applications as a raw material: A review', *Renewable and Sustainable Energy Reviews*, 27, pp. 118–127.

Tay, D. H. S., Ng, D. K. S., Kheireddine, H.& El-Halwagi, M. M. (2011) 'Synthesis of an integrated biorefinery via the C-H-O ternary diagram', *Clean Technologies and Environmental Policy*, 13(4), pp. 567–579.

Tay, D. H.S., Kheireddine, H., Ng, D. K.S., El-Halwagi, M.M.& Tan, R. R. (2011) 'Conceptual synthesis of gasification-based biorefineries using thermodynamic equilibrium optimization models', *Industrial and Engineering Chemistry Research*, 50(18), pp. 10681–10695.

Tevebaugh, A. D. and Cairns, E. J. (1965) 'Carbon Deposition Boundaries in the CHO System at Several Pressures', *Journal of Chemical and Engineering Data*, 10(4), pp. 359–362.

Tey, S., Wong, S. S., Lam, J. A.,Ong, N. Q. X., Foo, D .C .Y. &Ng, D.K. S. (2020) 'Extended hierarchical decomposition approach for the synthesis of biorefinery processes', *Chemical Engineering Research and Design*, 166, pp. 40–54.

Tey, T.O.,Chen,S., Cheong, Z.X., Choong, A.S.X., Ng, L.Y. & Chemmangattuvalappil, N. G (2021) 'Synthesis of a sustainable integrated biorefinery to produce value-added chemicals from palm-based biomass via mathematical optimisation', *Sustainable Production and Consumption*, 26, pp. 288–315.

Trifoi, A. R., Agachi, P. Ş. and Pap, T. (2016) 'Glycerol acetals and ketals as possible diesel additives. A review of their synthesis protocols', *Renewable and Sustainable Energy Reviews*, 62(2016), pp. 804–814.

Tursi, A. (2019) 'A review on biomass : importance , chemistry , classification , and conversion', *Biofeuel Research Journal*, 22, pp. 962–979.

Tsubaki, N., Ito, M. & Fujimoto, K. (2001) ' A new method of low- temperature methanol

synthesis', *Journal of Catalysis*, 197(1), pp.224-227.

Valliyappan, T., Bakhshi, N. & Dalai, A. (2008) 'Pyrolysis of Glycerol for the Production of Hydrogen or Syn gas', *Bioresource Technology*, 99, pp. 4476–4483.

Vivek, N., Sindhu, N., Madhavan, A., Anju, A.J., Castro, E., Faraco, V., Pandey, A. & Binod, P. (2017) 'Bioresource Technology Recent advances in the production of value added chemicals and lipids utilizing biodiesel industry generated crude glycerol as a substrate – Metabolic aspects , challenges and possibilities : An overview', *Bioresource Technology*, 239, pp. 507–517.

Wang, W. (2010) 'Thermodynamic analysis of glycerol partial oxidation for hydrogen production', *Fuel Processing Technology*, 91(11), pp.1401-1408.

Wang, X., Li, M., Wang, M.; Li, S., Wang, S. & Ma, X. (2009) 'Thermodynamic analysis of glycerol dry reforming for hydrogen and synthesis gas production', *Fuel*, 88(11), pp. 148–2153.

Wang, X.,Wang, Q., Song, X. & Chen, J. (2017) 'Dry autothermal reforming of glycerol with in situ hydrogen separation via thermodynamic evaluation', *Internation Journal of Hydrogen Energy*, 42(2), pp. 838–847.

World Bioenergy Association (WBA). 2018. Global Bioenergy Statistics 2018. http://www.worldbioenergy.org/uploads/181017%20WBA%20GBS%202018_Summary_hq.pdf. [Accessed on 27 December 2020]

Xie, H., Li,R.; Yu, Z.; Wang, Z.; Yu, Q. & Qin, Q.(2020) 'Combined steam/dry reforming of bio-oil for H2/CO syngas production with blast furnace slag as a heat carrier', *Energy*, 200, p. 117481.

Xuan, T. D., Diep, N.Q., Nakagoshi, X.D., Sakanishi, K., Fujimoto, S. S Minowa, T.(2012) 'Biorefinery : Concepts , Current Status , and Development Trends', *International Journal of Biomass and Renewables*, (January 2015), pp. 1–8.

Yang, J., Ma, W., Chen, D., Holmen, A. & Davis, B.H. (2014) ' Fischer-Tropsch synthesis: A review of the effect of CO conversion on methane selectivity', *Applied Catalysis A: General*, 470, pp.250-260.

Yi, J., Yeo, J., How, B.S., Teng, S. Y., Leong, W. D., Ng, W.P.Q., Lim, C.H., Ngan, S.L., Sunarso, J. & Lam, H.L.(2020) 'Synthesis of Sustainable Circular Economy in Palm Oil Industry Using Graph-Theoretic Method', *Sustainability*, 12, pp. 5–29.

Yuan, Z., Chen, B. and Gani, R. (2013) 'Applications of process synthesis : Moving from conventional chemical processes towards biorefinery processes', *Computers and Chemical Engineering*, 49, pp. 217–229.

Zhang, H., Hu, Z., Huang, L., Zhang, H., Song, K., Wang, L., Shi, Z., Ma, J., Zhuang, Y., Shen, W., Zhang, Y., Xu, H. & Tang, Y. (2015) 'Dehydration of Glycerol to Acrolein over Hierarchical ZSM - 5 Zeolites : Effects of Mesoporosity and Acidity', *Catalysis*, 5, pp. 2548–2558.

Zhou, C. H., Zhao, H., Tong, D. S., Wu, L. M. & Yu, W.H. (2013) 'Recent Advances in Ctalytic Conversion of Glycerol', *Catalysis Reviews*, 55(4), pp. 369–553.

Zondervan, E., Nawaz, M., de Haan, A. B., Woodley, J. M.& Gani, R. (2011) 'Optimal design of a multi-product biorefinery system', *Computers and Chemical Engineering*, 35(9), pp. 1752–1766.

CHAPTER THREE

3.0 METHODOLOGY

3.1 Introduction

Carbon, hydrogen, and oxygen (CHO) ternary systems play a significant role in chemical processes such as combustion, gasification, hydrogenation processes, and fuel cells (Cairns and Tevebaugh, 1964). Any chemical compound consisting of carbon, hydrogen, and oxygen can be represented as a unique point on the CHO ternary diagram based on its molar composition by using an equilateral triangle (Tay *et al.,* 2010)**.** Because biorefineries also consist of raw materials and chemical substances that are mostly made up of these three atoms, biorefinery systems can be represented as a CHO ternary system. Glycerol, as well as compounds produced from glycerol, consist of carbon, hydrogen, and oxygen, can be represented on a ternary diagram. From this diagram different glycerol conversion processes such as reforming and pyrolysis, can be considered and a conceptual design of a glycerol biorefinery can be conducted. It is assumed that the impurities present in glycerol are insignificant and won't impact the process in a major way.

The main objective of this chapter is to give an overview of different concepts that are going to be applied in the study. The methodology used in this study is split into two sections. The first section uses CHO ternary diagrams to represent different processes through which glycerol, as well as a mixture of glycerol with linear low-density polyethylene (LLDPE), can be transformed into syngas and to determine the process targets. These CHO ternary diagrams are plotted using a software known as ProSim Ternary Diagram. Acrobat Reader DC (Measuring Tool) is used for all distance measurements on the CHO ternary diagrams. This measuring tool is easy to use and provides an accurate measurement of the distance between two points (distance between two reactants or products). The second section uses Aspen Plus simulation software to develop and model different flowsheets based on CHO ternary. Figure 3.1 shows a summary of the methodology used in this study. The different steps presented in this figure will be discussed in more detail in the following sections.

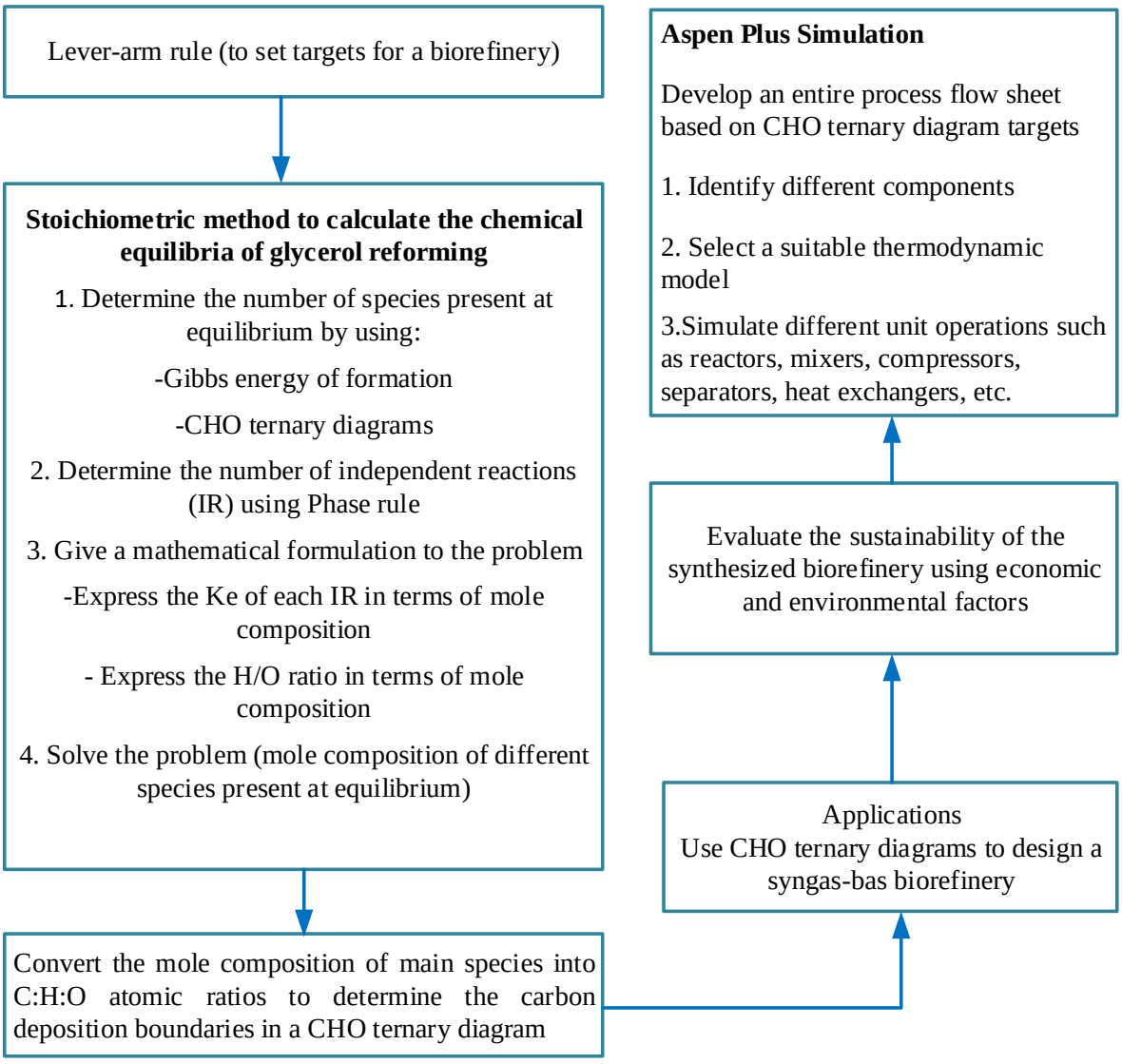

Figure 3. 1: Proposed Methodology

3.2 Fundamentals of CHO ternary diagrams

The CHO diagram (Figure 3.2) is represented by an equilateral triangular grid that is used to represent the different components and their compositions. Each corner of the triangle represents a pure component or atom. In other words, carbon, hydrogen, and oxygen are represented on each vertex of the triangle. Any mixture that consists of two atoms should lie on a side of the triangle. A ternary mixture that consists of the three atoms (carbon, hydrogen, and oxygen) will be represented inside the triangle.

Figure 3.2 shows a ternary diagram whereby the vertices represent 100 percent carbon, hydrogen, and oxygen. This figure is a simple representation but reveals important and insightful information on CHO systems.

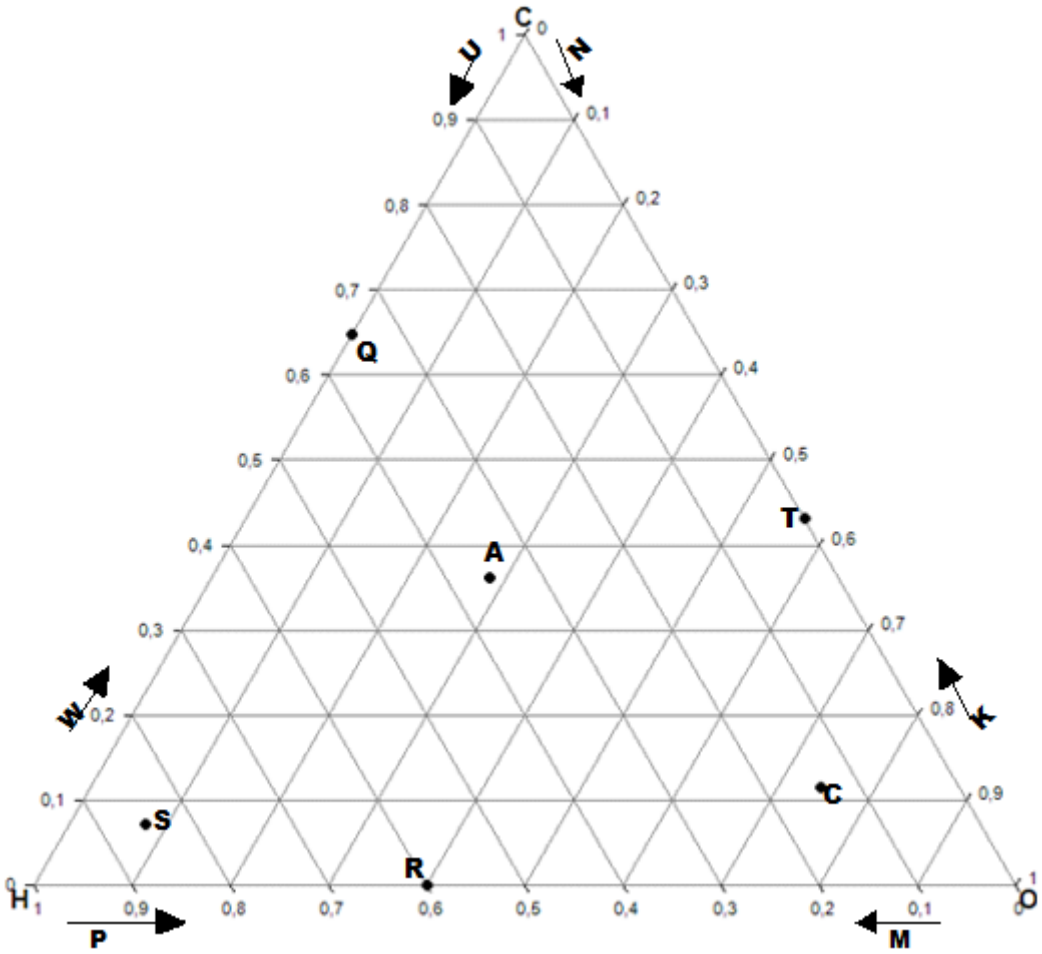

Figure 3. 2: Properties of CHO ternary diagrams

Figure 3.2 can be interpreted as follows: Arrow W represents a decreasing mole fraction of hydrogen (H). The H mole fraction decreases until it becomes zero at the vertex represented by carbon (C). Arrow U represents a decrease in carbon mole fraction. Point Q represents a chemical species constituted by only carbon and hydrogen (64.8% C and 35.2% H). Any chemical compound that consists of H and C can be plotted on the C-H side (e.g., methane, linear low-density polyethylene, propane). Arrow P indicates the decrease in hydrogen mole fraction whereas arrow M shows a decrease in oxygen mole fraction. Any chemical species that is constituted only by hydrogen and oxygen (such as water) must be plotted on the H-O side. This is the case of point R (60% H and 40% O). Arrows N and K represent the decrease

in carbon and oxygen mole fractions respectively. All chemical species whose constituents are carbon and oxygen are plotted on the C-O edge such as carbon monoxide and carbon dioxide. For example, point T represents a species with 43% C and 57% H. Points A, C and S are examples of chemical species that are constituted of all three atoms viz. carbon, hydrogen, and oxygen. For example, glycerol, acetic acid, biomass, ethanol would be plotted inside the CHO diagram.

3.3 Determining the C, H, and O composition of a compound using CHO ternary diagrams

The most effective way of determining compositions of carbon, hydrogen, and oxygen using a ternary diagram is by drawing lines passing through a specific point (any species with $C_x H_y O_z$ as general chemical formula), that is parallel to each side of the triangle (O-C, C-H or H-O). Figure 3.3 shows an arbitrary point O. Three lines are drawn parallel to each side of the triangle. Line segment xOx_1 is parallel to side H-C, yOy_1 is parallel to C-O and zOz_1 is parallel to side H-O. Using some fundamental basics of geometry, the proportion of each atom/element can be calculated as follows:

$$\text{Hydrogen proportion : } H_{\text{Proportion}} = \frac{yO}{HO} = \frac{y_1 C}{CH}$$

$$\text{Oxygen proportion : } O_{\text{Proportion}} = \frac{Hx}{HO} = \frac{x_1 C}{CO}$$

$$\text{Carbon proportion : } C_{\text{Proportion}} = \frac{zC}{CO} = \frac{z_1 H}{CH}$$

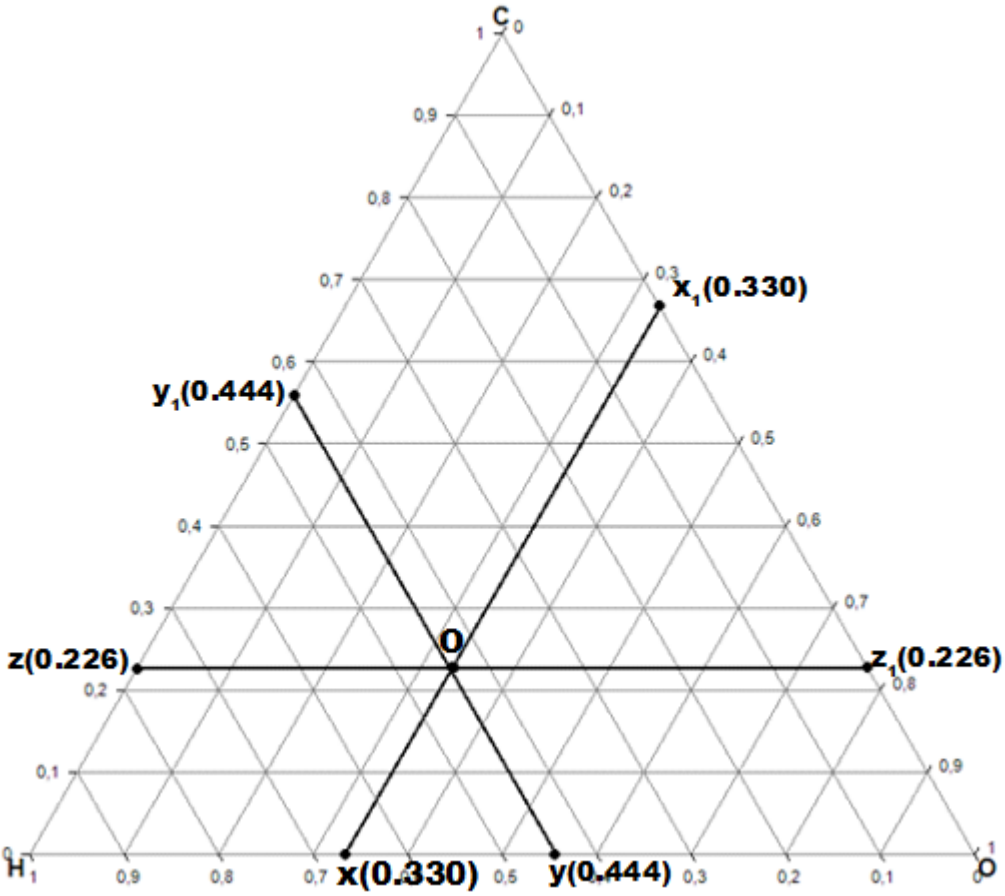

Figure 3. 3: Composition of an arbitrary point inside a CHO ternary diagram

Consequently, the composition of compound O is 22.6% carbon, 44.4% hydrogen and 33.0% oxygen.

3.4 Significance of CHO ternary diagrams in process design

In previous sections, it was shown how to determine the mole fractions of carbon, hydrogen, and oxygen using CHO ternary diagrams. This section focuses on using CHO ternary diagrams to determine the overall material balance. Material balances play an important role in chemical processes as it quantifies the flow of material. It is based on the theory of mass conservation which states that: the mass entering is equal to the mass leaving the system at a steady state. The material balance for chemical processes that involve multiple reactions, recycles, purge or bypass streams, and various unit operations can be quite complex and requires a considerable amount of detail and information regarding the process. At the early design stages, the material balance can be simplified by considering only the inputs and outputs. Once the input and output are known, CHO ternary diagrams can be used to determine targets for input and output required by employing the lever-arm rule, which can be considered as a graphical representation of the mass balance.

Consider two imaginary inputs D and E inside the ternary diagram as shown in figure 3.4. Point M is the mixing point. Atomic material balance can be performed at the mixing point M.

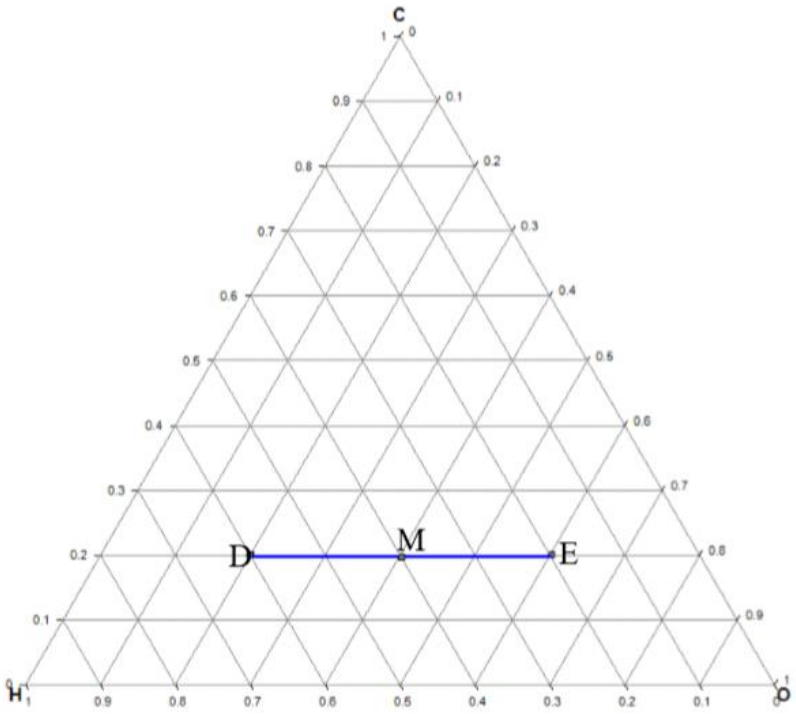

Figure 3. 4: Mass balance using CHO ternary systems

The overall material balance can be written as follows.

$$M - (D + E) = 0 \qquad 3.1i$$

$$\text{Hydrogen balance: } Mx_{HM} - (Dx_{HD} + Ex_{HE}) = 0 \qquad 3.1ii$$

$$\text{Carbon balance: } Mx_{CM} - (Dx_{CD} + Ex_{CE}) = 0 \qquad 3.1ii$$

Where, X_M: composition of stream M

X_E: composition of stream E

X_D: composition of stream D

X_{CD}: composition of carbon of stream D

X_{HD}: composition of hydrogen of stream D

The ratio of $\frac{D}{E}$ can be determined by using hydrogen and carbon balance (Litheko 2017).

$$\frac{D}{E} = \frac{X_{HE} - X_{HM}}{X_{HM} - X_{HD}} \quad 3.2$$

$$\frac{D}{E} = \frac{X_{CE} - X_{CM}}{X_{CM} - X_{CD}} \quad 3.3$$

Therefore

$$\frac{D}{E} = \frac{X_{HE} - X_{HM}}{X_{HM} - X_{HD}} = \frac{X_{CE} - X_{CM}}{X_{CM} - X_{CD}} = \frac{EM}{DM} \quad 3.4$$

From the same figure, it can be shown that the ratio of stream D to mixing point M is equal to the distance from E to M (segment of the tie line from E to M) divided by the total distance (DE). To determine the ratio of stream E to mixing point M, one will have to divide the DM (length of the tie line from D to M) with DE (total length of the tie line from D to E). These two relationships can be used to determine the composition of D and E.

To illustrate the importance of the lever-arm rule during the synthesis of a biorefinery, consider a process whereby 1 kmol of methanol is synthesized from glycerol and water.

$$aC_3H_8O_3 + bH_2O \implies 1CH_4O + cCO_2 \quad 3.5$$

Where a, b and c represent the respective molar quantity of $C_3H_8O_3$, H_2O, and CO_2 to produce 1 kmol of CH_4O

It must be noted that equation 3.5 represents an overall process for methanol synthesis from glycerol. To show this process on the CHO ternary diagram, the atomic mole fractions are first calculated (see Appendix A).

In figure 3.5, the blue line represents the input ($C_3H_8O_3$ and H_2O) while the black line represents the output (CH_4O and CO_2) and M the equilibrium point. This point indicates that the equilibrium state of the mixture of glycerol and water, as well as the mixture of methanol, and carbon dioxide is attained.

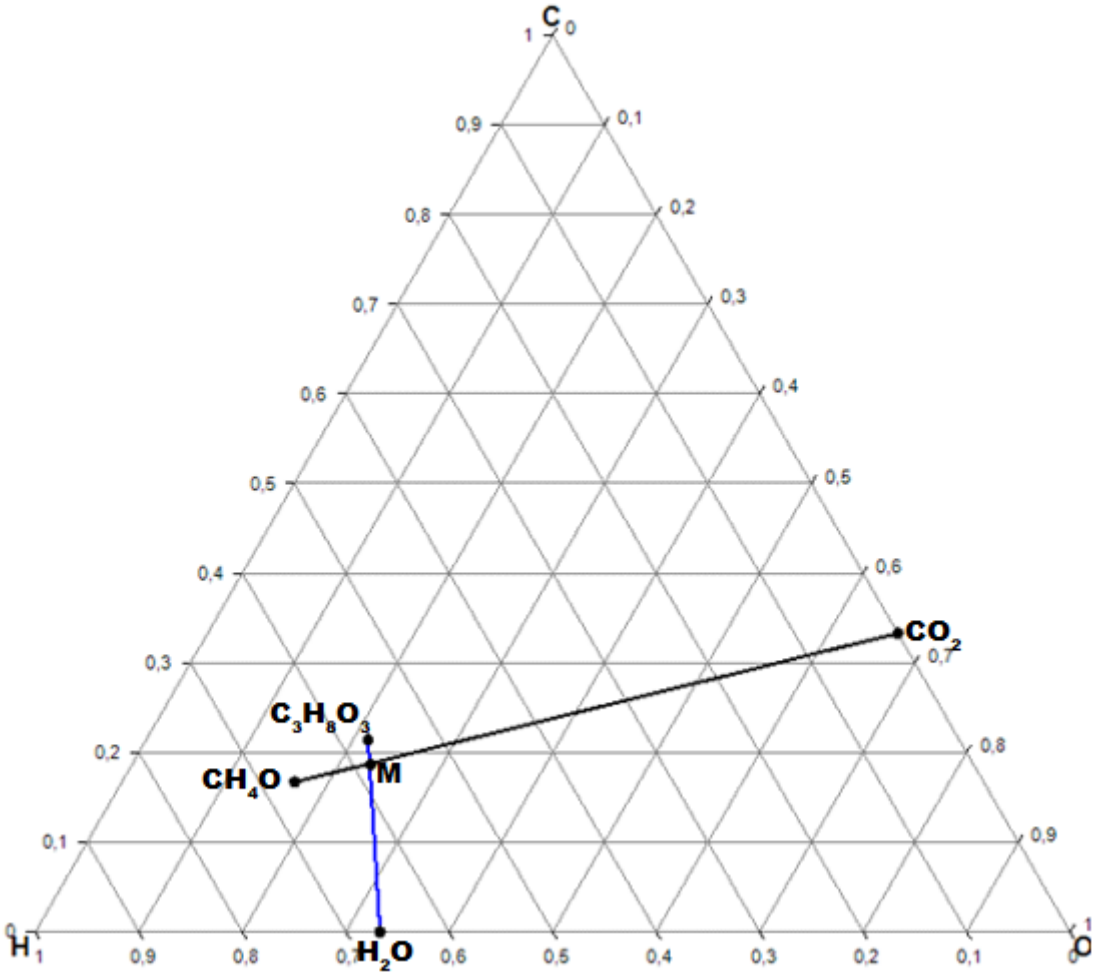

Figure 3. 5: Methanol synthesis from glycerol

To determine the minimum amounts of carbon dioxide, water as well as the amount of glycerol, the following steps are followed:

Step 1: Determine the distance between reactants and products. These distances, expressed in millimetres, are determined using Adobe Acrobat Reader DC measuring tool.

Figure 3.6 shows that streamline $C_3H_8O_3$- H_2O has two-line segments viz. $C_3H_8O_3$-M and M-H_2O. To determine the distance between $C_3H_8O_3$ and M, one must subtract M-H_2O from $C_3H_8O_3$- H_2O. The values of these line segments are shown in figure 3.6

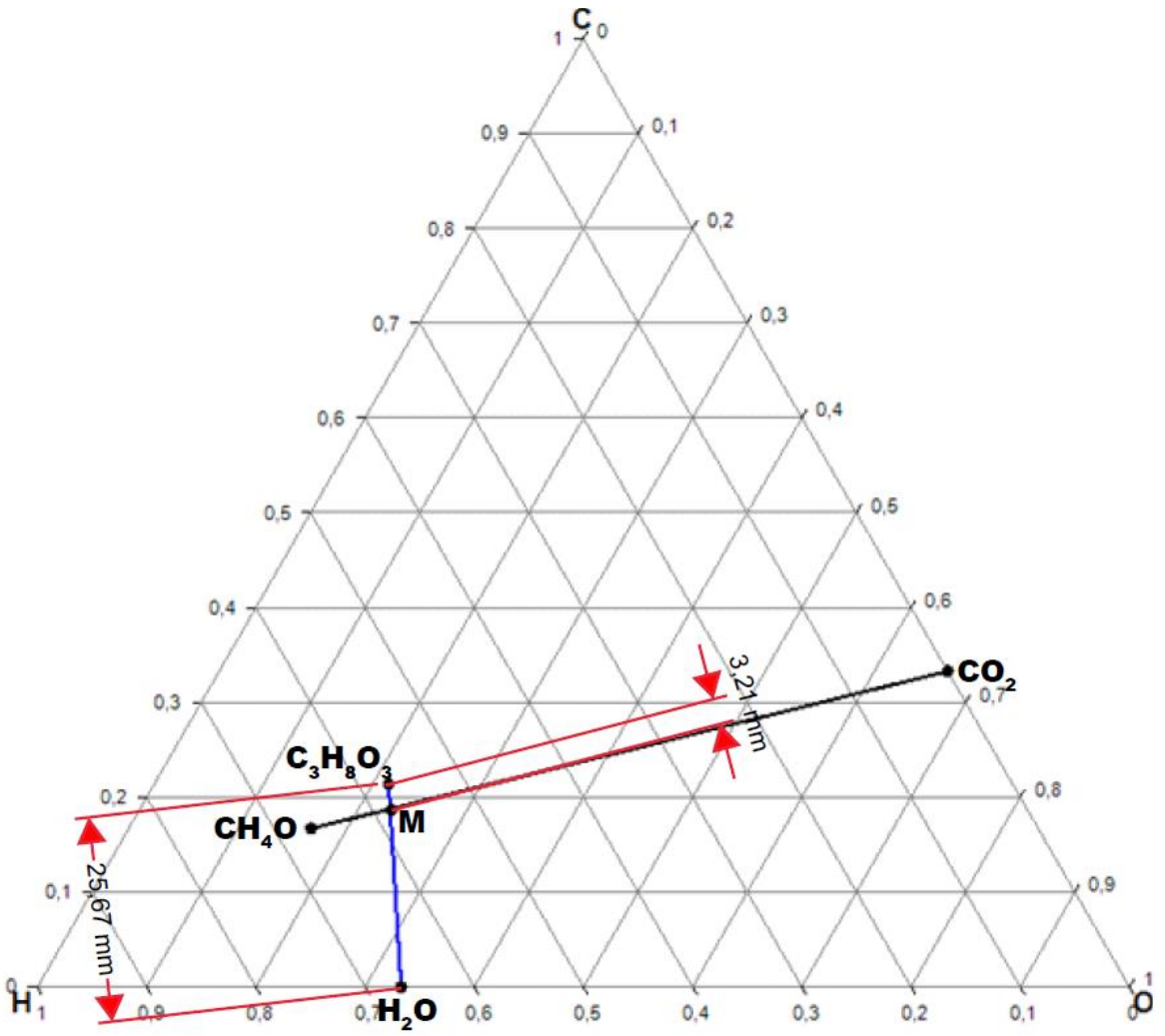

Figure 3. 6: Distance between reactants

Figure 3.7 shows the distance between CH_4O and CO_2 as well as the distance between M and CH_4O. The distance from M to CO_2 can be calculated by subtracting distance CH_4O- M from CH_4O-CO_2.

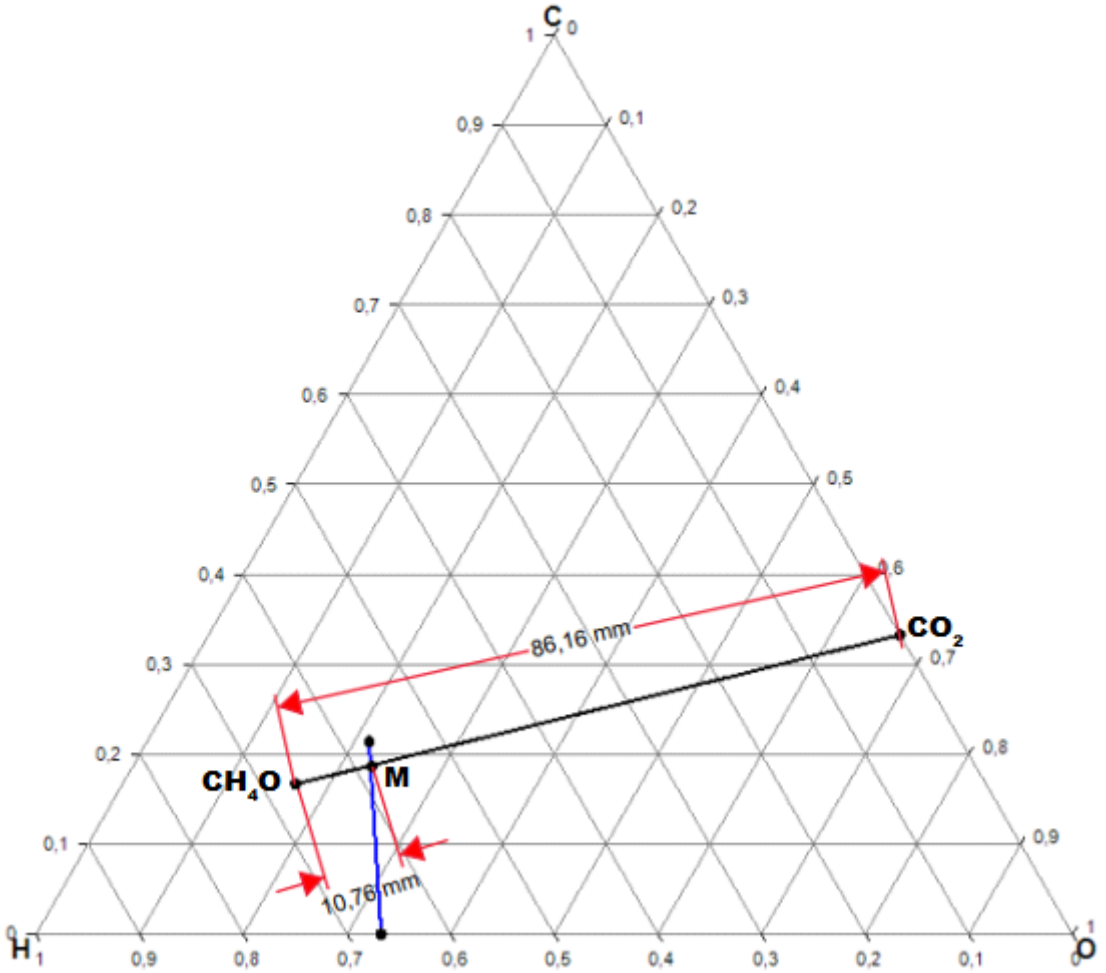

Figure 3. 7: Distance between products

Step 2: Calculate the relative distance of different species using the following equations.

$$D_{H_2O} = \frac{C_3H_8O_3 - M}{C_3H_8O_3 - H_2O} \quad \text{3.6i}$$

$$D_{C_3H_8O_3} = \frac{M - H_2O}{C_3H_8O_3 - H_2O} \quad \text{3.6ii}$$

$$D_{CH_4O} = \frac{M - CO_2}{CH_4O - CO_2} \quad \text{3.6iii}$$

$$D_{CO_2} = \frac{M - CH_4O}{CH_4O - CO_2} \quad \text{3.6iv}$$

Equations 3.6i, 3.6ii, 3.6iii and 3.6iv represent the respective distance of H_2O, $C_3H_8O_3$, CO_2 and CH_4O relative to point M. These distances are shown in figure 3.8.

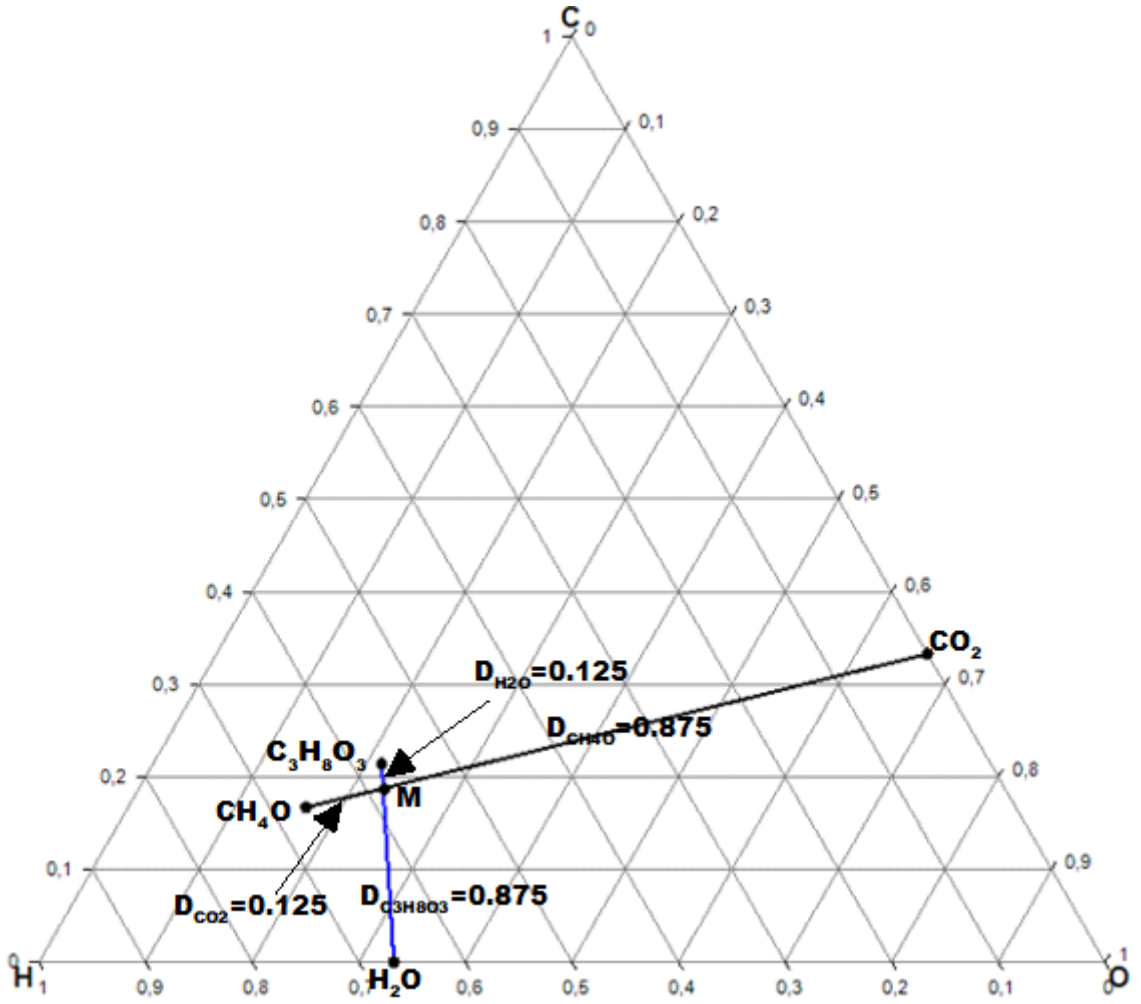

Figure 3. 8: Relative distance of H_2O, $C_3H_8O_3$, CO_2 and CH_4O relative to point M

Step 3: Determine the stoichiometric coefficient (SC) of each species

A relationship developed by Tay *et al.* (2011) can be used to determine the stoichiometric coefficient (SC) of each species. Equation 3.7 shows this relationship.

$$\frac{\text{Length of } D_{CH}}{\text{Total length between reactants or prodcuts}} = \frac{\text{SC x number of atoms in CH}}{\text{total number of atoms for all reactants or prodcuts}} \quad 3.7$$

Where, CH: Any reactant or product under consideration (in this case CH = glycerol, carbon dioxide and water).

SC: stoichiometric coefficient of species CH

The stoichiometric coefficients of H_2O, $C_3H_8O_3$, and CO_2 are calculated using equation 3.7 by considering 1 kmol of CH_4O. H_2O consists of 3 atoms, $C_3H_8O_3$ (14 atoms) and CO_2 (3 atoms). Calculations are shown in Appendix A. This overall process is represented by equation 3.8

$$0.4857C_3H_8O_3 + 0.2857H_2O \implies 1CH_4O + 0.2857CO_2 \quad 3.8$$

Figures 3.6, 3.7 and 3.8, illustrate that CHO ternary diagrams can be used as synthesis tools to determine the targets during the synthesis of glycerol biorefinery.

Atomic species balances can also be used as an accurate tool for the synthesis of a chemical process (Patel, 2007). Considering the same example (3.1), it is established that the lever rule and atomic balance yield same results. The calculations in terms of atomic balance are shown in Appendix B.

3.5 Thermodynamic equilibrium in CHO ternary diagrams

In previous sections, it was shown that one can use CHO ternary diagrams to determine the performance of a biorefinery at early stages. In other words, using a CHO ternary diagram insight-based approach one can determine the amount of raw materials required to produce a certain product as well as the amount of waste that can be generated from a particular process. It is also possible to use chemical and thermodynamic equilibria to set targets for a biorefinery during the early-stage design. For example, once the overall process is known one can use Gibbs energy as well as equilibrium constant to determine its spontaneity and feasibility. One can also use these thermodynamic tools (Gibbs energy and equilibrium constant) to determine the equilibrium composition of a particular chemical species (Kyle, 1984). For example, one can use Gibbs energy as well as the equilibrium constant to calculate the syngas equilibrium composition from biomass gasification at different temperatures.

The main objective of this study is to use CHO ternary diagrams (insight-based approach) to design a glycerol-based biorefinery via reforming pathway. To represent glycerol reforming on these CHO ternary diagrams, it is crucial to start by calculating the chemical equilibria. The next section discusses various thermodynamic aspects that will be used in calculating the chemical equilibria for CHO ternary diagrams.

3.5.1 Relationship between Gibbs energy and Equilibrium constant

Gibbs energy (ΔG) is a powerful tool used in process synthesis to identify the equilibrium state of the process (Koukkari, 2014). A process designer can use ΔG to determine whether a process is spontaneous or non-spontaneous. A positive of value of ΔG indicates that the process is non-spontaneous (reactants favoured at equilibrium) whereas a negative value of ΔG indicates that a process is spontaneous (products favoured at equilibrium). If $\Delta G = 0$, then products and reactants are favoured equally (Denbigh, 1981).

For a given process, Gibbs energy ΔG is related to the equilibrium constant (Ke) using equation 3.9 (Snoeyink and Jenkins, 1980).

$$\Delta G = \Delta G^{o} + RT\ lnQ \qquad 3.9$$

Where; ΔG^{o} is the standard Gibbs energy at standard conditions (kJ/mol)

T: absolute temperature (K)

R: gas constant (8.314 J/mol·K)

Q: reaction quotient = concentration of the products divided by the concentration of reactants

At equilibrium Q = Ke

Equation 3.9 becomes

$$lnKe = -\frac{\Delta G^{o}}{RT} \qquad 3.10$$

If ΔG is negative ($\Delta G < 0$), then Ke is positive ($Ke > 1$), this means that at equilibrium the products are more favoured over the reactants in other words, products are greater than the reactants at equilibrium. If ΔG is positive ($\Delta G > 0$), then Ke is negative ($Ke < 1$), this means that at equilibrium the products are less favoured over the reactants in other words, reactants are greater than products at equilibrium. If ΔG =0, and Ke =1, this means that at equilibrium neither the products nor the reactants are favoured (*ibid*).

The process designer can quickly determine whether a chemical process will take place and proceed to completion or not by checking the value of the Gibbs energy or the equilibrium constant (Ke). Any chemical process having an equilibrium constant less than 10^{-3} is unlikely to take place while processes with $Ke > 10^{3}$ are assumed to take place and proceed completely (Natarajan, 2014).

The equilibrium constant can also be expressed in terms of fugacity. Consider an ideal gas (j), the fugacity (f_j^{o}) and standard pressure ($P_j^{o} = 1$ atm)of this gas are equal. The equilibrium constant can now be expressed as follows (Walas, 1985).

$$Ke = \prod_i \left(\frac{\hat{f_j}}{P_j^{o}}\right)^{v_j} \qquad 3.11$$

It is known that

$$\hat{f_j} = \hat{\emptyset_j} P \qquad 3.12$$

Where $\hat{\emptyset_j}$ the fugacity coefficient

Equation 3.12 becomes

$$Ke = \prod_i \left(\frac{\hat{\emptyset_j} x_j P}{P_j^o} \right)^{v_j} \qquad 3.13$$

Where x_j the mole composition of ideal gas j

For an isobaric process ($P = P_j^o = 1$) and $\hat{\emptyset_j} = 1$, equation 3.13 becomes

$$Ke = \prod_i (x_j)^{v_j}$$

Where x_j and v_j the respective mole composition and stoichiometric coefficient of ideal gas j.

Consider now a typical gas phase chemical reaction where A and B are the reactants while C and Dare the products.

$$a\,A + b\,B \leftrightarrow c\,D + d\,D \qquad 3.14$$

The equilibrium constant of this reaction in terms of mole composition can be expressed as follows

$$Ke = \prod_i (x_i)^{v_i} = (x_A)^{-a} (x_B)^{-b} (x_C)^{c} (x_D)^{d} \qquad 3.15$$

3.5.2 Stoichiometric method to calculate the chemical equilibrium for glycerol reforming process

Reforming process is considered as one of the main processes used to produce syngas from glycerol. During this process, various chemical reactions take place, which produce different species (Schwenber *et al.*, 2016). The equilibrium composition of these different species can be determined using the stoichiometric method (as described in Chapter 2). This method plays a significant role in process synthesis because it uses chemical reactions to relate all these different species at equilibrium. Once these chemical reactions are known, the process designer can use CHO ternary diagrams to evaluate the composition of different species at equilibrium. There are four steps that are used to calculate the chemical equilibria for glycerol reforming via stoichiometric model (Kyle, 1984). These steps are summarized below.

1. Different species present at equilibrium (in significant composition) must be determined

2. Use phase rule to determine the degree of freedom, number of independent components and reactions
3. Give a mathematical formulation to the problem
4. Solve the mathematical problem

3.5.2.1 Using Gibbs energy to determine the predominant species at equilibrium

The CHO ternary systems are used together with Gibbs energy to determine the number of chemical species that are predominant at equilibrium in a particular chemical system. The Gibbs energy of different chemical species that can be formed during glycerol as well as a mixture of glycerol-LLDPE reforming are given in table 3.1 at a temperature range of 500-1500K.

Table 3. 1: Change in the Gibbs energy of formation for species involved in glycerol reforming at equilibrium (Yaws. 1999)

Temperature K	Gibbs Energy (ΔG_f^o) kJ/mol							
	CO	CO_2	CH_4	C(s)	H_2O	H_2	C_2H_4	C_2H_6
500	-155.6	-394.9	-32.60	0	-219.0	0	76.96	5.220
650	-169.2	-395.3	-18.01	0	-211.4	0	84.72	35.14
800	-182.7	-395.6	-2.56	0	-203.5	0	92.58	66.26
950	-196.2	-395.8	13.74	0	-195.3	0	100.5	98.60
1050	-205.1	-395.9	25.07	0	-189.7	0	106.0	120.83
1200	-218.5	-396.0	42.77	0	-180.9	0	114.0	155.20
1350	-231.7	-396.1	61.31	0	-171.8	0	122.2	190.74
1500	-244.9	-396.1	80.695	0	-162.4	0	130.5	222.75

Referring to table 3.1, it is apparent that both water and carbon dioxide molecules have a more negative Gibbs energy of formation values at high temperatures. This means they are predominantly present at equilibrium. All chemical species having positive Gibbs energy of formation values are present in insignificant quantities at equilibrium. In this case, C_2H_6 and C_2H_4 are considered not to be in significant quantities at equilibrium and therefore they are discarded (Kyle, 1984). At standard conditions, the Gibbs energy of formation of any chemical element or diatomic gases is always zero (Snoeyink and Jenkins, 1980). That is why, looking at table 3.1, the Gibbs energy of formation of H_2 and C(s) is zero. This implies that at

equilibrium only 6 chemical species are present in significant quantities (H_2, CO, CH_4, H_2O, CO_2, and C(s)) during glycerol reforming.

The CHO ternary diagram can also be used to determine these species predominating at equilibrium. Cairns and Tevebaugh. (1964) divided the CHO triangle into four areas to indicate in which area a particular chemical species should be present in a significant quantity. Figure 3.9 shows these different areas.

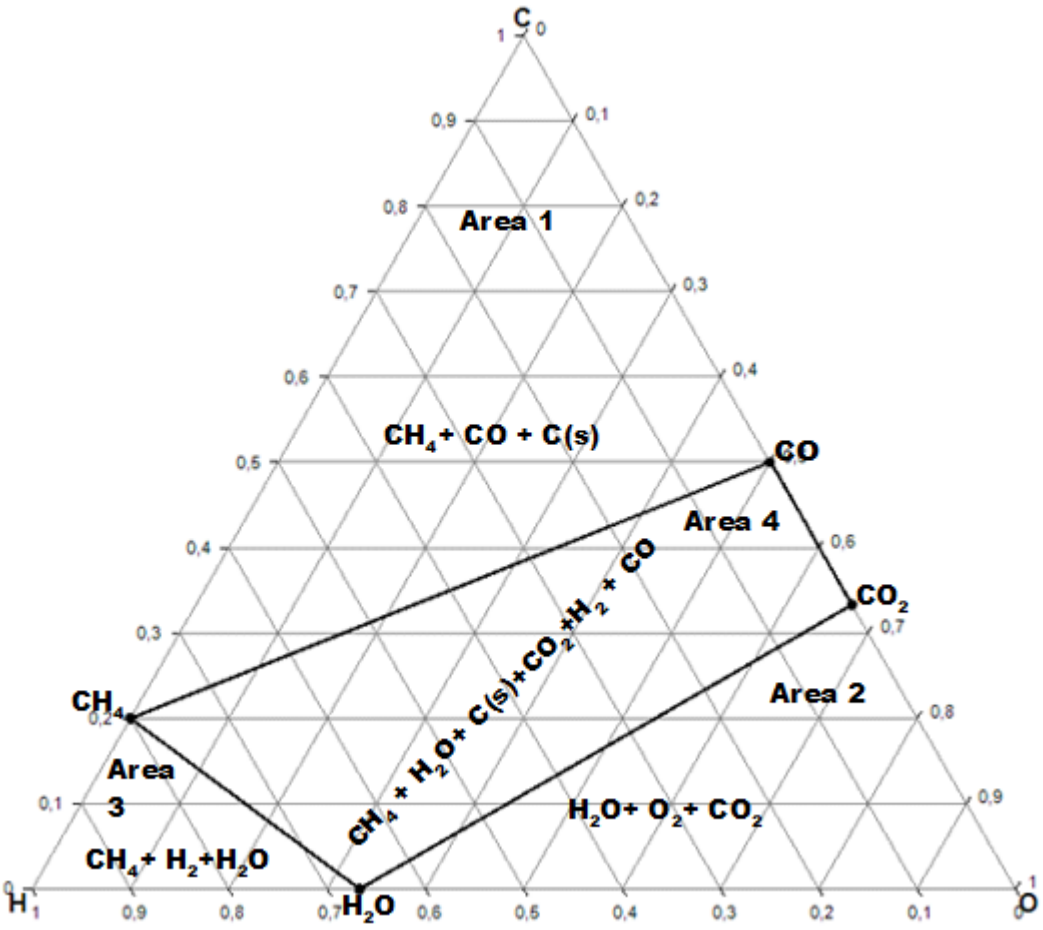

Figure 3. 9: Different regions in a CHO ternary diagram (ibid)

Area 1 is where solid carbon is present in significant amount; hydrogen and oxygen in this area exist as methane and carbon monoxide respectively. Area 2 is the area where oxygen predominates whereas hydrogen and carbon exist as a water molecule and carbon dioxide respectively whereas Area 3 shows that hydrogen is predominant, and carbon and oxygen are present as methane and water respectively. All species (excluding oxygen) are present at equilibrium in significant amounts in Area 4. Oxygen is considered as non-predominant in this

area since the Gibbs energy for the formation of H_2O and CO_2 are extremely negative. This makes the partial pressure of O_2 extremely low in this area. Therefore, based on these insights, only 6 species are present at equilibrium in significant composition.

The Gibbs energy and the CHO ternary systems give similar chemical species that are predominant at equilibrium. Since the number of chemical species is now known, it is now crucial to determine the number of independent reactions. This can be done by using Gibbs phase rule.

3.5.2.2 Gibbs phase rule and determination of independent components

Gibbs phase rule is a powerful tool used to determine the degree of freedom of any system that consists of multiple phases (multiphase system). This multiphase system should be at thermodynamic equilibrium. Due to this rule, there exists a relationship between the number of intensive thermodynamic properties which are independent and the number of phases for a specific system. At equilibrium, the phase rule can be described by the following mathematical expressions presented in Equations 3.16-3.18 (Denbigh, 1981):

$$F = 2 - \pi + C \qquad 3.16$$

Where; π is the number of phases that are present in the system, C is number components present in the system, and F is the number of degrees of freedom

The phase rule can be written in the following manner, in terms of species, and for the case of a reaction:

$$F = 2 - \pi + N - r \qquad 3.17$$

Where, r is the number of independent reactions and N the number of species present in the systems at equilibrium

Thus, the relationship between N and C.

$$C = N - r \qquad 3.18$$

To determine the degrees of freedom, the number of components and independent reactions must be determined first.

The number of independent components can be found from the atomic matrix of different species present at equilibrium. The chemical elements (atoms) form the columns and the chemical species form the rows. The rank of the formed matrix is equal to the number of

independent components. In the previous section, it was determined that the number of chemical species present at equilibrium during the reforming of glycerol is 6. Using these 6 species a matrix can be set as shown in table 3.2

Table 3. 2: Atomic matrix during the reforming of glycerol

Species	system atoms		
	C	H	O
CO_2	1	0	2
CO	1	0	1
CH_4	1	4	0
H_2	0	2	0
C	1	0	0
H_2O	0	2	1

The rank of this matrix can be solved easily since it has only three columns. The rank is found to be 3.

As stated earlier, the rank of a matrix corresponds to the number of independent components, therefore, the number of independent components C equals to 3. The number of independent chemical reactions is the only parameter remaining to determine the degree of freedom.

3.5.2.3 Calculation of independent chemical reactions

Using equation 3.18, the number of independent chemical reactions is calculated and found to be 3. This means that there are 3 independent reactions in the system. It must be noted that, in this case, the formation of solid carbon is taken into consideration. In the case where carbon formation is considered as negligible, the set of independent reactions becomes 2 (Mountouris *et al*., 2006). These three independent reactions can be used to find the equilibrium composition of the CHO ternary diagram with solid carbon deposition (Tassios, 1993).

It therefore follows that the degree of freedom is 3, which means that three variables can be used to define the system at equilibrium. These variables can be temperature, pressure and one material balance constraint. The material balance constraint can be selected as one mole of the total reactant that contains a fixed O/H, H/O, C/O or C/H ratio. Any of these three elemental

ratios can be used to relate the chemical species mole fraction (x) for the reforming of glycerol at equilibrium. In this study $\frac{H}{O}$ ratio is chosen.

Schwenber *et al*. (2016) give a summary of different chemical reactions that occur during glycerol reforming. However, the Gibbs phase rule revealed that from these different reactions, only three are independent and should contain all the six-chemical species. Appendix C shows how the three independent chemical reactions are determined. Reaction 1 is commonly known as a water- gas reaction and reaction 2 is known as a hydrogasification reaction (Basu. 2013). Reaction 3 is commonly known as Boudouard reaction (Ptasinski. 2015).

The three set of independent reactions are:

$$CO(g) + H_2O(g) \leftrightarrow CO_2(g) + H_2(g) \quad (1)$$

$$C(s) + 2H_2(g) \leftrightarrow CH_4(g) \quad (2)$$

$$2CO(g) \leftrightarrow C(s) + CO_2(g) \quad (3)$$

These three independent reactions contain all the six chemical species that are predominant at equilibrium and hence their equilibrium composition can be calculated. Tay *et al*. (2011) point out that any set of independent reactions that are used to represent the chemical species at equilibrium provide similar equilibrium composition. Methane decomposition, heterogeneous water-gas shift and water gas shift reactions were used to compute the mole fractions of major species at equilibrium *(ibid)*.

Determine the Gibbs energy of each independent reaction

Since all three independent reactions are now known, a thermodynamic analysis can be conducted by considering the Gibbs energy at different temperatures and a pressure of 1 atm. Using the Gibbs energy of each species in table 3.1, the following equation is used to determine the Gibbs energy of each reaction.

$$\Delta G_{reaction} = \sum n\,(\Delta G_f)_{products} - \sum n\,(\Delta G_f)_{reactants} \quad 3.19$$

Figure 3.10 shows the change in Gibbs energy of reaction 1,2 and 3 as a function of temperature.

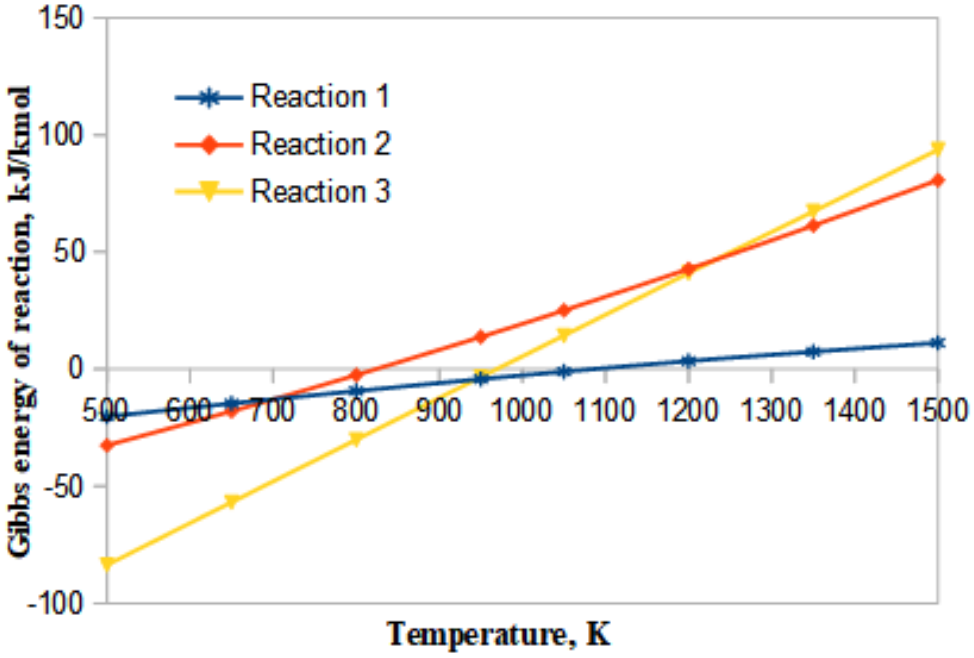

Figure 3. 10: Gibbs energy of the independent reactions at different temperatures

Figure 3.10 reveals that from 500 K to 1050 K reaction 1 is spontaneous (products favoured). At 1200 K up to 1500 K this reaction is no longer spontaneous, and reactants are favoured. However, it should be noted that the change in Gibbs energy over the temperature range is not very significant. Reaction 2 is spontaneous from 500 up to 800 K (products favoured) and becomes reactants favoured from 950 up to 1500 K. Reaction 3 becomes non- spontaneous (reactants favoured) from 1050 K until it reaches 1500K but at a temperature from 500 K up to 800 K it is a spontaneous reaction (products favoured).

3.5.2.4 Mathematical formulation

Determine the equilibrium constant of each independent reactions

One can now determine the equilibrium constants of the three independent reactions. The equilibrium constant for each independent reaction can be expressed in terms of partial pressure of each species as follows

$$K_{P1} = \frac{p_{H_2} p_{CO_2}}{p_{CO} p_{H_2O}} \qquad 3.20i$$

$$K_{P2} = \frac{p_{CH_4}}{(p_{H_2})^2} \qquad 3.20ii$$

$$K_{P3} = \frac{p_{CO_2}}{(p_{CO})^2} \qquad 3.20iii$$

Using Dalton's law, the following is obtained

$$P_t = \sum p_i \qquad 3.20iv$$

Where P_t the system total pressure and p_i the partial pressure of each chemical species

Expressing the partial pressure in terms of mole fraction and total pressure, the following relationship is obtained

$$P_i = x_i P_t \qquad 3.20v$$

Introducing equation 3.20v in 3.20i, 3.20ii and 3.20iii, the equilibrium constants of the three independent reactions can be expressed as follows

$$K_{eq\,1} = \frac{x_{H_2} x_{CO_2}}{x_{H_2O}\, x_{CO}} \qquad 3.21i$$

$$K_{eq\,2} = \frac{x_{CH_4}}{(x_{H_2})^2} \qquad 3.21ii$$

$$K_{eq\,3} = \frac{x_{CO_2}}{(x_{CO})^2} \qquad 3.21iii$$

It is known that,

$$\ln K_{eq} = \frac{-\Delta G}{RT} \qquad 3.21iv$$

The equilibrium constant of all the chemical species present at equilibrium at different temperatures can be determined. Table 3.3 shows the equilibrium constants of all three independent reactions as a function of temperature.

Table 3. 3: Equilibrium constants of the three independent reactions as a function of temperature

Temp, K	$\mathbf{K_{eq-1}}$	$\mathbf{K_{eq-2}}$	$\mathbf{K_{eq-3}}$
500	132.95	2545.30	$5.8\ 10^8$
650	15.18	28.022	37421.47
800	4.096	1.470	93.691
950	1.716	0.1755	1.537
1050	1.140	0.05660	0.1960
1200	0.712	0.01375	0.01640
1350	0.517	0.0035	0.00250
1500	0.4066	0.0015	0.00054

The equilibrium constants of all three reactions decrease with an increase in temperature. This is because all three reactions are exothermic in the forward reaction at all temperatures and according to the Le Chatelier's principle, increasing the temperature will move the equilibrium position of all three reactions in the reverse direction. In other words, an increase in temperature will result in more CO and H_2O being produced from reaction 1 and similarly, more H_2 and less CH_4 will be produced from reaction 2. In terms of reaction 3, there will be more CO and less CO_2 generated when the temperature is increased. When calculating the equilibrium composition of these different species, it is expected that more CO and H_2 and less methane, water, and carbon dioxide will be produced at high temperatures.

Linking atomic ratio to mole fractions of the 5 species

The only parameter remaining to calculate the gaseous equilibrium compositions of the different chemical species is the atomic ratio. It is known that the sum of mole fraction of all chemical species present in a system is always 1. This is expressed by equation 3.22i and 3.22 ii

$$\sum x_i = 1 \qquad 3.22i$$

$$x_{CH_4} + x_{CO} + x_{CO_2} + x_{H_2O} + x_{H2} = 1 \qquad 3.22ii$$

The atomic ratios can be summarized as follows.

$$\frac{H}{O} = \frac{4x_{CH_4} + 2\,x_{H2O} + 2x_{H2}}{x_{CO} + 2x_{CO_2} + x_{H_2O}} \qquad 3.22iii$$

$$\frac{C}{H} = \frac{x_{CH_4} + x_{CO} + x_{CO_2}}{4x_{CH_4} + 2x_{H_2O} + 2x_{H2}} \qquad 3.22iv$$

$$\frac{C}{O} = \frac{x_{CH_4} + x_{CO} + x_{CO_2}}{x_{CO} + 2x_{CO_2} + x_{H_2O}} \qquad 3.22v$$

Simultaneously solving equations 3.21i-3.22v, the equilibrium compositions of the major chemical species can be determined at a fixed atomic ratio. In this case, a ratio of $\frac{H}{O}$ is selected. To fully analyse the thermodynamic equilibrium of the CHO ternary diagrams, various H/O ratios should be used. The different H/O ratios used in this study are shown in (Appendix E)

Starting with a temperature of 500K and a $\frac{H}{O}$ = 0.0 at system pressure of 1 atmosphere, the following equation is obtained.

$$\begin{Bmatrix} 132.95\,\mathrm{x_{H2O}}x_{\mathrm{CO}} - \mathrm{x_{H_2}}x_{\mathrm{CO_2}} = 0 \\ 2545.3\left(\mathrm{x_{H_2}}\right)^2 - x_{\mathrm{CH_4}} = 0 \\ 5.8x10^8(\mathrm{x_{CO}})^2 - x_{\mathrm{CO_2}} = 0 \\ \mathrm{x_{CH_4}} + \mathrm{x_{CO}} + \mathrm{x_{CO_2}} + \mathrm{x_{H_2O}} + \mathrm{x_{H_2}} = 1 \\ 4\mathrm{x_{CH_4}} + 2\mathrm{x_{H_2O}} + 2\mathrm{x_{H2}} = 0 \end{Bmatrix}$$

3.5.2.5 Solving the problem

The above system of nonlinear and linear equations was solved using Wolfram Mathematica software with the following constraints: $x_i \geq 0$ and the solution is provided in Appendix D.

The amount of syngas/gaseous product can be determined by using equation 3.23 (Tay *et al.*, 2011). It must be noted that this equation is directly applied to glycerol.

$$\mathrm{n_{snygas}}[\mathrm{x_{CO}}(\mathrm{A_{CO}}) + \mathrm{x_{CO2}}(\mathrm{A_{CO2}}) + \mathrm{x_{CH4}}(\mathrm{A_{CH4}})] + \mathrm{mA_C} = \mathrm{A_{C_3H_8O_3}} \quad 3.23$$

Where, n the molar quantity of syngas/gaseous product per molar quantity of glycerol, x the mole fraction of CO, CO_2 and CH_4, A: number of carbon atoms and m the amount of carbon deposited (if any).

A similar approach is used to determine the equilibrium mole fractions of different chemical species at 500K, 650, 800, 950, 1050, 1200, 1350, and 1500K at different atomic ratios. The results are tabulated under Appendix E (table E.1). It must be noted that the selection of H/O ratios was not done randomly because there are certain H/O ratios in a range of 0 to 78 at which the solution to the non-linear systems could not be possible. For example, at a temperature of 500K and an H/O in the range of 0.001-0.02588, the solution of the non-linear system was not found.

3.6 Carbon deposition boundaries in CHO ternary diagrams

3.6.1 Background

One of the main challenges faced by chemical process industries is the undesired formation of carbon deposition from gaseous mixtures of carbon-hydrogen-oxygen (Jaworski and Pianko-Oprych, 2017). When designing a biorefinery via a thermochemical route, it is crucial to know at which conditions carbon deposition/precipitation may occur. A useful way to predict the formation of carbon deposition in CHO ternary systems is by means of triangular coordinates (Cairns and Tevebaugh. 1964). The ratios of the three atoms can predict whether carbon will form or not from a given feed composition (ibid).

Figure 3.11 gives an illustration of a carbon deposition boundary by using a CHO ternary diagram. Points B, R, and D represent the carbon deposition boundary. Consider point N which represents a chemical species, since this chemical species lies above curve BRD (carbon deposition boundary), at equilibrium the system will consist of two phases viz. solid (carbon) and gas phase. The equilibrium composition of this gas phase can be determined at point R. One can employ the lever-arm rule to determine the distance of point R and C relative to point N. Also consider the oxidation of methane (CH_4). The composition of this reaction moves from methane towards oxygen (O_2). Point A represents the system at equilibrium which consists of solid carbon and gas phase. The equilibrium composition of this gas phase can be determined at point B. Point D represents the amount of oxygen required to convert methane into gaseous species without carbon deposition. This amount can be determined by using the lever-arm rule. Lastly, CH_4-O_2 and CO_2-H_2O streams intersect at point Q. At this point, methane undergoes a complete combustion to produce CO_2 and H_2O with no carbon deposition.

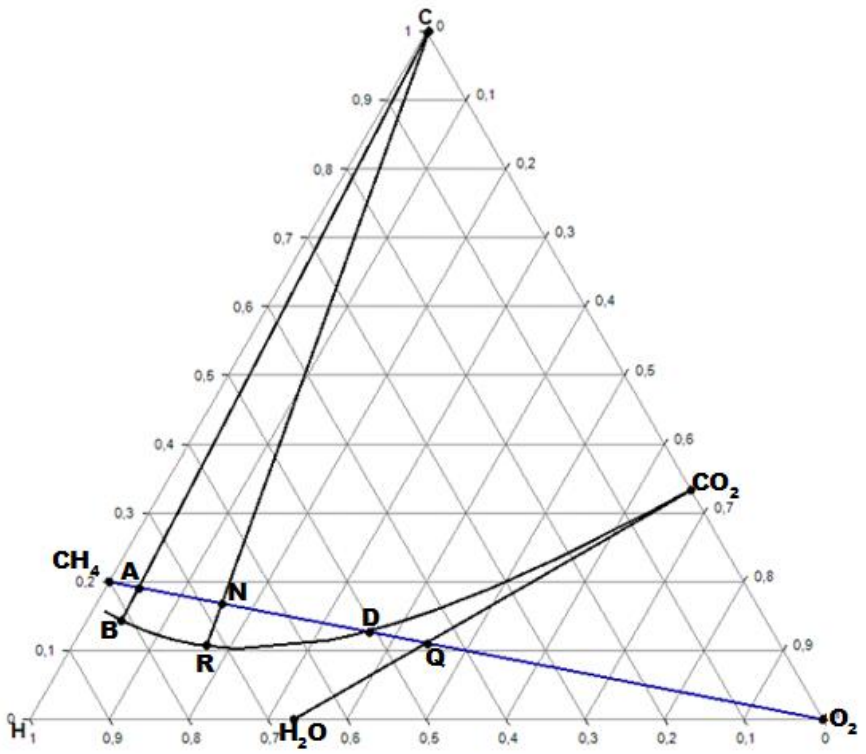

Figure 3. 11: Carbon deposition boundary for a CHO ternary system, (Kyle, 1984)

3.6.2 Conversion of equilibrium gaseous compositions into atomic percentages

To determine the carbon deposition boundaries inside a CHO ternary diagram at different temperatures, syngas equilibrium compositions are converted to an atomic ratio. It must be noted that Boudouard and hydrogasification reactions are the two selected reactions that

describe the formation of solid carbon. Equations 3.24i-3.24iii describe the conversion of the mole fractions into atomic ratios (C, H, and O).

$$H = 0.8x_{CH_4} + 0.667x_{H_2O} + x_{H_2} \quad 3.24i$$

$$O = 0.333x_{H_2O} + 0.5x_{CO} + 0.667x_{CO_2} \quad 3.24ii$$

$$C = 0.2x_{CH_4} + 0.5x_{CO} + 0.333\,x_{CO_2} \quad 3.24iii$$

These atomic ratios can be plotted on a CHO ternary diagram to determine the carbon deposition boundary at different temperatures. These ratios are tabulated in Appendix E (table E.2).

3.6.3 Using CHO ternary diagrams for the synthesis of a glycerol-based biorefinery

After determining the carbon deposition boundaries on the CHO ternary diagram at different temperatures, glycerol reforming processes can be analysed. From this analysis a glycerol-based biorefinery can be synthesized. It is also possible to study the reforming of other different compounds such as a mixture of glycerol and linear low-density polyethylene plastics (LLDPE) on these CHO ternary diagrams.

3.7 Evaluating the sustainability of a glycerol biorefinery

Various transformation pathways occur within a biorefinery, so it is important to evaluate its sustainability at an early stage. This will help the process designer screen out unnecessary alternatives. There are different tools that are used in evaluating a biorefinery sustainability (Zheng *et al.,* 2012). This study only considers 5 tools viz. Gibbs energy, atom economy, economic potential, carbon efficiency, and E-factor. Gibbs energy is used to analyse the thermodynamic feasibility of a process. It tells the designer whether a given reaction/alternative is thermodynamically feasible or not. Equation 3.19 can be used to determine the Gibbs energy at 298K. The second tool is the economic potential (EP). The process designer can calculate the profitability of each alternative by using equation 3.25i.

$$EP = \sum n_i P_{\text{product i}} - \sum n_j P_{\text{reactant j}} \quad 3.25i$$

Where; n and P are the stoichiometric coefficient and price of a chemical species.

An alternative is judged not economically feasible or profitable, if $EP < 0$ and if $EP > 0$, then the alternative is deemed profitable.

A biorefinery sustainability can also be evaluated by calculating the atom economy of each alternative. Consider a process whereby species A is the reactant and B is the product while C is the waste. The atom economy can be calculated using equation 3.25ii.

$$\%\ \text{atom economy} = \frac{\text{b}\,M_B}{\text{a}M_A} \times 100 \qquad 3.25\ \text{ii}$$

Where a and b the stoichiometric coefficients of A and B respectively, M_B and M_A the respective molecular weight of B and A. If the atom economy is high, then less waste will be generated.

Lastly, carbon efficiency (%C) and e-factor can be calculated using equation 3. 25iii and 3.25 iv respectively (Patel, 2015).

$$\%C = \frac{\text{moles of C in desired product}}{\text{moles of C in the feed}} \text{x}100 \qquad 3.25\text{iii}$$

$$\text{E} - \text{factor} = \frac{\text{mass of waste}}{\text{mass of desired product}} \qquad 3.25\text{iv}$$

A low E-factor means that the process generates less waste, whereas a high carbon efficiency means that significant amount of raw materials is converted into product.

3.8 Simulation of glycerol-biorefinery using Aspen Plus

The first part of this chapter focused on how CHO ternary diagrams can be used in setting targets for a biorefinery at an early stage. It was shown that before glycerol can be represented on these CHO ternary diagrams it is important to calculate their chemical equilibria first.

The second part shows how Aspen Plus is used for the simulation of glycerol reforming. Aspen Plus is a powerful tool used to design chemical processes. Once inputs and outputs are determined by means of an insight-based approach, Aspen Plus can be used to model the flowsheet of the process. Various studies have been carried out to study glycerol reforming processes using Aspen Plus simulation. For example, Unlu and Hilmioglu (2020) studied glycerol steam reforming to produce hydrogen in Aspen Plus. Three parameters were analysed viz. temperature, pressure, and steam to glycerol ratio. It was shown that a temperature of 773 K, pressure of 1 atm, and a steam to glycerol ratio of 9:1 were the most suitable conditions to produce hydrogen. At these conditions, the mole fraction of hydrogen was observed to be 98%. Hunpinyo and Narataruksa (2016) used Aspen Plus to design a process for the synthesis of hydrogen and FT-liquid fuels from glycerol reforming using steam as a reforming agent. It was

shown that using 160 kmol/day of glycerol can produce a hydrogen yield of 75%. It was further shown that the same feed was used to generate 2692 liters per day of FT-liquid fuels (C_5-C_{20}).

The next sections discuss different steps used in the simulation of glycerol reforming as well as a mixture of glycerol and LLDPE in Aspen Plus.

3.8.1 Entering components in Aspen Plus

Aspen Plus provides different types of components such as conventional, pseudo, non-conventional, solid, and polymer components. Taking the scope of this study into consideration, only conventional and non-conventional components are considered. $C_3H_8O_3$, CO, CO_2, CH_4, H_2O, H_2, and CH_4O are considered as conventional components while linear low-density polyethylene plastics (LLDPE) is considered as non-conventional components. The proximate and ultimate analysis of LLDPE is shown in table 3.4

Table 3. 4: Ultimate and proximate analysis of LLDPE (Farooq *et al.*, 2021)

Ultimate analysis %	Proximate analysis %
C: 85.8 H: 14.2	Moisture: 0, Volatile matter: 100, Ash: 0 and Fixed carbon: 0

3.8.2 Selecting a suitable property method in Aspen Plus

One of the most important steps during the simulation of a chemical process in Aspen Plus is the selection of a suitable thermodynamic property method. The property method is divided into three main groups viz. ideal model (considers ideal liquids and gases), activity coefficient-based model, equation of state (EOS) model. Non-Random-Two-Liquid (NRTL), Universal Functional activity coefficient (UNIFAC) models are examples of an activity coefficient-based model whereas PENG-ROB (Peng-Robinson) and RK-SOAVE (Redlich-Kwong Soave) are examples of the equation of state model (Unlu and Hilmioglu, 2020). To make the correct decision when selecting a suitable thermodynamic model during the simulation of glycerol-biorefinery, Carlson (1996) and Chaves *et al*. (2016) were used as guidelines.

Unlu and Hilmioglu (2020) point out that UNIFAC, Peng-Robinson, and Redlich-Kwong Soave models are more favourable during the simulation of glycerol reforming using a plug flow reactor i.e. kinetic model. However, it is important to emphasize that the composition of products (H_2, CO, CO_2, CH_4, and H_2O) generated during glycerol reforming in a Gibbs reactor was not affected by any of these three models. The three models produce the same molar

composition of H_2, CO, CO_2, CH_4, and H_2O when a Gibbs reactor is used. This study uses Peng-Robinson as the thermodynamic model during the simulation of glycerol biorefinery in Aspen Plus. This model is advantageous for chemical processes that require high pressures (Carlson, 1996). An example of such processes is the synthesis of methanol from syngas (50-100 bars) (Mevawala et al., 2017). The accuracy of this model is validated in Chapter 4 using data from (Adhikari *et al.*, 2007).

3.8.3 Simulation of different reactors in Aspen Plus

Reactors are viewed as the most important unit operations of a chemical process. This is because raw materials are transformed into different products in a reactor. Aspen Plus provides 7 reactor models viz. stoichiometric (RStoic), yield (RYield), equilibrium (REquil), Gibbs (RGibbs), plug flow (RPlug), continuous stirred tank (RCSTR) and batch (RBatch). Only Gibbs (reforming process), Yield (decomposition of LLDPE) and Plug flow (methanol synthesis) reactors are considered in this study.

Gibbs (calculation option: calculate phase equilibrium and chemical equilibrium P= 1 bar, T= 500-1500K,) reactor uses the minimization of Gibbs energy and does not require any chemical reactions to be specified. It is assumed that all components appear as products. Because several reactions take place during glycerol reforming, this reactor is used to convert glycerol as well as a mixture of glycerol and LLDPE into syngas. To convert raw materials into products using a yield reactor (P = 1 bar, T = 800K, Yield option: component yields) in Aspen Plus, the yield of different products should be specified. This reactor does not require any chemical reactions. In this study, a yield reactor is used to decompose LLDPE before it can be mixed glycerol. A plug flow reactor requires a chemical reaction as well as its kinetics. It is assumed that this reactor operates isothermally. Different expression models are available in Aspen Plus which are used to simplify the kinetics of a given reaction. The most common expressions are the Power Law and Langmuir-Hinshelwood-Hougen-Watson (LHHW) expressions. A plug reactor is used in this study for the synthesis of methanol from glycerol-derived syngas. The next paragraphs discuss in detail how a plug flow reactor is simulated in Aspen Plus using an LHHW expression.

Consider the following example (methanol synthesis) to illustrate how LHHW expression can be used in Aspen Plus:

$$\mathrm{CO_2(g) + 3H_2(g) \leftrightarrow CH_4O(g) + H_2O(g)} \qquad 3.26i$$

The rate law of equation 3.26ii in terms of CH_4O can be written as follows (Van-Dal and Douallou, 2013).

$$r = \frac{k_1 P_{CO_2} P_{H_2} - k_2 \frac{P_{CH_4O} P_{H_2O}}{P^2_{H_2}}}{\beta^3} \qquad 26.ii$$

Where $\beta = 1 + k_3 \frac{P_{H_2O}}{P_{H_2}} + k_4 P^{1/2}_{H_2} + k_5 P_{H_2O}$

This rate law equation has two expressions viz. driving force (numerator) and absorption expression (numerator). This equation must be rearranged so that Aspen Plus can recognize it. The different constant values from these expressions are shown in table 3.5 (ibid).

Table 3. 5: LHHW kinetic parameters for equation 3.26i

Parameter	A	B	C	D
k_1	-29.87	4811.2	0	0
k_2	17.55	-2249.8	0	0
k_3	8.147	0	0	0
k_4	-6.452	2068.4	0	0
k_5	-34.951	14928.9	0	0
$k_1 K_{b1}$	17.549	-2645.966	0	0

Table 3.5 can be used to enter the kinetics of equation 3.26i in Aspen Plus. It must be noted that, the driving force of this reaction contains two terms, and the adsorption expression contains four terms.

3.8.4 Process descriptions

The following section gives the description of different processes that are simulated in Aspen Plus. Firstly, CHO ternary diagrams are used to determine the inputs and outputs of these processes as well as operating conditions before Aspen Plus simulation can be carried out. Figure 3.12 (a & b) shows how Aspen Plus is used for the simulation of 1 kmol of glycerol using H_2O and CO_2 as a reforming agent respectively. The flowsheet consists of three main unit operations viz. heater (to convert water into steam), reactor (Gibbs reactor) and a separator (to separate water from syngas). In this case it is assumed that all components are present in product stream ($C_3H_8O_3$, H_2, H_2O, CO_2, CO, and CH_4). Streams GLY, H_2O and CO_2 contain pure glycerol, H_2O, as well as CO_2. Water is heated and transformed into steam. All three

streams are now fed into Gibbs reactor to convert glycerol into syngas. The reactor outlet stream PROD contains H_2, CO, CH_4, CO_2, and H_2O. The pressure inside the reactor is maintained at 1 bar. The separator operates at 298K. If stream CO_2 is zero, then the process becomes glycerol steam reforming.

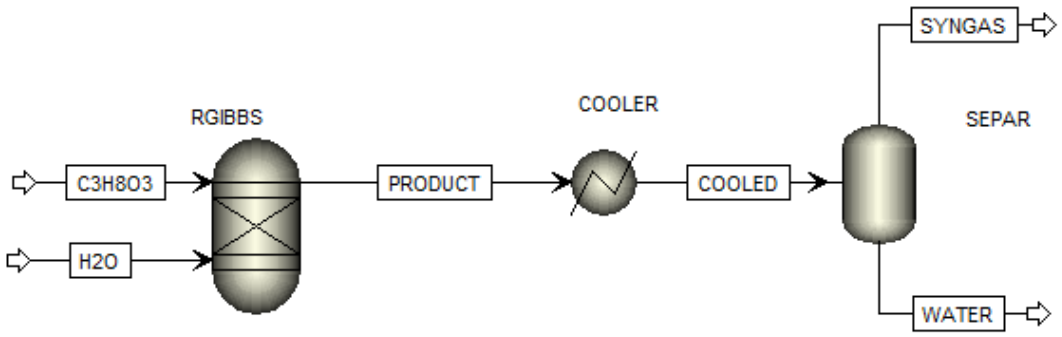

(a) Aspen Plus flowsheet for glycerol steam reforming process

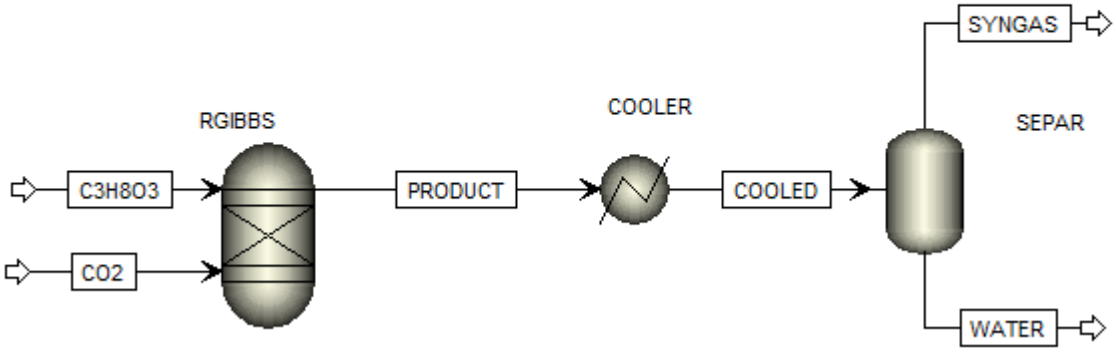

(b) Aspen Plus for glycerol dry reforming process

Figure 3. 12: Aspen Plus flowsheet for glycerol steam and dry reforming processes

Figure 3.13 depicts how glycerol and LLDPE are co-reformed in the presence of H_2O using Aspen Plus. This process consists of seven-unit operations viz. 3 heaters (HE-01, HE-02, and HE-03), one mixer and two reactors (R-01 and R-02). HE-01 pre-heats LLDPE before it can be fed into a yield reactor (R-01). This reactor (T= 873 K, P= 1 bar) decomposes LLDPE into its constituent atoms before it can be mixed with glycerol ($C_3H_8O_3$). The decomposed LLDPE (stream 2) is now mixed with glycerol and the mixture (stream 5) is fed into the reformer (R-02). HE-02 converts water into steam which is a reforming agent. The reformer is a Gibbs

reactor (operating at 1200K and 1 bar) whereby the stream 5 is converted into syngas (stream 6) in the presence of H_2O. Stream 6 is cooled using a cooler (HE-03) before it can be fed into a flash drum (SEP) whereby syngas is separated from water. This separator operates at 298 K and 13 bars.

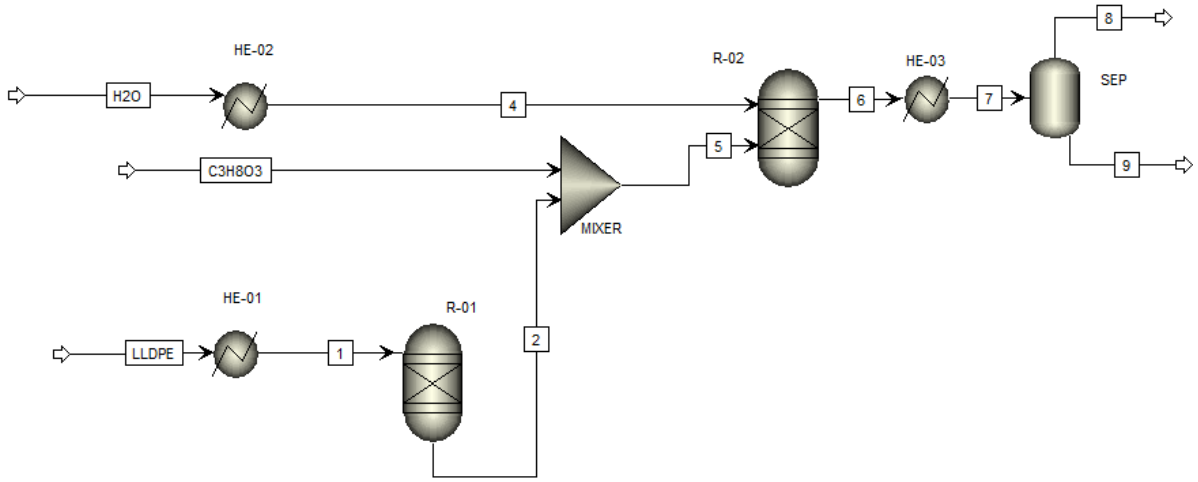

Figure 3. 13: Glycerol-LLDPE mixture reforming process flow diagram

CHO ternary diagrams are used to determine the amounts of $C_3H_8O_3$, CH_4, and H_2O required to produce methanol before developing a detailed flowsheet using Aspen Plus. Figure 3.14 shows an Aspen Plus flowsheet for methanol synthesis from glycerol. This flowsheet consists of 12-unit operations viz. two reactors (R-01 & R-02), three heat exchangers (HE-01, HE-02, & HE-03), one mixer (MX), two compressors (COMPR-1 and COMPR-2), two separators (T-01 & T-02), one valve (V-01), and one splitter (SPL). Glycerol, methane, and water are fed into R-01 which is a Gibbs reactor (operating at 1200K and 1 bar). The main function of this reactor is to transform the mixture of glycerol and methane into syngas (stream 1) in the presence of H_2O. This syngas is cooled using HE-01 (T_{in} = 1200 K and T_{out} = 423 K) and compressed from 1 bar to 55 bars using a two-stage compressor COMPR-1 ($\mathbf{P_{out}}$ = 55 bar, T_{out} = 493 K). The main reason of compressing the syngas to this pressure is because methanol synthesis requires high pressures in a range of 50-100 bars (Mevawala *et al.*, 2017). The compressor outlet stream (3) is fed into an R-02 (Plug reactor; catalyst density 1.775 g/cm^3, bed voidage: 0.5) to produce methanol (ibid). The kinetic data of different reactions that occur during the synthesis of methanol are taken from (Bussche and Froment, 1996), (Van-Dal and Douallou, 2013). Bussche and Froment (1996) showed that CO_2 participates in the synthesis of methanol using $Cu/ZnO/Al_2O_3$ as the catalysts.

The R-02 outlet (stream 5) is cooled using HE-02 (T_{in} = 493 K, T_{out} = 311 K) to create a two-phase mixture (liquid and vapor). The pressure of this two-phase mixture is reduced by means of a valve (V-01). To separate this mixture, a separator is used (T-01) whereby water and methanol are removed from unreacted H_2, CO, and CH_4. This separator operates at 311 K and 22 bars. The main reason of operating this separator at a high pressure is attributed to the fact that high pressures tend to decrease the vapour mole fraction of methanol in the recycle stream (1.43%). Stream 12 contains a mixture of water and methanol but also small amounts of CO_2, CH_4 (0.83 % and 0.26 % respectively). This stream is heated by HE-03 (T_{in} = 311 K, T_{out} = 348K) and fed into a distillation column (T-02) (P =2 bars) whereby methanol is produced from the top section of the column (stream 14) and water from the bottom (stream 15). The vapor phase from the separator (stream 8) is split using a splitter (SPL) to remove methane as a purge (stream 11) while CO, H_2, small fractions of CO_2 and CH_4O are recycled. The splitter was simulated in such a way that when the recycled syngas is mixed with the fresh one does not dramatically exceed a ratio of 2.1 (H_2-CO_2/CO+CO_2). This caused some amount of syngas (H_2 and CO) to be lost in the purge stream which in turn affected the overall conversion. The recycled syngas (stream 9) is compressed from 22 bars to 55 bars using a two-stage compressor (COMPR-2) before it can be mixed with the fresh feed. The main reason of compressing the recycled syngas to such high pressure is because the fresh feed is already at high pressure (55 bars).

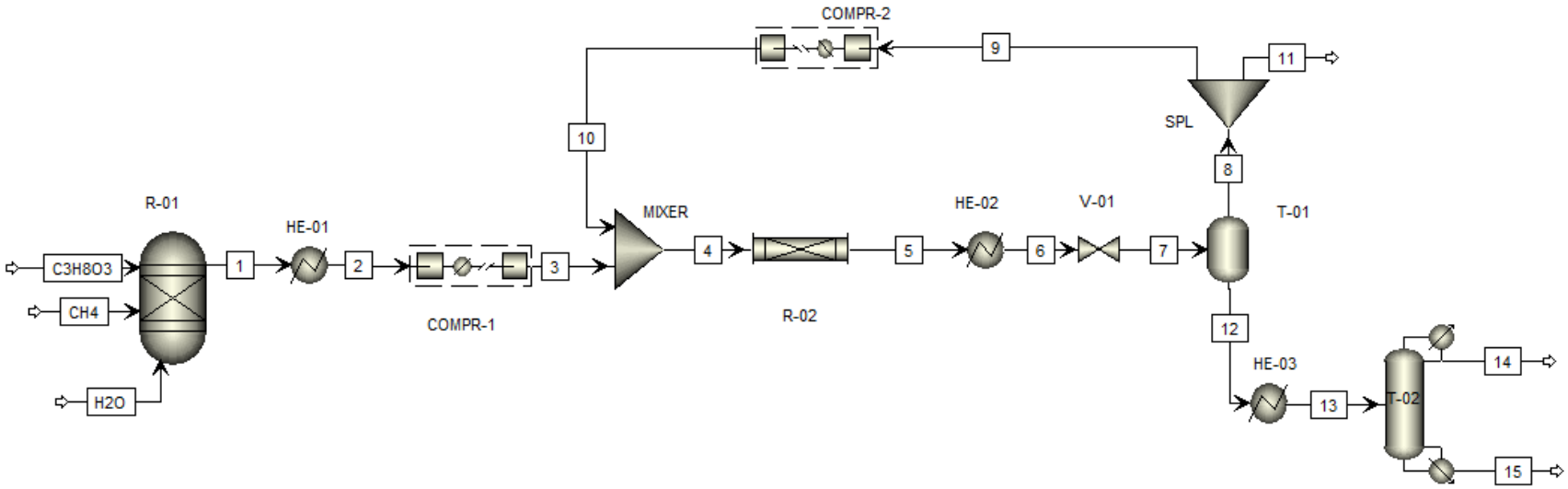

Figure 3. 14: Aspen flowsheet for methanol synthesis from glycerol

3.9 Conclusion

The main objective of this chapter was to describe the methodology that is used for the synthesis of a glycerol-based biorefinery via reforming processes. It was shown that CHO ternary diagrams can be used to set targets for the synthesis of a glycerol biorefinery. Since this biorefinery is a syngas-based biorefinery, the necessity of calculating the thermodynamic equilibria for CHO ternary diagrams arose. The main objective of calculating these thermodynamic equilibria was to determine the syngas equilibrium composition from which a glycerol-based biorefinery can be synthesized. It was further shown that CHO ternary diagrams can be used to determine at which conditions carbon depositions can occur during the synthesis of this biorefinery. A quick sustainability evaluation of glycerol biorefinery was presented to screen out any unnecessary alternatives during the synthesis. Finally, after determining glycerol biorefinery targets and evaluating all alternatives, the necessity of developing a flowsheet for the entire process arose. There are various tools that can be used to develop a flowsheet for a chemical process. This study uses Aspen Plus to develop a glycerol-based biorefinery flowsheet. Results from the CHO ternary diagrams as well as results from Aspen Plus are presented and discussed in Chapter 4.

3.10 References

Adhikari, S., Fernando, S., Gwaltney, S.R., To, S.D.F., Bricka, R.M., Steele, H. & Haryanto, A. (2007) 'A thermodynamic analysis of hydrogen production by steam reforming of glycerol', *International Journal of Hydrogen Energy*, 32 (14), pp. 2875–2880.

Basu, P. (2013) *Biomass Gasification, Pyrolysis and Torrefaction: Practical Design and Theory*. Second Ed.

Bussche, K. M.V. and Froment, G. F. (1996) 'A steady-state kinetic Model for Methanol Synthesis and the water gas shift reaction on a commercial $Cu/ZnO/Al_2O_3$', *Journal of Catalysis*, 161(0156), pp. 1–10.

Cairns, E. J. and Tevebaugh, A. D. (1964) 'CHO Gas Phase Compositions in Equilibrium with Carbon, and Carbon Deposition Boundaries at One Atmosphere', *Journal of Chemical and Engineering Data*, 9(3), pp. 453–462.

Carlson, E.C (1996), Do not Gamble with Physical Properties for Simulation. Available at http://www.cchem.berkeley.edu/cbe150b/docs/VLE/Guidelines.pdf. Accessed on 30th September 2021].

Chaves, I.D.G., Lopez, J.R.G., Zapata, J.L.G., Robayo, A.L. & Nino, G.R. (2016) *Process Analysis and simulation in chemical engineering. Springer, Cham Heidelberg, New York Dordrecht, London.*

Denbigh, K. (1981) *The Principles of Chemical Equilibrium with Applications in Chemistry and Chemical Engineering*. Fourth ed. Cambridge, University Press.

Farooq, A., Moogi, S., Jang, S.H., Kannapu, H. P. R., Valizadeh, S., Ahmed, A., Lam, S. S.& Park, Y.K. (2021) 'Linear low-density polyethylene gasification over highly active Ni/CeO_2-ZrO_2 catalyst for enhanced hydrogen generation', *Journal of Industrial and Engineering Chemistry*, 94, pp. 336–342.

Hunpinyo, P. & Narataruksa, P. (2016) 'Process Simulation and Costing Study for the FT-liquid Fuel Production from Steam Glycerol Reforming', *Chemical Engineering Transactions*, 52, pp. 241–246.

Jaworski, Z. & Pianko-Oprych, P. (2017) 'On thermodynamic equilibrium of carbon deposition

from gaseous C-H-O mixtures: updating for nanotubes', *Rev Chem Eng*, 33(3), pp. 217–235.

Koukkari, P. (2014) 'Introduction to constrained Gibbs energy methods in process and materials', *Energy and Chemistry*, p. 111. Available at: http://www.vtt.fi/inf/pdf/technology/2014/T160.pdf.

Kyle, B. G (1984) *Chemical and Process Thermodynamics*. Third ed. Edited by B. Goodwin. Englewood liffs, NJ: Prentice-Hall.

Litheko, L. A. (2017) *Conceptual design of gsification-based biorefineries using the C-H-O ternary diagrams*. University of South Africa, Pretoria.

Mevawala, C., Jiang, Y. and Bhattacharya, D. (2017) 'Plant-wide modeling and analysis of the shale gas to dimethyl ether (DME) process via direct and indirect synthesis routes', *Applied Energy*, 204, pp. 163–180.

Mountouris, A., Voutsas, E. and Tassios, D. (2006) 'Solid Waste Plasma Gasification: Equilibrium Model Development and Exergy Analysis', *Energy Conversion and Management*, 47, pp. 1723–1737.

Natarajan, K. (2014) 'Computing equilibrium constants of chemical reactions – A new approach', *International Journal of ChemTech Research*, 7(5), pp. 2361–2367.

Patel, B. (2015) 'A Thermodynamic targeting Approach for the Synthesis of Sustainable Biorefineries', in *12th International Symposium on Process Systems Engineering and 25th European Symposium on Computer Aided Process Engineering, 31 May-4 June, Copenhagen, Denmark*, pp. 1283–1288.

Patel, B. (2007) *Fundamental Targets for the Synthesis and Evaluation of Chemical Processes*. PhD Thesis, University of the Witwatersrand, Johannesburg.

Ptasinski, K.J. (2015) Efficiency of Biomass Energy: An Exergy Approach to Biofuels, power and biorefineries. Haboken, New Jersey: John Wiley & Sons.

Schwenber, C.A., Alves, H.J.,Schaffner, R.A., da Silva, F.A., Sequnel, R., Bach, V.R. & Ferracin, R.J. (2016) 'Overview of glyerol reforming for hydrogen production', *Renewable and Sustainable Energy Reviews*, 58, pp. 259–266.

Snoeyink, V. L. & Jenkins, D. (1980) *Water Chemistry*. New York: John Wiley & Sons.

Tassios, D. (1993) *Applied chemical engineering thermodynamics*. Berlin, Germany: Springer-Verlag.

Tay, D. H. S., Kheireddine, H., Ng, D.K.S. & El-halwagi, M.M. (2010) 'Synthesis of an integrated biorefinery via the C-H-O ternary diagram', *Chemical Engineering Transactions*, 21, pp. 1411–1416.

Tay, D. H. S., Kheireddine, H., Ng, D.K.S. & El-Halwagi, M.M. (2011) 'Conceptual synthesis of gasification-based biorefineries using thermodynamic equilibrium optimization models', *Industrial and Engineering Chemistry Research*, 50(18), pp. 10681–10695.

Unlu, D. & Hilmioglu, N. D.(2020) 'Application of Aspen Plus to renewable hydrogen production from glycerol by steam reforming', *International Journal of Hydrogen Energy*, 45(5), pp. 3509–3515.

Van-Dal, É. & Douallou, C. (2013) 'Design and Simulation of a methanol production plant from CO_2 hydrogenation', *Journal of Cleaner production*, 57, pp. 38–45.

Walas, S. M. (1985) *Phase Equilibria in Chemical Engineering.*, Place? Butterworth-Heinemann.

Yaws,C.L. (1999).Chemical Properties Handbook: Physical, Thermodynamic, Environmental, Transport, Safety, and health related Properties of organic and inorganic Chemicals. Texas: McGraw-Hill.

Zheng, K., Lou, H.H., Gangadharan, P. & Kanchi, K. (2012) 'Incorporating Sustainability into the Conceptual Design of Chemical Process-Reaction Routes Selection', *Industrial and Engineering Chemistry Research*, 51(27), pp. 9300–9309.

CHAPTER FOUR

4.0 RESULTS AND DISCUSSION

4.1 Validation of stoichiometric model

The stoichiometric equilibrium models were used in this study to compute the gaseous compositions of five species based on three independent chemical reactions. To validate the accuracy of this model, the results computed in this work are compared with previous results from the literature. Two steps are used to validate the model. Firstly, the equilibrium constant of the three independent reactions calculated from Gibbs energy at different temperatures are compared with previous works such as Litheko (2017), and Mountouris *et al*. (2006) and Tay *et al*.(2011). Figure 4.1 shows that equilibrium constant values of water gas shift and methanation reactions at 800, 1200, and 1500K from the current study and those from the three cited works are similar.

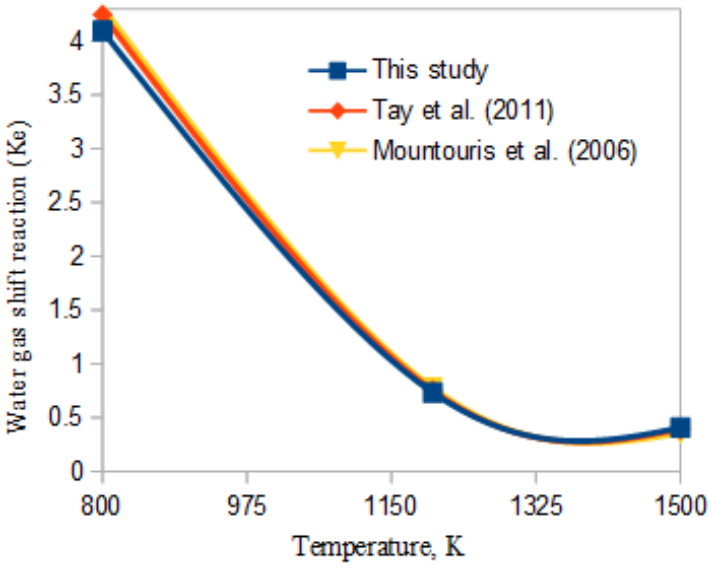

(a)

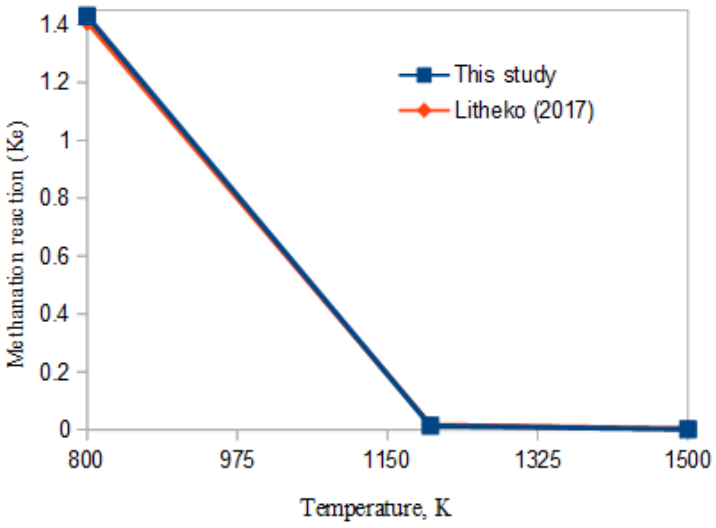

(b)

Figure 4. 1: Model validation using equilibrium constants, (a) water gas shift reaction, (b) methanation reaction

Lastly, the carbon deposition boundaries generated from the current study are compared with those generated by Litheko (2017) and Tay *et al*. (2011) at 800, 1200, and 1500K as shown in figure 4.2. It can be seen that all carbon deposition boundaries follow a similar trend at different temperatures. For example, at 800K the carbon boundaries are represented by a curve while at 1200K they are shown by straight lines joining CO and H_2. This simply means that at high temperatures, H_2 and CO are present in significant quantities. Based on these previous studies, this model is deemed valid and sufficiently accurate to perform the conceptual design.

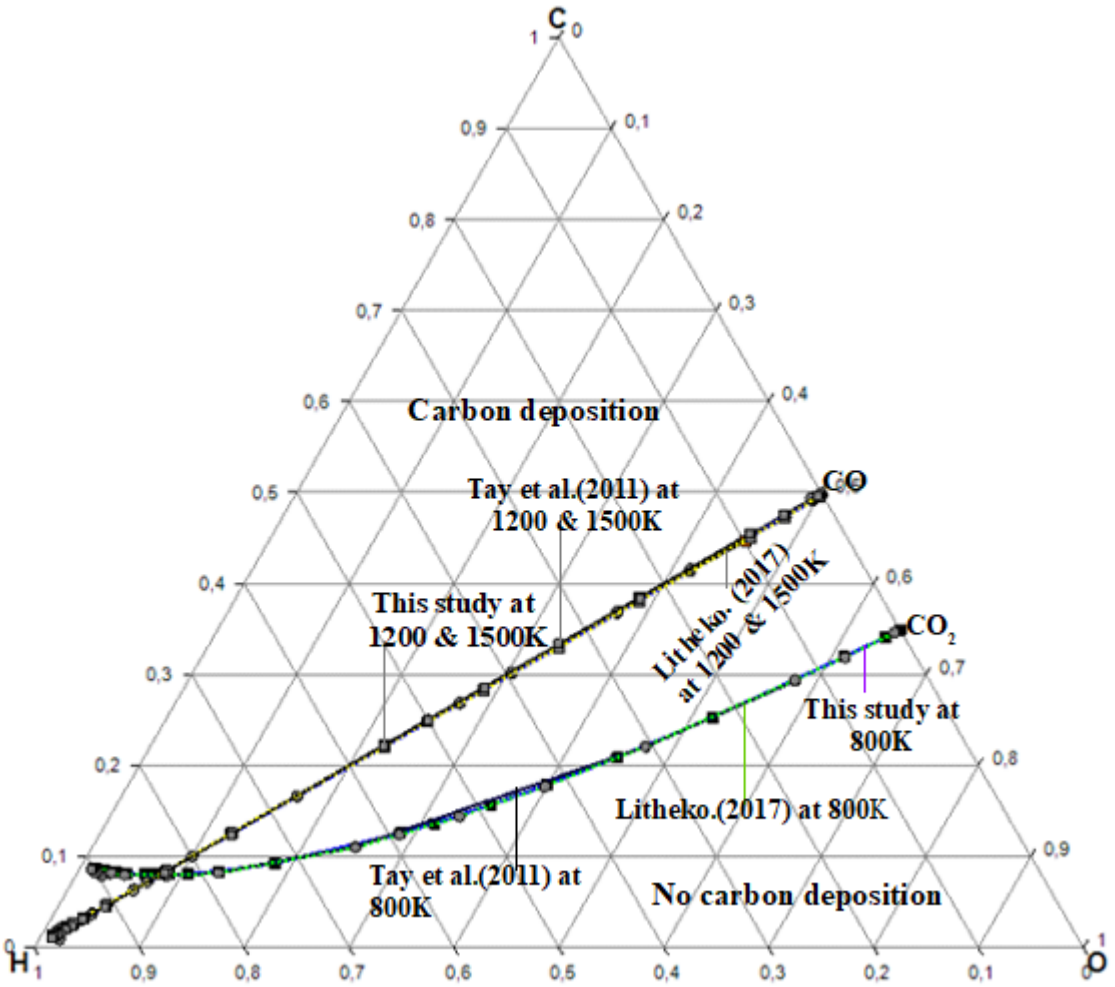

Figure 4. 2: Model validation based on carbon deposition boundaries

4.2 Carbon deposition boundaries in a CHO ternary diagram

Figure 4.3 shows the trend of carbon deposition boundaries in a temperature range of 500-1500K. Each point on a carbon deposition boundary at a particular temperature represents the composition of H_2, CO, CO_2, CH_4, and H_2O in equilibrium with solid carbon. Above this point, the deposition of solid carbon occurs whereas below this point there is no formation of carbon deposition. This figure also reveals other important information, and it should not be overlooked. The following can be deduced from figure 4. 3: from 500K up to 800K, all solid carbon deposition boundaries are represented by curves while from 950K up to 1500K these deposition boundaries are represented by straight lines joining CO and H_2. This means that, at low temperatures CO_2, CH_4, and H_2O are the most predominant species at equilibrium. Considering the methanation and

Boudouard reactions for example ($C + 2H_2 \Leftrightarrow CH_4$, and $2CO \Leftrightarrow C + CO_2$), the equilibrium of these reactions will shift to the right to produce more CH_4 and CO_2 at low temperatures. Increasing the temperature, carbon deposition boundaries move from CH_4-CO_2 composition lines towards CO-H_2 composition lines. This indicates that the equilibrium of methanation and Boudouard reactions shift to the left at high temperatures to generate more H_2 and CO.

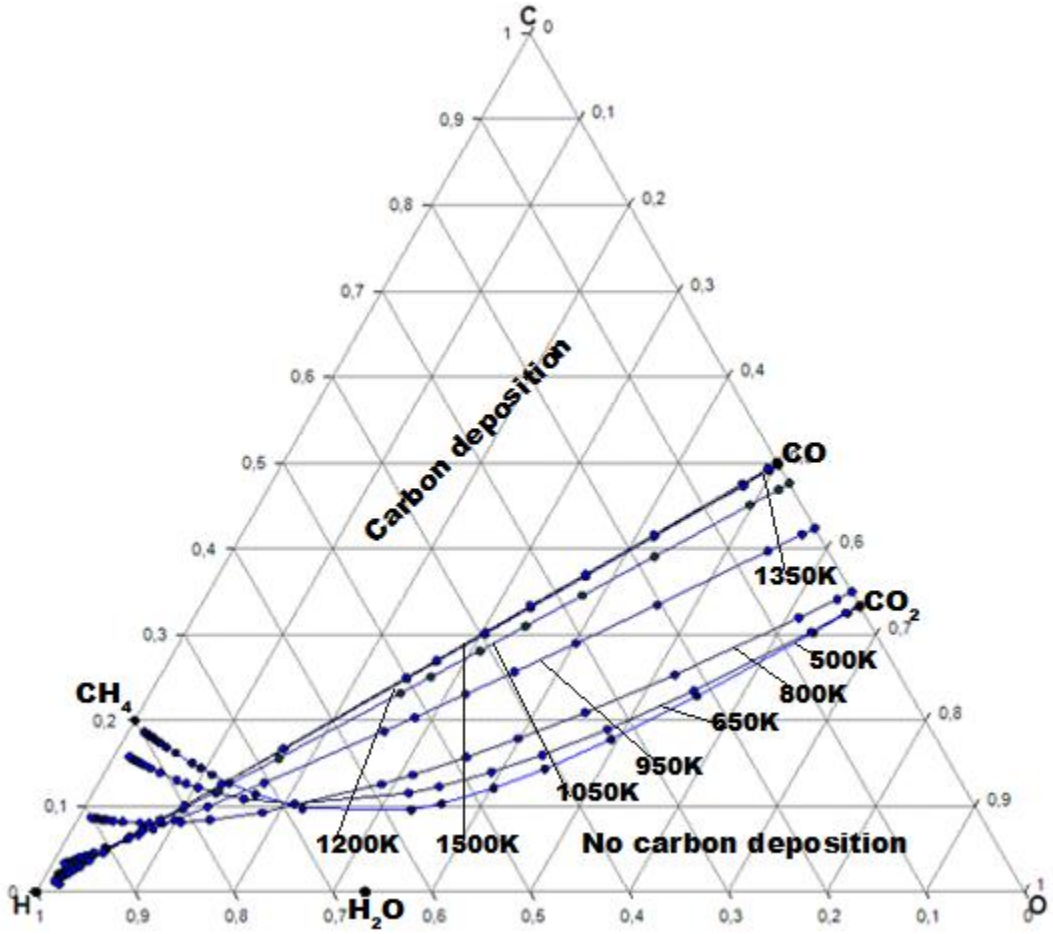

Figure 4. 3: Carbon deposition boundaries at a temperature range from 500 to 1500K

4.3 Pyrolysis of glycerol using CHO ternary diagrams

In this section, CHO ternary diagrams are used to determine syngas composition and carbon yield during the pyrolysis of glycerol. The pyrolysis of glycerol will be considered at 950 K, 1050K, and 1200K using CHO ternary diagrams.

In figure 4.4, a line is drawn from the carbon vertex (pure carbon) passing through glycerol to the carbon deposition boundary at 500 K forming different points. Each point on this line represents

the composition of syngas in equilibrium with solid carbon. For example, point a, b, and c represent the syngas composition in equilibrium with carbon at 950 K, 1050 K, and 1200 K respectively. The empirical formula of these points (a, b, and c) is $C_{0.17306}\,H_{0.60278}\,O_{0.22416}$ (H/O = 2.689), $C_{0.201}\,H_{0.580}\,O_{0.220}$ (H/O =2.636), and $C_{0.215}\,H_{0.570}\,O_{0.215}$ (H/O = 2.651) respectively. The lever-arm rule can be used to determine the amount of carbon deposited at these three temperatures (950 K, 1050 K, and 1200 K). The stoichiometric coefficient of carbon is determined using the lever-arm rule and is found to be 0.765, 0.237, and 0 at 950 K, 1050 K, and 1200 K respectively. These stoichiometric coefficients represent the amount of carbon deposited during the pyrolysis of 1 kmol of glycerol at 950 K, 1050 K, and 1200 K respectively.

To determine the amount of syngas from glycerol pyrolysis at 950K, 1050 K, and 1200 K, it is imperative to first determine its composition. At point a, b, and c, the hydrogen to oxygen ratio (H/O) is 2.689, 2.636, and 2.651 respectively. Using these ratios, the molar fraction of the five-chemical species (CO_2, H_2O, CO, H_2, and CH_4) is determined by interpolation (table E.1 in Appendix E) and is summarised in table 4.1

Table 4. 1: Gaseous composition from glycerol pyrolysis at 950, 1050 and 1200 K

$\frac{H}{O}$	Temperature K	Syngas targeted composition				
		x_{CH_4}	x_{H_2O}	x_{H_2}	x_{CO}	x_{CO_2}
2.689	950	0.0443	0.1090	0.4983	0.2498	0.0986
2.636	1050	0.0162	0.0346	0.5304	0.3884	0.0304
2.651	1200	0.0042	0.0054	0.5513	0.436	0.0033

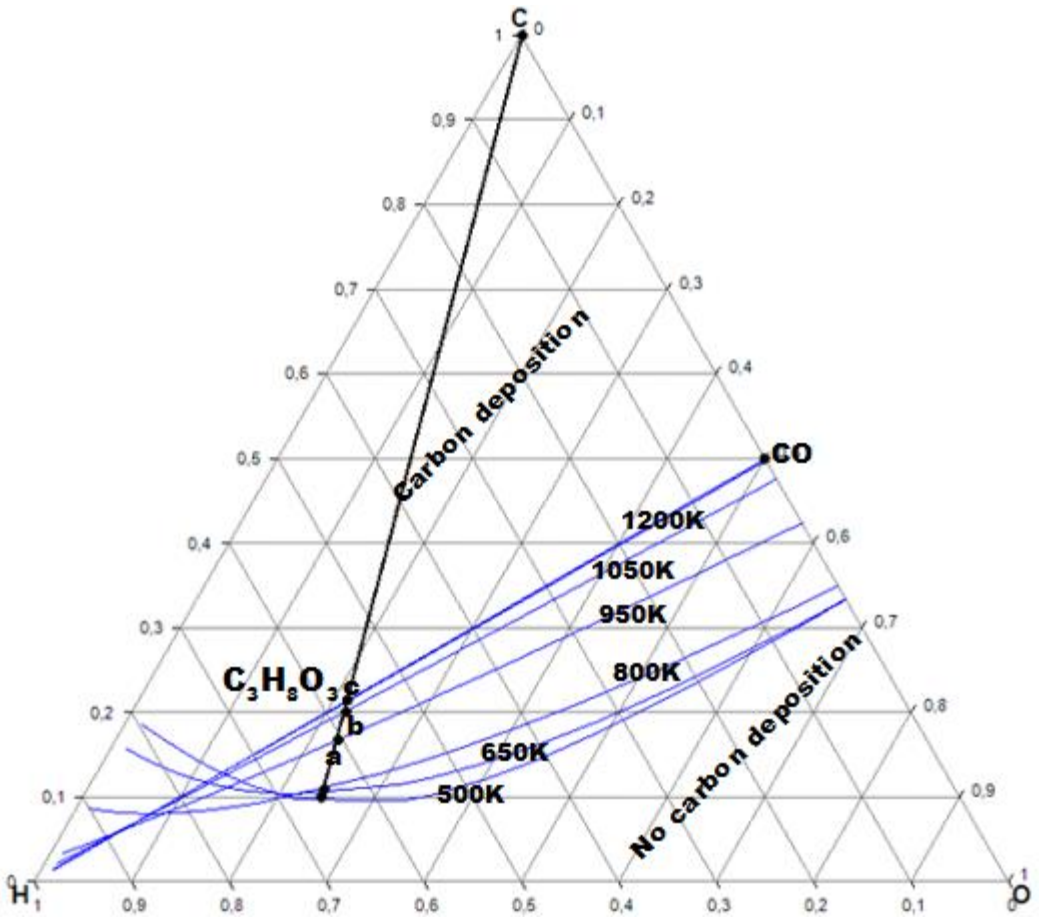

Figure 4. 4: Glycerol pyrolysis process using a CHO ternary diagram at different temperatures

Using table 4.1 the molar quantity of syngas produced per kmol of glycerol is 5.614 , 6.544, and 6.764 kmol/kmol of glycerol at 950 K, 1050 K, and 1200 K respectively.

A similar reasoning is followed to determine the amount of syngas produced as well as the amount of carbon deposited at 650, 800, 1350, and 1500K as indicated in figures 4.5, and 4.6. The composition of H_2 and CO increases with an increase in temperature (figure 4.5). The maximum composition of syngas at 1500K is found to be 0.5597 (H_2), and 0.4394 (CO). Figure 4.6 shows that the molar quantity of the syngas increases with a decrease in carbon formation. These results clearly show that the target for syngas composition from 1 kmol glycerol via pyrolysis is 6.818 kmol at 1500K with no carbon deposition.

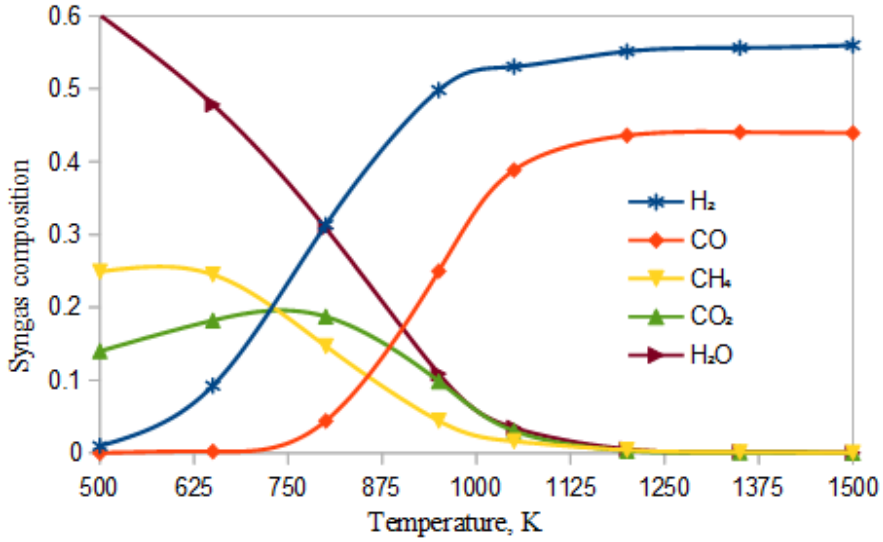

Figure 4. 5: Syngas composition from glycerol pyrolysis at various temperatures

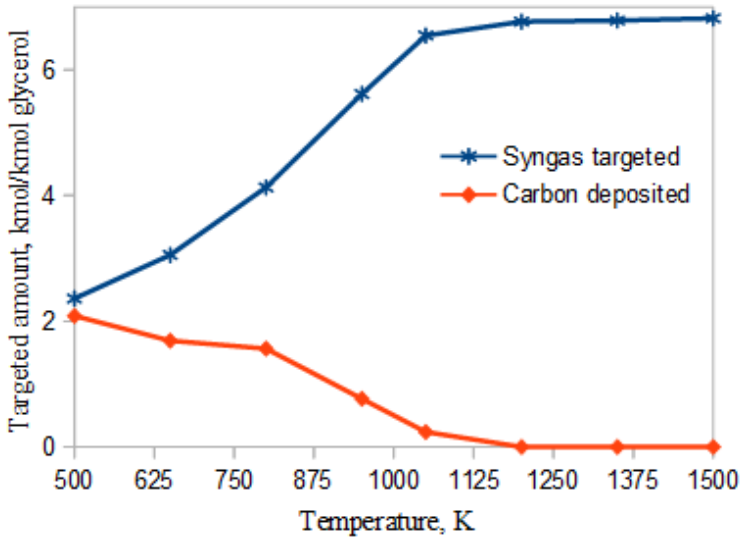

Figure 4. 6: Glycerol conversion into syngas and carbon deposition at different temperatures during pyrolysis

4.4 Syngas composition target from glycerol reforming using CHO ternary systems

During the pyrolysis of glycerol, no additional reactant is needed. In the case of reforming, glycerol is reacted with another reactant commonly known as reforming agent or oxidant. The most used

reforming agents are steam (H_2O), carbon dioxide (CO_2), and oxygen (O_2)/ air or a combination of these three. In the next sections, the CHO ternary diagrams are used to determine the optimum amount of reforming agent required to convert 1 kmol of glycerol into syngas at different temperatures with no carbon deposition.

4.4.1 Syngas composition target from glycerol partial oxidation (GPO) by means of CHO ternary diagrams

A process whereby sub-stoichiometric number of O_2 is used as an oxidizing agent to transform glycerol into syngas is known as partial oxidation process (PO). This is an exothermic process and hence no external heat is needed to drive the reaction (Roslan *et al.*, 2020). In this section, CHO ternary diagrams are used to study glycerol partial oxidation (GPO) at different temperatures.

For illustrative purposes, consider oxygen as the oxidizing agent for the reforming of glycerol at 950K, 1050 K, and 1200 K. The CHO ternary diagram is used to represent the reforming of glycerol with O_2. The main challenge is to determine the minimum amount of O_2 that will give an optimum production of syngas. This challenge, however, can be solved by using the lever-arm rule. The carbon deposition boundaries at 950 K, 1050 K, and 1200 K are also shown in figure 4.7. In the region below the carbon boundary, there is no formation of solid carbon whereas in the region above the boundary curve, there is a deposition of solid carbon. As shown in figure 4.7, an arbitrary point Q with an empirical formula of $C_{0.2111}H_{0.5428}O_{0.2461}$ (H/O =2.2056) is located above the 950 K boundary curve and on the glycerol-O_2 streamline. Thus, there will be a deposition of solid carbon and the syngas composition will be targeted at point V. Point R (represents the complete oxidation of $C_3H_8O_3$, producing H_2O and CO_2 as main species) intersects the glycerol-O_2 streamline and water-carbon dioxide streamline. This point also lies below the carbon deposition boundary, which means that no solid carbon deposition will occur. At this point, hydrogen and carbon monoxide which are the main syngas constituents undergo a complete oxidation process (combustion) to form water and carbon dioxide according to the following reactions (Equation 4.1) (Rabenstein and Hacker, 2008).

$$H_2 + 0.5O_2 \longrightarrow H_2O \text{ , and } CO + 0.5O_2 \longrightarrow CO_2 \qquad 4.1$$

To avoid complete oxidation (combustion) of hydrogen and carbon monoxide as well as the formation of solid carbon during the reforming of glycerol, the final product must be located at

point T on the carbon boundary lines. The empirical formula of this point T at 950 K, 1050 K, and 1200K are $C_{0.2054}H_{0.5245}O_{0.2701}$(H/O=1.942), $C_{0.2148}H_{0.5572}O_{0.2279}$ (H/O=2.445) and $C_{0.215}H_{0.570}O_{0.215}$ (H/O=2.651) respectively. The minimum amount of O_2 needed to convert 1 kilomole of glycerol into syngas can now be calculated as well as the syngas composition at point T. This point represents GPO with no carbon deposition at 950 K, 1050 K, and 1200 K.

The stoichiometric coefficients of oxygen at 950 K, 1050K, and 1200 K are calculated using the lever-arm rule and are found to be 0.5741, 0.1211 and 0 respectively. These stoichiometric coefficients represent the minimum amount of O_2 needed to convert 1 kmol of $C_3H_8O_3$ into syngas with no carbon deposition at 950K, 1050K, and 1200K. It can be shown in the same figure that the minimum amount of O_2 required to convert 1 kilomole of glycerol into syngas at 1200 K is zero. The main reason behind this is because syngas target point at 1200K intersects with the glycerol point. This process tends to the pyrolysis process (no oxidizing agent is required to convert glycerol into syngas).

It is also important to determine the molar quantity of syngas that can be obtained at point T when 0.5741 and 0.1211, and 0 kmol of O_2 are used to convert 1 kmol of glycerol. The empirical formulae of point T have already been determined using the CHO diagram. Using the H/O ratios at 950K, 1050K, and 1200K the syngas composition can be interpolated from table E.1 (in Appendix E). The syngas composition using these H/O ratios is summarized in table 4.2

Table 4. 2: Syngas composition from GPO at 950K, 1050 K and 1200 K

$\frac{H}{O}$	Temperature K	Syngas targeted composition				
		x_{CH_4}	x_{H_2O}	x_{H_2}	x_{CO}	x_{CO_2}
1.942	950	0.0346	0.1129	0.4438	0.2843	0.1244
2.445	1050	0.01530	0.0350	0.5155	0.4019	0.0323
2.651	1200	0.0042	0.0054	0.5513	0.436	0.0033

Performing a carbon balance (Equation 3.23), the syngas molar quantity at 950 K, 1050K, and 1200K is 6.767, 6.674, and 6.764 kmol per kmol of glycerol respectively. It can be shown that GPO produces higher syngas molar quantity than pyrolysis at 950 K and 1050 K. This can be attributed to the fact that there is a formation of solid carbon during the glycerol pyrolysis process

at these temperatures (950 K and 1050 K). It can also be observed that an increase in temperature results in higher syngas yield with lower oxygen requirements during GPO. Syngas composition (H_2 & CO) also increases with an increase in temperature.

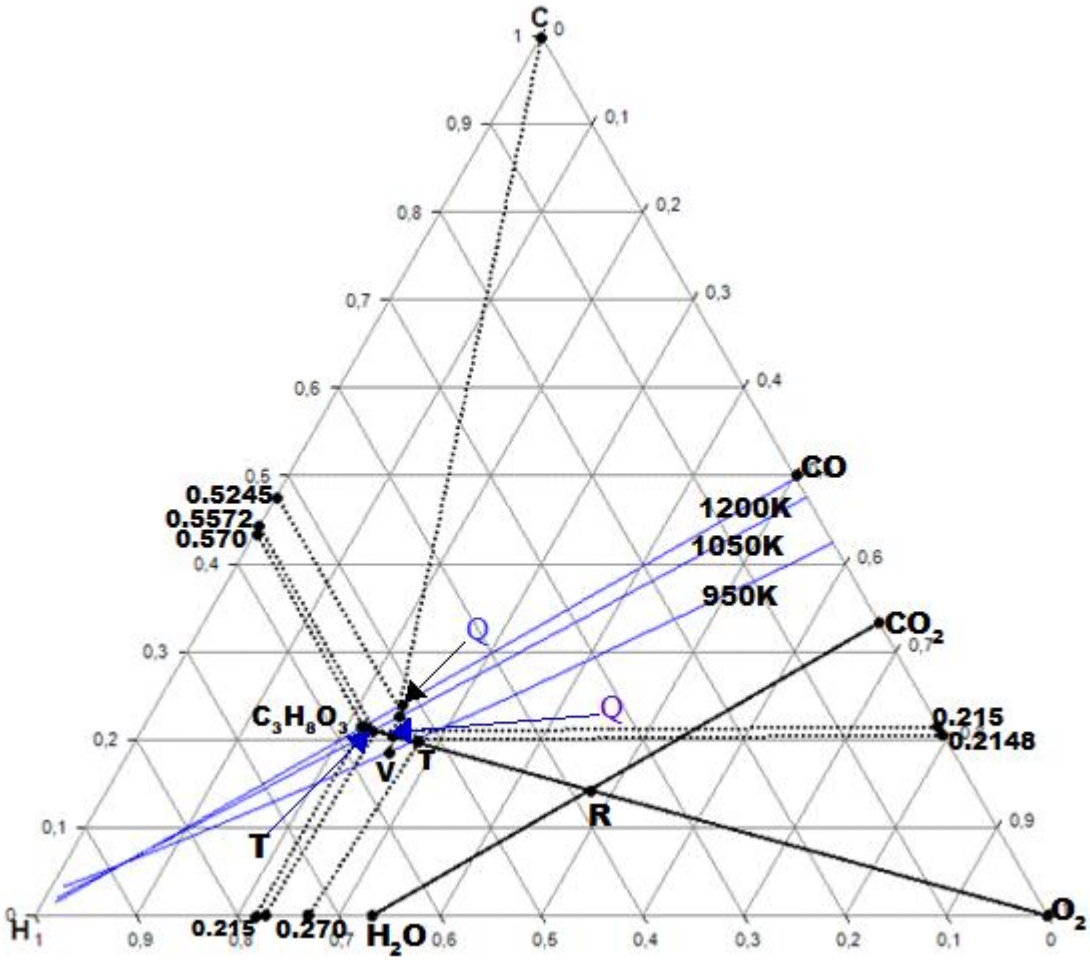

Figure 4. 7: PO of glycerol using CHO ternary systems at 950, 1050 and 1200 K

The same reasoning is followed at different temperatures keeping in mind that point T represents the composition of syngas during the reforming of glycerol with O_2. Syngas composition as well as the minimum amount of O_2 required to convert 1 kmol of glycerol without carbon deposition is shown in Appendix E (table E.4). The CHO ternary diagrams clearly show that the stoichiometric coefficient of O_2 decreases with an increase in temperature during GPO until it becomes zero from 1200 K up to 1500 K (pyrolysis). This indicates that at high temperatures glycerol is decomposed to form H_2 and CO as main constituents without forming solid carbon. For example, at 1500K the

syngas composition is found to be 55.8% H_2 and 44.1% CO. These results are in agreement with the work done by Wang (2010) whereby minimization of Gibbs energy was used to study the conversion of glycerol using O_2 as a reforming agent and found that at a temperature of 1500K, the maximum mole fraction of hydrogen and carbon monoxide were found to be 57.06% and 44.55% respectively.

It can be further shown that the amount of methane that can be targeted from GPO without any solid carbon formation is less than 5% from 950K up to 1500K. Low temperatures favour the production of CO_2, CH_4, and H_2O while high temperatures favour H_2 and CO production (see figure 4.8). This is caused by equilibrium reactions such as Boudouard ($CO + 2CO_2 \leftrightarrow 2\ CO$) and methanation ($C + \ H_2O \leftrightarrow CO + H_2$). High temperatures tend to shift the equilibrium to the right in order to produce more H_2 and CO while at low temperatures the equilibrium of these reactions tends to shift to the left to produce more H_2O and CO_2. For example, the amount of CO_2 and H_2O targeted from GPO at 500K is 44.63% and 50.18% respectively while at 1200K, these compositions become 0.33 % and 0.54 % respectively (CO_2 and H_2O). Figure 4.8 shows the composition of syngas target during the PO of glycerol in a temperature range of 500 K-1500K. This figure reveals that the maximum composition of H_2 and CO from GPO is below 60% at all temperatures.

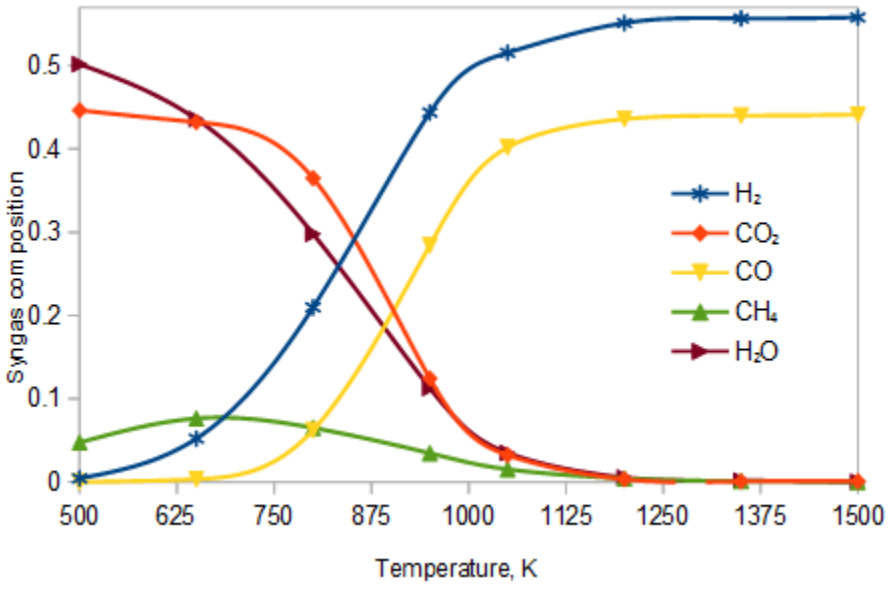

Figure 4. 8: Syngas target composition during glycerol partial oxidation at different temperatures

4.4.2 Syngas composition target from glycerol steam reforming by means of CHO ternary diagrams

Glycerol steam reforming (GSR) is a process whereby glycerol is co-fed with steam to produce H_2 and CO as the main species. This is the most commonly used method for syngas and H_2 production from fossil fuel resources (Roslan *et al.*, 2020)(Charisiou *et al.*, 2020). The GSR process can be represented on the CHO ternary systems at 950K, 1050 K, and 1200 K: A line joining the reactants (glycerol and steam) is drawn from glycerol to steam (see figure 4.9). Point Q (syngas target point) is the intersection point between the reactants line and the carbon formation boundary curves at 950K, 1050 K, and 1200K. The equilibrium composition of syngas is targeted at point Q and the empirical formula of this point is $C_{0.179046}H_{0.588172}O_{0.232782}$ (H/O =2.527), $C_{0.202}H_{0.577}O_{0.221}$ (H/O =2.611), $C_{0.215}H_{0.570}O_{0.215}$ (H/O =2.651) at 950 K, 1050 K, and 1200 K respectively. The distances of glycerol (D_{GL}), and steam (D_{H2O}) relative to point Q are determined and from these distances, the stoichiometric coefficient of H_2O can be calculated.

The optimum amount of steam needed to convert one kmol of glycerol into syngas without carbon deposition at 950 K, 1050K, and 1200 K is calculated using the lever-arm rule and found to be 1.20, 0.343, and 0 kmol per kmol of glycerol respectively. Table 4.3 shows syngas composition during GSR at 950 K, 1050 K, and 1200K. Performing a carbon balance and using table E.1 (linear interpolation), the molar quantity of syngas produced at point Q is 7.444, 6.865, and 6.764 kmol syngas/kmol glycerol without carbon deposition at 950 K, 1050 K, and 1200 K respectively.

Table 4. 3: Syngas target composition from glycerol at 950K, 1050 K and 1200 K

$\frac{H}{O}$	Temperature, K	Syngas targeted composition				
		x_{CH_4}	x_{H_2O}	x_{H_2}	x_{CO}	x_{CO_2}
2.527	950	0.0423	0.1100	0.4870	0.2569	0.1038
2.611	1050	0.0161	0.0346	0.5285	0.3902	0.0307
2.651	1200	0.0042	0.0054	0.5513	0.4360	0.0033

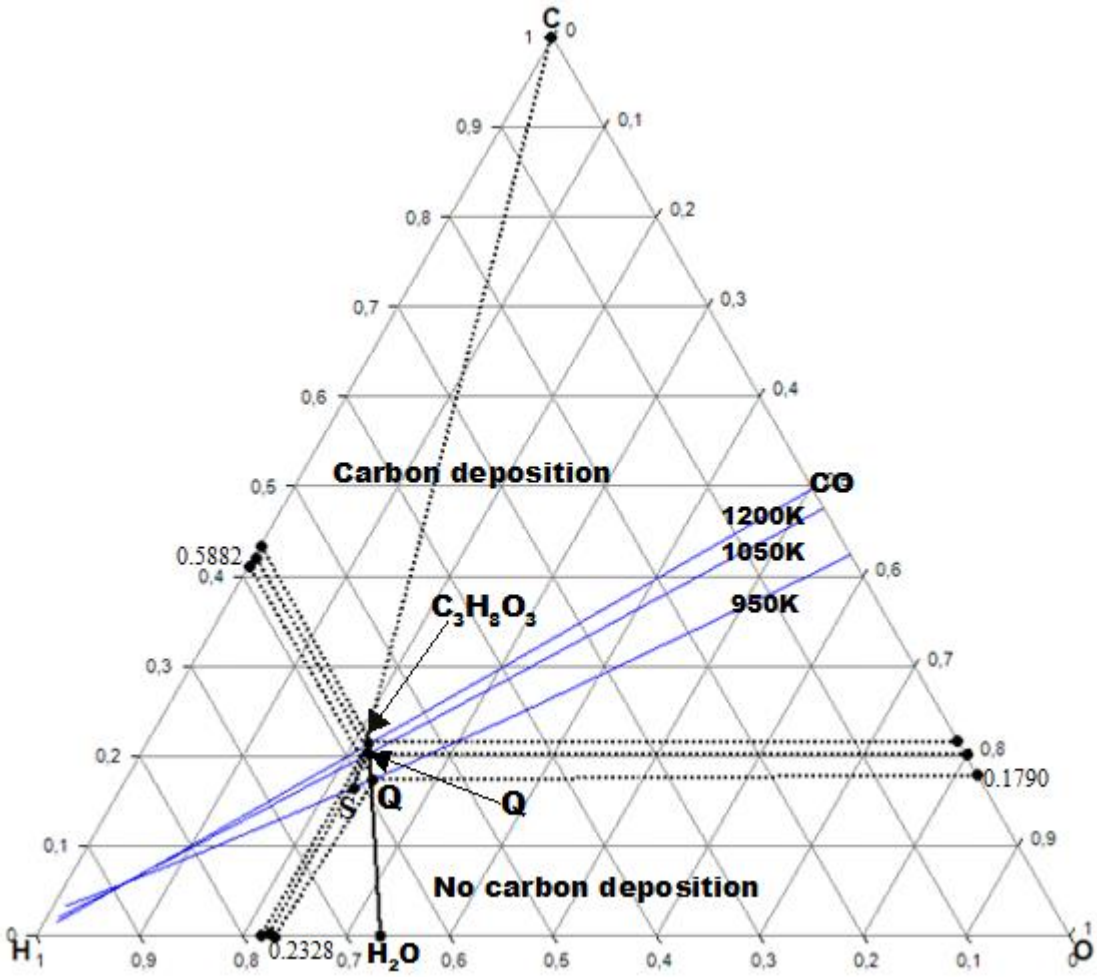

Figure 4. 9: Representation of glycerol reforming with steam in the CHO diagram at 950K, 1050 K and 1200 K

The reforming of glycerol using steam at 500 K, 650 K, 800 K, 1350 K, and 1500K is calculated in the same way. The amount of steam required to convert 1 kmol of glycerol into syngas at these different temperatures is summarized in Appendix E (table E.5). It can be shown that with an increase in temperature, the distance between the syngas target point Q and glycerol is decreasing. This causes the amount of steam needed to convert glycerol into syngas to decrease until it becomes zero at the glycerol point. At 1200K, 1350K, and 1500K, the minimum amount of steam (H_2O) required to convert glycerol is zero since the syngas target point intersects with glycerol at these three temperatures. This shows that at these three temperatures glycerol is now decomposed to form H_2 and CO as main species (pyrolysis process). For example, at 1200K the maximum composition of hydrogen and carbon monoxide that can be produced from glycerol is 55.13% and

43.60% respectively. In the same figure (4.9), taking into consideration carbon deposition, the syngas composition can be targeted at point S. The amount of carbon deposited can be determined in a similar way as in the previous section (pyrolysis). It is also interesting to observe that GSR produces more syngas molar quantity than pyrolysis in a temperature range of 500-1050 K. This is attributed to the fact that there is a formation of carbon during pyrolysis of glycerol which reduces syngas molar quantity (from Equation 3.23).

It is also important to visualize the mixture of glycerol-water in a CHO ternary diagram using different proportions. This helps the process designer determine the correct operating conditions such as temperature and water to glycerol ratios in order to avoid the deposition of solid carbon. Figure 4.10 shows how glycerol is co-fed with steam in different proportions (5% glycerol, and 95% steam, 10% glycerol, and 90% steam, etc.). These proportions are represented by blue points on the CHO ternary diagram. It can be shown that 10% and 5% glycerol proportions are located below all carbon deposition boundaries. This means that converting these glycerol proportions into syngas/gaseous species using steam will not lead to carbon deposition. Increasing glycerol proportion tends to form carbon deposition at certain temperatures. Consider, for example, a 30% glycerol-70% steam mixture (lies above 500 K, 650 K, and 800 K carbon deposition boundaries). This implies that using these low temperatures to convert 30% glycerol into syngas/gaseous species will favour the deposition of solid carbon. In the same figure, a 45% glycerol-55% H_2O mixture lies on the 950K carbon deposition boundary. This means that to convert this mixture into syngas without carbon deposition, a temperature of 950 K or higher than 950 K is required. The syngas composition can be targeted at this point by interpolating the data in Appendix E (table E.1) and using an H/O ratio of 2.474

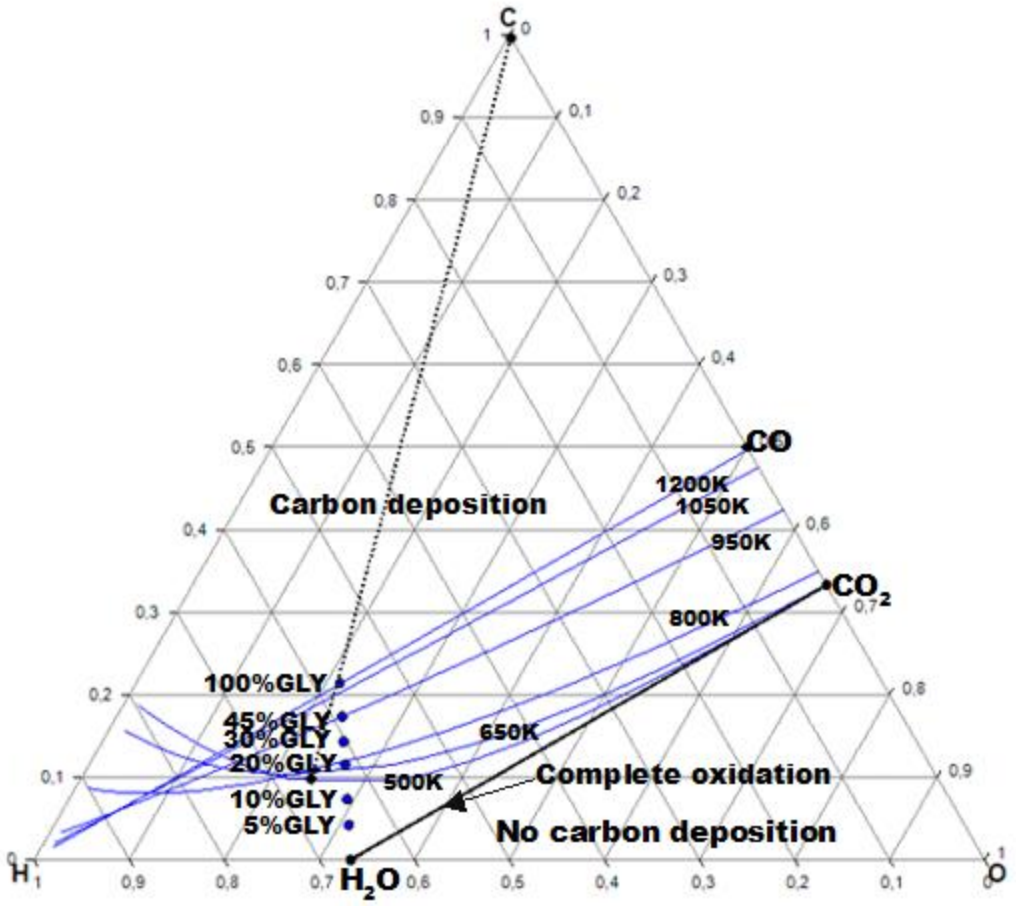

Figure 4. 10: Glycerol-steam mixtures on a CHO ternary diagram

Figure 4.11 shows that the composition of H_2 and CO increases with an increase in temperature until a respective maximum composition of 56.03% and 43.88% at 1500K is reached. The composition of CH_4 increases from 20.61% at 500K to 21.28% at 650K and starts to decrease from 800K up to 1500 K, whereas H_2O composition decreases with an increase in temperature. The composition of CO_2 increases slightly at 500 K, 650 K, and 800 K and starts to decrease from 950K until it reaches 0.0085% at 1500K (see figure 4.11). Two equilibrium reactions (can explain the variation of syngas composition from GSR):$CH_4 + CO_2 \leftrightarrow 2CO + 2H_2$ (methane dry reforming) and $CO + H_2O \leftrightarrow CO_2 + 2H_2$ (water gas shift reaction). At low temperatures, these reactions' equilibrium tends to shift to the left to increase the production of CH_4 and CO_2 while at high temperatures it tends to shift to the right in order to consume CH_4 and CO_2 and produce more syngas (Adhikari *et al.*, 2007).

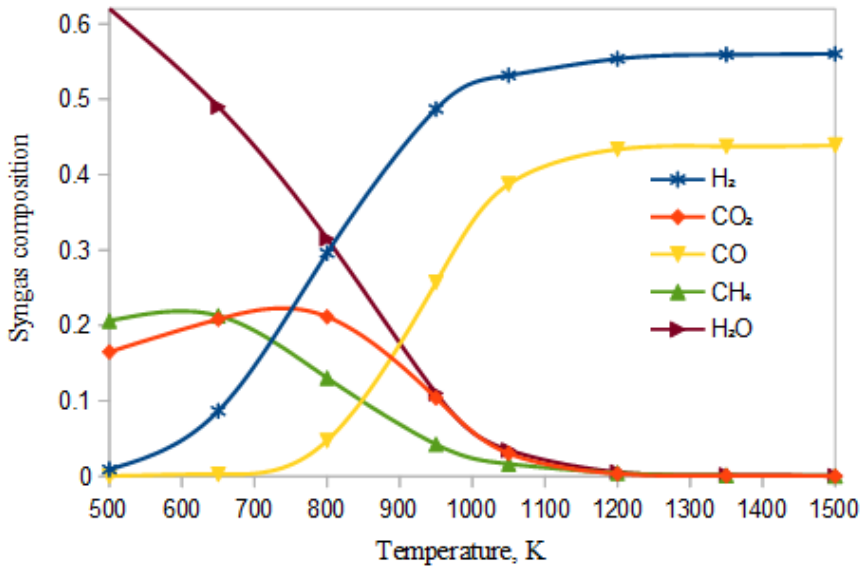

Figure 4. 11: Syngas composition target via GSR using CHO diagrams

4.4.3 Glycerol dry reforming using CHO ternary diagrams

Glycerol dry reforming (GDR) is a process whereby glycerol is converted into syngas by employing carbon dioxide as a reforming agent (Garcia *et al.*, 2001) (Arif *et al.*, 2019). In this section, CHO ternary diagrams are used to determine the composition of syngas from GDR at different temperatures without depositing any solid carbon.

The GDR process is considered at 950K, and 1050K graphically using a CHO ternary diagram in figure 4.12. A line is drawn from glycerol to carbon dioxide and point Q is the intersection between $C_3H_8O_3$-CO_2 streamline and carbon boundary lines at 950K and 1050K. The empirical formulae of this point Q that represents the syngas composition target at 950 K, and 1050K are $C_{0.250579}H_{0.412206}O_{0.337215}$, and $C_{0.2261}H_{0.5402}O_{0.2337}$ respectively. The $\frac{H}{O}$ ratios of this point at 950K, and 1050 K are 1.222 and 2.311 respectively. The composition of the syngas can be calculated by interpolation of the data in Appendix E (table E.1). Furthermore, the minimum amount of carbon dioxide needed to convert 1 kmol of glycerol into syngas (at point Q) at 950K and 1050K without carbon deposition can also be determined.

The stoichiometric coefficients of carbon dioxide at 950 K and 1050 K are found to be 1.8229, and 0.2720 respectively. These stoichiometric coefficients represent the minimum amount of carbon dioxide that can be used to convert 1 kmol of glycerol into syngas at point Q without forming solid carbon. Although syngas composition can be determined on the entire streamline that connects $C_3H_8O_3$ and CO_2, any point besides point Q will result in solid carbon formation. Table 4.4 represents the targeted syngas composition from GDR at point Q. This composition is determined through linear interpolation of table E.1 data (Appendix E).

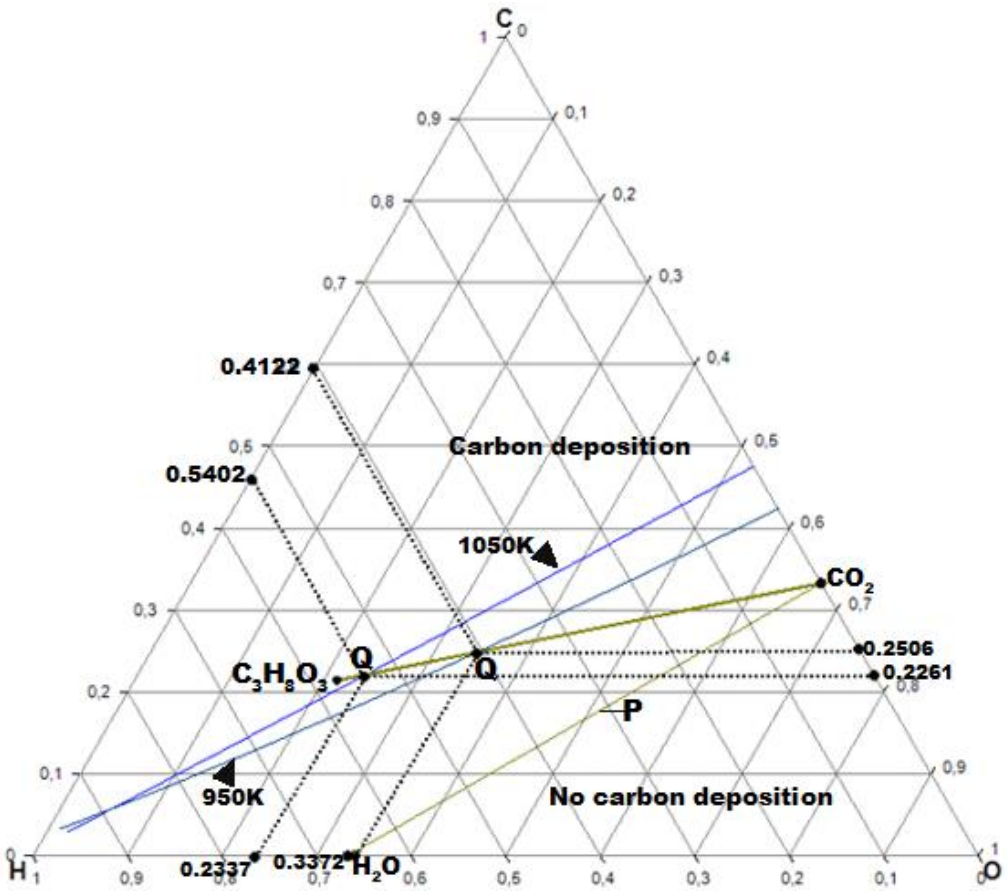

Figure 4. 12: Conversion of glycerol in the presence of carbon dioxide at 950 K and 1050 K using CHO ternary diagrams

Table 4. 4: Equilibrium syngas composition targeted from glycerol dry reforming at 950K and 1050K

$\frac{H}{O}$	Temperature, K	Syngas targeted composition				
		x_{CH_4}	x_{H_2O}	x_{H_2}	x_{CO}	x_{CO_2}
1.222	950	0.0208	0.10380	0.3392	0.34805	0.18820
2.311	1050	0.0146	0.0352	0.5051	0.4114	0.0334

Performing a carbon balance by using table 4.6, the targeted syngas molar quantities at 950 K, and 1050K (point Q) are found to be 5.386 and 6.530 kmol/kmol of glycerol respectively. This means that 1 kmol of glycerol can be converted into 5.386 kmol of syngas in the presence of 1.830 kmol of carbon dioxide without deposition of any solid carbon at 950 K, and at 1050 K, 1 kmol of glycerol needs 0.272 kmol of CO_2 to produce 6.530 kmol of syngas.

Syngas composition during glycerol dry reforming at other temperatures is calculated in the same way. Figure 4.13 gives a summary of GDR at different temperatures. At low temperatures glycerol dry reforming produces a low composition of H_2 and CO, but an increase in temperature gives a high composition of H_2 and CO. In a temperature range of 1200-1500 K, CHO ternary diagrams revealed that no CO_2 required to convert glycerol into syngas (this becomes a pyrolysis process). The highest H_2 and CO composition from GDR is targeted at 50.57 % and 41.14 % at 1050K using 1 kmol of glycerol as a feed.

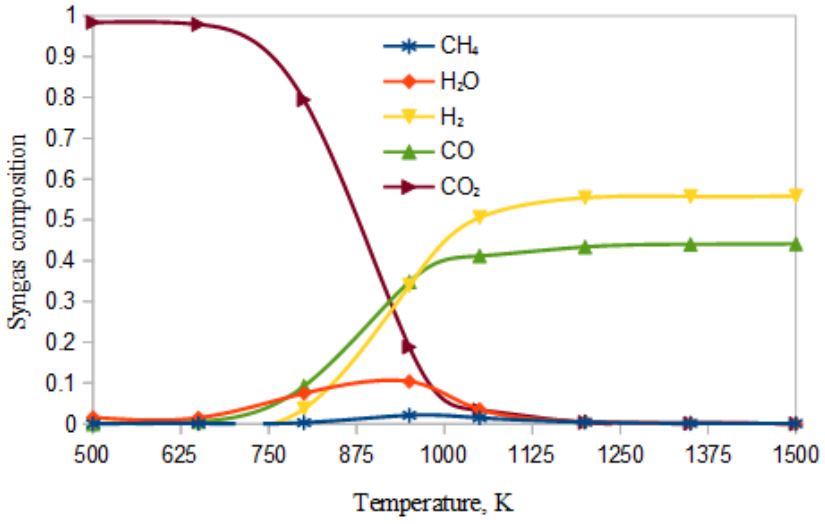

Figure 4. 13: Syngas composition target from glycerol dry reforming using CHO ternary systems

Figure 4.14 reveals that carbon boundaries at 500 K, and 650K intersect with glycerol-carbon dioxide streamline on the C-O axis. This indicates that syngas composition could be targeted at CO_2 point without carbon deposition. The minimum amount of CO_2 required to convert 1 kmol of glycerol at 500 K, and 650K is targeted at 354.31 kmol with no carbon deposition. This amount of CO_2 shows that glycerol dry reforming at low temperatures is not feasible as a significant amount of CO_2 is needed to produce a small quantity of syngas with no carbon deposition.

The same figure (4.14) shows GDR at 500 K, and 650 K on the CHO ternary diagram taking into consideration carbon deposition. Point M represents a $CO_2/C_3H_8O_3$ =1. Drawing a line from carbon vertex through M intersection points T_1 and T_2 are formed on carbon boundaries at 500 K and 650K respectively. The amount of carbon deposited is targeted at 3.06 and 2.142 kmol per kmol of glycerol at 500 K, and 650K respectively. Kale and Kulkarni (2010) studied GDR at 650 K and $CO_2/C_3H_8O_3$=1 and the amount of carbon deposited was found to be approximately 2.141 kmol. It can be seen that the amount of carbon deposited in this study is very close to Kale and Kulkarni (2010) with a percentage error of 0.047% . The composition of H_2 and syngas can be targeted at point M (H/O = 1.601) by linear interpolation of results in Appendix E (table E.1 data).

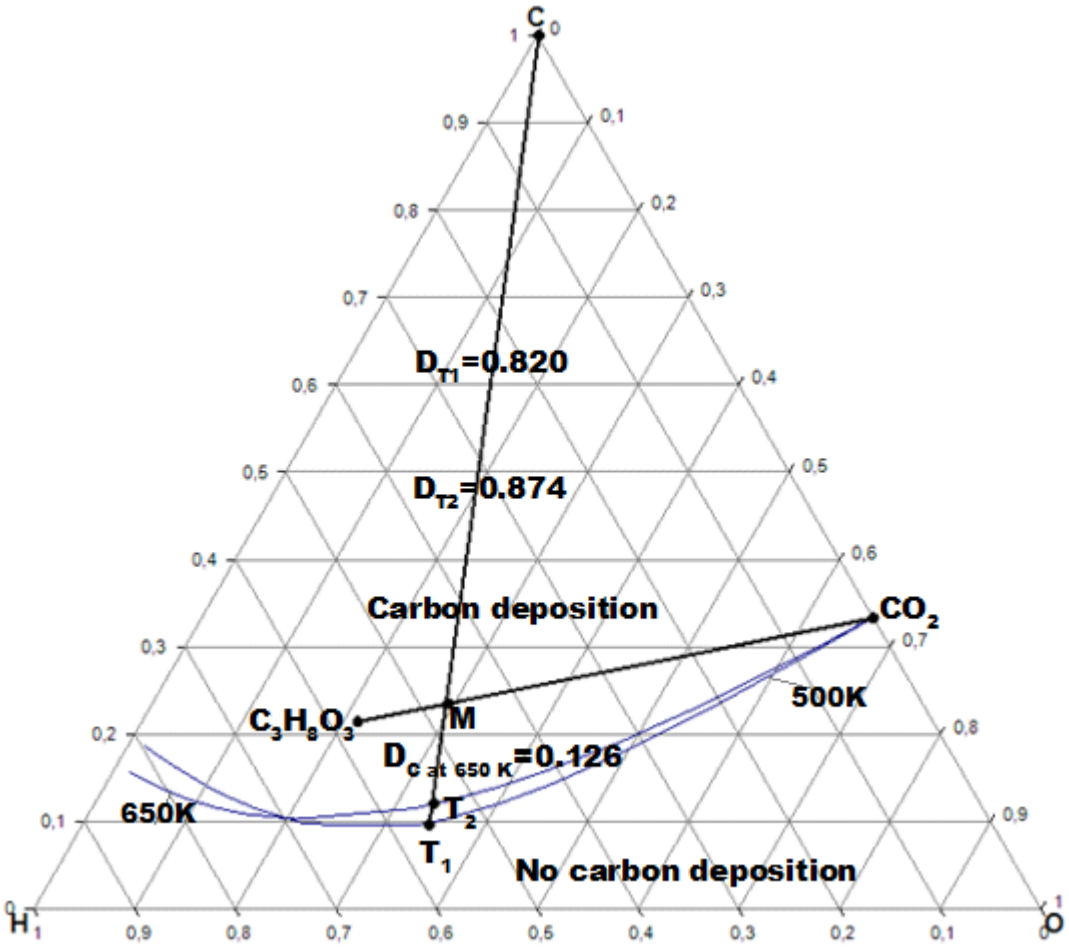

Figure 4. 14: Syngas target and carbon from glycerol at 500 and 650K using CO2 as a reforming agent

4.4.4 Effect of temperature on glycerol-derived syngas ratio via partial oxidation, steam, and dry reforming

Syngas ratio (H_2:CO) for the synthesis of chemicals is very crucial and most processes require a syngas ratio in the range of 1-3 (Kale and Kulkarni, 2010) (Cao *et al.*, 2008). For example, the synthesis of methanol requires a syngas ratio of 2.0 (Tay *et al.*, 2011). Figure 4.15 reveals that neither steam, dry reforming, nor partial oxidation of glycerol produces syngas that can be used for the downstream applications at 800K (syngas ratio out of the range of 1-3). From 950 K up to 1500K, the syngas produced from GSR, and GPO can be used for the synthesis of various chemicals because the H_2:CO ratio falls within the range. For example, GSR produces a syngas ratio of 1.895 at 950K while GPO generates an H_2: CO ratio of 1.561 at the same temperature. The

syngas ratio decreases with an increase in temperature for both glycerol steam reforming and partial oxidation because high temperatures favor the formation of H_2, and CO. Even though the syngas ratio decreases with an increase in temperature, glycerol steam reforming and partial oxidation are still favourable for syngas production. However, this syngas does not meet the requirement for downstream applications such as methanol synthesis. The synthesis of methanol from syngas requires a ratio (H_2:CO) of 2 (Tay *et al*., 2011). This syngas ratio it can be adjusted using different methods such as mixing glycerol with CH_4 (using steam as a reforming agent) or using water gas shift reaction.

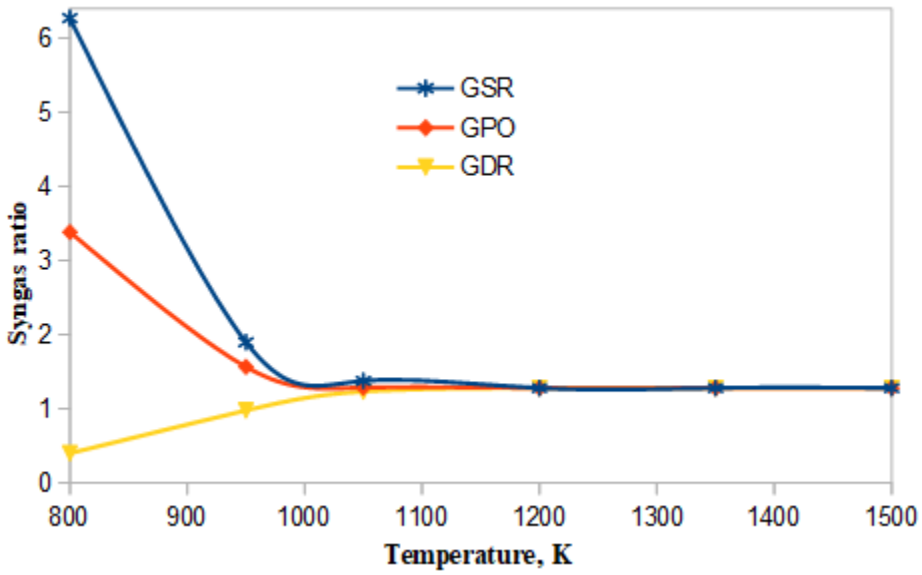

Figure 4. 15: Effect of temperature on glycerol-derived syngas ratio

The same figure (4.15) shows that from 1050K up to 1500K, GDR generates a syngas ratio (H_2:CO) that falls within the range (1-3). Therefore, this syngas could be favorable for downstream processes such as dimethyl ether. It is also interesting to observe that all three processes (GSR, GPO, and GDR) generate the same syngas ratio in a temperature range of 1200K-1500K. This is because at this temperature range (1200-1500K), all three processes tend to pyrolysis as shown in previous sections (4.3 and 4.4).

4.4.5 Comparing GSR with GDR and GPO using CHO ternary diagrams

4.4.5.1 Comparing steam reforming (GSR) with partial oxidation (GPO)

Table E.4 and E.5 (Appendix E) summarize the respective optimum amounts of O_2, and H_2O required to fully convert 1 kmol of glycerol to syngas with no solid carbon deposition. First, the distances from glycerol to H_2O, and O_2 are undoubtedly different (H_2O-$C_3H_8O_3$ = 25.69 mm and O_2-$C_3H_8O_3$ = 97.60 mm). This means that the optimum amount of O_2 and H_2O required to convert 1 kmol of glycerol will not be the same and this will result in different syngas compositions. The optimum amounts of O_2 and H_2O are related to temperature. In other words, these amounts decrease with an increase in temperature until they become zero from 1200 up to 1500K. At 500K, 1 kmol of glycerol requires 3.097 kmol of O_2 to produce syngas whereas this same amount of glycerol requires 5.908 kmol of H_2O. In the temperature range of 500-1050K, 1 kmol of glycerol requires more H_2O than O_2. At 1050K for example, the optimum amount of steam needed to fully convert glycerol into syngas is 0.343 kmol, and if O_2 were used as a reforming agent, 1 kmol of glycerol would require 0.121 kmol of O_2.

Both reforming agents produce different syngas composition since H/O ratios are different. For example, at 1050K (H/O = 2.6525) the syngas composition using H_2O is 1.63% CH_4, 3.46% H_2O, 53.17% H_2, 38.72% CO, and 3.02 % CO_2, whereas using O_2 at the same temperature (H/O = 2.445) the syngas composition is 1.53% CH_4, 3.50 % H_2O, 51.56% H_2, 40.20 % CO and 3.20 % CO_2 as shown figure 4.11, and 4.8. These results reveal that GSR produces a higher syngas ratio (H_2: CO=1.373) than GPO (H_2: CO = 1.283) at 1050K. But at this same temperature, GPO produces more CO_2 than GSR. Using the syngas composition target from both technologies, the optimum amount of syngas is 6.917 and 6.673 kmol per kmol of glycerol using O_2 and H_2O respectively. Using the same reasoning, GSR produces a higher amount of syngas than GPO in a temperature range of 500-1050K. The total hydrogen potential (sum of H_2 and CO composition) for both technologies is the same at a temperature range of 1200-1500K, this is because between this temperature range the syngas composition does not change significantly. For example, at 1200K both processes produce a total hydrogen potential of 98.7%.

4.4.5.2 Comparing GSR with GDR

GSR produces more H_2 than GDR at the temperature range used in this study (see figures 4.11 and 4.13). For example, at 1050K, GSR generates 3.678 kmol of H_2 per kmol of glycerol whereas GDR generates 3.302 kmol H_2 per kmol of glycerol. It must be pointed out that, GDR produces more CO than GSR at all temperatures and more CO_2 is produced through GDR technology. This is because there is more carbon in the feed during GDR than GSR. For example, at the same temperature (1050 K), the optimum amount of CO and CO_2 produced from 1 kmol of glycerol via GDR is targeted at 2.689, and 0.218 kmol respectively.

4.4.6 Syngas composition target from glycerol by combining two technologies on a single CHO ternary diagram

Thus far, CHO ternary systems have been used to determine the syngas composition from glycerol by using all three reforming agents separately. It may also be possible to determine the syngas composition target by combining two reforming agents such as H_2O/CO_2, CO_2/O_2, or H_2O/O_2. Figure 4.16 shows how syngas composition target can be calculated by using H_2O/CO_2, CO_2/O_2 and H_2O/O_2 as reforming agents. Points Q, U and P represent H_2/O_2 (1:1), H_2O/CO_2 (1:1), and CO_2/O_2 (1:1) respectively. These points (Q, U, and P) are obtained in the same way as described in previous sections. Point T represents the syngas composition target at 800K with no solid carbon deposition by co-feeding CO_2 with O_2. This point T is used to determine syngas composition at different temperatures and different technologies with no carbon deposition.

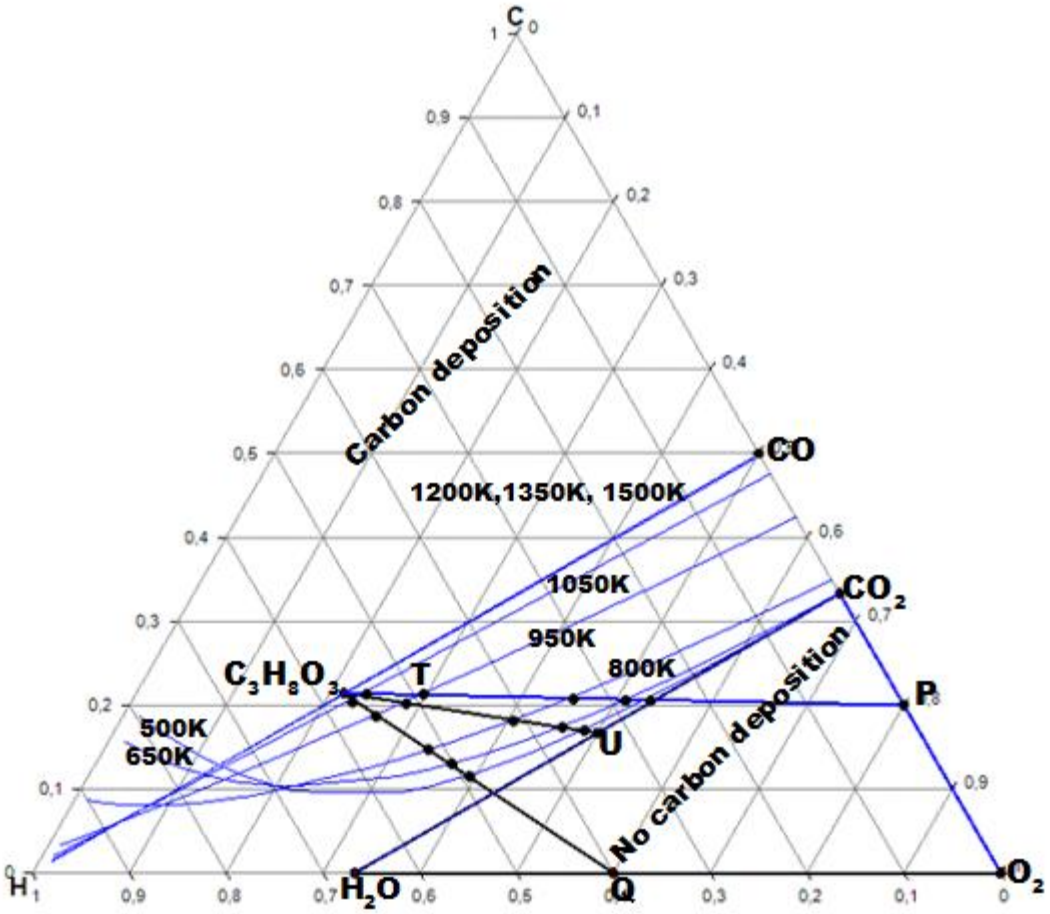

Figure 4. 16: Combined reforming technologies for glycerol conversion on a CHO ternary diagram

4.4.6.1 Targeting the optimum amount CO_2/ O_2, H_2O/CO_2 and H_2O/O_2 to fully convert 1 kmol of glycerol

It is important to determine the optimum amount of H_2O, CO_2 and O_2 required to fully convert 1 kmol of glycerol by means of the lever-arm rule when these reforming agents are combined (H_2O/CO_2, H_2O/O_2, and O_2/CO_2). Tables E.7-E.9 shows the summarized optimum amounts of CO_2, O_2, and H_2O required to convert 1 kmol of glycerol as well as the amount of syngas targeted per kmol of glycerol at different temperatures. The H_2O/O_2 co-feed requires the least amount of H_2O than H_2O/CO_2 co-feed to produce syngas from glycerol at all temperatures. For example, at 1050K, 1 kmol of glycerol requires 0.0398 kmol of H_2O to produce syngas via H_2O/O_2 co-feed whereas the same amount of glycerol requires 0.137 kmol of steam when H_2O/CO_2 co-feed are used. At this temperature (1050 K), 1 kmol of glycerol requires 0.0398 kmol of O_2 to produce syngas via H_2O/O_2 co-feed while it requires 0.0926 kmol of O_2 via O_2/ CO_2 co-feed. These results

show that glycerol auto-thermal reforming technology requires less amount of O_2 than dry auto-thermal reforming.

Both steam–dry (H_2O-CO_2 co-feed) and dry-partial oxidation (CO_2-O_2 co-feed) reforming processes use carbon dioxide as a feed to target syngas composition from glycerol. It is revealed that glycerol steam-dry reforming requires less amount of carbon dioxide than dry-partial oxidation reforming in a temperature range of 500 K-1050 K. For example, the optimum amount of CO_2 needed to convert 1 kmol of glycerol at 1050K into syngas via steam dry reforming is targeted at 0.137 kmol per kmol of glycerol while at the same conditions dry-partial oxidation reforming process utilizes 0.0926 kmol of CO_2 per kmol of glycerol.

4.4.6.2 Targeting the composition of H_2 and CO from glycerol by using H_2O/CO_2, H_2O/O_2, and O_2/CO_2

Figure 4.17 shows the H_2+CO composition using H_2O/CO_2 (molar ratio= 1:1), H_2O/O_2 (molar ratio =1:1), and O_2/CO_2 (molar ratio = 1:1) as main reforming agents. In a temperature range of 500 K-1050 K, the co-feeding of H_2O with O_2 generates the highest syngas composition from glycerol followed by H_2O/CO_2. An O_2/CO_2 co-feed produces the least syngas composition in a temperature range of 500 K-1050K. For example, at 950K, H_2O/O_2 produces a syngas composition of 74.11% while H_2O/CO_2 and O_2/CO_2 produce 72.34 % and 71.64 % respectively. This figure shows that at temperatures higher than 1050K, all three co-feeds produce the same syngas composition.

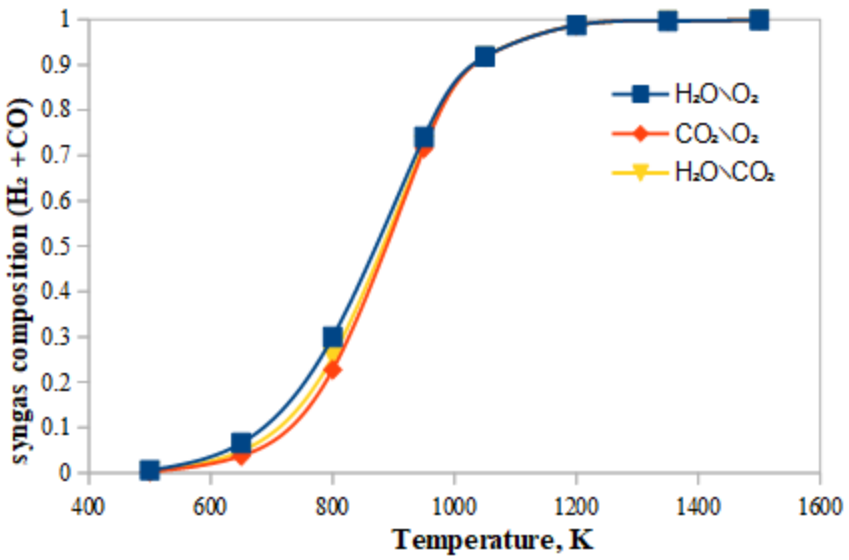

Figure 4. 17: Syngas composition target via different processes

4.4.6.3 Targeting the net composition of CO_2 generated from different glycerol reforming technologies

The optimum amount of CO_2 required to convert 1 kmol of glycerol into syngas via dry-partial oxidation and steam-dry reforming has been targeted at different temperatures. It is important to target the minimum composition of CO_2 that can be generated from these processes. As it has been shown in previous sections, in a temperature range of 1200 K-1500K the distance of $H_2O/O_2/CO_2$ relative to the syngas target point at these temperatures is zero. This resulted in zero minimum amount of reforming agent to convert glycerol into syngas on the CHO ternary systems.

However, at these temperatures both CO_2/O_2 and H_2O/CO_2 technologies produce the same composition of CO_2. For example, at 1200K the minimum amount of CO_2 generated from both technologies is 0.33% which corresponds to 0.0221 kmol per kmol of glycerol. But at temperatures lower than 1200K these processes produce different compositions of CO_2. For example, at 1050K, glycerol dry-partial oxidation (CO_2/O_2) reforming produces 3.314% (0.2182 kmol) of CO_2 while steam-dry reforming (H_2O/CO_2) generates 3.202% (0.2148 kmol) of CO_2. This simply means that dry-partial oxidation reforming of 1 kmol of glycerol utilizes 0.0926 kmol of CO_2 to emit 0.2182 kmol of CO_2 while steam-dry reforming utilizes 0.137 kmol of CO_2 to emit 0.2148 kmol of CO_2. Kale and Kulkarni (2010) define the net amount of carbon dioxide evolved as the difference

between the amount of CO_2 produced and CO_2 fed. The net amount of CO_2 generated from glycerol steam-dry reforming process at 1050K is targeted at 0.078kmol/kmol glycerol (0.215-0.137).

The dry reforming of glycerol at low temperatures requires a significant amount of CO_2 and ends up generating a high amount of CO_2. For example, at 650K, 1 kmol glycerol requires 354.31 kmol to produce an insignificant amount of syngas as indicated in figure 4.14. The amount of CO_2 generated at this temperature is targeted at 2.984 kmol per kmol of glycerol. At elevated temperatures, glycerol requires small amounts of CO_2 to produce syngas. For example, at 1050K, the minimum amount of CO_2 needed to transform glycerol into syngas without any solid carbon deposition is targeted at 0.272 kmol CO_2/kmol glycerol. The net amount of CO_2 evolved at this temperature (1050K) is targeted at 0 kmol per kmol of glycerol because the amount of CO_2 produced is less than the amount of CO_2 fed. Figure 4. 18 shows the composition of CO_2 that can be produced from glycerol by using different technologies at various temperatures.

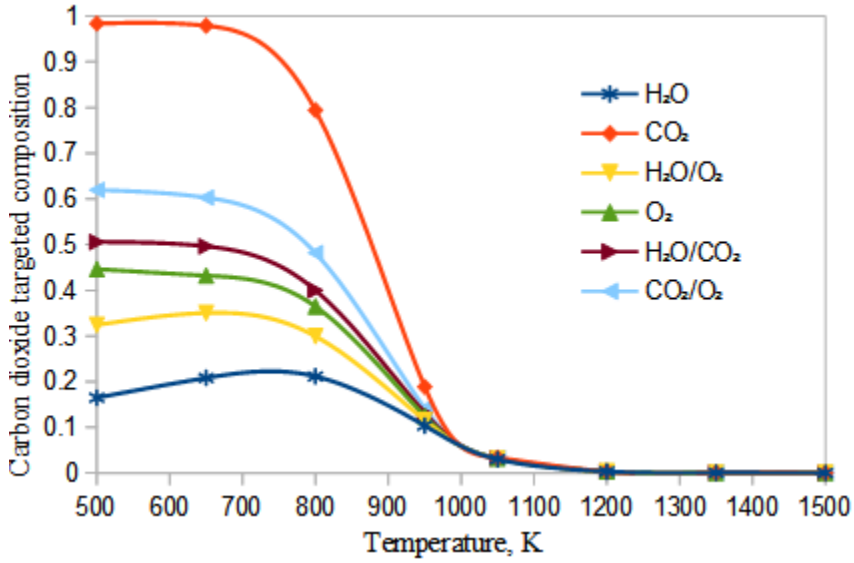

Figure 4. 18: Targeted composition of CO_2 from glycerol different reforming processes

4.4.7 Co-reforming glycerol and LLDPE using CHO diagrams

So far CHO ternary systems have been extensively used to target syngas composition from glycerol by employing different technologies. These CHO ternary systems revealed that at temperatures above 1050K, the carbon deposition boundary lines intersect with glycerol point. In

other words, at these temperatures, the syngas composition is targeted at the glycerol point. It was also shown that glycerol-derived syngas via different technologies cannot directly be used in downstream applications such as DME and methanol synthesis. Linear low-density polyethylene plastics (LLDPE) consist only of carbon and hydrogen; thus, it can be easily plotted on a CHO ternary diagram as a single point (on C-H side). From this point, different reforming processes can be used to convert LLDPE into syngas. It is also possible to mix glycerol with LLDPE into different proportions and these proportions can be presented as single points in a CHO ternary diagram. This study does not consider syngas production from pure LLDPE (100% LLDPE) but a mixture of glycerol and LLDPE. This section focuses on targeting syngas composition by mixing linear low-density polyethylene plastics (LLDPE) with glycerol and compare the targeted syngas with previous results. Various proportions can be obtained from a mixture of glycerol and LLDPE and this will have an impact on syngas ratio. Tay *et al*. (2011) showed that biomass steam gasification produces a lower syngas ratio compared to methane steam reforming at 1200 K. The main reason behind this difference can be attributed to the fact that methane lies on the C-H edge of the CHO diagram whereas biomass lies inside the triangle. The more one moves towards the C-H edge the higher the syngas ratio. In the case of a glycerol-LLDPE mixture, increasing the composition of LLDPE will eventually increase the syngas ratio. Figure 4.19 illustrates the reforming of 75% LLDPE-25% glycerol using O_2 and H_2O on a CHO diagram at different temperatures. To determine the optimum amount of reforming agents required to convert 1 kmol of 75% LLDPE-25% glycerol mixture is done in the same way as in previous sections. Results are summarized in Appendix E (table E.10 and E.11)

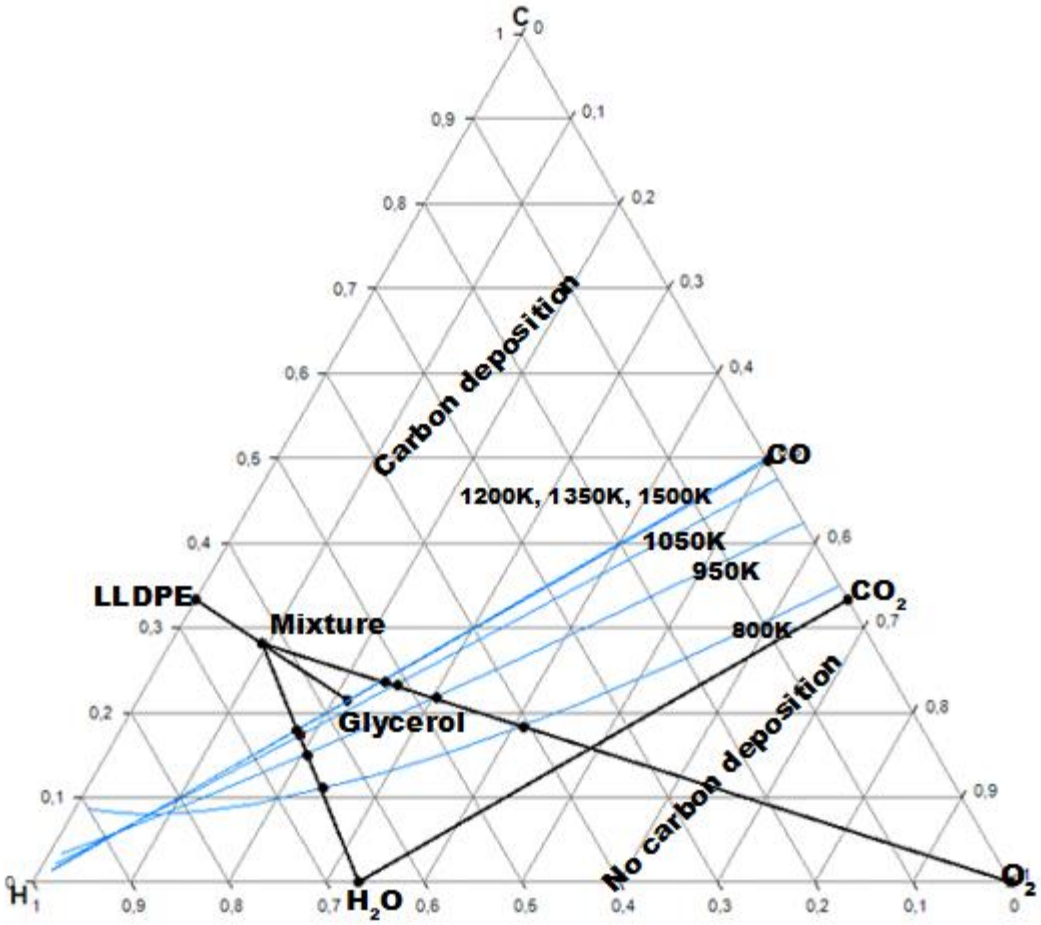

Figure 4. 19: Representation of a 75% LLDPE- 25% glycerol co-reforming on the CHO ternary diagrams using H_2O and O_2 as reforming agents

4.4.7.1 Targeting the optimum amount of H_2O and O_2 required to gasify 1 kmol of 75% $(C_2H_4)_n$ and 25% $C_3H_8O_3$ mixture

Figure 4.20 shows the optimum amount of H_2O and O_2 needed to convert 1 kmol of plastics and glycerol mixture into syngas at different temperatures. It can clearly be seen that 1 kmol of plastics and glycerol waste mixture requires more H_2O and less O_2 at all temperatures. For example, at a temperature of 1050K, 1 kmol of 75% LLDPE-25% glycerol mixture requires 1.7085 kmol of steam while it requires 0.8409 kmol of O_2 to be fully reformed. In terms of mass, 1 ton of 75% LLDPE-25% glycerol mixture requires 0.699 tons of steam to be fully converted at 1050K without depositing any solid carbon. If oxygen were used as a reforming agent instead of steam, 1 ton of the same mixture would require 0.6120 ton of oxygen to be fully gasified at 1050K.

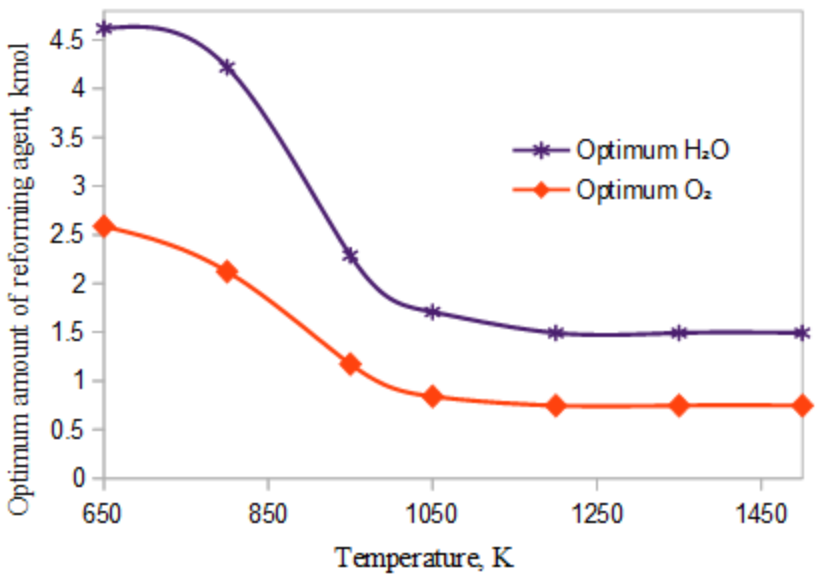

Figure 4. 20: Optimum amount of H_2O and O_2 required to fully convert 1 kmol of plastic and glycerol waste

Looking closely at figure 4.20, it may be tempting to conclude that oxygen is the best reforming agent used in the co-reforming of plastics and glycerol wastes at a temperature range of 650-1500K based on the amount of reforming agent required. But to identify a suitable oxidizing agent used to fully convert 1 kmol of 75% LLDPE-25% glycerol mixture, two criteria are considered. These criteria are explained below:

- Reforming agent that generates the least amount of CO_2 from 1 kmol of 75% LLDPE-25% glycerol mixture: figure 4.21 shows that 1 kmol of 75% LLDPE-25% glycerol mixture produces less amount of CO_2 when steam is used as a reforming agent than when O_2 and CO_2 at all temperatures. For example, at 1050K, the maximum amount of CO_2 that can be generated from 1 kmol of 75% LLDPE-25% glycerol mixture using steam as a reforming agent is 0.1303 kmol (2.113%). Whereas the maximum amount of CO_2 that could be produced from the same feed at 1050K is 0.1702 kmol (3.621%) if O_2 were used as a reforming agent and generates 3.34% CO_2.
- Oxidizing agent that produces more H_2 using the same feed (75% LLDPE-25% glycerol mixture): results once again reveal that, H_2O produces more hydrogen than O_2 from 1 kmol of 75% LLDPE-25% glycerol mixture. For example, at 1200K the maximum amount of H_2 that can be generated from this mixture is 3.8525 kmol (62.667%) when steam is used

as the reforming agent and when O_2 is used as reforming agent this mixture generates 2.4263 kmol (51.60%) of hydrogen.

These two criteria reveal that to produce H_2 and syngas from 1 kmol of 75% LLDPE-25% glycerol mixture, H_2O is a suitable reforming agent as it gives a high H_2 composition with less CO_2 emissions. Figure 4.21 shows the effect of temperature and reforming agent on the carbon dioxide composition.

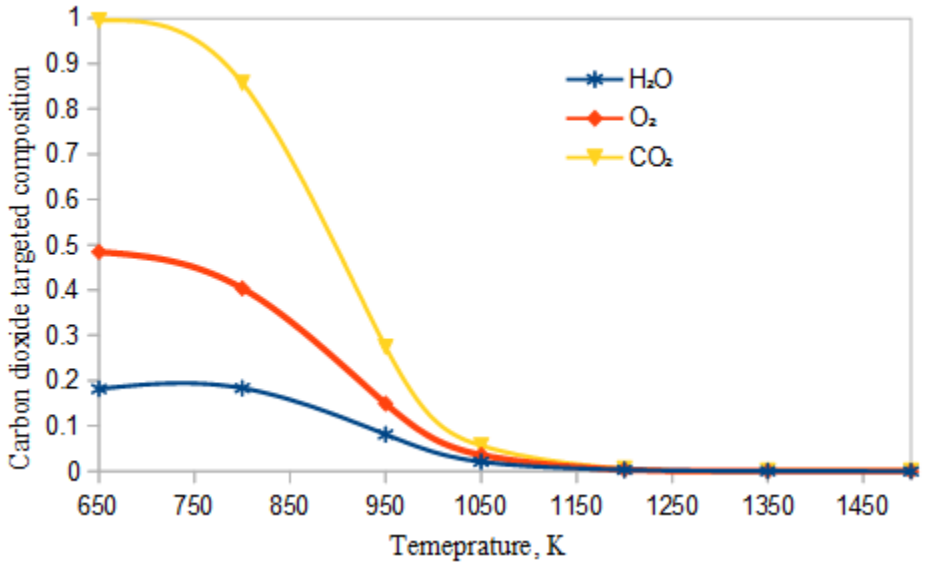

Figure 4. 21: CO_2 composition target from polyethylene-glycerol mixture using CHO ternary diagram using H_2O, CO_2 and O_2 as reforming agents

4.4.7.2 Optimal conditions for the co-reforming of glycerol and LLDPE using CHO ternary systems

Steam is the suitable reforming agent used to produce H_2 and syngas from 1 kmol of 75% LLDPE-25% glycerol mixture with less CO_2 emissions. However, a significant amount of CO_2 is produced at temperatures below 1050K with a low amount of H_2 and CO. This means that to convert 1 kmol of 75% LLDPE-25% glycerol mixture, low temperatures should be avoided. The optimal temperature at which 1 kmol of 75% LLDPE-25% glycerol mixture should be converted into H_2 and CO with the least amount of CO_2 produced is in the range of 1200-1500K.

4.4.8 Targeting the optimum net composition of CO_2 generated via CHO ternary systems

It is important to compare the net composition of CO_2 produced using crude glycerol as well glycerol-LLDPE mixture via different reforming technologies. Figure 4.22 shows the reforming of glycerol as well as the co-reforming of glycerol and LLDPE on a single CHO diagram. Points M and N represent the LLDPE-glycerol mixture and glycerol respectively. The three dashed lines represent glycerol reforming using H_2O, CO_2, and O_2 as reforming agents.

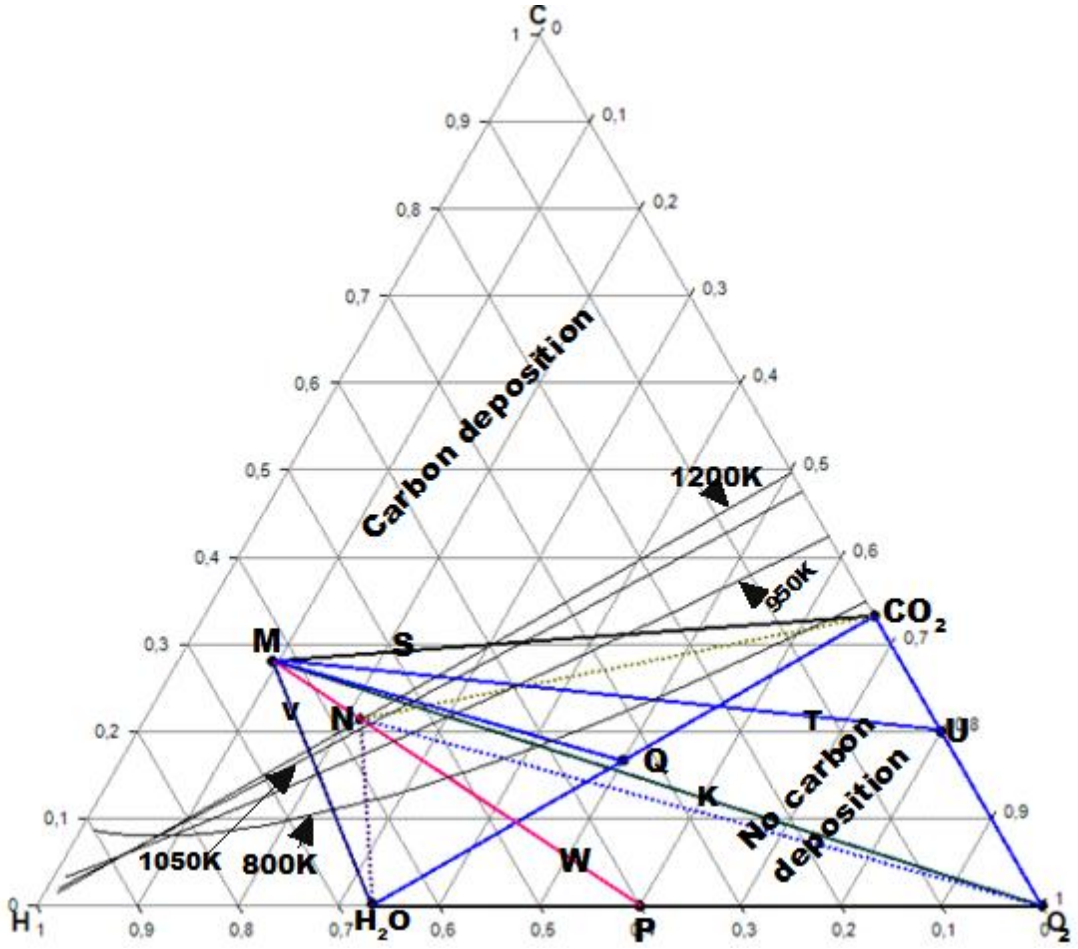

Figure 4. 22: Targeting CO_2 net amount emitted using CHO ternary systems

Lines V, S, and K represent the reforming of LLDPE-glycerol mixture using H_2O, CO_2, and O_2 as reforming agents respectively. The respective points Q, P, and U represent the co-feed of H_2O-CO_2, H_2O-O_2, and CO_2-O_2 as main reforming agents to produce syngas from 1 kmol of mixture M. A similar approach can be followed to represent the co-feed of H_2O-CO_2, H_2O-O_2, and CO_2-O_2 for glycerol reforming (on the same CHO diagram). Reforming lines intersect with carbon boundary lines at different temperatures and the points of intersection represent the syngas

composition target in equilibrium with carbon. These intersection points are not shown in figure 4.22 (this has been already shown in previous sections).

This figure presents insightful information regarding glycerol and linear low-density polyethylene plastics wastes reforming. Consider for example lines M-P and N-P which represent the reforming of glycerol and LLDPE-glycerol mixture using H_2O-O_2 as a reforming agent. It can be shown that glycerol and LLDPE-glycerol mixture reforming produce the same syngas composition using H_2O-O_2 as a reforming agent. This is explained by the fact that syngas composition target lies on the same line (from point M to P).

Using the lever-arm rule, the minimum amount of CO_2 needed to convert the mixture of LLDPE, and glycerol can be determined at different temperatures. For example, at 1050K, 1 kmol of 75% $(C_2H_4)_n$-25% $C_3H_8O_3$ mixture requires 1.929 kmol of CO_2 and the amount of CO_2 generated from 1 kmol of this mixture is 0.212 kmol (0.567%). It shows that the amount of CO_2 generated is less than the amount of CO_2 fed. This implies that the net amount of CO_2 evolved during the reforming of 1 kmol of 75% $(C_2H_4)_n$-25% $C_3H_8O_3$ mixture using CO_2 as reforming agent is negative. At this same temperature, crude glycerol requires 0.272 kmol of CO_2 to be fully converted without depositing any solid carbon and this leads to a negative net amount of CO_2 evolved. The reforming of 1 kmol of crude glycerol requires less amount of CO_2 than the co-reforming of 1 kmol of 75%C_2H_4-25% $C_3H_8O_3$ using CO_2 as a reforming agent at 1050K.

In the same figure (4.22), the composition of CO_2 generated using points Q, P, and V as reforming agents can be calculated at different temperatures using 1 kmol of 75%$(C_2H_4)_n$-25%$C_3H_8O_3$ as the feedstock. Using point P (H_2O/O_2) as the reforming agent, it is interesting to see that 1 kmol of crude glycerol and 1 kmol of 75%C_2H_4-25%$C_3H_8O_3$ mixture produce the same syngas composition. This means that both processes generate the same composition of CO_2 at all temperatures. Comparing point U(CO_2/O_2) with point Q (CO_2/ H_2O), it is found that 1 kmol of 75% $(C_2H_4)_n$-25%$C_3H_8O_3$ uses less amount of CO_2 when point Q is used as a reforming agent than point U at any temperature. For example, at 1050K, the amount of CO_2 needed to convert 1 kmol of 75%$(C_2H_4)_n$-25%$C_3H_8O_3$ when points U and Q are used as reforming agents is found to be 0.602 and 0.880 kmol. The amount of CO_2 generated using points U and Q is 0.171 and 0.190 kmol respectively (at 1050 K).

Figure 4.23 represents the composition targets of H_2, CO, CH_4, H_2O, and CO_2 produced from the co-reforming of a glycerol-LLDPE mixture by using various reforming technologies. Using H_2O as a reforming agent produces the highest composition of H_2 followed by H_2O/O_2 at all temperatures. CO_2 and CO_2/O_2 produce the least composition of H_2 at all temperatures. The composition of CO follows an inverse trend, as H_2O and H_2O/O_2 produce the least composition of CO at all temperatures. The highest composition of CO is produced by using CO_2 and CO_2/O_2 as reforming agents since these two technologies introduce more carbon in the feed ($C_3H_8O_3$ and CO_2) unlike in the case of other reforming technologies.

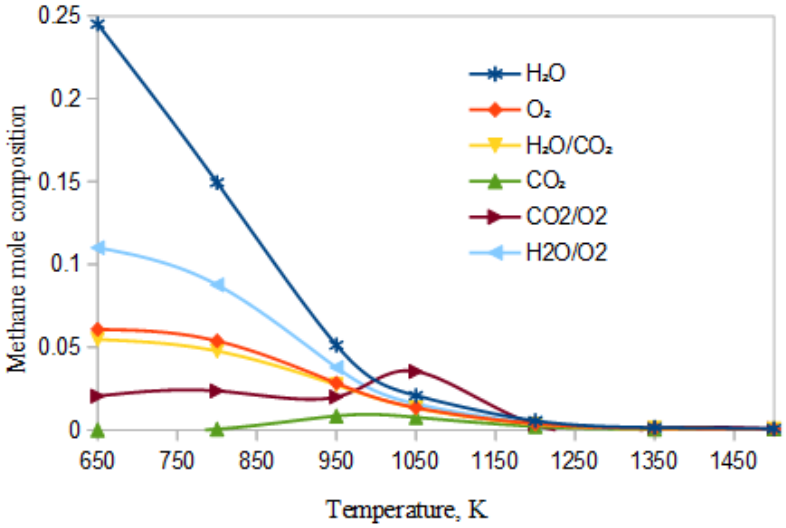
Methane mole composition
0.25
0.2
0.15
0.1
0.05
0
650
750
850
950
1050
1150
1250
1350
1450
Temperature, K
H₂O
O₂
H₂O/CO₂
CO₂
CO2/O2
H2O/O2

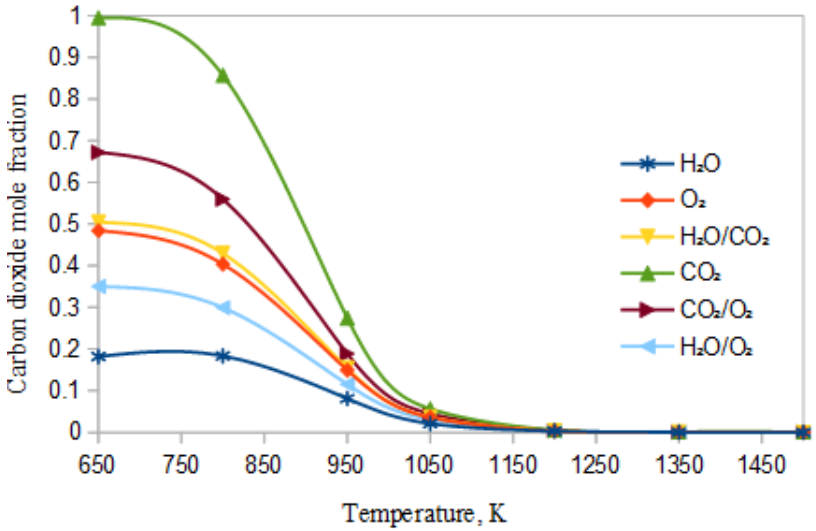
Carbon dioxide mole fraction
1
0.9
0.8
0.7
0.6
0.5
0.4
0.3
0.2
0.1
0
650
750
850
950
1050
1150
1250
1350
1450
Temperature, K
H₂O
O₂
H₂O/CO₂
CO₂
CO₂/O₂
H₂O/O₂

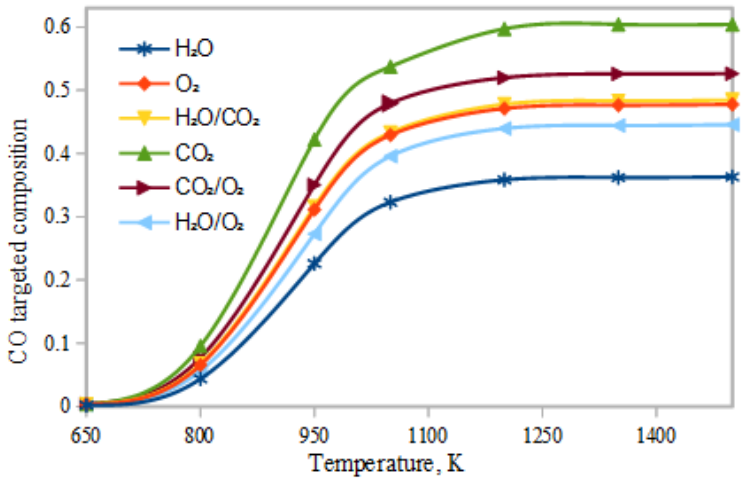
CO targeted composition
0.6
0.5
0.4
0.3
0.2
0.1
0
650
800
950
1100
1250
1400
Temperature, K
H₂O
O₂
H₂O/CO₂
CO₂
CO₂/O₂
H₂O/O₂

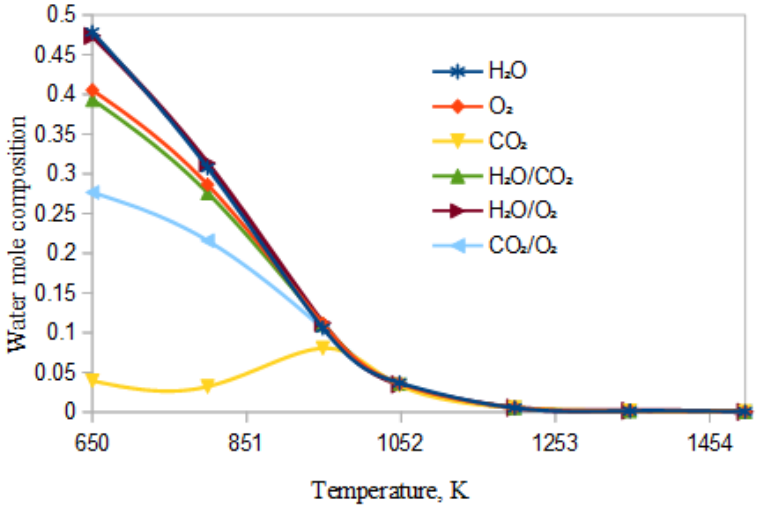
Water mole composition
0.5
0.45
0.4
0.35
0.3
0.25
0.2
0.15
0.1
0.05
0
650
851
1052
1253
1454
Temperature, K
H₂O
O₂
CO₂
H₂O/CO₂
H₂O/O₂
CO₂/O₂

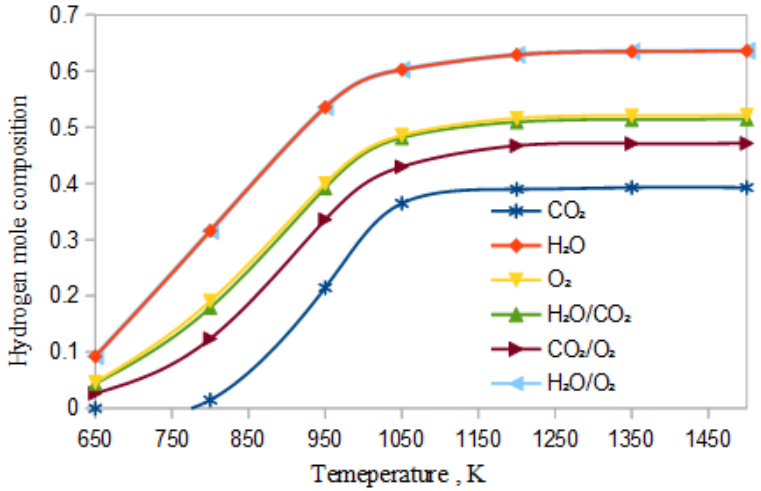

Figure 4. 23: Syngas composition target during the co-reforming of glycerol and plastics waste via different technologies

4.5 Summary of findings based on glycerol and polyethylene plastic wastes reforming

Table 4.5 provides a summary of the findings from glycerol (100% feed) and a mixture of 75% plastics-25% glycerol using different technologies at optimal conditions. As stated earlier, the CHO ternary diagrams revealed that at a temperature higher than 1050K the optimum amount of reforming agent needed to convert glycerol into syngas is zero. This is because glycerol and syngas target points are located at the same point on the CHO ternary diagram. Temperatures higher than 1050K produce syngas with an insignificant composition of CO_2, CH_4, and H_2O. GSR produces the highest syngas ratio (H_2: CO = 1.373) followed by GSR+ GPO (H_2: CO = 1.320). GDR produces the least syngas ratio (H_2: CO = 1.229) at 1050K. This implies that H_2O is the most suitable reforming agent to produce syngas from glycerol at 1050K. Also considering the mixture of glycerol-LLDPE, it was shown that H_2O is once again the most suitable reforming agent to convert this mixture into syngas at 1200K. Figure 4.24 shows the effect of temperature on syngas ratio generated from glycerol and glycerol-LLDPE mixture (MSR: mixture steam reforming, MDR: mixture dry reforming and MPO: mixture partial oxidation). It can be shown that mixing glycerol with LLDPE has an impact on the syngas ratio. For example, at a temperature of 1200K, GSR produces a syngas ratio (H_2: CO) of 1.280 whereas glycerol-LLDPE mixture produces a syngas ratio (H_2: CO) of 1.755 using steam as a reforming agent. Glycerol-LLDPE mixture produces syngas ratio higher than glycerol using O_2 as a reforming agent. For example, at 1200K GPO produces a syngas ratio of 1.280 whereas Glycerol-LLDPE mixture partial oxidation produces a syngas ratio of 1.095. This implies that glycerol-LLDPE mixture using oxygen as a reforming agent is favourable for downstream processes that require a syngas ratio close to 1. Whereas for downstream processes that require a syngas ratio close to 2, glycerol-LLDPE mixture using steam as reforming agent is favourable. It can be further shown that glycerol-LLDPE mixture steam reforming produces higher hydrogen composition than glycerol-LLDPE mixture partial oxidation, glycerol steam reforming, and glycerol partial oxidation. For example, at 1200K, glycerol-LLDPE mixture steam reforming produces 62.89% H_2, whereas glycerol steam reforming, glycerol partial oxidation, and glycerol-LLDPE partial oxidation produce 55.40%, 55.40 %, and 51.60 % H_2 respectively at the same temperature (1200K). These results are shown in Appendix E.

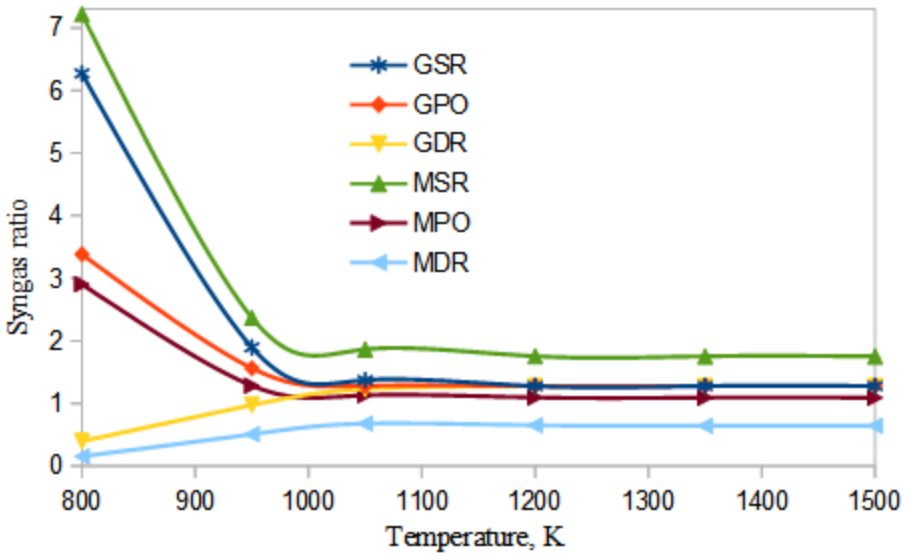

Figure 4. 24: Effect of temperature on glycerol and glycerol-LLDPE mixture derived syngas ratio, MSR: steam reforming of glycerol-LLDPE mixture, MPO and MDR: partial oxidation and dry reforming of glycerol-LLDPE mixture respectively.

Table 4. 5: Summary of product composition of glycerol and plastics reforming at optimal conditions

Feed: 1 kmol	Reforming agents	Temperature K	$\frac{H}{O}$	Optimum amount of oxidizing agent kmol/kmol glycerol	Syngas composition target					Optimum amount of syngas targeted kmol/kmol glycerol	$\frac{H_2}{CO}$
					x_{CH_4}	x_{H_2O}	x_{H_2}	x_{CO}	x_{CO_2}		
Glycerol	None	1200	2.651	None	0.0042	0.0054	0.5513	0.4360	0.0033	6.764	1.264
	H_2O	1050	2.653	0.34264	0.01630	0.03460	0.53174	0.3872	0.03024	6.9165	1.373
	O_2	1050	2.445	0.1211	0.0153	0.0350	0.5156	0.4019	0.0323	6.6734	1.283
	CO_2	1050	2.311	0.272	0.01460	0.0352	0.5057	0.4114	0.0334	6.5303	1.229
	H_2O/O_2	1050	2.533	0.0795	0.01571	0.03479	0.52240	0.3958	0.0315	6.7726	1.320
	H_2O/CO_2	1050	2.476	0.274	0.01543	0.03490	0.51796	0.39971	0.0320	6.7090	1.296
	O_2/CO_2	1050	2.365	0.1851	0.01489	0.03512	0.50932	0.4076	0.0331	6.5847	1.250
Glycerol and LLDPE	H_2O	1200	3.642	1.4930	0.00552	0.00511	0.62887	0.35836	0.0034	6.9165	1.755
	O_2	1200	2.266	0.7472	0.0037	0.0055	0.5160	0.47111	0.00370	4.70210	1.095
	CO_2	1200	1.30	1.555	0.0021	0.0054	0.3896	0.5971	0.0059	3.7189	0.653
	H_2O/O_2	1200	2.651	0.9923	0.0042	0.0054	0.5476	0.4396	0.00330	5.0324	1.246
	H_2O/CO_2	1200	2.651	1.455	0.0042	0.0054	0.5476	0.4396	0.0033	5.0324	1.246
	O_2/CO_2	1200	2.651	1.0474	0.0042	0.0054	0.5476	0.4396	0.00330	5.0324	1.246

4.6 Applications of glycerol-derived syngas in downstream processes

Up to this point, it has been shown that glycerol can be used as a feedstock to target syngas production via steam, partial oxidation, and dry reforming processes but also using a combination of these three by means of a graphical approach. Using this graphical approach, the optimum amount of reforming agent needed to completely transform glycerol into syngas was targeted. It was revealed that at high temperatures glycerol is decomposed producing two main species viz. H_2 and CO (pyrolysis). The composition of these two main species were targeted at glycerol point on the CHO diagrams due to the fact there was no relative distance of reforming agents to syngas target point at these high temperatures. The temperature limit at which the optimum amount of reforming agent was targeted is 1050K. However, at this temperature limit, the syngas generated contains significant composition of CO_2, H_2O, and CH_4 which is unfavorable for downstream processes. It was also shown that the syngas generated from 100% glycerol at all temperatures cannot directly be used in downstream processes because the H_2:CO ratio is less than 2 for mixed alcohols, methanol and DME (direct route) synthesis. For the synthesis of DME via indirect route this syngas ratio (H_2:CO) should be 1 (Mevawala *et al*., 2017).

In this study, the co-reforming of 75% LLDPE-25% glycerol mixture was also considered to compare the syngas composition targeted by reforming 100% glycerol with the one targeted from 75% LLDPE-25% glycerol mixture via different reforming processes. This comparison was done in previous sections using the same graphical approach. It was revealed that the co-reforming of 75% LLDPE with 25% glycerol increased the syngas ratio up to 1.755 using steam as reforming agent. Even though this syngas ratio increased it does not meet the requirement for synthesis of the above-mentioned chemicals.

This section focuses on different methods used to adjust the syngas ratio targeted from 75% LLDPE-25% glycerol mixture and 100% glycerol to meet the requirement for the synthesis of methanol and DME (via direct route). In this study two methods are used to adjust the H_2:CO ratio which are the introduction of CH_4 in the reformer to increase the H_2:CO up to 2 (methanol synthesis from glycerol) and using H_2O/CO_2 to adjust the H_2:CO to 1 (DME synthesis from glycerol-LLDPE mixture).

Studies such as Gutiérrez Ortiz *et al.* (2013) and Mahabir *et al.* (2021) have used Aspen Plus simulation to synthesize methanol from glycerol via supercritical water and autothermal reforming

processes respectively. Even though these studies provide important guidelines in producing methanol from glycerol, there is a lack of evaluating the performance of this process at early design stages. Thus, this section uses CHO ternary diagrams to determine the performance (screen out unnecessary alternatives) of methanol synthesis from glycerol. The section further uses these CHO ternary diagrams for the synthesis of DME from glycerol-LLDPE mixture.

4.6.1 Methanol synthesis from glycerol using CHO ternary diagrams

4.6.1.1 Using CHO ternary to determine the overall material balance

It is important to determine the overall material for CH_4O synthesis from $C_3H_8O_3$ using CHO ternary diagram. Figure 4.25 shows the overall mass target for methanol synthesis from glycerol. Point P_1 represents a region whereby water is not required nor produced during the synthesis of methanol. The lever-arm rule reveals that the minimum amount of $C_3H_8O_3$ needed for the synthesis of 1 kmol of CH_4O is 0.5 kmol. At this point (P_1) the process uses 0.25 kmol of O_2 and generates 0.5 kmol CO_2. Point P_3 represents a region whereby O_2 is not needed nor produced. The minimum amount of $C_3H_8O_3$ needed for the synthesis of 1 kmol of CH_4O at this point is targeted at 0.4286 kmol. The process utilizes 0.2857 kmol of H_2O and, generates 0.2857 kmol of CO_2 as waste. A process that does not required or produce CO_2 is presented by point P_2 and the minimum amount of $C_3H_8O_3$ needed to produce 1 kmol of CH4O is targeted at 0.333 kmol. At this point, the process uses 0.667 kmol of H_2O and generates 0.333 kmol O_2.

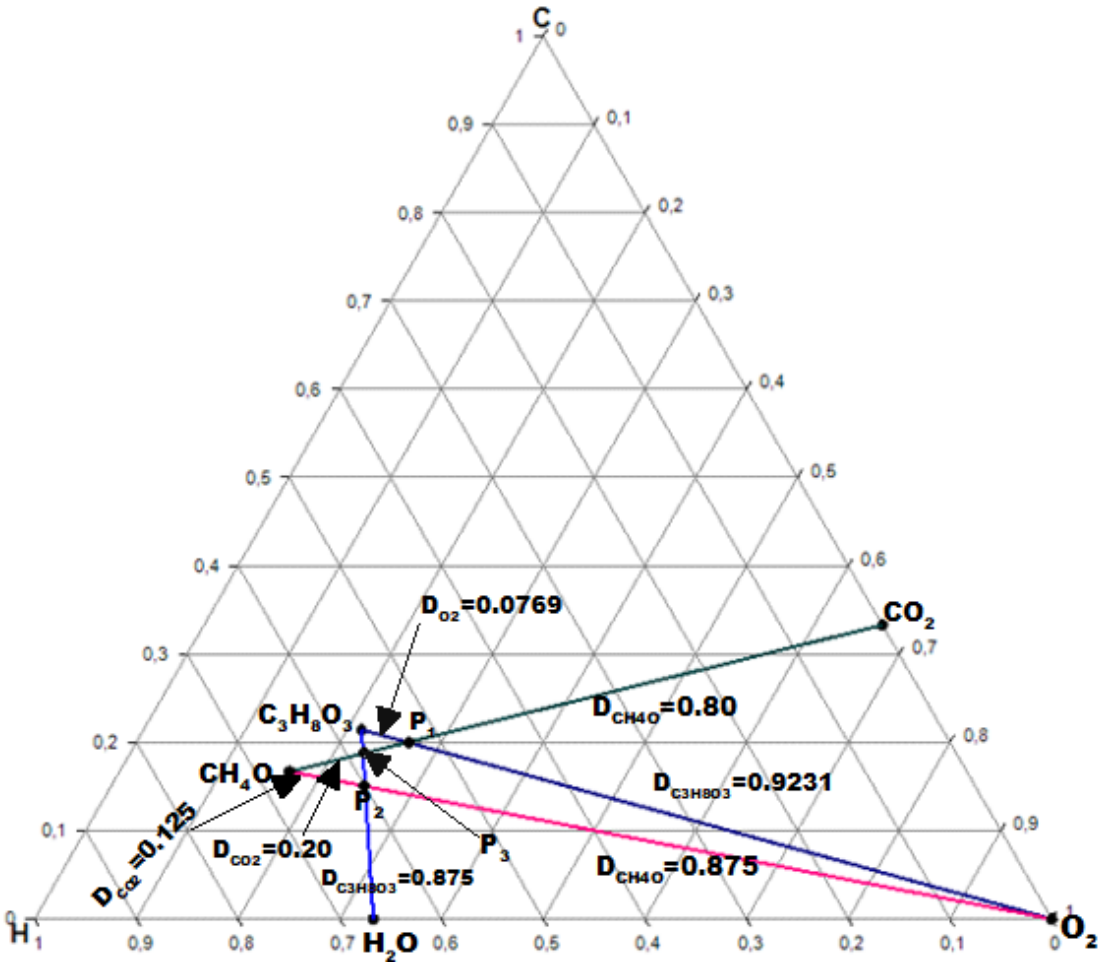

Figure 4. 25: Overall mass balance target for methanol synthesis from glycerol

4.6.1.2 Evaluating the sustainability of methanol from glycerol process

CHO ternary diagrams have shown that there are three alternatives during the synthesis of methanol from glycerol (P_1, P_2 & P_3). It is important to screen out any alternative that is not feasible using different tools as discussed in chapter 3. Table 4.6 gives a summary of the sustainability of each alternative. The first step in evaluating the sustainability of each alternative is to determine the Gibbs energy. Table 4.6 shows that alternative P_2 is not feasible from a thermodynamic point of view because its Gibbs energy is greater than zero. Therefore, P_2 should be screened out. Since alternative P_1 and P_3 have both a negative Gibbs energy, other tools are used in order to screen out either P_1 or P_3. Comparing the atom economy of alternative P_1 and P_3 it is revealed that P_3 has the highest atom economy. The higher the atom economy the more sustainable an alternative (high

percentage of raw materials is converted into product). This means that P_3 is more sustainable than P_1. It is also shown that P_3 has higher carbon efficiency and less E-factor than P_1. The evaluation of the three alternatives during the synthesis of methanol from glycerol is summarized in table 4.6 (using Gibbs energy, atom economy, carbon efficiency, and E-factor)

Table 4. 6: Evaluating glycerol biorefinery for methanol synthesis

Tool	**P_1**	**P_2**	**P_3**
Gibbs energy, kJ/mol	-140.56	139.29	-20.58
Atom economy, %	59.26	75.04	71.79
Carbon efficiency, %	66.67	100	77.77
E-factor	0.687	0.333	0.393

The remaining sustainability indicator to evaluate the glycerol biorefinery is the economic potential (EP). This can be done by using Equation 3.25i. It is important to study the effect of change of glycerol price on the economic potential (alternative P1, P2, and P3). This is because the price of glycerol will not remain constant once any alternative has been evaluated.

Figure 4.26 shows the effect of a change in glycerol price on the economic potential. As it can be seen a dramatic increase in glycerol price reduces the economic potential of all three alternatives (P1, P2, and P3). For example, at a glycerol price of 0.025 $/kg, the approximate economic potential of alternative P1, P2, and P3 is $123.61, $139.62, and $130.47 million per year respectively. Whereas the economic potential of these 3 alternatives (P1, P2, and P3) is found to be -$13.01, $48.63, and $13.39 million per year at a glycerol price of $0.4/kg ($400 /ton). This shows that, if the price of glycerol were fixed at $0.4/kg, alternative P1 can be automatically screened out (negative economic potential). It was earlier shown that alternative P2 is not feasible from a thermodynamic point of view. Comparing the economic potential of alternative P1 and P3, it is evident to see that P3 is more feasible in a glycerol range of $0.025/Kg- $0.6/Kg (although its EP is lower than P2). This implies that the process designer can use alternative P3 for the synthesis of methanol from glycerol.

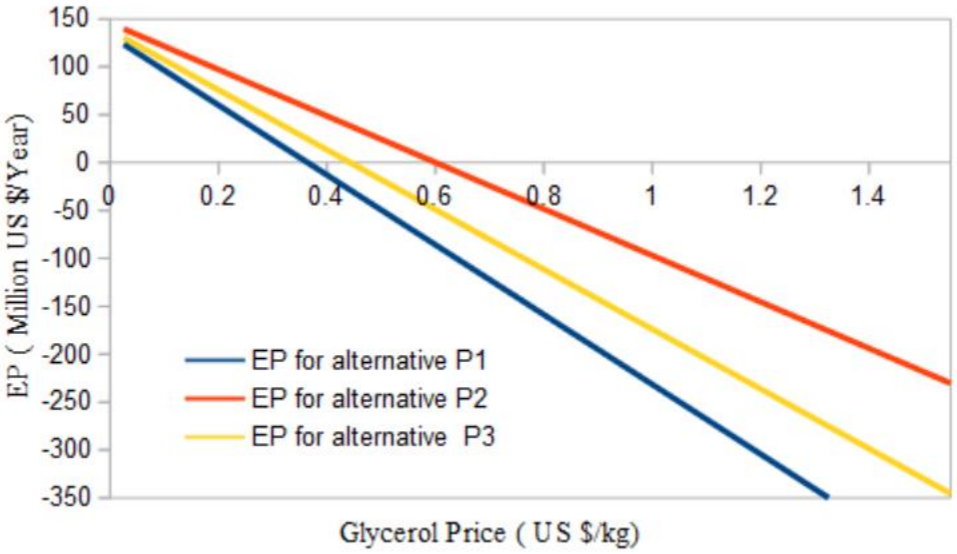

Figure 4. 26: Effect of glycerol price on economic potential

The overall material target for CH_4O synthesis from $C_3H_8O_3$ (at point P_3) is summarized as follows:

$$0.4286C_3H_8O_3 + 0.2857H_2O \implies 1CH_4O + 0.2857CO_2 \qquad 4.2$$

In terms of mass, 1 ton of $C_3H_8O_3$ requires 0.1304 ton of H_2O to produce 0.8116 ton of CH_4O and 0.3189 ton of CO_2. It must be noted that this represents the overall material balance and is not a one-step process as glycerol must be converted into syngas first.

4.6.1.3 Using glycerol-derived syngas for methanol synthesis

The production of methanol from glycerol is a two-step process. The first step consists of converting glycerol into syngas while the second step utilizes the glycerol-derived syngas for methanol synthesis. The requirements for methanol synthesis from syngas are as follows $H_2/CO \geq 2$ and $CO_2/CO \leq 0.6$ (Tay *et al.*, 2011). Looking at figure 4.15, none of the three reforming agents (H_2O, O_2, and CO_2) produces syngas that fulfil methanol synthesis specifications in terms of H_2/CO. At a temperature range of 500-1050 K, GSR produces the highest syngas ratio (see figure 4.15). At a temperature range of 1200-1500 K, all glycerol reforming processes produce the same syngas ratio because at these temperatures, the syngas target point intersects with the glycerol point as shown in previous sections. Huang *et al.* (2018) have shown experimentally that, introducing methane in glycerol steam reforming can produce a syngas that fulfils the methanol synthesis requirement$\left(\frac{H_2}{CO} \sim 2\right)$.

4.6.1.3.1 Using CHO ternary diagrams to determine the overall mass balance when $C_3H_8O_3$ is co-fed with CH_4

Figure 4.27 gives a summary of mixing glycerol with methane in the presence of steam to produce 1 kmol of methanol. Point V (intersects CH_4-$C_3H_8O_3$ streamline) is formed by drawing a line from water point to CH_4-$C_3H_8O_3$ streamline passing through methanol point. The distance of water relative to methanol is calculated and found to be 0.20. Point T (intersects $C_3H_8O_3$-H_2O streamline) is obtained by drawing a line from methane point to $C_3H_8O_3$-H_2O streamline passing through methanol point. The distance of methane relative to methanol is also calculated and found to be 0.33. Lastly, point P is formed by drawing a line from glycerol point to H_2O-CH_4 streamline passing through methanol point. The line segment from methanol to point P represents the distance of glycerol relative to methanol. This distance is calculated and found to be 0.469. The stoichiometric coefficients of water, methane, and glycerol are calculated using these different relative distances and found to be 0.4, 0.4, and 0.2 respectively.

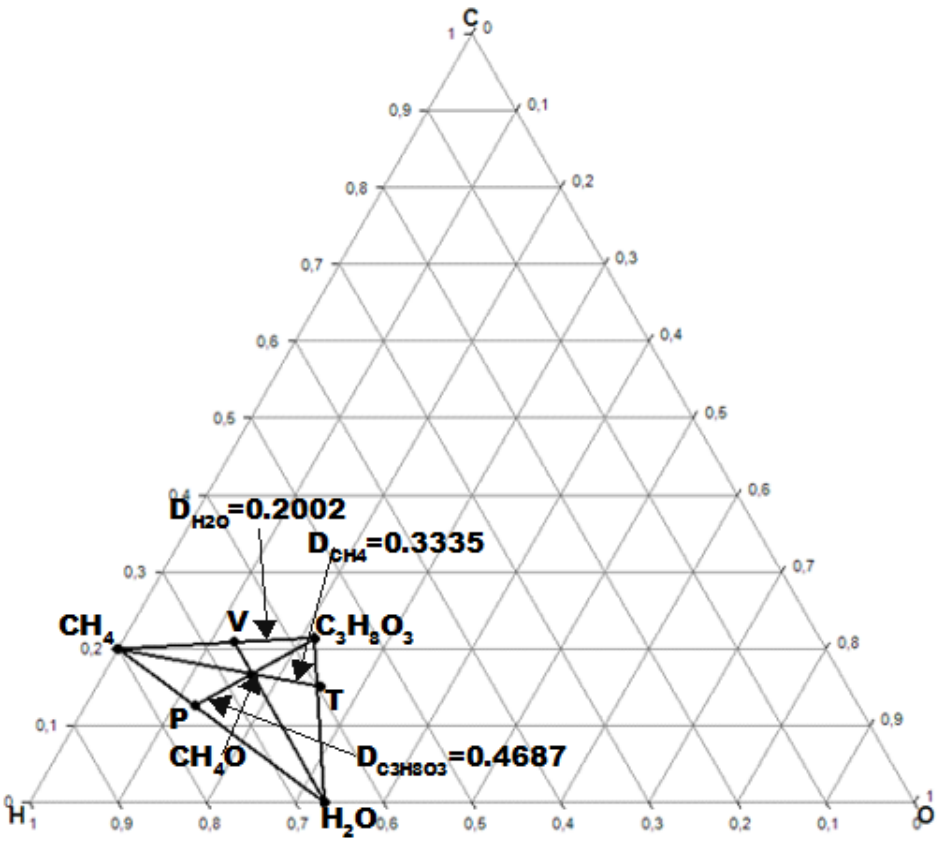

Figure 4. 27: Overall material balance for the synthesis of 1 kmol of methanol from glycerol, methane, and water

This shows that 0.2 kmol of glycerol can be co-fed with 0.4 kmol of methane in the presence of 0.4 kmol of water to produce 1 kmol of methanol. Scaling this process up, 10.87 kmol of glycerol require 21.74 kmol methane in the presence of 21.74 kmol of water to produce 54.35 kmol of methanol. It must be noted that this is a two-step process, meaning that glycerol and methane should be transformed into syngas in the presence of steam and this syngas can be used to produce methanol. The next section shows this approach by means of a CHO ternary diagram.

Figure 4.28 shows how the optimum amount of syngas derived from methane reforming can be mixed with glycerol-derived syngas. Point R represents the decomposition of glycerol at 1200 K (since steam is not needed to convert it into syngas), point P represents the syngas composition target that meets the requirement for methanol synthesis (H_2:CO= 2). Point S represents the steam reforming of methane at 1200K.

4.6.1.3.2 Determining the mixing ratio between glycerol-derived syngas with methane derived syngas

Let β be the mixing ratio of methane steam reforming- derived syngas to glycerol derived -syngas. The lever-arm rule reveals that the value of β is 0.551:0.449. This means that 1 kmol of glycerol derived syngas should be mixed with 1.227 kmol of methane steam reforming derived syngas to achieve a syngas ratio of 2. The amount of syngas produced from glycerol at 1200K is targeted at 6.802 kmol/kmol glycerol. At this temperature, the minimum amount of H_2O required to convert 1 kmol of glycerol into syngas is 0. This is explained by the fact that at this temperature, syngas target composition point intersects with glycerol point. The methane steam reforming produces 8.8404 kmol/kmol methane at the same temperature to meet the methanol synthesis requirement (H_2:CO=2). In terms of mass, 1 ton of glycerol produces 1.0021 ton of syngas 73.938 kmol. This implies that 73.935 kmol of this glycerol derived syngas require 90.735 kmol from methane steam reforming derived syngas to fulfil the requirement for methanol synthesis. This is summarized in table 4.7 and 4.8. Following the same reasoning as shown in figure 4.28, the mixing ratio (in terms of moles) between glycerol and methane is found to be 1/2. This means that 10.87 kmol (1 ton) of glycerol requires 21.74 kmol (0.3478 ton) of methane. This means that 10.87 kmol of glycerol should be mixed with 21.74 kmol of methane to achieve a syngas ratio of 2.

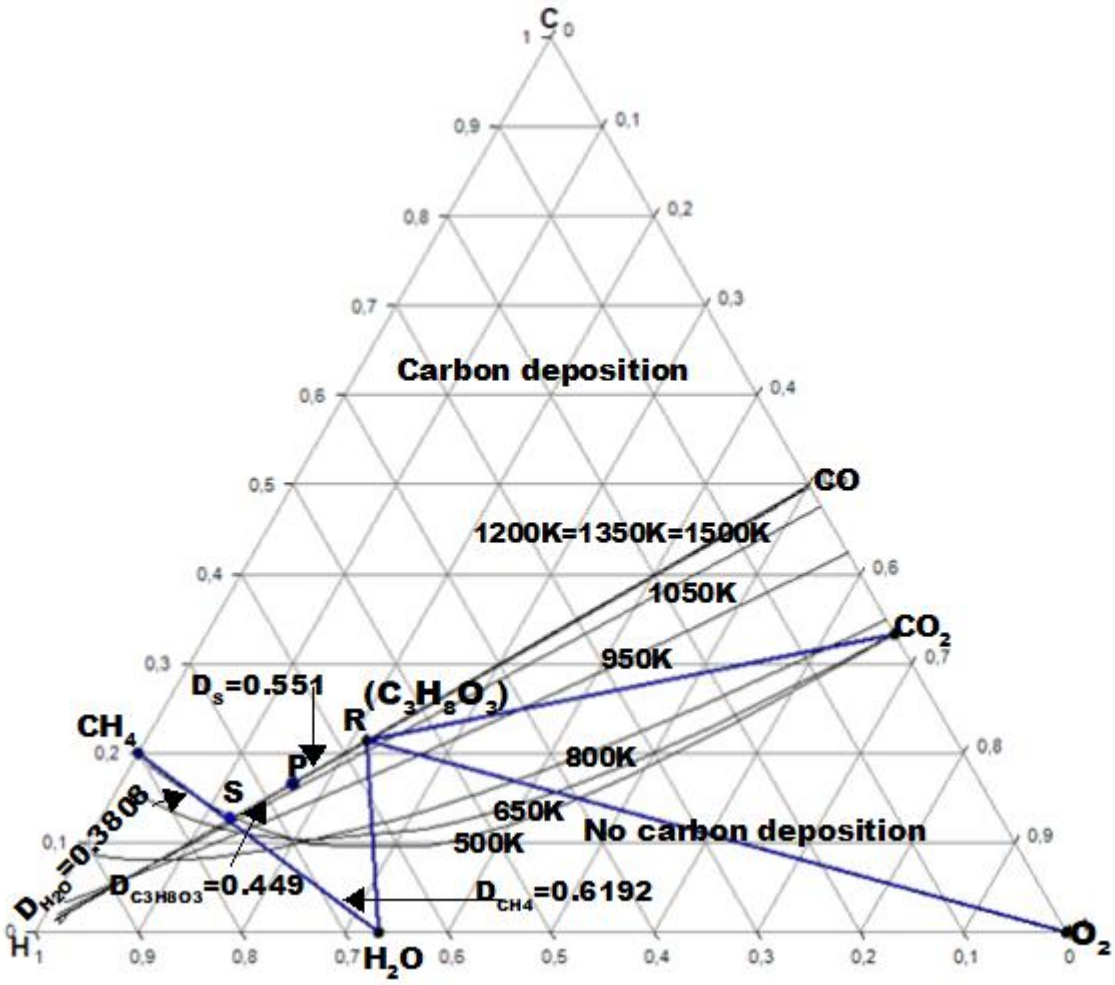

Figure 4. 28: Mixing methane derived syngas with glycerol derived syngas at 1200K to meet methanol synthesis requirement

It is now important to determine the amount of steam required to convert $C_3H_8O_3$-CH_4 into syngas that fulfils the ratio requirement (H_2: CO =2) for methanol synthesis. The lever-arm reveals that, 21.74 kmol (0.391 ton) of steam is needed to produce a syngas that fulfils this requirement.

Table 4. 7: Syngas composition target at point R and S

$\frac{H}{O}$	Temperature K	Syngas targeted composition					H_2/CO
		x_{CH_4}	x_{H_2O}	x_{H_2}	x_{CO}	x_{CO_2}	
2.725 (R)	1200	0.0043	0.00538	0.5536	0.4335	0.0033	1.277
6.270(S)	1200	0.00736	0.0042	0.7469	0.2457	0.00011	2.9325

It must be noted that using two reformers to produce syngas from glycerol and methane can be costly. Thus, both glycerol and methane are co-reformed in a single reformer using steam as a reforming agent. The total syngas from this process is shown in table 4.8

Table 4. 8: Amount of syngas that meets methanol synthesis requirement at 1200K

Targeting point	On a molar basis (kmol)		In terms of mass (ton)	
	CO	H_2	CO	H_2
R	32.051	40.93	0.8974	0.08186
S	22.294	67.77	0.6242	0.1355
Total	54.345	108.70	1.5220	0.2174
H_2/CO	2.00			

4.6.1.3.3 Targeting the maximum amount of methanol

From table 4.8, a mixture of glycerol-methane can produce 54.35 kmol of CO and 108.70 kmol of H_2 for the synthesis of methanol. Figure 4.29 shows a simplified process for methanol synthesis from a glycerol-methane mixture. From this figure, it can be seen that the total production of methanol from 1 ton of glycerol, 0.3478 ton of methane, and 0.3913 ton of steam is targeted at 1.7392 ton (based on a 100% CO conversion). Tay *et al*. (2011) used 1 ton of biomass ($CH_{1.4}O_{0.59}$) to produce methanol via steam gasification. It was shown that this process does not produce syngas that meets methanol synthesis requirement (H_2:CO = 2). Tay *et al*. (2011) showed that methane steam reforming-based syngas must be mixed with gasification steam reforming-based syngas to fulfil methanol synthesis requirement. The total amount of syngas from these two technologies was found to be 2.497 ton (2.124 ton of CO, and 0.375 ton of H_2). Based on a 50% CO conversion, the total amount of methanol that can be produced from this process was targeted at 1.214 ton. Comparing Tay *et al*. (2011) results (methanol from biomass gasification- methane reforming technologies) with the current study's results it can be shown that glycerol/methane steam reforming produces a lower amount of methanol than biomass steam gasification/methane steam reforming. For example, considering a 50 % CO conversion, glycerol/methane reforming produces 0.870 ton of methanol whereas biomass steam gasification/methane steam reforming produces 1.214 ton of methanol. This corresponds to an increase of approximately 39.60%. The main reason

for this difference in methanol production can be attributed to the fact that glycerol and biomass have different C:H:O atomic ratios. This means that both feedstocks (glycerol and biomass) will produce different syngas composition at the same temperature (1200K). Another reason behind this difference is due to the fact that glycerol does not require any steam to produce syngas at 1200K, whereas biomass requires steam. When performing an overall material balance glycerol-methane mixture will produce less amount of methanol than a biomass-methane mixture.

Comparing figure 4.29 with the overall target from equation 4.2, it can be shown that introducing methane in the reformer increases syngas ratio as well as the amount of methanol.

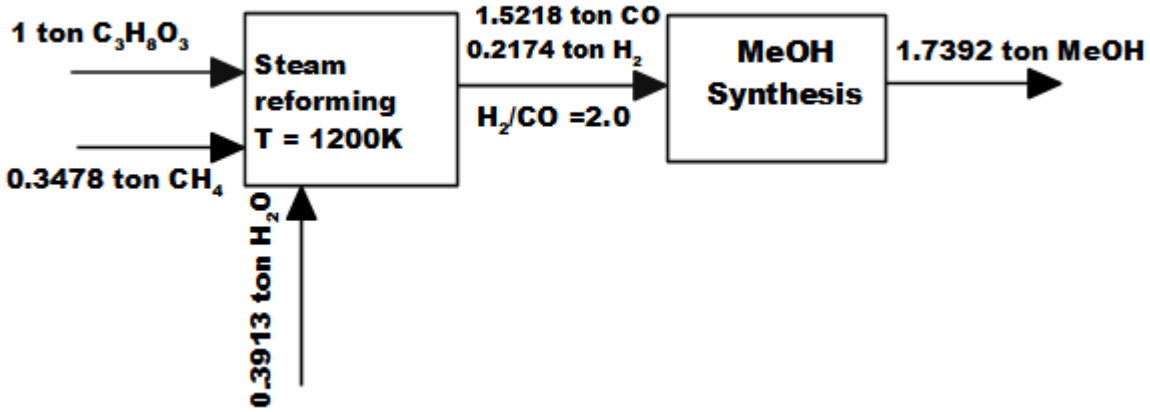

Figure 4. 29: Simplified block diagram for methanol synthesis from glycerol

Considering the same figure (4.29), the atom economy, carbon efficiency as well as E-factor are calculated and found to be 100%, 100% and 0 respectively. The economic potential of this process can now be calculated using equation 3.25i. Because the price of glycerol might fluctuate, it is imperative to perform a sensitivity analysis as indicated in figure 4.30. Comparing the economic potential values from figure 4.30 with the values in figure 4.26 (P3), it can be seen that introducing methane in the reformer increases also the overall economic potential.

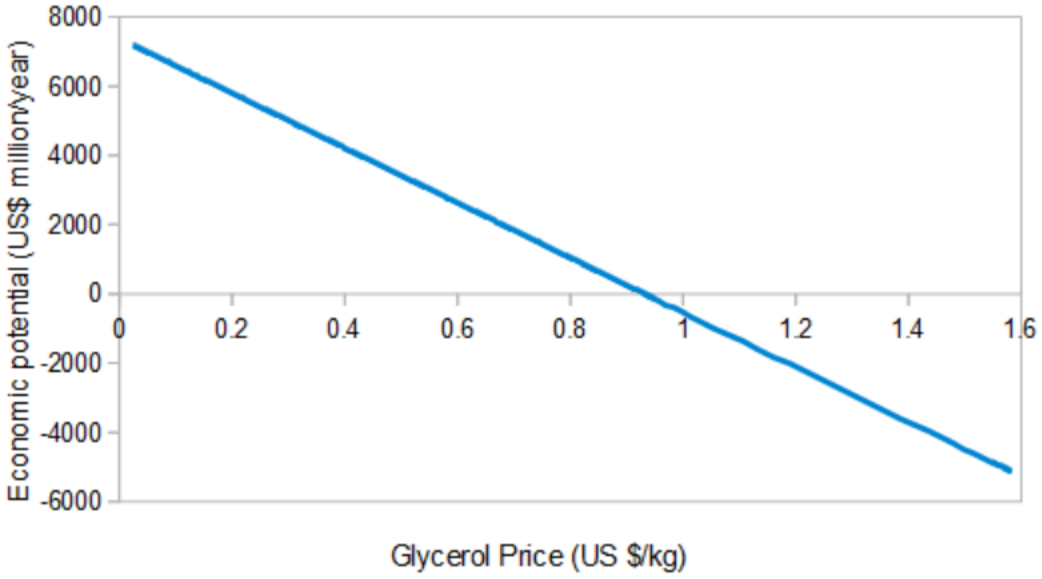

Figure 4. 30: Effect of glycerol price on economic potential during the synthesis of methanol

It is interesting to see that the synthesis of methanol from a mixture of glycerol and methane will remain economically feasible as long as the price of raw glycerol is less than $0.95/kg. Table 4.9 gives a summary of methanol synthesis from glycerol and methane in the presence of steam.

Table 4. 9: Summary of methanol synthesis from glycerol

METHANOL BIOREFINERY	
Overall process	
Feed	
Glycerol	1 ton
CH_4	0.3478 ton
H_2O	0.3913 ton
Products	
Methanol	1.7392 ton
Reforming stage	
Feed	
Glycerol	1 ton

CH_4	0.3478 ton
Operating conditions	
Temperature	1200 K
Pressure	
Reforming agent	1 bar
H_2O	0.3913 ton
Product: Syngas	
Total mass flow rate	1.7392 ton
CO	1.5218 ton
H_2	0.2174 ton
Methanol synthesis stage	
Feed	
CO	1.5218 ton
H_2	0.2174 ton
Product	
Methanol	1.7392 ton
Sustainability evaluation	
Atom economy	100 %
Carbon efficiency	100 %
E-factor	0.0
The approximate economic potential at a glycerol price range of \$0.025/kg- \$ 0.90/kg	\$7169.12-\$239.12 million per year

4.6.2 DME synthesis from LLDPE-glycerol mixture via direct method

The main objective of this section is to show how to adjust the syngas ratio (H_2:CO) to 1 and DME is used as an illustration. Following the same reasoning as in previous sections, it can be shown that the synthesis of 1 kmol DME requires 0.72 kmol of LLDPE, 0.24 kmol of glycerol as well as 0.6 kmol of water. But also 0.16 kmol of CO_2 is generated as waste. This is represented by the following process.

$$0.72(C_2H_4)_n + 0.24C_3H_8O_3 + 0.6H_2O \implies 1C_2H_6O + 0.16CO_2 \qquad 4.3$$

In terms of mass, 1 ton of $(C_2H_4)_n - C_3H_8O_3$ requires 0.2560 ton of H_2O to produce 1.089 ton of DME and 0.167-ton CO_2. It must be noted that this is not a single process meaning that $(C_2H_4)_n - C_3H_8O_3$ mixture must be reformed first, and the syngas generated can now be used for the synthesis of DME. The atom economy, carbon efficiency and E-factor of this process are calculated and found to be 86.73%, 92.60 %, and 0.153 respectively. Equation 4.4 shows the synthesis of DME from syngas via indirect route.

$$3H_2 + 3CO \rightarrow C_2H_6O + CO_2 \qquad 4.4$$

This reveals that the syngas ratio (H_2:CO) for DME synthesis via direct route is 1.0 and looking in figure 4.24 there is no reforming agent that generates a syngas that meets this requirement at a temperature range of 1200K-1500 K; all the H_2:CO> 1. The H_2:CO ratio can be adjusted by combining two reforming agents in a correct proportion. In figure 4.22, it was shown how to combine two reforming agents on a single CHO ternary diagram for syngas production, but an arbitrary proportion was chosen. In this section, CHO ternary diagram is used to determine the correct proportion of the reforming agents that produce a syngas ratio of 1 (H_2:CO =1). The direct route for DME synthesis is used to illustrate this approach.

Figure 4.31 reveals that to produce a syngas with a ratio (H_2:CO) of 1 from a mixture of LLDPE-glycerol, H_2O can be combined with CO_2. In the same figure, point T represents the syngas target (H_2:CO = 1), point V shows how H_2O is co-fed with CO_2 in a correct proportion to produce a H_2:CO ratio of 1.

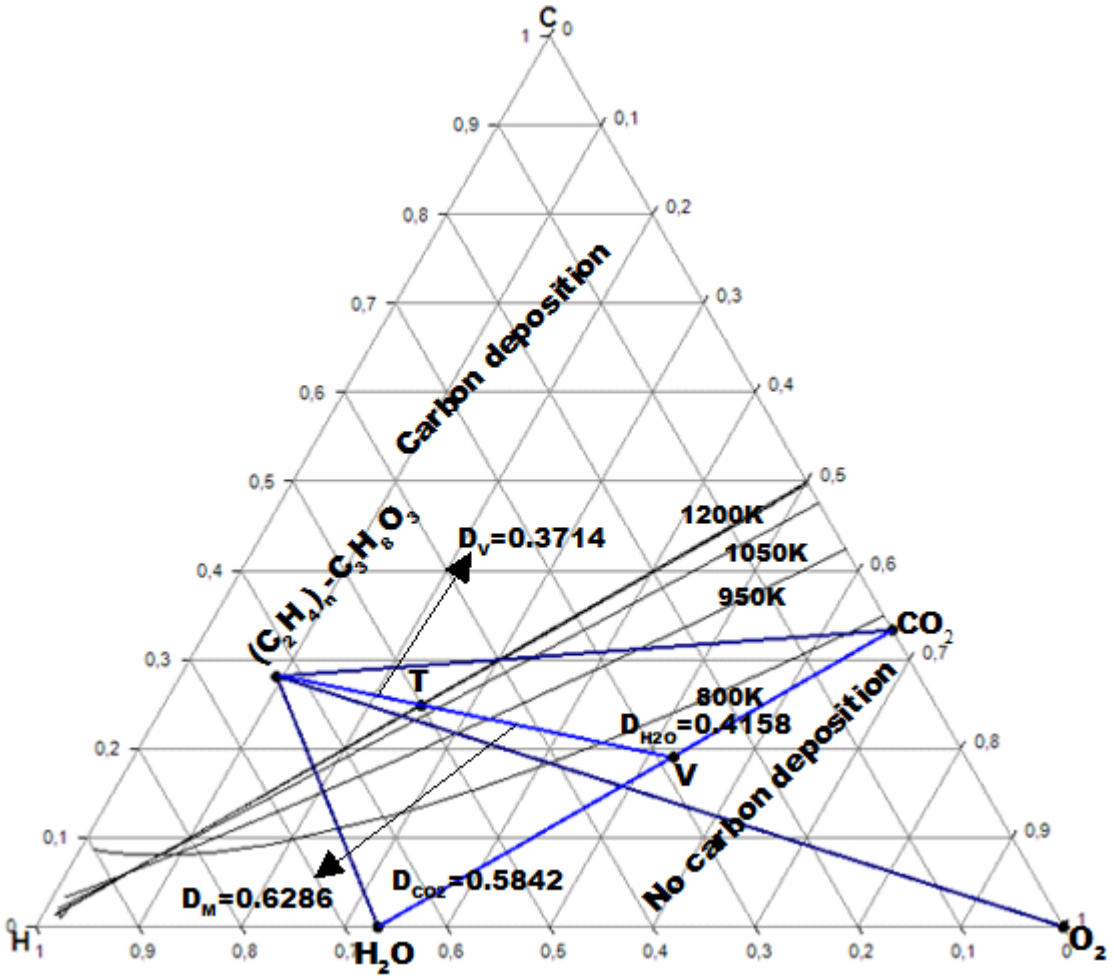

Figure 4. 31: Syngas target from LLDPE-glycerol mixture by co-feeding H_2O with CO_2 for DME synthesis

The atomic ratio of point V is given as follows 0.192: 0.280:0.528 and it can be written as $C_{0.192}H_{0.280}O_{0.528}$. The distances of H_2O and CO_2 relative to point V are shown in figure 4.31. Using these distances, the minimum amount of H_2O and CO_2 is targeted at 0.6213 and 0.8730 kmol respectively. This implies that to produce DME from 1 kmol of $(C_2H_4)_n - C_3H_8O_3$ mixture, this mixture must be reformed with 0.6213 kmol of H_2O and 0.8730 kmol of CO_2 without depositing any solid carbon at 1200K. The following process balance summarizes how a mixture of 1 kmol $(C_2H_4)_n - C_3H_8O_3$ is converted into syngas by co-feeding H_2O with CO_2.

$$1\,[(C_2H_4)_n - C_3H_8O_3] + 0.6213H_2O + 0.873CO_2 \implies 3.12CO + 3.12H_2 \qquad 4.5$$

In terms of mass, 0.75 ton of $(C_2H_4)_n$ is mixed with 0.25 ton of $C_3H_8O_3$ by using a combination of 0.254 ton (14.22 kmol) of H_2O and 0.873 ton ((19.843 kmol) of CO_2 as gasifying agent to produce 0.142 ton of H_2 (70.918 kmol) and 1.986 ton of CO (70.918 kmol).

The syngas generated from 1 kmol of $(C_2H_4)_n - C_3H_8O_3$ mixture can now be used for the synthesis of DME via direct method. The following process gives a summary of this method.

$$70.918\ H_2 + 70.918\ CO \implies 23.6393 C_2H_6O + 23.6393 CO_2 \qquad 4.6$$

In terms of mass 1.0874 ton of C_2H_6O is produced from 1 ton of $(C_2H_4)_n - C_3H_8O_3$ by co-feeding 0.254 ton of H_2O with 0.873 ton of CO_2 as reforming agents. But this process produces 1.040 tons of CO_2 as waste. The amount of CO_2 emitted from this process is calculated in the same way as in previous sections and is found to be 0.167 ton. This means that 0.873 ton of CO_2 must be recycled. Figure 4.32 shows the summary of the process.

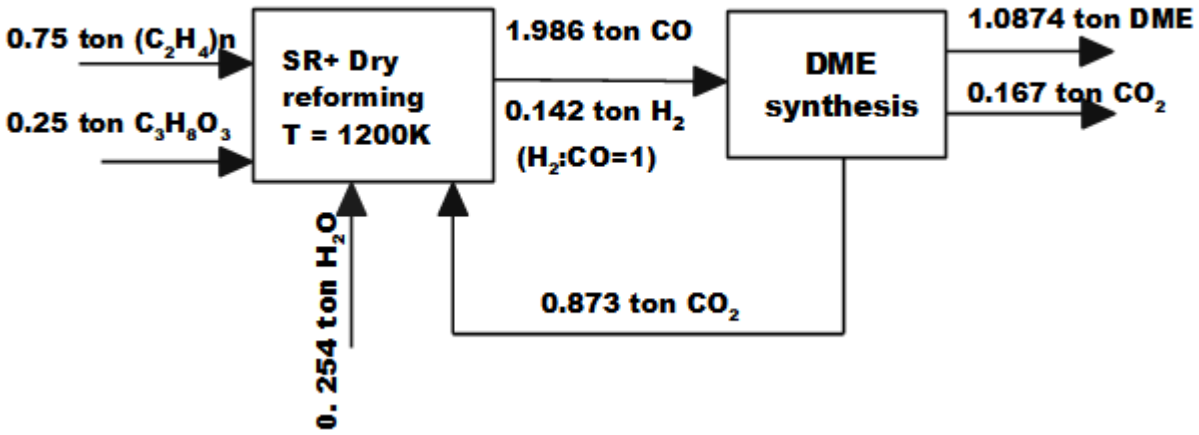

Figure 4. 32: Simplified block diagram for DME synthesis from LLDPE-glycerol mixture

Figure 4.32 shows that it is possible to produce DME from glycerol-LLDPE mixture via direct route. Litheko (2017) showed that 1 ton of biomass requires 0.280 ton of steam and 0.106 ton of CO_2 to synthesize 0.708 ton of DME via direct method. It was also shown that this process produced 0.678 ton of CO_2 per ton of biomass. Comparing the current results with Litheko (2017) it can be shown that 1 ton of glycerol-LLDPE mixture steam reforming can potentially produce more DME than biomass ($CH_{1.4}O_{0.59}$) steam gasification at 1200K.

The sustainability of DME synthesis from glycerol-LLDPE mixture can now be evaluated using different tools as discussed in chapter 3. The atom economy, carbon efficiency, as well as the E-factor are calculated and found to be 86.72 %, 76.60 % and 0.154 respectively. This indicates that the process is feasible, and less waste is generated. The approximate economic potential of the process is calculated using equation 3.25i and found to be $ 1435 million per annum (using a glycerol price of $0.1453/Kg).

4.6.2.1 Summary of findings for DME synthesis from glycerol-LLDPE mixture

Table 4.10 gives a summary of DME synthesis from 1 ton glycerol-LLDPE mixture. This process consists of two stages viz. reforming of glycerol-LLDPE mixture and DME synthesis from syngas. 1 ton of glycerol-LLDPE mixture requires 0.254 and 0.873 ton of H_2O and CO_2 to produce 2.128 tons of syngas at 1200K. This syngas is utilized to produce 1.0874 ton of DME as the main product and 0.167 ton of CO_2 (waste).

Table 4. 10: Summary of findings during the synthesis of DME

DME BIOREFINERY (DIRECT METHOD)	
Overall process	
Feed	
LLDPE	0.75 ton
Glycerol	0.25 ton
CO_2	0.873 ton
H_2O	0.254 ton
Product	
DME	1.0874 ton
Waste	
CO_2	0.167 ton
Reforming stage	
Feed	
LLDPE	0.75 ton
Glycerol	0.25 ton
Operating conditions	

Temperature	1200 K
Pressure	1 bar
Reforming agent(s)	
CO_2	0.873 ton
H_2O	0.254 ton
Product: Syngas	
Total mass flow rate	2.128 ton
CO	1.986 ton
H_2	0.142 ton
DME synthesis (Direct method) stage	
Feed	
CO	1.986 ton
H_2	0.142 ton
Product	
DME	1.0874 ton
Waste	
CO_2	0.167 ton
Sustainability evaluation	
Atom economy	86.72 %
Carbon efficiency	76.60 %
E-factor	0.154
Approximate economic potential	$ 1435 million per year

4.7 Developing an entire process flowsheet based on CHO ternary diagram targets

The first part of this chapter discussed glycerol reforming processes using the CHO ternary diagram. It was shown that glycerol as well as a mixture of glycerol and LLDPE can be plotted on a CHO ternary diagram to target the minimum amount of reforming agent needed to produce syngas. It was further shown that syngas derived from glycerol and glycerol-LLDPE mixture can be used for the synthesis of methanol and DME respectively via the CHO ternary diagrams. This section focuses on using CHO ternary diagram targets to develop an entire Aspen Plus flowsheet for methanol synthesis from glycerol (DME from glycerol-LLDPE mixture is not simulated in this study). The following processes are simulated in Aspen Plus:

- Glycerol reforming using steam as a reforming agent: This process is simulated in Aspen Plus to validate the thermodynamic model during the synthesis of methanol (reforming stage)
- Glycerol reforming using CO_2 as reforming agent: It is crucial to utilize CO_2 as a feedstock during the conversion of glycerol into syngas since it contributes to global warming.
- Reforming of glycerol-LLDPE mixture using H_2O as reforming agent: there is no study in the literature conducted to target syngas composition from a mixture of glycerol-LLDPE. It was shown in section 4.4.7 that steam is the most suitable reforming agent used to convert this mixture into syngas. It is crucial to simulate this process using Aspen Plus to gain some insights.
- Synthesis of methanol from glycerol and methane using H_2O as reforming agent: CHO ternary diagrams (section 4.6.1) showed that is possible to use glycerol-methane mixture in the presence of steam for the synthesis of methanol. It is important to use these targets to construct an entire process flowsheet using Aspen Plus.

4.7.1 Reformer Model validation

To validate the method used during the simulation of glycerol reforming, the results generated are compared with (Adhikari *et al.*, 2007). Aspen Plus flowsheet for glycerol steam reforming is shown in chapter 3. Figure 4.33 (a) shows the effect of temperature and steam to glycerol ratio (SGR) on hydrogen mole fraction. It can be shown that low SGR and high temperature favour the

production of hydrogen. For example, at 950K and at an SGR of 3:1, the mole fraction of hydrogen is found to be approximately 48% whereas an SGR of 6:1 at 950 K produces approximately 43% of hydrogen. The trend of hydrogen mole fraction at different temperatures and SGRs is in full agreement with Adhikari *et al*. (2007). Adhikari *et al*. (2007) showed that a high mole fraction of hydrogen is produced at high temperatures and low SGRs. For example, at 950 K and an SGR of 3:1, the mole fraction of hydrogen was found to be approximately 48% while an SGR of 6:1 produced approximately 43% of hydrogen. Figure 4.33 (b, c, and e) shows the effect of temperature and SGR on carbon monoxide, carbon dioxide, and methane mole fraction. The temperature and SGR have a significant impact on carbon monoxide mole fraction. Increasing both temperature and SGR reduces the mole fraction of carbon monoxide. For example, at 950 K and an SGR of 3:1, the mole composition of carbon monoxide is found to be approximately 17%, whereas at 950K and an SGR of 6:1, carbon monoxide mole fraction is reduced to approximately 10% (see figure 4. 33b). Figure 4.33c the mole fraction of carbon dioxide increases in a temperature range of 600-750 K at an SGR of 3:1 and starts to decrease from 800K, while it increases in a temperature range of 600-800K at an SGR of 6:1 and 9:1. The same figure indicates that high temperature and low SGR and high temperature reduce the production of carbon dioxide (see figure 4.33c). Figure 4.33e shows that low SGR favours the production of methane in a temperature range of 600-1000K. A similar trend was observed by Adhikari *et al*. (2007). Adhikari. (2007) showed that a decrease in SGR reduces the production of methane. Besides similar trends between the figures from Adhikari et al. (2007) and the current figures, the mole fraction of major species (H_2, CO, CH_4, CO_2, and H_2O) is also the same. Taking the observation of Adhikari *et al*. (2007) into consideration, this method is deemed valid and can be used to glycerol reforming processes.

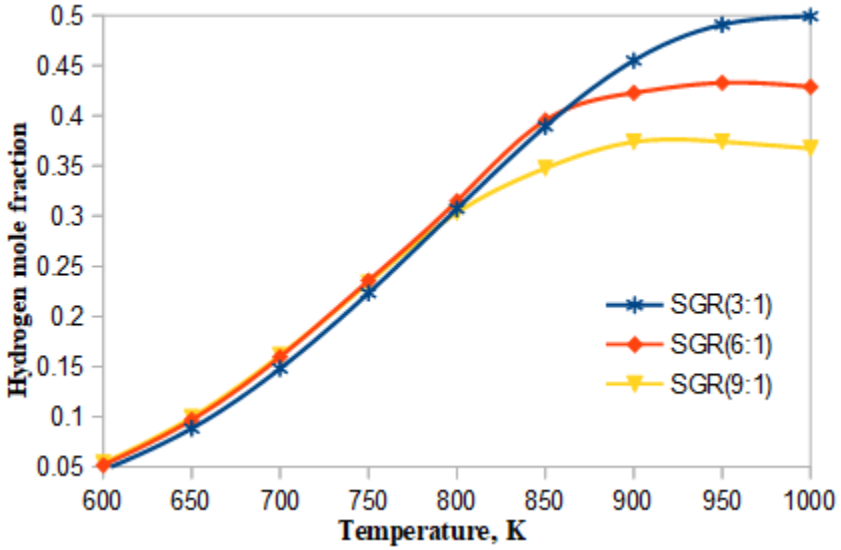

(a) Effect of temperature and SGR on hydrogen mole fraction

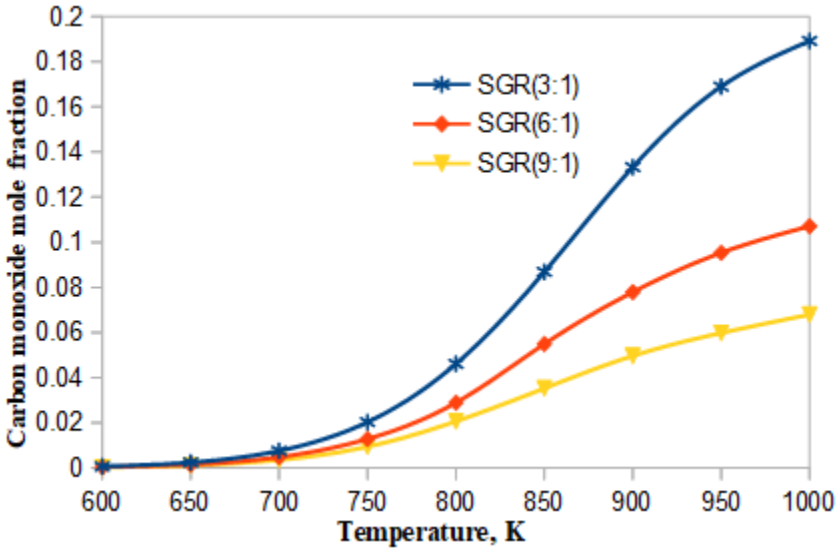

(b) Effect of temperature and SGR on CO mole fraction

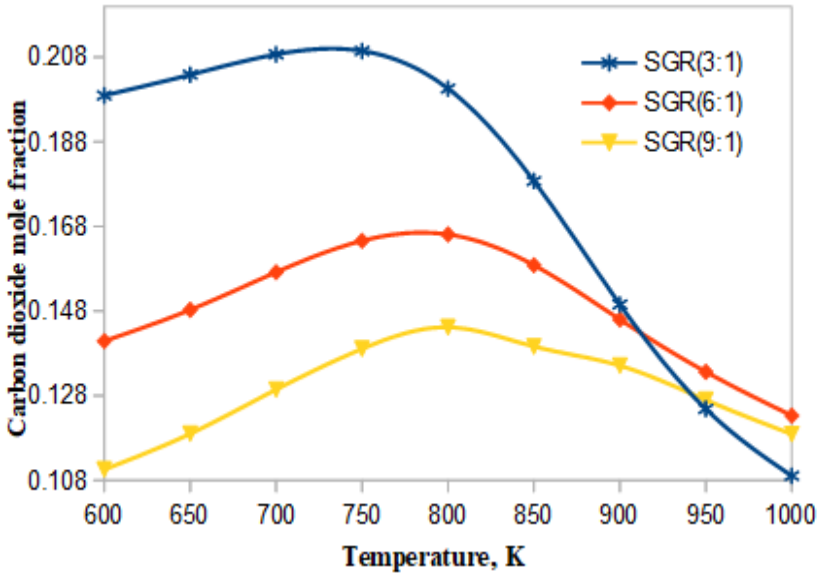

(c) Effect of temperature and SGR on CO_2 mole fraction

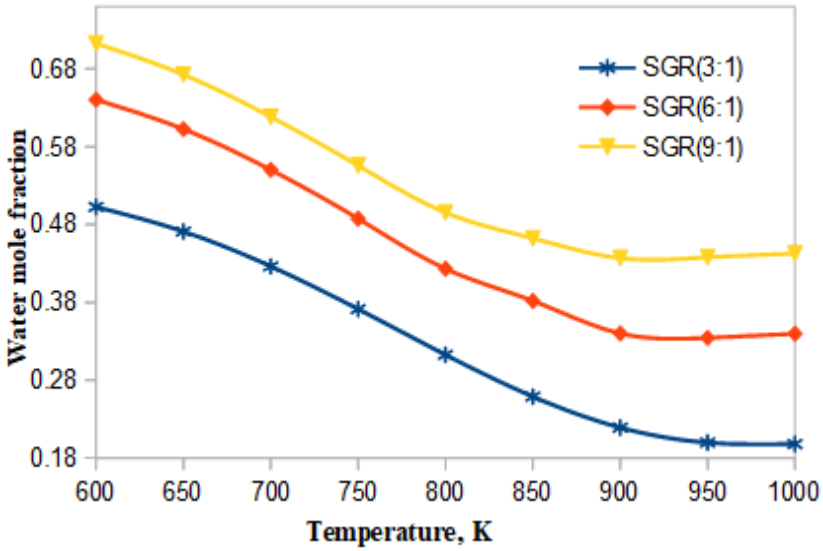

(d) Effect of temperature and SGR on H_2O mole fraction

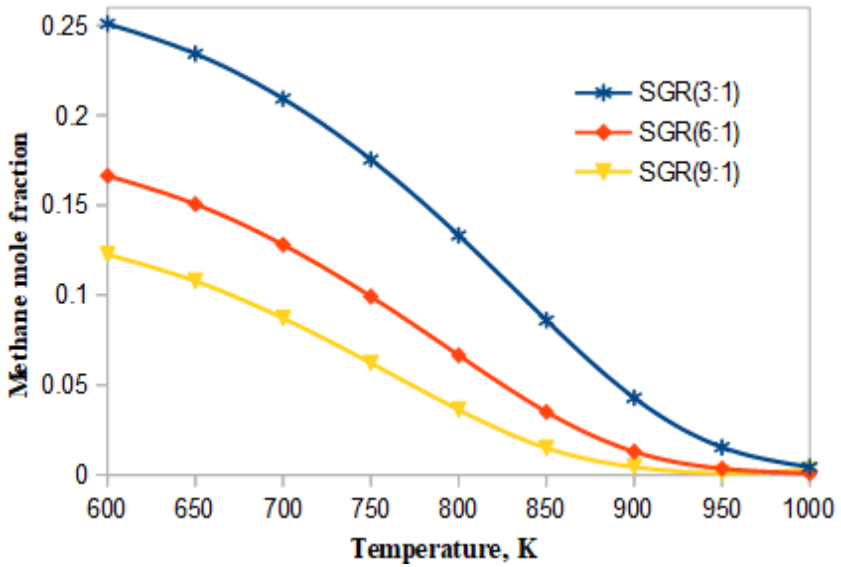

(e) Effect of temperature and SGR on methane mole fraction

Figure 4. 33: Simulation of glycerol steam using Aspen Plus at 1 bar

4.7.2 Comparison between CHO ternary diagrams and Aspen Plus during GSR

CHO ternary diagrams were used to determine at which conditions glycerol steam reforming can be converted into syngas without carbon deposition. The minimum amount of steam needed to convert one kilomole of glycerol at different temperatures was also determined. These operating conditions (such as steam to glycerol ratios) were now used for the simulation of GSR in Aspen Plus. Figure 4.34 (a-d) shows the similarities and differences between CHO ternary diagrams and Aspen Plus in terms of syngas mole fraction at different temperatures. It can be seen that the syngas mole fraction generated from the two methods follows a similar trend (increasing with an increase in temperature). Even though a similar trend is observed, the syngas mole fraction from the two methods is not the same at all temperatures. For example, the mole fraction of H_2, CO, CO_2, and CH_4 from CHO ternary diagrams is found to be 53.17%, 38.72 %, 3.02% and 1.63% at 1200K respectively, whereas Aspen Plus generates 54.12% H_2, 37.56% CO, 2.97% CO_2, and 1.744% CH_4 at the same temperature. The difference between CHO ternary diagrams and Aspen Plus is attributed to the fact that in Aspen Plus an equation of state was used to determine the molar composition of these species whereas in CHO ternary diagrams it was assumed that all species follow an ideal gas behavior. It must be noted that this difference between the two methods is not significant as the percentage error is less than 7%.

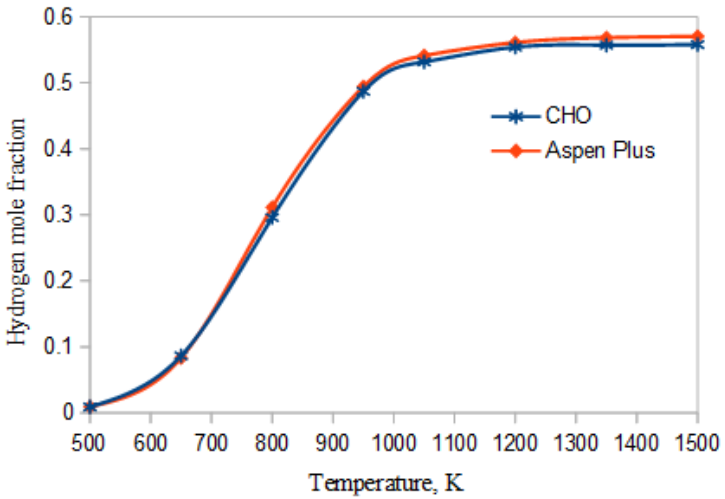

(a) Effect of temperature on hydrogen mole fraction

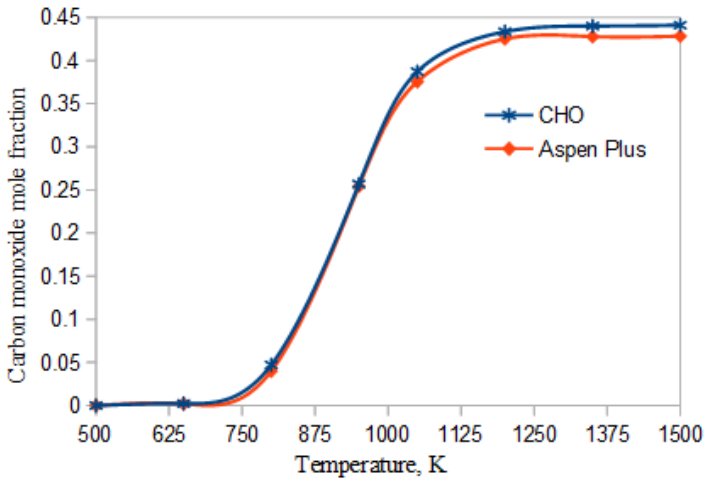

(b) Effect of temperature on carbon monoxide mole fraction

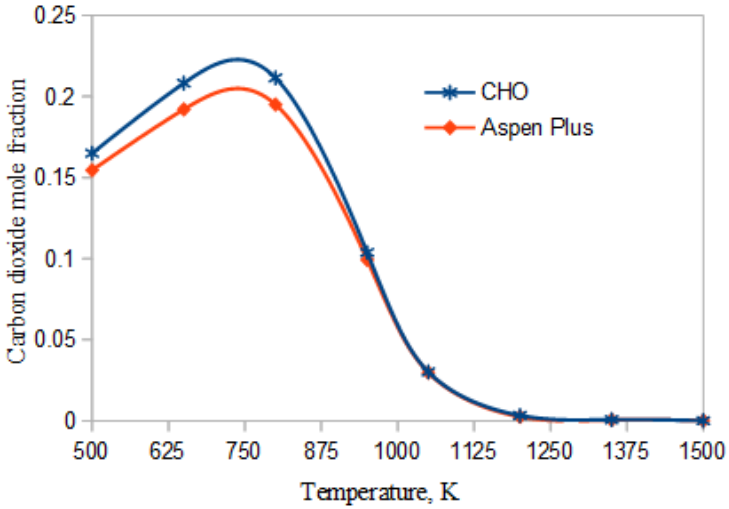

(c) Effect of temperature on carbon dioxide mole fraction

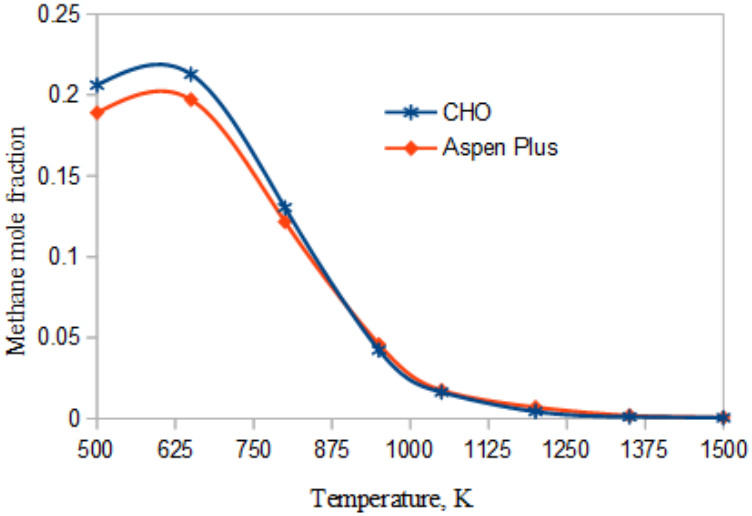

(d) Effect of temperature on methane mole fraction

Figure 4. 34: Comparison between CHO diagrams and Aspen Plus

4.7.3 Simulation of glycerol in the presence of CO_2

CHO ternary diagrams have shown that it is possible to produce syngas from glycerol reforming by using a CO_2 as reforming agent (GDR). It is important to use these CHO ternary diagram targets to develop an Aspen Plus flowsheet for glycerol dry reforming (see figure 3.12b). A sensitivity analysis was performed to study the effect of $CO_2/C_3H_8O_3$ ratio (ratio = 1:1 and 0.5:1) as well as temperature to syngas composition and at a pressure of 1 bar as shown in figure 4.35. Figure 4.35 (a) shows that $CO_2/C_3H_8O_3$ ratio has an impact on hydrogen mole fraction at fixed temperatures. Considering for example a temperature of 950K, a $CO_2/C_3H_8O_3$ ratio of 0.5/1 produces 44.25% hydrogen whereas $CO_2/C_3H_8O_3$ ratio of 1/1 generates 41.1% of hydrogen at the same temperature (950K). This corresponds to a percentage decrease in hydrogen mole fration of approximately 7.12%. A similar trend is observed at temperatures higher than 950K. The same figure (4.35a) reveals that an increase in temperature tends to increase the production of hydrogen at a fixed $CO_2/C_3H_8O_3$ ratio. For example, using a $CO_2/C_3H_8O_3$ ratio of 1/1, the mole fraction of hydrogen increases from 41.10% to 46.10% at 950K and 1200K respectively. Fixing also the $CO_2/C_3H_8O_3$ ratio at 0.5/1, the respective mole fraction of hydrogen at 950K and 1200K is found to be 44.25% and 51.34%. Taking the above observations into consideration, it is revealed that a $CO_2/C_3H_8O_3$ ratio of 0.5:1 is more suitable than a ratio of 1:1 for hydrogen production from GDR. Figure 4.35 (b-d) shows the effect of $CO_2/C_3H_8O_3$ ratio and temperature on carbon monoxide, carbon dioxide, and methane mole fraction. The $CO_2/C_3H_8O_3$ ratio does not have an impact on carbon monoxide in a temperature range of 500K- 950 K. But from 950 K up to 1500 K, a significant impact of $CO_2/C_3H_8O_3$ ratio on carbon monoxide composition is observed. A high $CO_2/C_3H_8O_3$ ratio generates more carbon monoxide. Figure 4.35 (c) shows that a high $CO_2/C_3H_8O_3$ ratio produces more carbon dioxide mole fraction at all temperatures. This implies that a $CO_2/C_3H_8O_3$ ratio of 0.5/1 is recommendable over 1:1 during the conversion of glycerol into syngas as it produces less CO_2. Looking in figure 4.35 (d), it is interesting to observe that methane mole fraction is not influenced by $CO_2/C_3H_8O_3$ ratio at high temperatures.

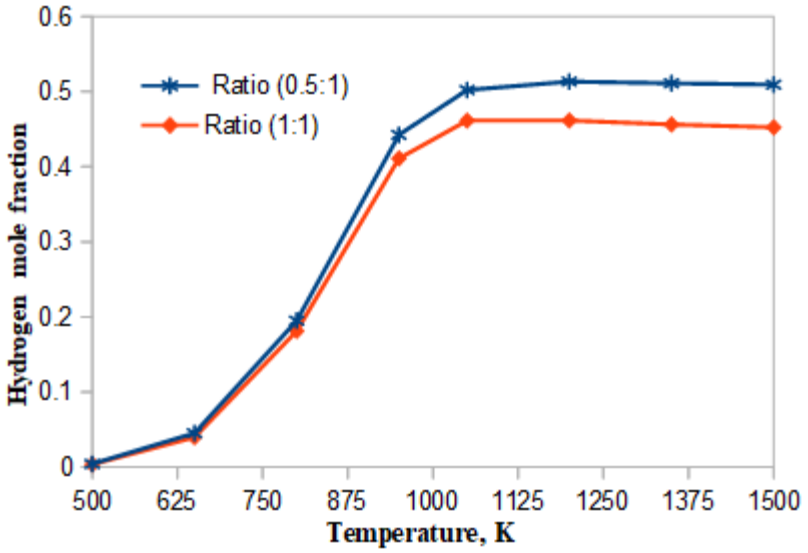

(a) Effect of $CO_2/C_3H_8O_3$ ratio on hydrogen mole fraction

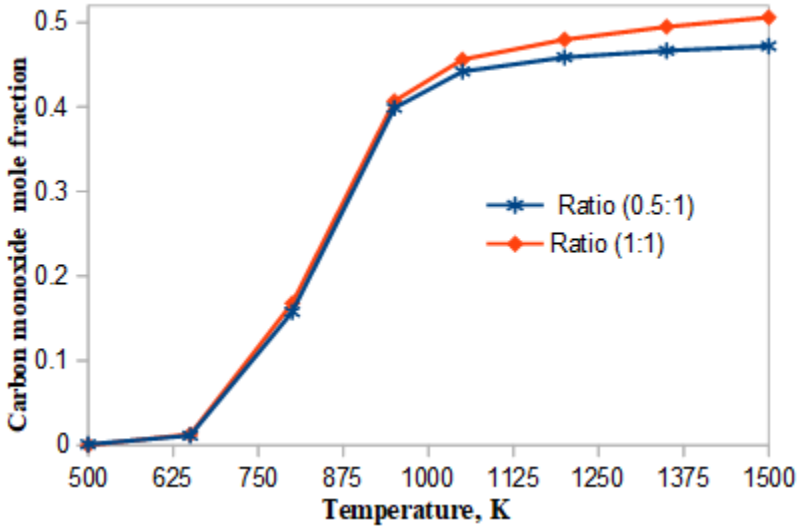

(b) Effect of $CO_2/C_3H_8O_3$ ratio on carbon monoxide mole fraction

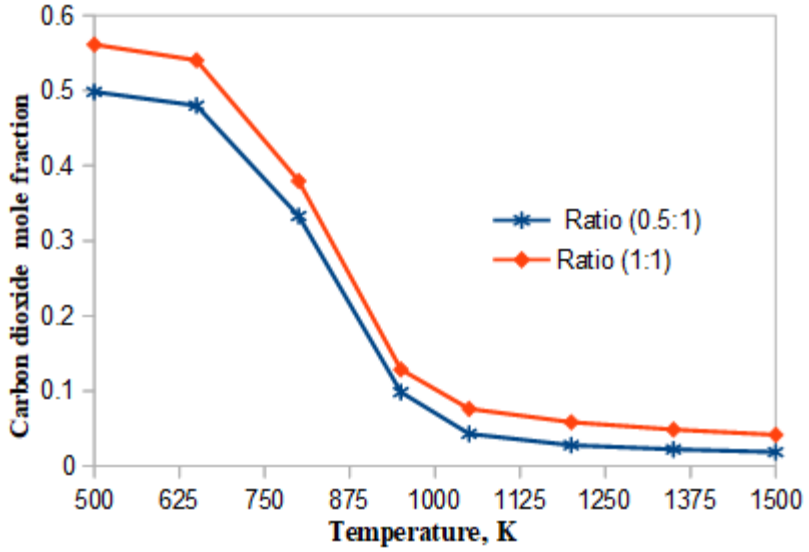

(c) Effect of $CO_2/C_3H_8O_3$ ratio on carbon dioxide mole fraction

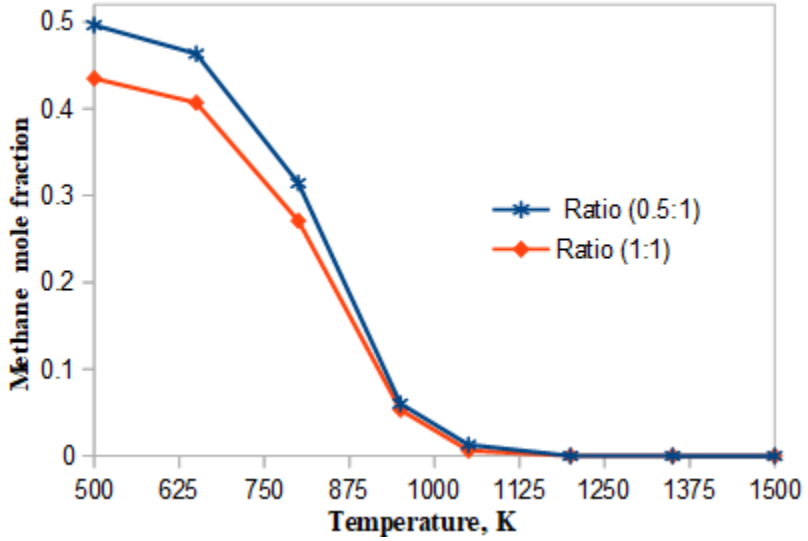

(d) Effect of $CO_2/C_3H_8O_3$ ratio on methane mole fraction

Figure 4. 35: Effect of $CO_2/C_3H_8O_3$ ratio on syngas composition at different temperatures

4.7.4 Simulation of glycerol-LLDPE mixture in the presence of H_2O

Section 4.4.7 demonstrated that it is possible to mix glycerol with LLDPE (25% glycerol and 75% LLDPE) to produce syngas using different reforming agents such as H_2O, CO_2, and O_2. This section focuses on using the targets set by CHO ternary diagrams to simulate glycerol-LLDPE

mixture in Aspen Plus. The Aspen Plus flowsheet for glycerol-LLDPE mixture reforming using H_2O as a reforming agent is shown in figure 3.13

A quick sensitivity analysis was performed to study the effect of steam to glycerol-LLDPE mixture ratio (SMiR) at different temperatures and at a fixed pressure (1 bar). Figure 4.36 (a-c) shows the effect of Gibbs reactor temperature on syngas composition at an SMiR of 1:3, 1:2, and 1:6 respectively. It can be shown that an SMiR has a significant impact on CO, CO_2, CH_4, and H_2O composition and less impact on H_2 composition at different temperatures. For example, at a temperature of 1250 K and an SMiR of 1:3, the approximate molar composition of H_2 and CO is found to be 58 % and 30 % respectively. But at the same temperature and an SMR of 1:6, the composition of H_2 remains the same whereas CO composition increases up to 38%. It can be further shown that an SMiR of 1:2 produces a significant amount of H_2O and CO_2 at different temperatures while an SMiR of 1:3 and 1:6 produce less amount of H_2O and CO_2. This clearly indicates that it is recommendable to use an SMiR of 1:3 or 1:6 to produce syngas from glycerol-LLDPE mixture.

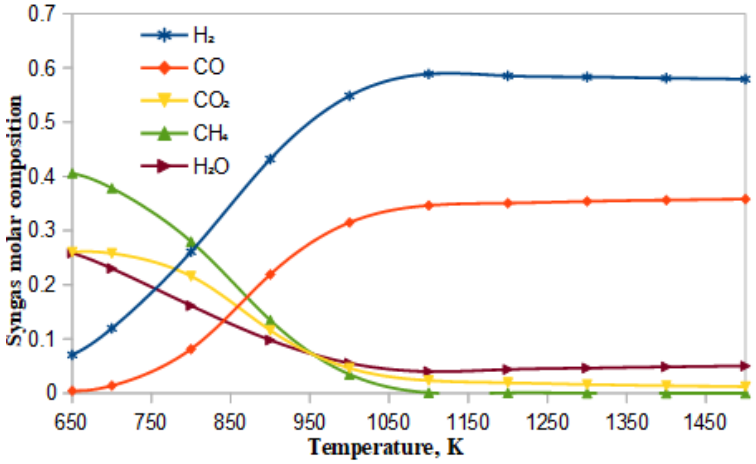

(a) SMiR=1:3

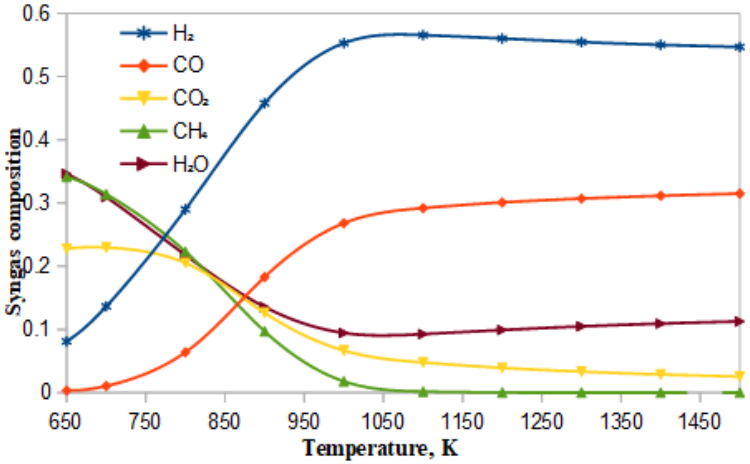

(b) SMiR = 1:2

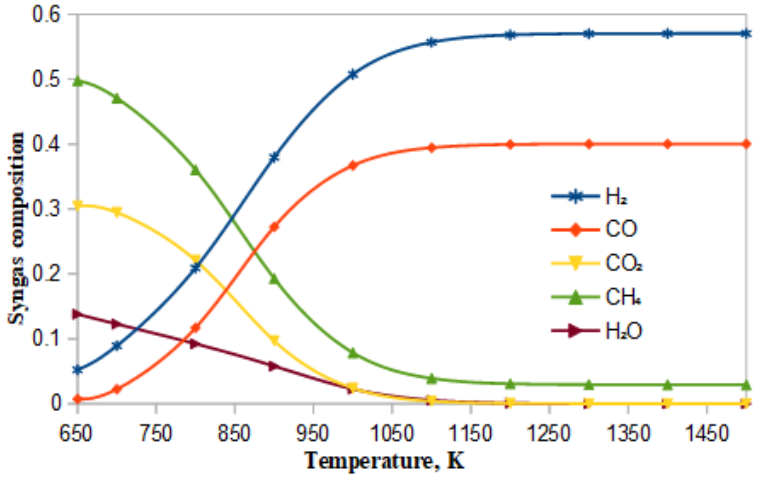

(c) SMiR = 1:6

Figure 4. 36: Simulation of glycerol-LLDPE mixture using Aspen Plus

4.7.5 Methanol synthesis from glycerol using Aspen Plus

4.7.5.1 Process description

Figure 4.25 revealed that it is possible to use glycerol as a raw material to produce methanol. This is a two-step process, meaning that glycerol must be reformed first to produce syngas and this syngas can now be utilized to produce methanol. CHO ternary diagrams revealed that glycerol reforming using H_2O, O_2 or CO_2 as a reforming agent does not produce a syngas that meets methanol synthesis requirement (H_2:CO =2). These CHO ternary diagrams further revealed that to produce a syngas from glycerol that meets the requirement of methanol synthesis, steam should be co-fed with methane (fig 4.28 and 29). The Aspen Plus flowsheet as well as process description for methanol production from glycerol in the presence of CH_4-H_2O co-feed is shown in figure 3.14, and the material balance is shown in Appendix F.

4.7.5.2 Methanol synthesis reactor model validation

The validation of the glycerol reforming process was done in section 4.6.1. This section focuses on the validation of methanol synthesis reactor based on LLHW method. To check the accuracy of methanol synthesis from glycerol and methane mixture in the presence of steam, feed flowrate from (Zhang *et al*., 2020) (32.1 kmol/h of H_2, 13.786 kmol/h of CO, 1.141 kmol/h of CO_2, and 0.175 kmol/h of CH_4) was used as an input to the simulation. The flow rate of methanol in this study was found to be 7.9 kmol/h while Zhang *et al*. (2020) found a molar flow rate of 8.04 kmol/h. The percentage error between these two results is roughly 1.74%. The reason behind this error can be attributed to the kinetic model that is used in the simulation. In this study, the adsorption expression has 4 terms whereas Zhang *et al*. (2020) used 2 terms. Zhang et al. (2020) did not specify the thermodynamic used in the simulation and this can also contribute to the difference. Therefore, the model proposed is deemed valid and can be used for the synthesis of methanol from glycerol.

4.7.5.3 Sensitivity analysis

Operating conditions such as pressure and temperature play a crucial role during the synthesis of methanol from syngas. A temperature and pressure range of 493-563K, and 50-100 bar respectively are required during the synthesis of methanol. Increasing the reactor temperature can damage the catalyst while low temperatures reduce the reaction rate (activation energy) (Gutiérrez Ortiz *et al.*, 2013). Taking these operating conditions into consideration, a pressure of 55 bar is selected to study the effect of reactor temperature (493-563 K) on methanol synthesis (see figure 4.37).

It can be shown from figure 4.37 that an increase in temperature decreases the molar flow rate of methanol. It can further be shown that a temperature of 493 K produces the highest molar flow rate of methanol (approximately 51.60 kmol/h). Therefore, 493 K is an optimal temperature for methanol synthesis at a fixed pressure of 55 bar. Puig-Gamero *et al.* (2018) used pine-derived syngas for the synthesis of methanol. It was shown that at a fixed pressure of 55 bar, a temperature of 493 K produced a high yield of methanol (32 kg/h).

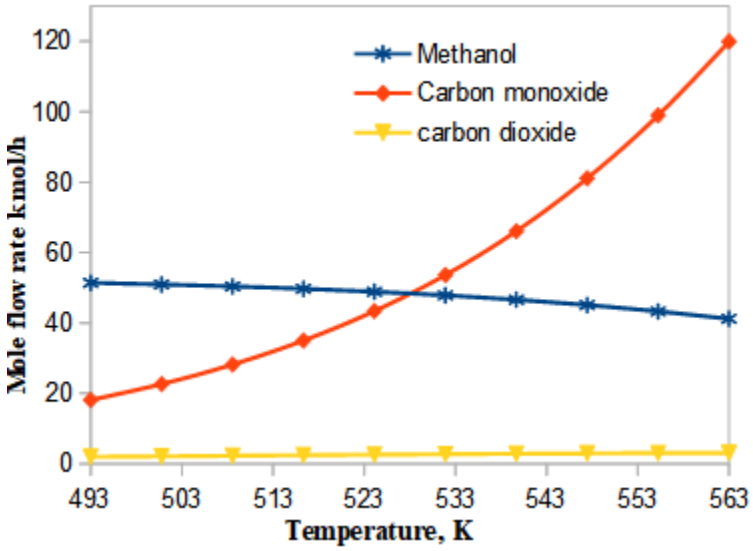

Figure 4. 37: Effect of plug reactor temperature on methanol synthesis

It is also important to study the effect of plug flow reactor length on methanol production as indicated in figure 4.38. The reactor maximum length was assumed to be 12.2 m (Luyben, 2010).

It can be shown that methanol flow rate approximately increases from 0.007 kmol/h to 50 kmol/h in a reactor length range of 0-4.9 m. From 4.9 m to 12.2 m methanol flow rate increases slightly. The same figure shows that the mole flow rate of CO increases with an increase in reactor length.

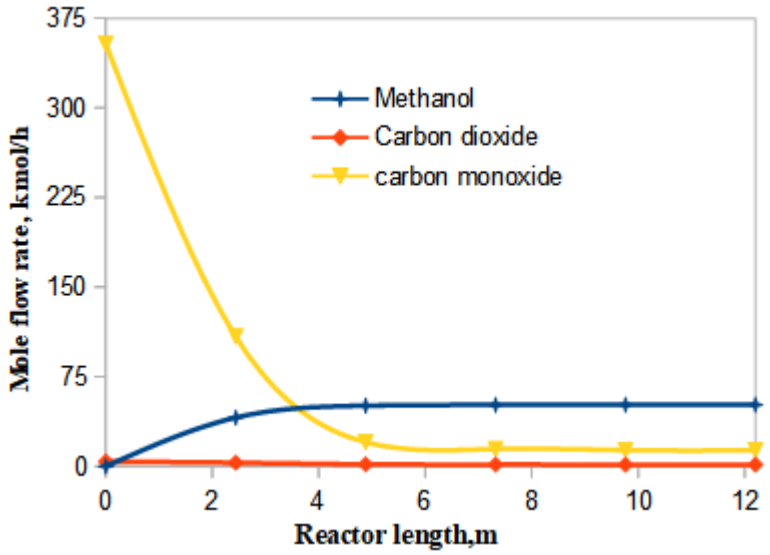

Figure 4. 38: Effect of plug reactor length on methanol synthesis

4.7.5.4 Comparison between CHO ternary diagrams and Aspen Plus for methanol synthesis

CHO ternary diagrams played a crucial role in setting targets for methanol synthesis from glycerol. It was shown that 1 ton of glycerol requires 0.348 and 0.391 ton of CH_4 and H_2O respectively to produce 1.739 ton of methanol (maximum methanol production). These inputs were now used in Aspen Plus to develop the entire flowsheet for methanol synthesis from glycerol. Table 4.11 gives a summary of Aspen Plus and CHO ternary diagrams results during the synthesis of methanol from glycerol. The percentage error between CHO ternary diagrams and Aspen Plus is below 2.5% (reforming stage) and approximately less than 5 % (methanol synthesis). The reason behind this percentage error can be due to:

- During the synthesis of methanol via CHO ternary diagrams, it was assumed that all syngas (H_2 & CO) is converted into methanol (100 % conversion). In Aspen Plus, it was observed that all syngas was not converted into methanol as certain amount of this it was

lost in the purge stream. The main purpose of this purge stream was to remove methane which is considered as an inert material. The amount of syngas and methane in this purge stream was found to be 7.412 kmol/h (26.90% CO & 73.10 % H_2) and 0.453 kmol/h respectively. The Aspen Plus syngas overall conversion was found to be approximately 79% (due to the purge stream). This purge stream also reduced the carbon efficiency as well as atom economy.

- During the stoichiometric calculation, it was assumed that all chemical species at equilibrium follow an ideal gas behavior, whereas in Aspen Plus simulation an equation of state was used.

It can be shown that results from CHO ternary diagrams collaborate with Aspen Plus results as the percentage error is not significant (less than 2.5% for reforming stage and less than 5% for methanol synthesis stage). Furthermore, Aspen Plus simulation does not exceed the limit set by CHO ternary diagrams in terms of methanol production. Therefore, CHO ternary diagrams are adequate tools for the conceptual and targeting for integrated biorefineries prior to a detailed design.

Table 4. 11: Comparison between Aspen Plus and CHO ternary diagram

Aspen Plus simulation	**CHO ternary diagrams**
Reforming stage	
Inputs	**Inputs**
Glycerol: 1 ton	Glycerol: 1 ton
Methane: 0.3478 ton	Methane: 0.3478 ton
Steam: 0.3913 ton	Steam: 0.3913 ton
Outputs (main species)	**Outputs (main species)**
H_2: 0.216 ton	H_2: 0.217 ton
CO: 1.486 ton	CO: 1.522 ton
H_2/CO (molar ratio) = 2.02	H_2/CO (molar ratio) = 2.0
Operating conditions:	**Operating conditions:**
Temperature: 1200K	Temperature: 1200K
Pressure: 1 bar	Pressure: 1 bar

Methanol synthesis stage	
Inputs (major species)	**Inputs (major species)**
H_2: 0.216 ton	H_2: 0.217 ton
CO: 1.486 ton	CO: 1.522 ton
Outputs (major species)	**Outputs**
CH4O: 1.654 ton	CH_4O: 1.739 ton
CO: 0.3766 ton	CO: None
H_2: 0.0730 ton	H_2: None
Operating conditions	Operating conditions
Temperature: 493K	Temperature: None
Pressure: 55 bar	Pressure: None
Metrics	
Atom economy: 94.96%	Atom economy:100%
Carbon efficiency: 95.0%	Carbon efficiency: 100%

4.8 References

Adhikari, S., Fernando, S., Gwaltney, S.R., To, S.D.F. & Bricka, R.M. (2007) 'A thermodynamic analysis of hydrogen production by steam reforming of glycerol', *International Journal of Hydrogen Energy*, 32, pp. 2875–2880.

Arif, N. N. M., Abidin, S.Z., Osazuwa, O. U., Vo, D. V. N., Azizan, M.T. &Taufiq-Yap, Y.H. (2019) 'Hydrogen production via CO_2 dry reforming of glycerol over Re-Ni/CaO catalysts', *International Journal of Hydrogen Energy*, 44(37), pp. 20857–20871.

Cao, Y., Gao, Z., Jin, J., Zhou, H., Cohron, H., Liu, H. & Pan, H. (2008) 'Synthesis Gas Production with an Adjustable H_2/CO Ratio through the Coal Gasification Process: Effects of Coal Ranks And Methane Addition', *Energy & Fuels*, 22, pp. 1720–1730.

Charisiou, N. D., Italiano, C., Pino, L., Sebastian, V., Vita, A. & Goula, M. A. (2020) 'Hydrogen production via steam reforming of glycerol over Rh/γ-Al2O3 catalysts modified with CeO_2, MgO or La_2O_3', *Renewable Energy*, 162(2020), pp. 908–925.

Garcia, L., Salvador, M.L., Arauzo, J. & Bilbao, R. (2001) 'CO_2 as a gasifying agent for gas production from pine sawdust at low temperatures using a Ni/Al coprecipitated catalyst', *Fuel Processing Technology*, 69, pp. 157–174.

Gutiérrez Ortiz, F.J ., Serrera, A., Galera, S. & Ollero, P. (2013) 'Methanol synthesis from syngas obtained by Supercritical water reforming of glycerol', *Fuel*, 105, pp. 739–751.

Huang, C., Xu, C., Wang, B., Hu, X., Li, J., Liu, J.& Li, C. (2018) 'High production of syngas from catalytic steam reforming of biomass glycerol in the presence of methane', *Biomass and Bioenergy*, 119, pp. 173–178.

Kale, G. R. & Kulkarni, B. D. (2010) 'Thermodynamic analysis of dry autothermal reforming of glycerol', *Fuel Processing Technology*, 91, pp. 520–530.

Litheko, L. A. (2017) *Conceptual design of gsification-based biorefineries using the C-H-O ternary diagrams*. University of South Africa, Pretoria.

Luyben, W.L (2010) ' Design and Control of a Methanol Reactor/Column Process', Ind. Eng. Chem. Res., 49, pp.6150-6163.

Mahabir,J., Koylass, N., Samaroo, N., Narine, K. & Ward, K. (2021) 'Towards resource circular biodiesel production through glycerol upcycling', *Energy Conversion and Management*, 233(December 2020), p. 113930.

Mevawala, C., Jiang, Y. and Bhattacharya, D. (2017) 'Plant-wide modeling and analysis of the shale gas to dimethyl ether (DME) process via direct and indirect synthesis routes', *Applied Energy*, 204, pp. 163–180.

Mountouris, A., Voutsas, E. & Tassios, D. (2006) 'Solid Waste plasma Gasification: Equilibrium Model Development and Exergy Analysis', *Energy Conversion and Management*, 47, pp. 1723–1737.

Puig-Gamero, M., Argudo-Santamaria, J., Valverde, J.L., Sanchez, P. & Sanchez-Silva, L. (2018) 'Three integrated process simulation using aspen plus: Pine gasification, syngas cleaning and methanol synthesis', *Energy Conversion and Management*, 117, pp. 416–427.

Rabenstein, G. & Hacker, V. (2008) 'Hydrogen for fuel cells from ethanol by stam-reforming, partial oxidation and combined auto-thermal reforming : A thermodynamic analysis', *Journal of Power Sources*, 185, pp. 1293–1304.

Roslan, N. A., Asmawati, A., Sumaiya, Z., Ideris, A. & Vo, D.V.N. (2020) 'A review on glycerol reforming processes over Ni-based catalyst for hydrogen and syngas productions', *International Journal of Hydrogen Energy*, 45(36), pp. 18466–18489.

Tay, D. H. S., Kheireddine, H., Ng, D.K.S., El-Halwagi, M.M. & Tan, R.R. (2011) 'Synthesis of an integrated biorefinery via the C-H-O ternary diagram', *Clean Technologies and Environmental Policy*, 13(1), pp. 567–579.

Wang, W. (2010) 'Thermodynamic analysis of glycerol partial oxidation for hydrogen production', *Fuel Processing Technology*, 91, pp. 1401–1408.

Zhang, Z., Delcroix, B., Rezazgui, O. & Mangin, P. (2020) 'Methanol Production from Pyrolysis oil Gasification-Model Development and Impacts of Operating conditions', *Appl. Sci.*, 10(20), pp. 7371.

CHAPTER FIVE

5.0 CONCLUSION AND RECOMMENDATIONS

5.1 Conclusion

This study intended to investigate the valorization of glycerol by using it as a raw material for a biorefinery using the CHO ternary diagram. Because glycerol only consists of carbon, hydrogen, and oxygen, it was shown that this compound can be plotted on CHO ternary diagrams as a single point. These CHO ternary diagrams were used to analyse different reforming processes as well as pyrolysis processes. It was found that glycerol can be used to produce syngas via reforming and pyrolysis routes. Reforming agents such as H_2O, O_2, CO_2, H_2O/O_2, H_2O/CO_2, O_2/CO_2 were used to convert glycerol into syngas via a reforming pathway at different temperatures and pressure of 1 bar. It was shown that temperature has a significant impact on syngas composition as well as reforming agent requirement. An increase in temperature increased syngas composition but decreased the amount of reforming agent required to produce this syngas. In a temperature range of 1200 K-1500 K, no reforming agent was required to convert glycerol into syngas because at these temperatures syngas target composition intersected with glycerol point. During glycerol pyrolysis process, no reforming agent was needed to convert glycerol into syngas. It was also revealed that an increase in temperature increased glycerol-derived syngas composition but significantly decreased the amount of carbon via pyrolysis process.

A mixture of glycerol-LLDPE was also represented on the CHO ternary diagrams to determine the syngas composition at different temperatures. It was further shown that the syngas target composition from glycerol cannot directly be used in different downstream processes such as the synthesis of methanol. However, a mixture of glycerol-LLDPE was directly used for the synthesis of DME via direct route.

Taking into consideration the results generated in this study, the following conclusions can be drawn:

- Glycerol is a valuable waste, and this waste can undergo different reforming processes to produce syngas. Among different glycerol reforming processes studied, steam reforming

was the most suitable as a high composition of syngas was obtained with the least composition of CO_2.

- In a temperature range of 500-1050K, GDR produced the highest composition of CO_2 per 1 kmol of glycerol, followed by partial oxidation-dry reforming process (O_2/CO_2) and GSR produces the least composition of CO_2. In this temperature range, GSR produced the highest syngas ratio (H_2: CO) followed by GPO.
- It is possible to use glycerol-derived syngas for the synthesis of methanol and this methanol can still be used in the production of biodiesel. This indicates that glycerol biorefinery is a good promotor of circular (bio) economy. CHO ternary diagrams revealed that 1 ton of glycerol can be co-reformed with 0.3478 ton of methane in the presence of 0.391 ton of steam to produce 1.522 ton of CO and 0.217 ton of H_2. This syngas was now utilized to produce 1.739 ton of methanol (based on 100 % conversion of CO).
- The sustainability of methanol synthesis from glycerol was evaluated using different tools such as economic potential, carbon efficiency, atom economy, and E-factor. A sensitivity analysis was conducted to study the effect of raw glycerol price on the economic potential during the synthesis of methanol. It was found that the economic potential decreases with an increase in raw glycerol price. The raw glycerol price range that generated a positive economic potential was found to be \$0.025/kg - \$ 0.90/kg. At this raw glycerol price range the approximate economic potential of the entire process was found to be \$ 7169.12 to 239.12 \$ million per year. The carbon efficiency, atom economy, and E-factor were calculated and found to be 100%, 100 %, and 0 respectively. This showed that all syngas was converted into product with no waste generated.
- It is also possible to obtain targets for the syngas composition from a mixture of glycerol-LLDPE via different reforming processes. CHO ternary diagrams further revealed that 1 ton of glycerol-LLDPE (0.75-ton LLDPE and 0.25-ton glycerol) mixture can produce 1.0874 ton of DME and 0.167 ton of CO_2 by using 0.254 ton of steam as a reforming agent. To produce a syngas that meets the requirement of DME (H_2: CO = 1.0) production, 0.873 ton of CO_2 was recycled in the reformer. Producing DME from a mixture of LLDPE-glycerol has an approximate economic potential of 1435 million per year at a raw glycerol price of \$ 0.1543/kg. Other tools such as carbon efficiency, atom economy, and E-factor were used to evaluate the sustainability of DME synthesis from glycerol-LLDPE mixture

prior to a detailed design. It was shown that this process has an atom economy, carbon efficiency, and E-factor of 86.72 %, 76.6%, and 0.154 respectively. This low carbon efficiency shows that some amount of CO was converted into waste (CO_2).

The second part of this study focused on the simulation of different glycerol reforming processes such as steam and dry reforming using Aspen Plus. The first process was GSR, it was shown that the molar composition of H_2 and CO was increasing with an increase in temperature, and this was in collaboration with CHO ternary diagram results. The effect of SGR on product composition was also studied. Results revealed that an increase in SGR decreased the composition of H_2 but increased the composition of CO.

The second process used CO_2 as a reforming agent to convert glycerol into syngas. A quick sensitivity analysis was carried out to study the effect of $CO_2/C_3H_8O_3$ ratio and temperature on syngas composition at a fixed pressure (1 bar). It was found that $CO_2/C_3H_8O_3$ ratio has a significant impact on hydrogen and carbon monoxide mole fraction at high temperatures. Low $CO_2/C_3H_8O_3$ ratio favoured the production of hydrogen whereas a high $CO_2/C_3H_8O_3$ ratio favoured the production of carbon monoxide at high temperatures.

The third process used a mixture of glycerol-LLDPE in the presence of H_2O as a reforming agent. The effect of steam to glycerol-LLDPE mixture ratio (SMiR) and temperature was analysed using a sensitivity analysis at a fixed pressure (1 bar). It was observed that among all different SMiRs used, an SMiR of 1:3 or 1:6 is suitable to produce syngas from glycerol-LLDPE mixture using steam as a reforming agent.

Lastly, Aspen Plus was used to synthesize methanol from a mixture of glycerol and methane based on CHO ternary diagram targets. CHO ternary diagrams assisted in determining the minimum amount of methane required to be mixed with 1 ton of glycerol as well as the amount of steam needed to convert this mixture into syngas that meets methanol synthesis requirement. It was shown that 1 ton of glycerol required 0.348 ton of methane to produce 1.486 ton of CO and 0.216 ton of H_2. The amount of steam needed to produce this syngas was 0.391 ton. Using this syngas, 1.654 ton of methanol was produced. A quick sensitivity analysis was performed to study the effect of reactor temperature on methanol production at a fix pressure (55 bars). It was found that an increase in temperature decreases methanol flow rate. The maximum methanol flow rate was

achieved at a temperature of 493K (51.539 kmol/h). The carbon efficiency and atom economy were found to be 95 and 94.96 % respectively. It was also revealed that Aspen Plus did not exceed targets set by CHO ternary diagrams (in terms of methanol production, carbon efficiency, and atom economy). Taking this observation into consideration it can be confirmed that CHO ternary diagrams is an important tool used in determining the performance of a biorefinery prior to a detailed design.

5.2 Recommendations

The conversion of glycerol into value-added products is a relatively recent area of research. To valorise glycerol as biorefinery raw material via reforming processes, the following recommendations are suggested for future studies:

- Use Aspen Plus to study the feasibility of glycerol-LLDPE reforming process in the presence of different reforming agents. Parameters such as glycerol-to- LLDPE ratios, pressure as well as reforming agent- glycerol-LLDPE ratios should be analyzed during this process.
- Study the thermodynamic analysis of glycerol using a combination of H_2O/CO_2 as a reforming agent. Analyze the effect of H_2O/CO_2, $H_2O/CO_2/C_3H_8O_3$, temperature as well as pressure on product composition.
- Use CHO ternary diagrams to obtain targets for syngas composition from glycerol reforming at high pressures.
- Use Aspen Plus simulation for the synthesis of DME from glycerol-LLDPE mixture and perform an economic analysis as well as heat integration
- Perform experimental study to evaluate the feasibility of glycerol reforming using a combination of steam and dry reforming. This is because there are no available experimental nor simulation data on this technology.
- Use Aspen Plus simulation to perform a heat integration calculation during the production of methanol from a mixture of glycerol-methane in the presence of steam.
- Aggregating the economic and sustainability criteria should be considered once the detailed design is completed.
- Further research should be conducted to develop aggregated methods that can be used for conceptual design and targeting purposes.

APPENDICES

Appendix A: Atomic percentage calculations

$C_3H_8O_3$: C = $\frac{3}{14} = 0.2143\ (21.43\%), \mathrm{H} = \frac{8}{14} = 0.5714\ (57.14\%), \mathrm{O} = \frac{3}{14} = 0.2143\ (21.43\%)$

H_2O: $\mathrm{C} = \frac{0}{3} = 0, \mathrm{H} = \frac{2}{3} = 0.6667\ (66.67\%), \mathrm{O} = \frac{1}{3} = 0.3333\ (33.33\%)$

CO_2: $\mathrm{C} = \frac{1}{3} = 0.3333\ (33.33\%), \mathrm{H} = \frac{0}{3} = 0.00\ \%\ , \mathrm{O} = \frac{2}{3} = 0.6667\ (66.67\%)$

CH_4O: $\mathrm{C} = \frac{1}{6} = 0.1667\ (16.67\%), \mathrm{H} = \frac{4}{6} = 0.6667\ (66.67\%), \mathrm{O} = \frac{1}{6} = 0.1667\ (16.67\%)$

Appendix B: Atomic balance to set targets for glycerol biorefinery

$$aC_3H_8O_3 + bH_2O \Longrightarrow 1CH_4O + cCO_2 \qquad 3.5$$

$$\begin{cases} \text{C balance}: 3\,a = 1 + c & (1) \\ \text{H balance}: 8a + 2b = 4 & (2) \\ \text{O balance}: 3a + b = 1 + 2c & (3) \end{cases}$$

From equation (1), $c = 3a - 1$ (1i) and from equation (3), $c = 1.5a + 0.5b - 0.5$ (3i)

Bearing in mind that equation 1i = 3i, we get the following

$b = 3a - 1$ (4)

Substituting equations 1i and 4 into equation 2 we get

$$8a + 2(3a - 1) = 4 \Leftrightarrow a = 0.42857, b = c = 0.2857$$

$$0.42857C_3H_8O_3 + 0.2857H_2O \Longrightarrow 1CH_4O + 0.2857CO_2$$

Appendix C: Determination of independent reactions

$$C\,(s) + \frac{1}{2}O_2\,(g) \rightarrow CO(g) \qquad A.1$$

$$C(s) + O_2\,(g) \rightarrow CO_2(g) \qquad A.2$$

Since oxygen is not involved among the number of chemical species predominantly present at equilibrium it can be eliminated as follows:

$$C + \frac{1}{2}O_2 \quad = CO \qquad (x2)$$

$$C + O_2 \quad = CO_2 \qquad (x\text{-}1)$$

$$2C + O_2\,(g) \quad = 2\,CO$$

$$-\,C - O_2 \quad = -\,CO_2$$

Adding these two equations leads to:

$$C = 2CO - CO_2$$

$$C + CO_2 = 2CO \qquad A.3$$

$$C(s) + 2H_2\,(g) = CH_4\,(g) \qquad A.4$$

$$3H_2\,(g) + CO\,(g) = CH_4\,(g) + H_2O\,(g) \qquad A.5$$

$$2H_2\,(g) + 2\,CO\,(g) = CH_4\,(g) + CO_2\,(g) \qquad A.6$$

Arranging reactions A.5 and A.6, we get reaction A.7

$$H_2\,(g) + CO_2\,(g) = CO\,(g) + H_2O\,(g) \qquad A.7$$

Appendix D: Composition of major chemical species at 500K and at a ratio of H/O =0.0

$x_{CH_4} = 0.00\%, x_{H_2O} = 0.00\%, x_{H_2} = 0.00\%, x_{CO} = 0.0042\%, x_{CO_2} = 99.9958\%$

Appendix E: Equilibrium composition of major species and atomic ratios

Table E. 1: Equilibrium composition of major species at different temperatures and H/O ratios

	500K					650 K				
H/O	x_{CH_4}	x_{H_2O}	x_{H_2}	x_{CO}	x_{CO_2}	x_{CH_4}	x_{H_2O}	x_{H_2}	x_{CO}	x_{CO_2}
0.00	0.00	0.00	0.00	0.00	1.0	0.0	0.0	0.0	0.0050	0.9950
0.026	5.00E-05	0.0254	0.0001	4.0E-05	0.974	0.0001	0.0235	0.00190	0.0051	0.969
0.1	8.00E-04	0.0931	5.00E-04	4.0E-05	0.9055	0.0014	0.0850	0.0070	0.0049	0.9020
0.4	0.0113	0.30835	0.0021	3.5E-05	0.678	0.0180	0.2670	0.0253	0.00430	0.6853
0.7	0.0317	0.4506	0.0035	3.0E-05	0.514	0.0455	0.3757	0.04032	0.00378	0.5347
1.0	0.0596	0.541	0.00484	2.5E-05	0.3945	0.0780	0.4392	0.0527	0.00340	0.4267
1.3	0.0925	0.5945	0.0060	2.3E-05	0.3070	0.1120	0.4746	0.0632	0.00305	0.3471
1.7	0.1404	0.627	0.0074	2.0E-05	0.2250	0.1566	0.4955	0.0747	0.00270	0.2705
2.0	0.1770	0.6330	0.0083	2.0E-05	0.1815	0.18840	0.4990	0.0820	0.00250	0.2281
4.0	0.3860	0.5410	0.0123	1.0E-05	0.0609	0.3531	0.4390	0.1123	0.00160	0.0941
6.0	0.5190	0.437	0.0143	7.3E-06	0.0296	0.45530	0.36540	0.1275	0.00120	0.0506
8.0	0.6051	0.3620	0.0154	5.6E-06	0.0174	0.522419	0.308657	0.13654	0.00092	0.031470
10	0.6650	0.3077	0.0161	4.5E-06	0.0114	0.569419	0.265856	0.14255	0.000756	0.021420
12	0.7080	0.2670	0.0167	3.8E-06	0.0080	0.60404	0.23299	0.146820	0.000644	0.015507
14	0.7410	0.2360	0.0171	3.2E-06	0.0060	0.630555	0.207140	0.15001	0.000560	0.01174
20	0.8050	0.1740	0.0178	2.3E-06	0.0030	0.68243	0.15504	0.15605	0.000403	0.00610
26	0.842	0.1380	0.0182	1.8E-06	0.0018	0.71277	0.12372	0.15950	0.0003	0.0037
32	0.8660	0.1140	0.0184	1.5E-06	0.0012	0.73267	0.10288	0.16170	0.000256	0.0025
38	0.8830	0.0973	0.0186	1.2E-06	0.0010	0.74672	0.08803	0.16324	0.00022	0.0018
44	0.8960	0.0848	0.0188	1.1E-06	0.0006	0.75717	0.07691	0.16438	0.00019	0.001350
50	0.9054	0.0752	0.0189	9.5E-07	0.0005	0.765240	0.06829	0.165253	0.00017	0.001051
60	0.9175	0.0632	0.0190	8.0E-07	0.0003	0.775259	0.057532	0.166331	0.00014	0.00074
66	0.9230	0.0577	0.01904	7.2E-07	0.0003	0.779873	0.052563	0.166825	0.00013	0.00061
72	0.9280	0.0530	0.0191	6.6E-07	0.0002	0.78374	0.04838	0.16724	0.00012	0.00052

78	0.9320	0.0491	0.0191	6.1E-07	0.0002	0.787042	0.04482	0.16759	0.00011	0.00044
800K						**950**				
H/O	x_{CH_4}	x_{H_2O}	x_{H_2}	x_{CO}	x_{CO_2}	x_{CH_4}	x_{H_2O}	x_{H_2}	x_{CO}	x_{CO_2}
0.00	0.00	0.00	0.00	0.09811	0.90189	0.00	0.00	0.00	0.54443	0.45557
0.026	0.00008	0.01665	0.0075514	0.096855	0.87890	3.0E-05	0.006	0.0125	0.5375	0.4440
0.1	0.001135	0.059404	0.027790	0.093451	0.81822	4.0E-04	0.0214	0.0462	0.5186	0.4134
0.4	0.01361	0.180207	0.096222	0.081877	0.628083	0.0044	0.0644	0.1580	0.4550	0.3182
0.7	0.03242	0.247756	0.14851	0.07293	0.49838	0.0103	0.08802	0.2420	0.4062	0.2536
1.0	0.052965	0.28571	0.18982	0.065804	0.40570	0.01658	0.10116	0.3074	0.36740	0.20746
1.3	0.073304	0.306364	0.223309	0.059980	0.33704	0.02275	0.10826	0.36003	0.33572	0.17323
1.7	0.09879	0.31831	0.25924	0.053680	0.26997	0.03040	0.11236	0.41610	0.30150	0.13970
2.0	0.116365	0.320352	0.28135	0.049780	0.23215	0.03560	0.11305	0.45042	0.28023	0.12070
4.0	0.20248	0.28705	0.37118	0.034027	0.105258	0.060960	0.10127	0.58935	0.19185	0.05657
6.0	0.25485	0.24255	0.41637	0.025467	0.06076	0.07601	0.08640	0.65813	0.14650	0.03299
8.0	0.28887	0.207934	0.44329	0.020568	0.03940	0.085854	0.07436	0.69943	0.1187	0.02166
10	0.312770	0.18117	0.46126	0.01717	0.027625	0.09280	0.06502	0.72704	0.09985	0.01532
12	0.330449	0.160208	0.474125	0.014772	0.020446	0.09788	0.0577	0.74683	0.08620	0.01142
14	0.34405	0.14345	0.483790	0.01296	0.015745	0.10183	0.05175	0.76172	0.07586	0.00884
20	0.370855	0.108958	0.502277	0.0094837	0.0084267	0.109607	0.03951	0.7903	0.05582	0.00480
26	0.38667	0.087731	0.512877	0.007478	0.005240	0.11421	0.03191	0.80671	0.04417	0.0030
32	0.397109	0.073395	0.51975	0.006173	0.003571	0.11725	0.026760	0.817383	0.036550	0.00205
38	0.40451	0.063074	0.52460	0.005257	0.00260	0.1194	0.02303	0.8249	0.031176	0.00149
44	0.410029	0.05529	0.52814	0.004577	0.00196	0.12103	0.02022	0.83044	0.02720	0.0011
50	0.414305	0.04922	0.53090	0.004053	0.00154	0.12230	0.01801	0.83472	0.02410	0.0009
60	0.419623	0.04160	0.53430	0.003404	0.0011	0.1238	0.01524	0.84003	0.020260	0.0006
66	0.42208	0.03806	0.53585	0.003105	0.00090	0.12456	0.01395	0.8425	0.01849	0.0005
72	0.42415	0.035077	0.537156	0.002855	0.00076	0.12520	0.01287	0.84451	0.01701	0.0004
78	0.425908	0.032530	0.538270	0.002642	0.00065	0.12570	0.01194	0.84625	0.01575	0.0004

1050K						1200K				
H/O	x_{CH_4}	x_{H_2O}	x_{H_2}	x_{CO}	x_{CO_2}	x_{CH_4}	x_{H_2O}	x_{H_2}	x_{CO}	x_{CO_2}
0.00	0.00	0.00	0.00	0.85630	0.1437	0.00	0.00	0.00	0.98412	0.01588
0.026	9.2E-06	0.002	0.013	0.8453	0.1400	2.2E-06	0.0003	0.0127	0.9715	0.01550
0.1	0.0001	0.007	0.0473	0.8156	0.1304	3.0E-05	0.00102	0.04723	0.93730	0.01441
0.4	0.0015	0.0201	0.1638	0.71450	0.1001	0.0004	0.00312	0.16522	0.82025	0.01103
0.7	0.0036	0.0277	0.2530	0.63631	0.07936	0.0010	0.0043	0.25675	0.72931	0.0087
1.0	0.0060	0.0320	0.3237	0.57370	0.06455	0.0015	0.00499	0.3299	0.65660	0.0071
1.3	0.0082	0.03426	0.3811	0.5228	0.05360	0.0021	0.005360	0.38964	0.59706	0.00585
1.7	0.0111	0.0356	0.4428	0.4676	0.04286	0.0030	0.00557	0.4542	0.5327	0.00465
2.0	0.0131	0.03583	0.48090	0.43340	0.03681	0.0033	0.0056	0.49415	0.49290	0.0040
4.0	0.02290	0.03194	0.63662	0.29185	0.01670	0.0060	0.0050	0.65824	0.32903	0.0020
6.0	0.02883	0.027053	0.7143	0.2203	0.0095	0.0075	0.0042	0.74030	0.2470	0.0010
8.0	0.03272	0.02315	0.76101	0.1770	0.0061	0.00860	0.0036	0.78951	0.19770	0.0006
10	0.03546	0.02015	0.7922	0.14792	0.00429	0.0093	0.00312	0.822340	0.16480	0.0004
12	0.03748	0.01780	0.81450	0.12708	0.003165	0.009836	0.00275	0.84580	0.14130	0.0003
14	0.039040	0.01592	0.83122	0.11140	0.002432	0.01025	0.002460	0.86338	0.12366	0.0002
20	0.04210	0.012066	0.86324	0.08130	0.00130	0.01106	0.001860	0.8970	0.08997	0.0001
26	0.04391	0.0097	0.88160	0.06401	0.0008	0.01154	0.00150	0.91620	0.07071	0.0001
32	0.04510	0.0081	0.89346	0.05280	0.0005	0.01186	0.00124	0.92860	0.058241	6.0E-05
38	0.04595	0.00696	0.90178	0.0449	0.0004	0.01208	0.001070	0.93730	0.04951	4.0E-05
44	0.04660	0.00610	0.90794	0.03910	0.0003	0.01225	0.0010	0.94373	0.043056	3.0E-05
50	0.047064	0.00543	0.91270	0.03460	0.0002	0.01240	0.0008	0.94868	0.038090	2.0E-05
60	0.04767	0.0046	0.91855	0.02903	0.0002	0.01253	0.0007	0.95480	0.031950	2.0E-05
66	0.04795	0.00420	0.92124	0.026450	0.0001	0.01261	0.00064	0.95760	0.029131	1.0E-05
72	0.04820	0.0040	0.92350	0.02434	0.0001	0.01267	0.0006	0.95995	0.02677	1.0E-05
78	0.04840	0.0036	0.9254	0.02252	0.0001	0.01272	0.0005	0.96195	0.02476	1.0E-05

1350K						1500K				
H/O	x_{CH_4}	x_{H_2O}	x_{H_2}	x_{CO}	x_{CO_2}	x_{CH_4}	x_{H_2O}	x_{H_2}	x_{CO}	x_{CO_2}
0.00	0.00	0.00	0.00	0.9966	0.0034	0.00	0.00	0.00	0.9995	0.0005
0.026	0.00	8.0E-05	0.0128	0.9840	0.0033	0.00	2.0E-05	0.01282	0.98663	0.0005
0.1	8.0E-06	0.0003	0.0475	0.9492	0.0031	0.00	6.0E-05	0.047580	0.95870	0.0005
0.4	0.0001	0.0009	0.1661	0.83053	0.00234	0.0001	0.0010	0.1661	0.83052	0.00234
0.7	0.0002	0.00125	0.2584	0.73825	0.00185	0.0002	0.00125	0.25840	0.73825	0.0018
1.0	0.0004	0.0014	0.3322	0.6644	0.00150	0.00017	0.00030	0.3329	0.66636	0.0002
1.3	0.0005	0.00156	0.39262	0.60404	0.00124	0.00054	0.0015	0.39262	0.60404	0.0012
1.7	0.0007	0.0016	0.45790	0.53875	0.0010	0.0007	0.00162	0.45790	0.53875	0.0010
2.0	0.0009	0.00163	0.49830	0.49835	0.0008	0.0004	0.0003	0.49934	0.49982	0.0001
4.0	0.00154	0.00145	0.66440	0.33225	0.0004	0.0007	0.0003	0.6657	0.3332	0.00006
6.0	0.002	0.0012	0.74741	0.24920	0.0002	0.0008	0.0002	0.74891	0.24996	0.00003
8.0	0.0022	0.0010	0.79723	0.19940	0.0001	0.0009	0.0002	0.79883	0.200	0.00002
10	0.0024	0.0009	0.83044	0.16614	0.0001	0.0010	0.0002	0.83210	0.1666	0.00001
12	0.00255	0.0008	0.85420	0.14241	0.00007	0.0011	0.0002	0.85587	0.14285	0.00001
14	0.00266	0.0007	0.87200	0.12461	0.00005	0.0011	0.0001	0.87370	0.1250	0.000
20	0.00287	0.0005	0.90593	0.09063	0.00003	0.00123	0.0001	0.90774	0.09091	0.000
26	0.0030	0.00043	0.92543	0.07121	0.000020	0.00123	0.0001	0.92720	0.07143	0.000
32	0.00310	0.00040	0.93791	0.05864	0.000010	0.0013	0.0001	0.93980	0.0588	0.000
38	0.0031	0.0003	0.94670	0.04984	0.000	0.00135	0.00006	0.94858	0.0500	0.000
44	0.0032	0.0003	0.95320	0.0434	0.000	0.00135	0.00005	0.95510	0.04350	0.000
50	0.0032	0.0002	0.95820	0.03834	0.000	0.00138	0.00005	0.9610	0.03850	0.000
60	0.0032	0.0002	0.9644	0.0321	0.000	0.0014	0.00004	0.96630	0.03230	0.000
66	0.00330	0.00020	0.9672	0.0293	0.000	0.0014	0.0004	0.96914	0.0294	0.000
72	0.0033	0.0002	0.96960	0.02694	0.000	0.0014	0.00003	0.97152	0.02703	0.000
78	0.00330	0.0001	0.97161	0.02572	0.000	0.0014	0.00003	0.97354	0.02500	0.000

Table E. 2: Atomic ratios from equilibrium compositions at different temperatures

500K				650 K			800K			950 K		
H/O	H	O	C	H	O	C	H	O	C	H	O	C
0.00	0	0,667	0,333	0	0,666138	0,333862	0	0,650616	0,349384	0	0,57608	0,42392
0.026	0,017082	0,658136	0,324782	0,017629	0,656963	0,325375	0,018721	0,640198	0,341117	0,016526	0,566896	0,416578
0.1	0,063238	0,635004	0,301758	0,06473	0,632226	0,30303	0,06832	0,61226	0,31942	0,060794	0,542164	0,397042
0.4	0,216809	0,555124	0,228066	0,217881	0,548186	0,233935	0,227308	0,519879	0,252812	0,204475	0,461185	0,334341
0.7	0,329464	0,49297	0,177566	0,327335	0,483623	0,189048	0,339699	0,451387	0,20891	0,308949	0,401562	0,289489
1.0	0,413367	0,443316	0,143317	0,408097	0,432524	0,15937	0,422761	0,398645	0,178593	0,388138	0,355762	0,2561
1.3	0,476562	0,402749	0,12069	0,469358	0,391121	0,139518	0,486297	0,356815	0,156885	0,450439	0,319455	0,230106
1.7	0,537999	0,358876	0,103125	0,530478	0,346783	0,122748	0,550585	0,312907	0,136498	0,515364	0,281346	0,20329
2.0	0,572334	0,331826	0,09584	0,565546	0,319578	0,114876	0,588117	0,286411	0,125469	0,554304	0,258268	0,187428
4.0	0,681829	0,220692	0,09748	0,687512	0,209721	0,102763	0,724626	0,182808	0,09256	0,705665	0,16738	0,126955
6.0	0,721024	0,165334	0,113641	0,735465	0,156037	0,108496	0,782031	0,13403	0,083937	0,776567	0,124026	0,099408
8.0	0,741021	0,132195	0,126785	0,760349	0,124233	0,115423	0,813078	0,105806	0,081178	0,817711	0,098559	0,08373
10	0,753423	0,110117	0,136461	0,775411	0,103195	0,121395	0,832316	0,08734	0,080338	0,844648	0,081795	0,073557
12	0,761336	0,094359	0,144305	0,785456	0,088251	0,126294	0,845343	0,074373	0,080284	0,86362	0,069931	0,066449
14	0,767225	0,082548	0,150226	0,792616	0,077088	0,1303	0,854711	0,064751	0,080533	0,877701	0,061059	0,06124

20	0,777937	0,059997	0,162066	0,805406	0,055899	0,138719	0,871636	0,046645	0,081719	0,904339	0,044268	0,051393
26	0,783849	0,047129	0,169022	0,812237	0,043817	0,143936	0,88073	0,036449	0,082818	0,919362	0,034712	0,045926
32	0,787515	0,038796	0,173689	0,816457	0,036055	0,147495	0,886392	0,029909	0,083697	0,929032	0,028553	0,042415
38	0,790116	0,033015	0,176869	0,819332	0,030625	0,150053	0,890278	0,025366	0,084396	0,935781	0,024251	0,039968
44	0,791915	0,028656	0,179429	0,821415	0,026606	0,151979	0,893042	0,022007	0,084947	0,940751	0,021067	0,038182
50	0,79337	0,025376	0,181254	0,822994	0,023527	0,153483	0,895174	0,019444	0,0854	0,944573	0,018648	0,03678
60	0,795134	0,021246	0,18362	0,824912	0,019722	0,155368	0,897746	0,016289	0,085993	0,949235	0,015605	0,03516
66	0,795926	0,019415	0,18466	0,825783	0,017975	0,156243	0,8989	0,014827	0,086268	0,951453	0,014224	0,034324
72	0,796554	0,017799	0,185646	0,826501	0,016517	0,156981	0,899872	0,013615	0,086511	0,953254	0,013058	0,033688
78	0,79712	0,016484	0,186396	0,827119	0,015274	0,15761	0,900694	0,012587	0,086719	0,954774	0,012118	0,033108

	1050 K			**1200 K**			**1350K**			**1500 K**		
H/O	H	O	C	H	O	C	H	O	C	H	O	C
0.00	0	0.523998	0.476002	0	0.502652	0.497348	0	0.500568	0.499432	0	0.500084	0.499917
0.026	0.014341	0.516696	0.468963	0.012902	0.496188	0.49091	0.012853	0.494228	0.492919	0.012833	0.493655	0.493512
0.1	0.052049	0.497108	0.450843	0.047934	0.478601	0.473465	0.047707	0.476768	0.475526	0.04762	0.479703	0.472677
0.4	0.178407	0.43071	0.390883	0.167621	0.418521	0.413858	0.16678	0.417125	0.416094	0.166847	0.417154	0.415999

0.7	0.274356	0.380312	0.345332	0.260418	0.37189	0.367692	0.259394	0.370775	0.369831	0.259394	0.370742	0.369864
1.0	0.349844	0.340561	0.309595	0.334428	0.334697	0.330874	0.333454	0.333667	0.33288	0.333236	0.333413	0.333351
1.3	0.410511	0.30856	0.280929	0.394895	0.304217	0.300888	0.394061	0.303367	0.302573	0.394053	0.30332	0.302628
1.7	0.475425	0.274242	0.250332	0.460315	0.271306	0.268378	0.459527	0.270575	0.269898	0.459541	0.270581	0.269878
2.0	0.515279	0.253184	0.231538	0.500525	0.250983	0.248492	0.500107	0.250251	0.249641	0.49986	0.250077	0.250063
4.0	0.676244	0.1677	0.156056	0.666375	0.167514	0.166111	0.666599	0.166875	0.166526	0.66646	0.16674	0.1668
6.0	0.755408	0.125495	0.119097	0.749101	0.125566	0.125333	0.74981	0.125133	0.125057	0.749683	0.125067	0.12525
8.0	0.802627	0.100278	0.097095	0.798791	0.100449	0.10076	0.799657	0.1001	0.100243	0.799683	0.10008	0.100237
10	0.834008	0.083531	0.082461	0.831861	0.083706	0.084433	0.83296	0.083436	0.083603	0.833033	0.083373	0.083593
12	0.856357	0.071578	0.072065	0.855503	0.071766	0.072731	0.856774	0.071518	0.071708	0.856883	0.071498	0.071618
14	0.873071	0.062624	0.064306	0.873221	0.062783	0.063997	0.874595	0.062571	0.062834	0.874647	0.062533	0.06282
20	0.904968	0.045535	0.049497	0.907089	0.045671	0.04724	0.90856	0.04550 2	0.045939	0.908791	0.045488	0.045721
26	0.923198	0.035769	0.041033	0.926433	0.035921	0.037646	0.928117	0.035762	0.036122	0.928251	0.035748	0.036001
32	0.934943	0.029431	0.035627	0.938915	0.029573	0.031511	0.940657	0.02946	0.029883	0.940894	0.029448	0.029658
38	0.943182	0.025034	0.031783	0.947678	0.025138	0.027184	0.94938	0.02502	0.0256	0.9497	0.02502	0.02528
44	0.949289	0.021781	0.02893	0.954197	0.021881	0.023922	0.95596	0.0218	0.02224	0.956213	0.021767	0.02202
50	0.953973	0.019242	0.026785	0.959134	0.019325	0.021542	0.960893	0.019237	0.01987	0.972083	0.01925	0.008667

60	0.959754	0.01618	0.024066	0.965291	0.016221	0.018488	0.967093	0.016117	0.01679	0.967442	0.016144	0.016414
66	0.962401	0.01469	0.022908	0.968115	0.014785	0.0171	0.969973	0.014717	0.01531	0.970527	0.014833	0.01464
72	0.964728	0.013569	0.021703	0.970486	0.013591	0.015922	0.972373	0.013537	0.01409	0.97266	0.013525	0.013815
78	0.966521	0.012526	0.020953	0.97246	0.012553	0.014987	0.974317	0.012893	0.01279	0.97468	0.01251	0.01281

Table E. 3: Pyrolysis of glycerol at different temperatures

Temp. (K)	H/O	Measurement			Relative distance (mm)		Carbon deposited (kmol)	Syngas produced (Kmol)
		Carbon vertex-point U (mm)	Carbon vertex-Glycerol (mm)	Glycerol-Point U (mm)	D_C	D_U		
500	2.6897	103.80	88.38	15.42	0.1484	0.8516	2.0840	2.3597
650	2.6874	100.86	88.69	12.170	0.12066	0.87934	1.6893	3.0535
800	2.7074	107.08	95.13	11.95	0.11160	0.88840	1.5624	4.1274
950	2.689	88.39	83.56	4.830	0.05464	0.94536	0.76496	5.6626
1050	2.636	94.66	93.06	1.60	0.01690	0.9831	0.2366	6.3478
1200	2.651	92.47	91.73	0.74	0.00	1.00	0.0	6.47970
1350	2.7042	80.20	80.20	0.00	0.00	1.00	0.00	6.7832
1500	2.7048	80.20	80.20	0.00	0.00	1.00	0.00	6.8183

Table E. 4: Syngas target through glycerol partial oxidation at different temperatures

Temperature K	H/O	Syngas composition					Relative distance (mm)		Min. O_2 required (kmol)	Syngas target (kmol/kmol glycerol)
		x_{CH_4}	x_{H_2O}	x_{H_2}	x_{CO}	x_{CO_2}	$D_{Glycerol}$	D_{O2}		
500	0.870	0.0475	0.5020	0.0043	0.00	0.4464	0.6933	0.3067	3.0966	6.07450
650	0.9846	0.0763	0.436	0.0521	0.003	0.4322	0.7287	0.2713	2.6061	5.8600
800	1.1785	0.0651	0.298	0.2097	0.062	0.365	0.79401	0.20599	1.8160	6.09445
950	1.942	0.0346	0.1130	0.4440	0.284	0.1244	0.9242	0.0758	0.5741	6.7673
1050	2.4450	0.0153	0.0350	0.5156	0.402	0.0323	0.9830	0.0170	0.1211	6.6734
1200	2.651	0.0042	0.0054	0.5513	0.436	0.0033	1.00	0.00	0.00	6.7656
1350	2.7042	0.0011	0.0016	0.5570	0.440	0.0007	1.00	0.00	0.00	6.7924
1500	2.7048	0.0005	0.0003	0.5579	0.441	0.0001	1.00	0.00	0.00	6.7910

Table E. 5: Syngas target via glycerol steam reforming at different temperatures

Temperature (K)	H/O	Syngas composition					Relative distance (mm)		Min. H_2O required (kmol	Syngas target (kmol)/kmol glycerol
		x_{CH_4}	x_{H_2O}	x_{H_2}	x_{CO}	x_{CO_2}	$D_{Glycerol}$	D_{H2O}		
500	2.2758	0.2061	0.6202	0.009	0.0000	0.1650	0.4413	0.5587	5.908	8.0869
650	2.2970	0.2128	0.4901	0.0865	0.0024	0.2082	0.5081	0.4919	4.5179	7.0839
800	2.3249	0.1304	0.3149	0.2960	0.0472	0.2115	0.5560	0.4440	3.72662	7.7099
950	2.527	0.0423	0.110	0.4870	0.2569	0.1038	0.7955	0.2045	1.1997	7.4437
1050	2.611	0.0163	0.0346	0.5317	0.3872	0.0302	0.9316	0.0684	0.34264	6.9165
1200	2.651	0.0043	0.0054	0.5540	0.4335	0.0033	1.00	0.00	0.00	6.8016
1350	2.7042	0.0011	0.0016	0.5570	0.440	0.0007	1.00	0.00	0.00	6.8210
1500	2.7048	0.0005	0.0003	0.5579	0.441	0.0001	1.00	0.00	0.00	6.8283

Table E. 6: Dry reforming of glycerol via CHO ternary systems

Temperature (K)	H/O	Syngas composition					Relative distance (mm)		Min. CO_2 required (kmol	Syngas target (kmol)/kmol glycerol
		x_{CH_4}	x_{H_2O}	x_{H_2}	x_{CO}	x_{CO_2}	$D_{Glycerol}$	D_{CO2}		
500	0.0153	0.0	0.0156	0.00	0.00	0.9839	0.013	0.987	354.31	3.0491
650	0.0153	0.0008	0.0146	0.0011	0.0052	0.979	0.013	0.987	354.31	3.0457
800	0.1378	0.0027	0.0746	0.0364	0.0920	0.7943	0.136	0.864	29.65	3.3746
950	1.222	0.0208	0.1038	0.3392	0.3481	0.1882	0.717	0.283	1.842	5.3850
1050	2.311	0.0146	0.0352	0.5057	0.4114	0.0334	0.945	0.0550	0.272	6.5303
1200	2.651	0.0043	0.0054	0.5540	0.4335	0.0033	1.00	0.00	0.00	6.7340
1350	2.7042	0.0011	0.0016	0.5570	0.440	0.0007	1.00	0.00	0.00	6.7446
1500	2.7048	0.0005	0.0003	0.5579	0.441	0.0001	1.00	0.00	0.00	6.7476

Table E. 7: Co-feeding H_2O with O_2 to produce syngas from glycerol

Temperature K	H/O	Co-feeds	Relative distance mm		Optimum amount H_2O kmol/kmol glycerol	Optimum amount O_2 kmol/kmol glycerol	Optimum amount CO_2 kmol/kmol glycerol	Syngas target kmol/kmol glycerol
		H_2O/O_2	$D_{Glycerol}$	D_{H_2O/O_2}				
500	1.241	H_2O/O_2	0.5306	0.4694	2.477	2.477	0.0	7.3126
650	1.387	H_2O/O_2	0.6002	0.3998	1.865	1.865	0.0	6.4711
800	1.524	H_2O/O_2	0.6805	0.3195	1.315	1.315	0.0	6.7636
950	2.165	H_2O/O_2	0.8765	0.1235	0.3945	0.3945	00.0	7.0416
1050	2.533	H_2O/O_2	0.9860	0.0140	0.03975	0.03975	0.0	6.7726
1200	2.651	H_2O/O_2	1.00	0.00	0.0	0.0	0.0	6.7099
1350	2.651	H_2O/O_2	1.00	0.00	0.0	0.0	0.0	6.7249

1500	2.651	H_2O/O_2	1.00	0.00	0.0	0.0	0.0	6.7236

Table E. 8: Co-feeding CO_2 with O_2 to produce syngas from glycerol

Temperature K	H/O	Co-feeds	Relative distance mm		Optimum amount H_2O kmol/kmol glycerol	Optimum amount O_2 kmol/kmol glycerol	Optimum amount CO2 kmol/kmol glycerol	Syngas target kmol/kmol glycerol
		CO_2/O_2	$D_{Glycerol}$	D_{CO_2/O_2}				
500	0.5070	CO_2/O_2	0.4697	0.53030	0.00	3.162	3.162	4.6997
650	0.5640	CO_2/O_2	0.4963	0.5037	0.00	2.842	2.842	4.6871
800	0.7540	CO_2/O_2	0.5921	0.4079	0.00	1.929	1.929	5.0893
950	1.6770	COO/O_2	0.8626	0.1374	0.00	0.446	0.446	6.3150
1050	2.651	CO_2/O_2	0.968	0.032	0.00	0.093	0.093	6.5847
1200	2.651	CO_2/O_2	1.00	0.00	0.00	0.00	0.00	6.7099
1350	2.651	CO_2/O_2	1.00	0.00	0.0	0.0	0.0	6.7249
1500	2.651	CO_2/O_2	1.00	0.00	0.0	0.0	0.0	6.7236

Table E. 9: Co-feeding H_2O with CO_2 to produce syngas from glycerol

Temperature K	H/O	Co-feeds	Relative distance mm		Amount H_2O kmol/kmol glycerol	Amount O_2 kmol/kmol glycerol	Amount CO_2 kmol/kmol glycerol	Syngas target kmol/kmol glycerol
		H_2O/CO_2	$D_{Glycerol}$	D_{H_2O/CO_2}				
500	0.7210	H_2O/CO_2	0.063	0.937	33.028	0.00	33.028	5.5611
650	0.8063	H_2O/CO_2	0.146	0.854	13.649	0.00	13.649	5.3851
800	1.0240	H_2O/CO_2	0.332	0.668	4.695	0.00	4.695	5.7677

950	1.8330	H_2O/CO_2	0.769	0.2310	0.6995	0.00	0.6995	6.5782
1050	2.4760	H_2O/CO_2	0.944	0.0560	0.137	0.00	0.137	6.7090
1200	2.651	H_2O/CO_2	1.00	0.00	0.00	0.00	0.00	6.7099
1350	2.6510	H_2O/CO_2	1.00	0.00	0.00	0.00	0.00	6.7249
1500	2.6510	H_2O/CO_2	1.00	0.00	0.00	0.00	0.00	6.7236

Table E. 10: Syngas composition target from 75% LLDPE -25% Glycerol mixture using O_2 as a reforming agent

Temperature (K)	$\frac{H}{O}$	x_{CH_4}	x_{H_2O}	x_{H_2}	x_{CO}	x_{CO_2}	D_{O_2}	D_M	Optimum amount of O_2(kmol)	Optimum amount of syngas (kmol)	Total hydrogen potential
650	0.840	0.0607	0.4053	0.0461	0.0036	0.4843	0.393	0.607	2.5876	4.10135	0.04972
800	1.008	0.0537	0.2863	0.1907	0.0656	0.40387	0.3467	0.6533	2.1227	4.30021	0.25636
950	1.6140	0.02821	0.11120	0.40003	0.31131	0.14931	0.2268	0.7732	1.1733	4.60283	0.71134
1050	2.060	0.01339	0.03571	0.48557	0.42915	0.03621	0.1737	0.8263	0.8409	4.69974	0.91472
1200	2.266	0.0037	0.0055	0.5160	0.47111	0.00370	0.1574	0.8426	0.7472	4.70210	0.98711
1350	2.266	0.00098	0.00160	0.52039	0.47630	0.00075	0.1574	0.8426	0.7472	4.70682	0.99669
1500	2.266	0.00035	0.00030	0.52147	0.47766	0.00001	0.1574	0.8426	0.7472	4.70751	0.99913

Table E. 11: Syngas composition target from 75% LLDPE -25% Glycerol mixture using H_2O as a reforming agent

Temp. (K)	$\frac{H}{O}$	x_{CH_4}	x_{H_2O}	x_{H_2}	x_{CO}	x_{CO_2}	D_{H_2O}	D_M	Amount of H_2O (kmol)	Amount of syngas (kmol)	Total hydrogen potential
650	2.689	0.24513	0.47832	0.09242	0.002165	0.18196	0.6339	0.3661	4.617	5.2420	0.09460
800	2.766	0.14935	0.30760	0.315755	0.043750	0.18355	0.6128	0.3872	4.2204	5.9737	0.35951
950	3.227	0.05116	0.10582	0.53565	0.2260	0.08136	0.4619	0.5381	2.28904	6.2758	0.76165
1050	3.559	0.02074	0.03669	0.60228	0.323062	0.02113	0.3905	0.6095	1.7085	6.1655	0.92534
1200	3.642	0.00552	0.00511	0.62887	0.35836	0.0034	0.3589	0.6411	1.4930	6.1261	0.98723
1350	3.642	0.00143	0.00148	0.63467	0.361982	0.00050	0.3589	0.6411	1.4930	6.1828	0.99665
1500	3.642	0.00065	0.00030	0.63592	0.36302	0.00007	0.3589	0.6411	1.4930	6.1857	0.99894

Table F. 1: Material balance during the production of methanol from 1 ton of glycerol

Stream No	1	2	3	4	5	6	7	8	9	10	11	12	13	14	15	$C_3H_8O_3$	CH_4	H_2O
Mole Flow kmol/h																		
CO	53.03886	53.03886	53.03886	64.34187	13.43921	13.43921	13.43921	13.29641	11.30195	11.30301	1.994462	0.142801	0.142801	0.142801	1.41E-17	0	0	0
H_2	107.3381	107.3381	107.3381	138.0416	36.11972	36.11972	36.11972	36.11992	30.70132	30.70345	5.417879	0.000528	0.000528	0.000528	5.87E-22	0	0	0
CO_2	0.628373	0.628373	0.628373	1.540348	1.5015	1.5015	1.5015	1.072853	0.911925	0.911975	0.160928	0.428647	0.428647	0.428647	5.96E-16	0	0	0
CH_4O	0	0	0	0.66039	51.6019	51.6019	51.6019	0.776894	0.66036	0.66039	0.116534	50.82501	50.82501	50.8245	0.000508	0	0	0
H_2O	0	0	0	0.000154	0.039002	0.039002	0.039002	0.000181	0.000154	0.000154	2.72E-05	0.038821	0.038821	3.88E-08	0.038821	0	0	21.72045
CH_4	0.587484	0.587484	0.587484	3.156344	3.156344	3.156344	3.156344	3.022174	2.568848	2.56886	0.453326	0.13417	0.13417	0.13417	4.04E-17	0	21.67956	0
GLYCEROL	0	0	0	0	0	0	0	0	0	0	0	0	0	0	0	10.85839	0	0
Mass Flow kg/h																		
CO	1485.64	1485.64	1485.64	1802.242	376.4377	376.4377	376.4377	372.4378	316.5721	316.6019	55.86567	3.9999	3.9999	3.9999	3.94E-16	0	0	0
H_2	216.3808	216.3808	216.3808	278.2753	72.81303	72.81303	72.81303	72.81197	61.89017	61.89446	10.92179	0.001064	0.001064	0.001064	1.18E-21	0	0	0
CO_2	27.65458	27.65458	27.65458	67.79041	66.08072	66.08072	66.08072	47.21604	40.13363	40.13583	7.082406	18.86468	18.86468	18.86468	2.62E-14	0	0	0
CH_4O	0	0	0	21.16032	1653.436	1653.436	1653.436	24.89336	21.15936	21.16032	3.734004	1628.543	1628.543	1628.527	0.016285	0	0	0
H_2O	0	0	0	0.002772	0.702629	0.702629	0.702629	0.003261	0.002772	0.002772	0.000489	0.699368	0.699368	6.99E-07	0.699367	0	0	391.3
CH_4	9.424864	9.424864	9.424864	50.63647	50.63647	50.63647	50.63647	48.48401	41.2114	41.2116	7.272601	2.152463	2.152463	2.152463	6.48E-16	0	347.8	0
GLYCEROL	0	0	0	0	0	0	0	0	0	0	0	0	0	0	0	1000	0	0

Total Flow kmol/h	161.5929	161.5929	161.5929	207.7407	105.8577	105.8577	105.8577	54.28771	46.14455	46.14784	8.143156	51.56997	51.56997	51.53064	0.039329	10.85839	21.67956	21.72045
Total Flow kg/h	1739.1	1739.1	1739.1	2220.107	2220.107	2220.107	2220.107	565.8464	480.9694	481.0069	84.87696	1654.26	1654.26	1653.545	0.715653	1000	347.8	391.3
Temperature C	926.85	149.85	220.01	219.9895	219.9895	76.85	71.15722	37.85	37.85	220.01	37.85	37.85	74.85	82.54225	119.765	25	25	25
Pressure atm	0.986923	2.96077	54.28078	54.28078	54.28078	44.41155	19.73847	19.73847	19.73847	54.28078	19.73847	19.73847	3.947693	1.973847	1.973847	0.986923	0.986923	0.986923
Vapor Frac	1	1	1	1	1	0.520197	0.543103	1	1	1	1	0	0	1	0	0	1	0
Liquid Frac	0	0	0	0	0	0.479803	0.456897	0	0	0	0	1	1	0	1	1	0	1
Enthalpy cal/mol	-2527.14	-8216.78	-7636.28	-7822.87	-26909	-32300.2	-32300.2	-9799.58	-9799.58	-8476.23	-9799.58	-57727.8	-56654.2	-47672.1	-66863.3	-157160	-17802.8	-68993.4
Entropy cal/mol-K	18.32831	8.575812	3.980645	3.446626	-14.0432	-26.8049	-25.8498	0.150459	0.150459	1.387249	0.150459	-58.5212	-55.1969	-29.8742	-34.0812	-141.786	-19.234	-38.9675
Density gm/cc	0.000108	0.000915	0.013894	0.013784	0.02888	0.054163	0.02526	0.007615	0.007615	0.013403	0.007615	0.765993	0.714157	0.002237	0.861862	1.269308	0.000648	0.961076
Average MW	10.76223	10.76223	10.76223	10.68691	20.97256	20.97256	20.97256	10.4231	10.4231	10.42317	10.4231	32.07798	32.07798	32.08857	18.19655	92.09472	16.04276	18.01528